

# POLITECNICO DI TORINO

Dipartimento di Ingegneria Meccanica e Aerospaziale (DIMEAS)

Master's Degree Thesis in Biomedical Engineering



## **Realization and Evaluation of a Prosthetic Foot Multibody Model in Quasi-Static and Dynamic Conditions**

### **Supervisor:**

Prof. Carlo Ferraresi

### **Co-supervisors:**

Ing. Carlo De Benedictis

Ing. Giovanni Milandri

Ing. Federico Tessari

### **Candidate:**

Elisa Catto

December 2019



*Vivi con pazienza, sii forte, credi in te stesso  
non sei in ritardo e non sei in anticipo,  
sei nel tuo tempo.*





# Abstract

---

Nowadays, innovations in lower limb prosthetics head towards active prostheses development or cheaper prostheses affordable by a wider group of people. Evaluation and optimization of prostheses' passive components, like the foot component of a lower limb prosthesis, could be useful to improve patients' comfort and physiological response, as well as simplify the role of the active components.

This study proposes to utilize multibody analysis to reproduce the elastic behaviour of a commercial prosthetic foot in order to run a dynamic simulation of gait stance phase. The multibody model realization is carried out with different CAD software and completed in MATLAB®, while the static and dynamic analysis of the prosthetic foot are performed within Simulink® environment. Most of the Simulink®'s blocks utilized to build the multibody model are taken from Simscape Multibody library. All simulations will be conducted on a Vari-Flex® foot (Össur).

Although the optimization of a generic flexible body is usually performed by means of Finite Element Analysis (FEA), the use of a multibody analysis could cut down computational time effort required to perform a dynamical simulation. The dynamic simulation of gait stance phase performed in this study lasts few minutes (less than 7) and present results comparable to those obtained experimentally, while a complete FEA (Finite Element Analysis) could take more than 1 hour. On the other hand, the simple multibody model proposed in this Thesis could not describe properly the quasi-static behaviour of the prosthetic foot.

Another key feature of the model is that joint's viscoelastic values are easily computed using an analytical formula obtained from a quasi-static model: a wedged beam loaded at the free end.

The steps followed to achieve the explained results are listed below:

1. Definite stiffness' starting value;
2. Segment the prosthetic foot real model in order to realize a multibody model;
3. Reproduce quasi-static loading simulation on Vari-Flex® foot;
4. Tune joints' stiffness using the results obtained by quasi-static mechanical simulations in previous works;
5. Simulate gait effects on the multibody model in order to evaluate the errors committed calculating foot deflection and Roll-Over Shape (ROS) over gait.

*This Thesis is part of a project by Fondazione IIT (Istituto Italiano di Tecnologia) – Department of Rehab Technologies funded by INAIL (Istituto Nazionale Assicurazione Infortuni sul Lavoro). The project's purpose is developing limb prosthetic solutions for the Italian Sistema Sanitario Nazionale.*



# Index

---

<b>Abstract .....</b>	<b>I</b>
<b>Index .....</b>	<b>III</b>
<b>Figures Index .....</b>	<b>VII</b>
<b>Tables Index .....</b>	<b>XVII</b>
<b>Equations Index .....</b>	<b>XIX</b>
<b>1. Fundamentals .....</b>	<b>1</b>
1.1 <i>Foot Anatomy and Biomechanics .....</i>	<i>1</i>
1.2 <i>Human Locomotion .....</i>	<i>9</i>
1.3 <i>Foot Amputation Causes.....</i>	<i>12</i>
1.4 <i>Lower Limb Prosthetics.....</i>	<i>14</i>
1.5 <i>Foot Prosthetics.....</i>	<i>17</i>
<b>2. Multibody Model Implementation .....</b>	<b>27</b>
2.1 <i>Simscape Multibody.....</i>	<i>27</i>
2.2 <i>Stiffness Issue.....</i>	<i>28</i>
2.3 <i>Highlander® Multibody Model – Preliminary Study .....</i>	<i>38</i>
2.4 <i>Vari-Flex® Segmentation.....</i>	<i>44</i>
2.5 <i>Vari-Flex® Multibody Model.....</i>	<i>56</i>
<b>3. Quasi-Static Simulations &amp; Multibody Model Tuning .....</b>	<b>61</b>

3.1	<i>Experimental Quasi-Static Tests and FEM Simulations.....</i>	61
3.2	<i>Simulation of Quasi-Static Test with Vari-Flex® Multibody Model .....</i>	65
3.3	<i>Parameters Estimation MATLAB®'s Tool.....</i>	72
3.4	<i>Tuning Process .....</i>	74
<b>4.</b>	<b>Gait Data Acquisition .....</b>	<b>79</b>
4.1	<i>Equipment.....</i>	79
4.2	<i>Gait Protocol .....</i>	82
4.3	<i>Data Processing .....</i>	84
4.4	<i>Final Gait Data .....</i>	86
<b>5.</b>	<b>Dynamic Simulations .....</b>	<b>95</b>
5.1	<i>Dynamic Simulation of Stance Phase .....</i>	95
5.2	<i>Model Changes .....</i>	106
<b>6.</b>	<b>Results .....</b>	<b>109</b>
6.1	<i>Quasi-Static Simulations on Vari-Flex® Model.....</i>	109
6.2	<i>Dynamic Simulation of Stance Phase on Vari-Flex® Model .....</i>	113
<b>7.</b>	<b>Discussion and Future Developments .....</b>	<b>121</b>
7.1	<i>Multibody Model Design .....</i>	121
7.2	<i>Quasi-Static Tests .....</i>	121
7.3	<i>Quasi-Static Simulations Future Developments .....</i>	122
7.4	<i>Dynamic Tests.....</i>	123
7.5	<i>Dynamic Simulations Future Developments.....</i>	124
<b>8.</b>	<b>Conclusions .....</b>	<b>127</b>

<b>A. Appendix A – MATLAB® Scripts .....</b>	<b>131</b>
<i>Theoretical wedged beam model – ‘bar_model_theoretical.m’.....</i>	<i>131</i>
<i>Analytical wedged beam model - ‘bar.m’.....</i>	<i>134</i>
<i>Cartesian Coordinates Segmentation Method – ‘segmentation_auto_DEF.m’.....</i>	<i>137</i>
<i>Quasi-Static Simulation (with Geometrical Information) – ‘load_test_geom.m’.....</i>	<i>140</i>
<i>2-Segments Beam Model to Be Tuned – ‘bar_optimization.m’.....</i>	<i>144</i>
<i>Import of Gait Data, Recognition of Stance Phase and Data Filtering - ‘data_import.m’ .....</i>	<i>146</i>
<i>Calculation of Gait Data Mean Values and Standard Deviations - ‘data_elaboration.m’.....</i>	<i>149</i>
<i>Dynamic Simulation – ‘variflex_model.m’.....</i>	<i>151</i>
<i>Other Functions .....</i>	<i>159</i>
 <b>B. Appendix B – Simulink® Schemes .....</b>	 <b>161</b>
<i>Simulink®/Simscape’s Blocks Legend.....</i>	<i>161</i>
<i>5-Segments Wedged Beam Model – ‘bar_model_5.slx’ .....</i>	<i>163</i>
<i>Highlander® multibody model – ‘sim_highlander_v6.slx’ .....</i>	<i>164</i>
<i>Vari-Flex® multibody model - ‘sim_vari_flex_16_9_geom.slx’.....</i>	<i>165</i>
<i>Quasi-Static Simulation 20 Heel Vari-Flex® Model – ‘sim_vari_flex_mech_test_heel_20.slx’.....</i>	<i>166</i>
<i>2-Segments Beam Model to Be Tuned – ‘bar_model_opt_2.slx’ .....</i>	<i>167</i>
<i>Former Dynamic Vari-Flex® Model – ‘sim_vari_flex_dyn_16_9.slx’ .....</i>	<i>168</i>
<i>Modified Dynamic Vari-Flex® Model – ‘sim_vari_flex_dyn_1sr_locked.slx’ .....</i>	<i>169</i>
<i>Subsystems .....</i>	<i>170</i>
 <b>References .....</b>	 <b>171</b>

<b>Ringraziamenti .....</b>	<b>177</b>
-----------------------------	------------

# 1. Figures Index

---

Figure 1.1.1 – Upper view of the foot bones. Tarsal bones are not coloured (ivory); metatarsal bones are coloured in pink, phalanges are coloured in yellow, violet and green. [ <a href="https://cdn.britannica.com/07/99107-004-B9666996.jpg">https://cdn.britannica.com/07/99107-004-B9666996.jpg</a> ] .....	2
Figure 1.1.2 – Plantar view of the foot ligaments. [ <a href="https://upload.wikimedia.org/wikipedia/commons/d/dc/Gray358.png">https://upload.wikimedia.org/wikipedia/commons/d/dc/Gray358.png</a> ] .....	3
Figure 1.1.3 – Foot arches. [ <a href="https://cdn.shopify.com/s/files/1/1708/5797/files/arches_of_the_foot.jpg?v=1505218403">https://cdn.shopify.com/s/files/1/1708/5797/files/arches_of_the_foot.jpg?v=1505218403</a> ] .....	3
Figure 1.1.4 – Foot joints. [ <a href="http://d1yboe6750e2cu.cloudfront.net/i/38dc4e75f20e66de7b6c3de2adc2bf5e7410b8f2">http://d1yboe6750e2cu.cloudfront.net/i/38dc4e75f20e66de7b6c3de2adc2bf5e7410b8f2</a> ] .....	4
Figure 1.1.5 – On the left: medial view of the foot. It is possible to notice the superior and inferior extensor retinacula and peroneal retinacula. [ <a href="https://radiologykey.com/wp-content/uploads/2016/07/C8-FF7-7.gif">https://radiologykey.com/wp-content/uploads/2016/07/C8-FF7-7.gif</a> ]. On the right: lateral view of the foot. The flexor retinaculum is shown. [ <a href="https://www.podiatryinthepines.com/storage/app/media/img-tarsal-tunnel.jpg">https://www.podiatryinthepines.com/storage/app/media/img-tarsal-tunnel.jpg</a> ] .....	5
Figure 1.1.6 – Foot dorsal muscles. [ <a href="https://teachmeanatomy.info/wp-content/uploads/The-Dorsal-Layer-of-Muscles.jpg">https://teachmeanatomy.info/wp-content/uploads/The-Dorsal-Layer-of-Muscles.jpg</a> ] .....	5
Figure 1.1.7 - Windlass effect explanation [2] .....	6
Figure 1.1.8 – A) First layer's structures. [ <a href="https://musculoskeletalkey.com/wp-content/uploads/2016/06/B9781455725311000171_f08-04a-9781455725311.jpg">https://musculoskeletalkey.com/wp-content/uploads/2016/06/B9781455725311000171_f08-04a-9781455725311.jpg</a> ] B) Second and third layers' structures [ <a href="https://musculoskeletalkey.com/wp-content/uploads/2016/06/B9781455725311000171_f08-04b-9781455725311.jpg">https://musculoskeletalkey.com/wp-content/uploads/2016/06/B9781455725311000171_f08-04b-9781455725311.jpg</a> ] .....	7
Figure 1.1.9 – Anatomic planes of the foot. A) Frontal plane with the relative frontal axes (or anterior-posterior axis). B) Transverse plane with the relative transverse axis (or inferior-superior axis). C) Sagittal plane with the relative sagittal axis (or medio-lateral axis). [ <a href="https://daniz53y71u1s.cloudfront.net/library/image1.jpg">https://daniz53y71u1s.cloudfront.net/library/image1.jpg</a> ] .....	8
Figure 1.1.10 – Physiological movements of the foot. Inversion and eversion develop around the X-axis (frontal axis); dorsiflexion and plantarflexion develop around the Y-axis (sagittal axis); external and internal rotation develop around the Z-axis (transverse axis). [ <a href="https://media.springernature.com/original/springer-static/image/chp%3A10.1007%2F978-1-4939-1732-7_18/MediaObjects/31137_3_En_18_Fig2_HTML.gif">https://media.springernature.com/original/springer-static/image/chp%3A10.1007%2F978-1-4939-1732-7_18/MediaObjects/31137_3_En_18_Fig2_HTML.gif</a> ] .....	8
Figure 1.1.11 – A) Supination of the foot. B) Pronation of the foot. [ <a href="https://www.bestrunning-shoes.com/wp-content/uploads/2017/10/Best-running-shoes-for-overpronation-bying-guide.jpg">https://www.bestrunning-shoes.com/wp-content/uploads/2017/10/Best-running-shoes-for-overpronation-bying-guide.jpg</a> ] ...	9
Figure 1.2.1 – Gait cycle terms and corresponding percentage of gait cycle [ <a href="https://www.physio-pedia.com/images/b/b0/Figure2.jpg">https://www.physio-pedia.com/images/b/b0/Figure2.jpg</a> ] .....	10
Figure 1.3.1 Risk factors and mechanism that may lead to foot ulcer and amputation [25] .....	14
Figure 1.4.1 - Lower limb amputation's levels. Going from left to right: ankle/foot disarticulation, transtibial amputation, knee disarticulation, transfemoral amputation, hip disarticulation, hemipelvectomy. [ <a href="http://chirurgiadelmoncone.org/L'amputazione.html">http://chirurgiadelmoncone.org/L'amputazione.html</a> ] .....	15

Figure 1.4.2 – Different types of foot amputation. Going from left to right: toes disarticulation or amputation, Transmetatarsal amputation, Lisfranc amputation, Chopart amputation, Pirogof amputation, Syme amputation. [ <a href="http://chirurgiadelmoncone.org/L'amputazione.html">http://chirurgiadelmoncone.org/L'amputazione.html</a> ] .....	15
Figure 1.4.3 – Lower limb prostheses' components. ....	15
Figure 1.4.4 – From left to right: prosthesis' foot component, below-knee prosthesis, above-knee prosthesis, hip disarticulation/hemipelvectomy prosthesis. ....	16
Figure 1.5.1 – Examples of rigid feet. On the left there is an example of SACH foot. On the right is represented a dynamic foot. [27] .....	18
Figure 1.5.2 – Examples of articulated prosthetic feet. [27] .....	18
Figure 1.5.3 – Examples of ESAR feet. On the right there is the Vari-Flex® foot, the one that will be analysed in this work.....	19
Figure 1.5.4 – Examples of sport purpose foot for running.....	19
Figure 1.5.5 – Overview of the foot prosthetic issues and the parameters and characteristics who are related with.....	20
Figure 1.5.6 – In Morgenroth et al. study were tested different foot: a dynamic (conventional) foot, an ESAR foot (prescribed) and a CESR (Controlled Energy Storage and Return) foot designed by them. The image shows the correlation between prosthetic foot-ankle push-off power and intact knee external adduction moment for each type of foot. As it can be seen, as the foot-ankle push-off power increases, intact knee EAM decreases. A decreased intact knee EAM means a lower load on the intact knee, resulting in a lower probability for the amputee subject to develop osteoarthritis [36]. ....	21
Figure 1.5.7 – Left figure: representation of the radius and the centre of curvature. The black curve is the imaginary ROS curve, with its own radius of curvature and the relative centre of curvature. The dashed circle in red is the ROS curve's osculating circle. [ <a href="https://en.wikipedia.org/wiki/Center_of_curvature#/media/File:Radius_of_curvature.svg">https://en.wikipedia.org/wiki/Center_of_curvature#/media/File:Radius_of_curvature.svg</a> ]. Right figure: different configurations of foot centre of curvature. [38] .....	22
Figure 1.5.8 – The figure shows the relationship between the net metabolic rate and the normalized (over leg length, L) arc foot radius. The curve shows a minimum where the arc foot radius is approximatively equal to 0.3 L. [39].....	22
Figure 1.5.9 – A) ROS of the two feet tested by Curtze et al. The figure on the left is referred to an Esprit foot, while the figure on the right is the ROS of a Vari-Flex® foot. B) COP forward travels of the Esprit® foot (left) and the Vari-Flex® foot (right). C) Radii of curvature of the Esprit foot (left) and Vari-Flex® foot (right) [38].....	23
Figure 2.2.1 – Schematic representation of a wedged beam subjected to bending. ....	29
Figure 2.2.2 - How $k_i$ and $l_i$ are considered in the multibody scheme. ....	30
Figure 2.2.3 – The blue line represents the theoretical force sensed at the weld joint. The red line is the force sensed in simulations with 1, 2, 5, 10 and 20 segments. ....	32
Figure 2.2.4 – The blue line represents the theoretical torque sensed at the weld joint. The red line is the torque sensed in simulations with 1, 2, 5, 10 and 20 segments. ....	32



Figure 2.2.5 - Vertical deflection achieved by the different models. The dashed thicker line is the theoretical result, while the other lines represent the deflection obtained by the simulated models. ....	32
Figure 2.2.6 – The blue dots represent the error that each simulated model present with respect to the theoretical maximum deflection at the beam’s loaded end. ....	33
Figure 2.2.7 – Representation of a 1-rigid-segment model of wedged beam loaded with a bending force at the free end.....	34
Figure 2.2.8 - Representation of a 2-rigid-segments model wedged beam loaded with a bending force at the free end.....	35
Figure 2.2.9 – Representation of a 3-rigid-segments model of wedged beam loaded with a bending force at the free end.....	36
Figure 2.2.10 – Maximum deflection’s error found using the analytical formula for rotational stiffness.....	37
Figure 2.2.11 – Wedged beam’s elastic line obtained with the analytical rotational stiffness’ formula. ....	38
Figure 2.3.1 – Schematic representation of the Highlander® lumped parameters model realized by Fey et al. [33]. The revolute joints highlighted with blue circles have viscoelastic properties, while the others have been considered as locked joints: they are pulled by the other segments, but do not allow relative rotations. The ankle joint is the origin of the reference system and it is fixed in space. ....	38
Figure 2.3.2 – A) Lateral view of the Highlander® model realized with Simscape. B) Isometric view of the same model.....	39
Figure 2.3.3 – A) Definition of foot flex extension angle: is the angle that the anterior-posterior axis of the foot and the line that connects the big toe and the ankle form. B) Trend of the foot flex-extension angle in healthy people over stance phase.....	40
Figure 2.3.4 – COP amputee displacement. The graph particularly represents the COP displacement along anterior-posterior direction, as the figure on the left explains. The time axis is referred to the stance phase only [11]. ....	40
Figure 2.3.5 – Vertical ground reaction force trend over stance phase. ....	40
Figure 2.3.6 – COP posterior-anterior displacement referred to the Highlander foot length. ....	41
Figure 2.3.7 – How inputs are given to the model. Foot flex-extension angle and vertical ground reaction force depend only on time, while COP posterior-anterior displacement is a function of both time and space.....	41
Figure 2.3.8 – The graph on the left shows the COP motion from hindfoot to forefoot over stance phase. Dots of same colour are related to the same segment’s midpoint highlighted in the figure on the right. ....	42
Figure 2.3.9 – Segments’ lengths referred to total body height, H. [49].....	42
Figure 2.3.10 – Other segments information as densities, masses, centre of mass (COM)’s position and radius of gyration. Masses are referred to total body weight (M). COM’s position and radius of gyration are expressed as a percentage of the segment’s length. Finally, density is expressed in g/cm <sup>3</sup> . [49].....	43

Figure 2.3.11 – From left to right: hip joint's flex-extension angle; knee joint's flex-extension angle; hip joint's flex-extension angle. Data taken from Bovi et al. study [48].....	43
Figure 2.3.12 – Representation of the lower limb multibody model simulated. The foot segment is realized with the Highlander® multilink model.....	43
Figure 2.4.1 – Schematic representation of the segmentation process. The software I have used are SolidWorks®, Rhinoceros® and MATLAB®.....	44
Figure 2.4.2 – Solidworks® CAD model of the Vari-Flex® foot.....	44
Figure 2.4.3 – Rhinoceros® IGES model of the Vari-Flex® foot.....	44
Figure 2.4.4 – Silhouette of the two laminas forming the elastic structure of the Vari-Flex foot.....	45
Figure 2.4.5 – Order in which the points must to be created to perform the further segmentation steps. The points must be created starting from position 1 and following the arrows. Blue number and arrow refer to the keel spline, while the red ones refer to the heel spline. ....	45
Figure 2.4.6 – Points taken on the Vari-Flex's silhouette. The green points form the keel silhouette, while the yellow points form the heel silhouette.....	45
Figure 2.4.7 – Vari-Flex®'s silhouette points imported in MATLAB®.....	46
Figure 2.4.8 – The splines that will be further considered to segment the foot model are highlighted in green (heel spline) and yellow (keel spline).....	46
Figure 2.4.9 – Relevant measures for polar-coordinates-based segmentation.....	48
Figure 2.4.10 – Relationship between points' relative orientation and cumulative spline length. The former relationship of the nominal splines is coloured in black, while the approximant function found is coloured in black. The graphic on the left is referred to the keel spline, while the one on the right refers to the heel spline.....	48
Figure 2.4.11 – Reconstructed splines using polar coordinates segmentation method. ....	49
Figure 2.4.12 - Relevant variables for cartesian-coordinates-based segmentation .....	49
Figure 2.4.13 – Comparison between the two segmentation methods. The one on the left (PCSM) introduces a significant geometrical error, especially where the two splines touch and on the heel. The segmentation on the right (CSSM) better approximates the nominal curves. ....	50
Figure 2.4.14 – Comparison of the nominal relationship between x and y coordinates and the cumulative spline length and the approximant function. Going from left to right and from up to down, the figures refers to heel spline x coordinate, heel spline y coordinate, keel spline x coordinate and keel spline y coordinate relationships with the cumulative spline length. ....	50
Figure 2.4.15 – On the left, the original reference system and the new desired origin are shown. On the right the new reference system derived from the coordinates shift is presented. ....	51
Figure 2.4.16 – Segmented keel spline.....	52
Figure 2.4.17 – 'Figure 3' generated by the segmentation script. It helps the user to decide how many segments keel and heel spline have in common and which is the ID number of the heel junction point. ....	53
Figure 2.4.18 – Basic information to give to MATLAB® Command Window (together with heel segments number) to perform the heel segmentation. ....	54

Figure 2.4.19 – Example of segmented multibody models that respect the requirements described before. Especially, the third model here presented will be the one used to conduct the further analysis. ....	55
Figure 2.4.20 – Example of a segmented model that does not fulfil the requirements. ....	55
Figure 2.5.1 – Vari-Flex® parts detailed. The rubber sole will be not considered in the multibody model. ....	57
Figure 2.5.2 – Details of pylon junction modeling – rigid body. ....	57
Figure 2.5.3 – Details of heel lamina modeling – flexible body. ....	57
Figure 2.5.4 – a) Simple multibody model. b) Complex multibody model. ....	58
Figure 3.1.1 – Fatigue testing machine Instron 8801. [51] ....	61
Figure 3.1.2 – Details of the crescent-shaped special support designed by L.Cavallaro et al. [51] ....	62
Figure 3.1.3 – Crescent-shaped support with the Vari-Flex® screwed on it. [51] ....	62
Figure 3.1.4 – a) 20° Heel touch configuration. b) 10° Heel touch configuration. c) 10° Toe touch configuration. d) 20° Toe touch configuration. ....	63
Figure 3.1.5 – Force-deflection diagram for 20° toe touch loading condition. ....	63
Figure 3.1.6 – Force-deflection diagram for 10° toe touch loading condition. ....	64
Figure 3.1.7 – Force-deflection diagram for 10° heel touch loading condition. ....	64
Figure 3.1.8 – Force-deflection diagram for 20° heel touch loading condition. ....	64
Figure 3.2.1 – Schematization of the external force's application point in the different configurations: a) 20° heel touch; b) 10° heel touch; c) 10° toe touch; d) 20° toe touch. ....	65
Figure 3.2.2 – External forces profiles: a) 20° heel touch; b) 10° heel touch; c) 10° toe touch; d) 20° toe touch. ....	66
Figure 3.2.3 – Results of preliminary tests at 20° heel touch. ....	68
Figure 3.2.4 - Results of preliminary tests at 10° heel touch. ....	68
Figure 3.2.5 – Results of preliminary tests at 10° toe touch. ....	68
Figure 3.2.6 - Results of preliminary tests at 20° toe touch. ....	69
Figure 3.2.7 – Example of the error area between computational force-deflection curve and experimental one. ....	70
Figure 3.2.8 - Results of Young modulus tests at 20° heel touch. ....	70
Figure 3.2.9 - Results of Young modulus tests at 10° heel touch. ....	70
Figure 3.2.10 – Results of Young modulus tests at 10° toe touch. ....	71
Figure 3.2.11 – Results of Young modulus tests at 20° toe touch. ....	71
Figure 3.2.12 – Total error area for different Young modulus' values. The results are presented for each loading conditions and then summed up and reported in “TOTAL” graphic. ....	71
Figure 3.3.1 – Parameters Estimation's Graphic User Interface (GUI). ....	72
Figure 3.3.2 – In ‘New Experiment – Edit Experiment’ section (on the left) it is possible to configure the local parameter that are specific for the experiment. In ‘Select Parameters – Edit Estimated	

<i>Parameters' section (on the right) it is possible to declare the parameters that have to be tuned considering all the loaded experiments.....</i>	<i>73</i>
<i>Figure 3.3.3 – 'Estimation Options' GUI. The menu were to find them is highlighted in yellow.....</i>	<i>74</i>
<i>Figure 3.4.1 – Schematic representation of a 2-segments beam model loaded with a vertical force at the free end.....</i>	<i>75</i>
<i>Figure 3.4.2 - a) Elastic line before tuning. b) Elastic line after tuning. c) Mid-point deflection before tuning; d) Midpoint deflection after tuning. e) Loaded-end deflection before tuning. f) Loaded-end deflection after tuning. ....</i>	<i>76</i>
<i>Figure 3.4.3 – Estimated stiffness variations over tuning iterations. ....</i>	<i>77</i>
<i>Figure 3.4.4 – Example of 'experimental' and 'linear' force profiles.....</i>	<i>78</i>
<i>Figure 4.1.1 – Subject wearing the adapter with Power Knee and Vari-Flex mounted. ....</i>	<i>79</i>
<i>Figure 4.1.2 – Schematic representation of the experimental set up [51]. ....</i>	<i>80</i>
<i>Figure 4.1.3 – Vicon Vero® camera.....</i>	<i>80</i>
<i>Figure 4.1.4 – AMTI treadmill. The two force plates are mounted under the blue sliding mat.....</i>	<i>81</i>
<i>Figure 4.1.5 – Experimental marker set with markers' names. ....</i>	<i>81</i>
<i>Figure 4.1.6 – Schematic representation of the pylon angle with respect to and ideal line perpendicular to the ground.....</i>	<i>82</i>
<i>Figure 4.2.1 – Trial phases. a) Prosthetic limb landing on the first force plate. b) Sound limb landing on the second force plate. c) Prosthetic limb passes the sound limb before the subjects stops the gait. ....</i>	<i>83</i>
<i>Figure 4.3.1 – Schematic resume of gait data processing. ....</i>	<i>84</i>
<i>Figure 4.3.2 – Considered marker distances. ....</i>	<i>85</i>
<i>Figure 4.3.3 – Schematic representation of the logic behind Equation 4.3.1.....</i>	<i>86</i>
<i>Figure 4.4.1 – Reference axes which ground reaction forces are referred to. ....</i>	<i>86</i>
<i>Figure 4.4.2 – Inferior-superior ground reaction force. The black lines are filtered data referring to each trial. The thicker red line is the averaged inferior-superior ground force. ....</i>	<i>87</i>
<i>Figure 4.4.3 – Inferior-superior ground reaction forces. In the upper figure experimental processed data are presented: averaged data are represented with a black thick line, while the red and green line are respectively averaged data plus or minus the standard deviation. In the lower figure there is the inferior-superior GRF for a healthy subject [56]. ....</i>	<i>87</i>
<i>Figure 4.4.4 – Posterior-anterior ground reaction forces. In the upper figure experimental processed data are presented: averaged data are represented with a black thick line, while the red and green line are respectively averaged data plus or minus the standard deviation. In the lower figure there is the anterior-posterior GRF for a healthy subject [56]. ....</i>	<i>88</i>
<i>Figure 4.4.5 – Posterior-anterior ground reaction force. The black lines are filtered data referring to each trial. The thicker red line is the averaged posterior-anterior ground force.....</i>	<i>89</i>
<i>Figure 4.4.6 – Medio-lateral ground reaction forces. In the upper figure experimental processed data are presented: averaged data are represented with a black thick line, while the red and green</i>	

line are respectively averaged data plus or minus the standard deviation. In the lower figure there is the medio-lateral GRF for a healthy subject [56].....	89
Figure 4.4.7 – Medio-lateral ground reaction force. The black lines are the filtered data referring to each trial. The thicker red line is the averaged medio-lateral ground force. ....	90
Figure 4.4.8 - Posterior-anterior COP displacement. Averaged data are represented with a black thick line, while the red and green line are respectively averaged data plus or minus one standard deviation.....	90
Figure 4.4.9 – Posterior-anterior COP displacement for a healthy subject [11].....	91
Figure 4.4.10 – Posterior-anterior COP displacement. The black lines are filtered data referring to each trial. The thicker red line is the averaged posterior-anterior COP displacement.....	91
Figure 4.4.11 – Legislation ISO 22675 for fatigue test on prosthetic feet. The tilt angle refers to the already described pylon angle. In this case, the angle is referred to a period that is typically the duration of the stance phase.....	92
Figure 4.4.12 – Pylon angle. The angle is negative when the foot is ahead of an imaginary line perpendicular to the ground and passing through the hip joint, while is negative when the foot is behind it. The black lines are the filtered data of all trials. The thicker red line is the averaged inferior-superior ground force. ....	92
Figure 4.4.13 – Posterior-anterior COP displacement. In the upper figure experimental processed data are presented: averaged data are represented with a black thick line, while the red and green line are respectively averaged data plus or minus the standard deviation. ....	92
Figure 4.4.14 – Distance between FootFront markers and TibiaUpFront markers over stance phase. ....	93
Figure 4.4.15 – Distance between FootMid markers and TibiaUpFront markers over stance phase. ....	93
Figure 4.4.16 – Distance between FootBack markers and TibiaUpFront markers over stance phase. ....	94
Figure 5.1.1 – Frames on foot sole’s segments.....	97
Figure 5.1.2 – COP progression over Vari-Flex® foot multibody model. Each vertical red line represents the instant when the COP switches from one segment to the following one.....	97
Figure 5.1.3 – First strategy’s forces profiles. The upper image refers to the vertical ground reaction forces, while the lower one refers to horizontal ground reaction forces. Each vertical line represent the instant when the previous segment is unloaded and the following one becomes loaded. ....	98
Figure 5.1.4 – Second strategy’s forces profiles. The upper image refers to the vertical ground reaction forces, while the lower one refers to horizontal ground reaction forces. It can be noticed how ‘reconstructed’ force profiles (black thick line) and ‘real’ force profile (red thick line) are the same because they are not distinguishable. ....	99
Figure 5.1.5 – COP progression for different loading conditions. The black dashed thick line represent the experimental COP posterior-anterior progression. Blue curve is the COP progression when the model is loaded following the first strategy for force application. Green curve is the COP progression when the model is loaded following the second strategy for force application. ....	100

Figure 5.1.6 – Markers' modeling resuming scheme. In the upper part of the image there is the Simscape scheme created to simulate one marker. In the lower part there is the model visualization. ....	101
Figure 5.1.7 – Calculation of distance between simulated markers. The Transform sensor block is set on Distance calculation. The reference frame is Base. In this specific case the base segment will always be The geometrical centre of TibiaUpFront marker. ....	101
Figure 5.1.8 – Schematic explanation of the instruments used (on the left) and the parameters considered (on the right) to calculate ROS in A. Hansen et al. study [58]. ....	102
Figure 5.1.9 – Schematic representation of parameters used to evaluate ROS of Vari-Flex multibody model. ....	103
Figure 5.1.10 – Transform Sensor block settings to properly calculate COPx – ANKLE <sub>x</sub> (Translation – X), COP <sub>y</sub> – ANKLE <sub>y</sub> (Translation – Y) and d (Translation – Distance). The measurement frame is set on Base, which in this case is the ankle joint (ANKLE). ....	105
Figure 5.1.11 – Experimental (in black) and FEA (in red) fitted ROS obtained by L. Cavallaro. ....	105
Figure 5.2.1 – Deflection of the markers on hind, mid and fore foot, calculated as explained in Paragraph 5.1.4. As it can be noticed from experimental data, when the heel lamina is loaded (from 0% to approximatively 55% of the stance phase) the forefoot marker should come closer to TibiaUpFront marker, but this effect is not replicated by Multibody Simulations (MBS). The same issue may be seen when the forefoot is loaded: the backfoot marker does not move away from the TibiaUpFront marker. ....	106
Figure 5.2.2 – Schematic representation of the Vari-Flex® multibody model after changes in junction modeling. The image on the right is the Simulink® junction model. ....	107
Figure 5.2.3 - Deflection of the markers on hind, mid and fore foot, calculated with the updated model. ....	107
Figure 5.2.4 – Different modeling of the junction between the two laminas. The letters refer to the bulleted list above the figure. The red dots are rotational joints, while the blue lines are weld joints. a) “Single” model. b) “Double” model. c) “Triple model”. d) “Single2” model. ....	108
Figure 6.1.1 – Force vs. deflection experimental and simulated curves for each loading conditions. Each image refers to the tuning executed considering the single mechanical test. a) 20° heel touch. b) 10° heel touch. c) 10° toe touch. d) 20° toe touch. ....	109
Figure 6.1.2 – Sets of tuned stiffness for each trial condition. The thick blue line represents the nominal stiffness. ....	110
Figure 6.1.3 – Averaged tuned stiffnesses with standard deviation. ....	110
Figure 6.1.4 - Sets of tuned damping for each trial condition. The thick blue line represents the nominal damping. ....	110
Figure 6.1.5 - Averaged tuned stiffnesses with standard deviation. ....	111
Figure 6.1.6 - % RMSE between the stiffnesses of each testing condition. ....	111
Figure 6.1.7 – Force vs. deflection diagram of 20° heel touch mechanical test. Experimental results are presented with a thick blue line. The orange line represents multibody model results before tuning. The green line represents multibody model results after tuning. ....	112

Figure 6.1.8 - Force vs. deflection diagram of 10° heel touch mechanical test. Experimental results are presented with a thick blue line. The orange line represents multibody model results before tuning. The green line represents multibody model results after tuning.....	112
Figure 6.1.9 - Force vs. deflection diagram of 10° toe touch mechanical test. Experimental results are presented with a thick blue line. The orange line represents multibody model results before tuning. The green line represents multibody model results after tuning.....	112
Figure 6.1.10 – Force vs. deflection diagram of 20° toe touch mechanical test. Experimental results are presented with a thick blue line. The orange line represents multibody model results before tuning. The green line represents multibody model results after tuning.....	113
Figure 6.1.11 – Force vs. deflection curves obtained from other tuning trials executed on 20° toe touch testing conditions.....	113
Figure 6.2.1 - Deflection of the markers on hind, mid and fore foot, computed using “Single” model.....	114
Figure 6.2.2 - Deflection of the markers on hind, mid and fore foot, computed using “Double” model.....	115
Figure 6.2.3 - Deflection of the markers on hind, mid and fore foot, computed using “Triple” model.....	115
Figure 6.2.4 - Deflection of the markers on hind, mid and fore foot, computed using “Single2” model.....	115
Figure 6.2.5 - Deflection of the markers on hind, mid and fore foot, computed using “Single” model and a Young modulus value equal to 60 GPa. ....	116
Figure 6.2.6 - Deflection of the markers on hind, mid and fore foot, computed using “Single” model and a Young modulus value equal to 65 GPa. ....	116
Figure 6.2.7 - Deflection of the markers on hind, mid and fore foot, computed using “Single” model and a Young modulus value equal to 60 GPa. ....	117
Figure 6.2.8 - Deflection of the markers on hind, mid and fore foot, computed using “Single” model and a Young modulus value equal to 75 GPa. ....	117
Figure 6.2.9 - Deflection of the markers on hind, mid and fore foot, computed using “Single” model and a damping value equal to $0.01 \text{ N} \cdot \text{m} \cdot \text{s} \cdot \text{rad} - 1$ .....	118
Figure 6.2.10 - Deflection of the markers on hind, mid and fore foot, computed using “Single” model and a damping value equal to $0.1 \text{ N} \cdot \text{m} \cdot \text{s} \cdot \text{rad} - 1$ .....	118
Figure 6.2.11 - Deflection of the markers on hind, mid and fore foot, computed using “Single” model and a damping value equal to $10 \text{ N} \cdot \text{m} \cdot \text{s} \cdot \text{rad} - 1$ .....	118
Figure 6.2.12 - Deflection of the markers on hind, mid and fore foot, computed using “Single” model and a damping value equal to $100 \text{ N} \cdot \text{m} \cdot \text{s} \cdot \text{rad} - 1$ .....	119
Figure 6.2.13 – ROS computed by multibody model. As it can be noticed, the radius value is like the one found by L. Cavallaro (46 cm).....	120
Figure 7.2.1 – Force-deflection curves for 20° heel touch quasi-static. The blue curve represents the experimental relationship. The red curve is the force-deflection relationship obtained switching the external force on two different foot sole’s segments. ....	122

*Figure 7.5.1 – On the left: schematic representation of the inverse dynamic analysis scheme for the lower limb. On the right: workflow to determine intersegmental (“joint”) forces and moments. [63]*  
.....125



## Tables Index

---

<i>Table 1.3.1 - Age-specific estimates of prevalence by sex, race and ethnicity, and Etiology (in thousands): year 2005, United States [12]. Highlighted in yellow there is the reported total amount of lower limb amputation. Highlighted in green there is the reported amount of lower limb amputation caused by dysvascular diseases related to diabetes.....</i>	<i>12</i>
<i>Table 1.5.1 – Effects that stiffness variations on different parts of foot have on biomechanical outcomes.....</i>	<i>24</i>
<i>Table 2.2.1 - Material and geometrical properties of the simulated wedged beam.....</i>	<i>31</i>
<i>Table 2.2.2 – Simulation’s parameters .....</i>	<i>31</i>
<i>Table 2.2.3 – Stiffnesses and cross-sectional moment values obtained from Equation 2.2.4 and Equation 2.2.6.....</i>	<i>31</i>
<i>Table 3.1.1 – Quasi-static testing condition’s resume [51] .....</i>	<i>62</i>
<i>Table 3.1.2 – New quasi-static testing condition’s resume.....</i>	<i>63</i>
<i>Table 3.2.1 – Model’s parameter for quasi-static simulations. ....</i>	<i>66</i>
<i>Table 3.2.2 – Complex model segments’ thickness and width. ....</i>	<i>67</i>
<i>Table 3.4.1 – 2-segments beam initial tuning parameters. ....</i>	<i>75</i>
<i>Table 3.4.2 – Initial parameters for Vari-Flex® model.....</i>	<i>77</i>
<i>Table 3.4.3 – Tuning process settings.....</i>	<i>78</i>
<i>Table 5.1.1 – Material and simulation parameters for the Vari-Flex dynamic simulation. ....</i>	<i>96</i>
<i>Table 5.1.2 - %RMSE of segmented and smoothed COP with respect to the experimental COP...100</i>	
<i>Table 6.2.1 – Simulation time difference when varying the number of weld joints and keeping a fixed damping value. ....</i>	<i>119</i>
<i>Table 6.2.2 - Simulation time difference when varying the damping value and keeping the same number of weld joints.....</i>	<i>120</i>
<i>Table 6.2.3 – ROS radius computed using different damping values.....</i>	<i>120</i>
<i>Table B.0.1 – Legend of the Simulink/Simscape’s blocks utilized.....</i>	<i>161</i>



# Equations Index

---

<i>Equation 2.1.1– Torsional harmonic oscillator’s equation of motion.</i>	28
<i>Equation 2.2.1 – Stress sensed at the weld joint</i>	29
<i>Equation 2.2.2 – Momentum sensed at the weld joint</i>	29
<i>Equation 2.2.3 – Theoretical beam ’s vertical deflection</i>	29
<i>Equation 2.2.4 – Cross-sectional moment of inertia for a beam with a rectangular section</i>	29
<i>Equation 2.2.5 – Beam’s maximum deflection at the loaded end</i>	30
<i>Equation 2.2.6 – Formulation of the ith joint’s stiffness as proposed by Fey et al. and Miller et al. [33] [45]</i>	30
<i>Equation 2.2.7 - Rotational stiffness expression for a 1-segment beam loaded at the free end.</i>	33
<i>Equation 2.2.8 – Rotational stiffness expression deriving from Equation 2.2.2 and Equation 2.2.7.</i>	34
<i>Equation 2.2.9 . Relation between angular and linear coordinates under the condition of small displacements.</i>	34
<i>Equation 2.2.10 - Rotational stiffness obtained considering eq. Equation 2.2.2, Equation 2.2.8 and Equation 2.2.9.</i>	34
<i>Equation 2.2.11 – Analytical rotational stiffness equation for a 1-rigid-segment model of wedged beam.</i>	34
<i>Equation 2.2.12 – System of two linear equation that describes the 2-rigid-segments model of wedged beam.</i>	34
<i>Equation 2.2.13 – Relation between relative rotations <math>\theta_1</math> and <math>\theta_2</math>.</i>	35
<i>Equation 2.2.14 – Total beam deflection expression for a 2-rigid-segment model of beam.</i>	35
<i>Equation 2.2.15 - <math>\theta_2</math> expression for a 2-rigid-segments model of beam.</i>	35
<i>Equation 2.2.16 – Rotational stiffness’ analytical value for a 2-rigid-segments model of wedged beam.</i>	35
<i>Equation 2.2.17 - System of three linear equation that describes the 3-rigid-segments model of wedged beam.</i>	35
<i>Equation 2.2.18 - Relationship between <math>\theta_1</math> and <math>\theta_3</math>.</i>	36
<i>Equation 2.2.19 – Relationship between <math>\theta_2</math> and <math>\theta_3</math>.</i>	36
<i>Equation 2.2.20 – Total beam’s deflection expression for a 3-rigid-segment model of beam.</i>	36
<i>Equation 2.2.21 – Total beam’s deflection referred to <math>\theta_3</math> and L.</i>	36
<i>Equation 2.2.22 – <math>\theta_3</math> expression.</i>	36
<i>Equation 2.2.23 – Rotational stiffness’ analytical value for a 3-rigid-segments model of wedged beam.</i>	36

<i>Equation 2.2.24 – Rotational stiffness' multiplying coefficients for 1-rigid-segment, 2-rigid-segments, 3-rigid-segments and N-rigid-segments wedged beam's models. ....</i>	<i>37</i>
<i>Equation 2.2.25 – Numerical coefficients multiplying <math>3EJ/L</math> in a N-rigid-segments wedged beam model. ....</i>	<i>37</i>
<i>Equation 2.2.26 – Rotational stiffness expression for a N-rigid-segments wedged beam model.....</i>	<i>37</i>
<i>Equation 2.4.1 – Relationship between approximant segment distance, points coordinates and relative orientation between two following points for the keel spline.....</i>	<i>47</i>
<i>Equation 2.4.2 – Relationship between approximant segment distance, points coordinates and relative orientation between two following points for the heel spline.....</i>	<i>47</i>
<i>Equation 4.3.1 – Trigonometric equation to determine the angle that the pylon forms with an imaginary line that is perpendicular to the ground. ....</i>	<i>85</i>
<i>Equation 5.1.1 – ROS calculation in shank-based coordinate system implemented by A. Hansen et al. [58].....</i>	<i>103</i>
<i>Equation 5.1.2 – Mathematical formula that allows to compute the distance between COP and ANKLE in Vari-Flex multibody model. ....</i>	<i>104</i>
<i>Equation 5.1.3 - Mathematical formula that allows to compute the angle between ANKLE – COP and the line perpendicular to the ground and passing through ANKLE.....</i>	<i>104</i>
<i>Equation 5.1.4 - Mathematical formula that allows to compute <math>\beta</math> angle in Vari-Flex multibody model. ....</i>	<i>105</i>





# 1. Fundamentals

---

Basic information to address and understand the further work will be introduced in this Chapter. The main issues that will be presented are:

- Foot Anatomy and Biomechanics
- Gait cycle
- Foot amputation causes
- Lower limb and foot prosthesis

## 1.1 Foot Anatomy and Biomechanics

The human foot is divided into three regions:

- *Hindfoot* or *rearfoot* (ivory section in Figure 1.1.1, next page) – It comprehends the tarsal bones.
- *Midfoot* (pink section in Figure 1.1.1, next page) – The metatarsal bones form this region.
- *Forefoot* (yellow, blue and green sections in Figure 1.1.1, next page) – The phalanges (or toe bones) are contained in this region

The foot acts as a *rigid* structure during weight-bearing and forward propulsion [1], but it can also work as a *flexible* structure to conform to uneven terrain [2]. This bivalent behaviour is hard to reproduce with prostheses. Also, the foot does not only provide a base of support, but it also contributes with dorsiflexion in decreasing energy expenditure during gait cycle swing phase and stance phase [3].

Therefore, the foot and the ankle have different functions as: supporting body weight, providing balance, shock-absorbing and transferring ground reaction forces to the upper limb structures.

### 1.1.1 Bones

The human foot is composed of 26 bones [4]:

- 7 thick and irregular *tarsal* bones (rearfoot region).
- 5 *metatarsal* bones through all the midfoot region. Their main purpose is to support the body weight and promote gait. This function is mainly achieved by metatarsal heads.
- 14 *phalanges* that form the toes in the forefoot region.

The tarsal bones are *talus* (or anklebone), *calcaneus* (or heel bone), *navicular bone*, *cuboid* and *cuneiform bones* (lateral, intermediate and distal). Their main functions are supporting bodyweight and transferring it from the mid and forefoot to the upper limb body segments.

The metatarsal bones confer stability while in an upright position. They are five and they have a *head* and a *basis*. The metatarsal bases are connected to the tarsal bones in the midfoot, while the heads connect with the proximal phalanges of the toes. Phalanges role is to grant firm support while walking. The hallux has only two phalanges, while the other toes have three phalanges each.

### 1.1.2 Ligaments

Foot bones form bridge-like structure, the so-called *arches* of the foot. Foot ligaments help supporting these structures [4].

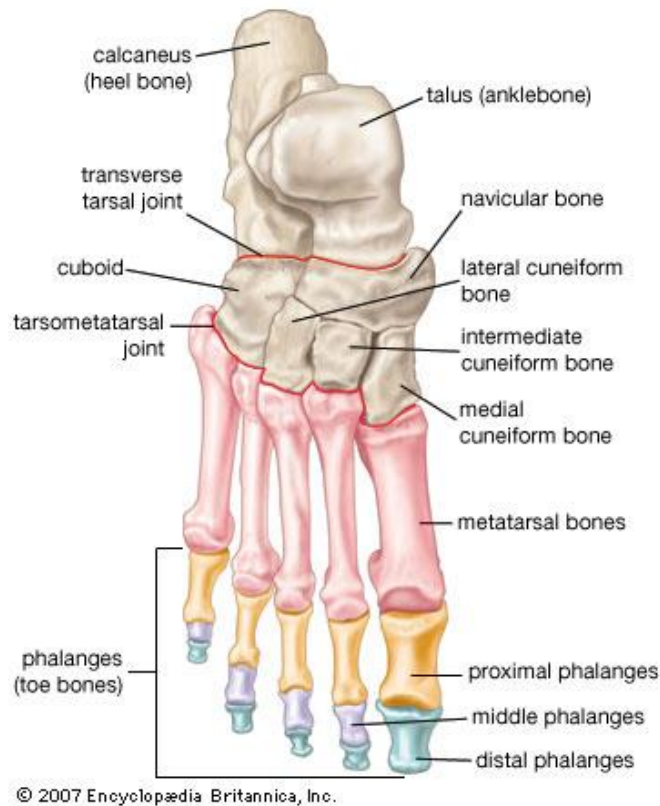


Figure 1.1.1 – Upper view of the foot bones. Tarsal bones are not coloured (ivory); metatarsal bones are coloured in pink, phalanges are coloured in yellow, violet and green. [<https://cdn.britannica.com/07/99107-004-B9666996.jpg>]

The three main foot ligaments are located on the foot plantar surface (Figure 1.1.2, next page) and they are:

- *Plantar calcaneonavicular ligament* – It connects the calcaneus with the navicular bone. It starts from the talus (a groove located on the calcaneus) and ends at the back of the navicular bone. It helps to sustain the foot longitudinal arch.
- *Long plantar ligament* – It goes from calcaneus lower side to the cuboid and the metatarsal bones.
- *Plantar calcaneocuboid ligament* (or *short plantar ligament*) – It is located under the long plantar ligament and it spreads from the frontal side of the calcaneus lower surface to the cuboid.

Other foot ligaments are *plantar intermetatarsal ligament*, *plantar tarsometatarsal ligament*, *plantar cuneonavicular ligament* and *plantar cuboideonavicular ligament*.

### 1.1.3 Arches

Foot arches grant flexibility, permit to walk on irregular terrains and support body weight [2] [4]. Foot prostheses try to replicate these structures; especially, the longitudinal arc could be easily noticed in certain ESAR (Energy Storage and Return) feet.



The human foot is composed of three arches (Figure 1.1.3, next page):

- *Medial longitudinal arch* – It is the highest and the most important arch above the two longitudinal arches. It is composed of calcaneus, talus, navicular bone, cuneiform bones and the first three metatarsal bones [4].
- *Lateral longitudinal arch* – It is lower and flatter than the previous one. The evidence is that the bones it is composed of (calcaneus, cuboid, fourth and fifth metatarsal bones) touch the ground while standing straight [4] (the contact with the floor is responsible for the footprint).
- *Transverse arch* – It spreads along the foot width. It is sustained by longitudinal arches and it is composed by the metatarsal bones' bases, the cuboid and the cuneiform bones [4].

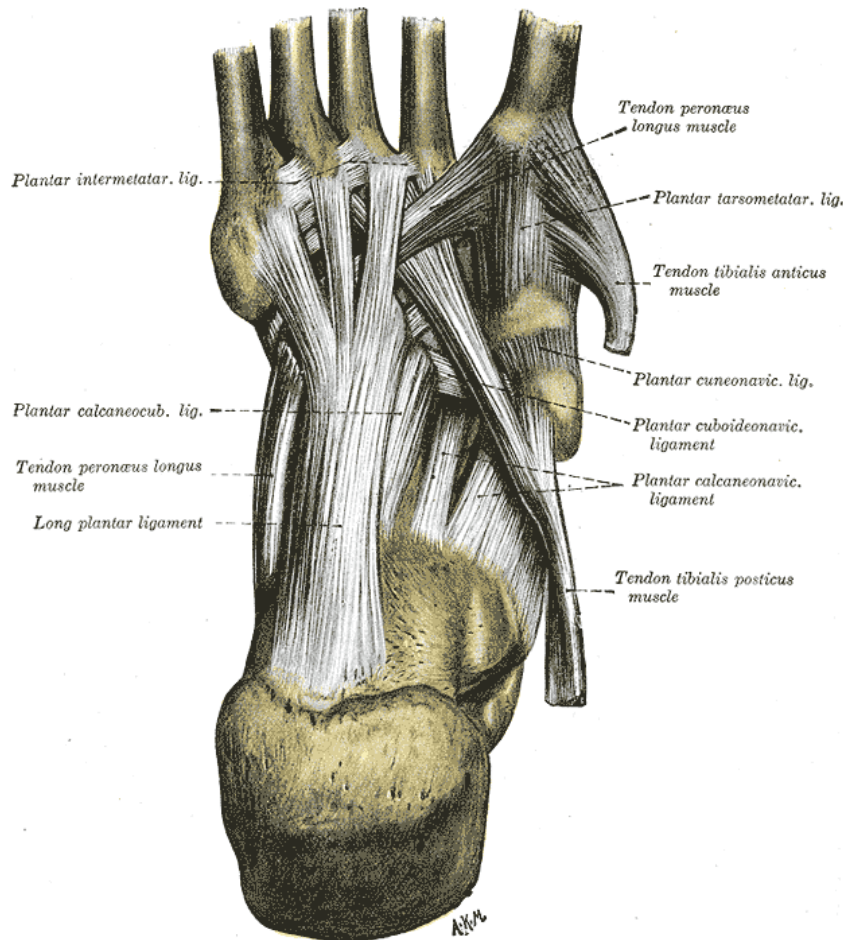


Figure 1.1.2 – Plantar view of the foot ligaments. [<https://upload.wikimedia.org/wikipedia/commons/d/dc/Gray358.png>]

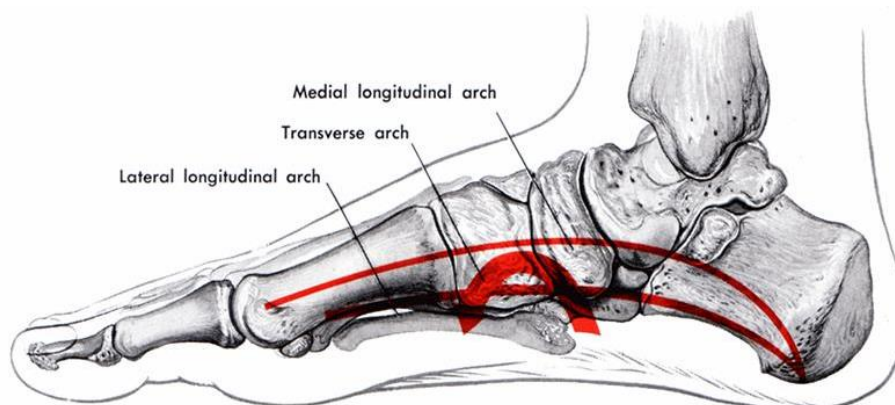


Figure 1.1.3 – Foot arches. [[https://cdn.shopify.com/s/files/1/1708/5797/files/arches\\_of\\_the\\_foot.jpg?v=1505218403](https://cdn.shopify.com/s/files/1/1708/5797/files/arches_of_the_foot.jpg?v=1505218403)]

Arches absorb the weight both in the longitudinal and the transverse direction: they basically work as dampers.

### 1.1.4 Joints

The foot and ankle joints are what defines ankle-foot system's kinematic and function. Foot joints are also used by surgeons as reference levels for amputation.

The main joints of the ankle-foot structure (Figure 1.1.4) are [2]:

- *Talocrural (TC) joint* – It is commonly known as the ankle joint. It is a hinge joint and allows dorsiflexion and plantarflexion: movements taking place on the sagittal plane.
- *Subtalar (ST) joint* – It connects the three talus facets with the calcaneus.
- *Midtarsal (MT) joint* – Also known as transverse tarsal joints or Chopart joint, it is the sum of two smaller joints – the *talonavicular (TN) joint* and *calcaneocuboid (CC) joint*. MT joint, when locked, allows the body forward propulsion during stance phase [5]. During heel strike, the joint unlocks and becomes flexible to adjust to the ground surface. Also, when a partial foot amputation becomes necessary, the MT joint helps the surgeon to define the amputation level (the associated amputation is called *Chopart amputation*) [4].
- *Tarsometatarsal (TMT) joint complex* – Also known as Lisfranc joint, it is where the distal tarsal rows articulate with the metatarsal bases to form the TMT complex. The TMT complex too is used as a benchmark when a foot amputation is required. As for Chopart joint, Lisfranc joint gives the name to the corresponding amputation.
- *Metatarsophalangeal (MTP) joints* and *interphalangeal (IP) joints* – The MTP joints connect the metatarsal heads to the corresponding bases of the proximal phalanges. The IP joints, instead, are located between the toe phalanges. Each toe has a proximal MTP joint and a distal IP joints except for the hallux, which only has one IP joint.

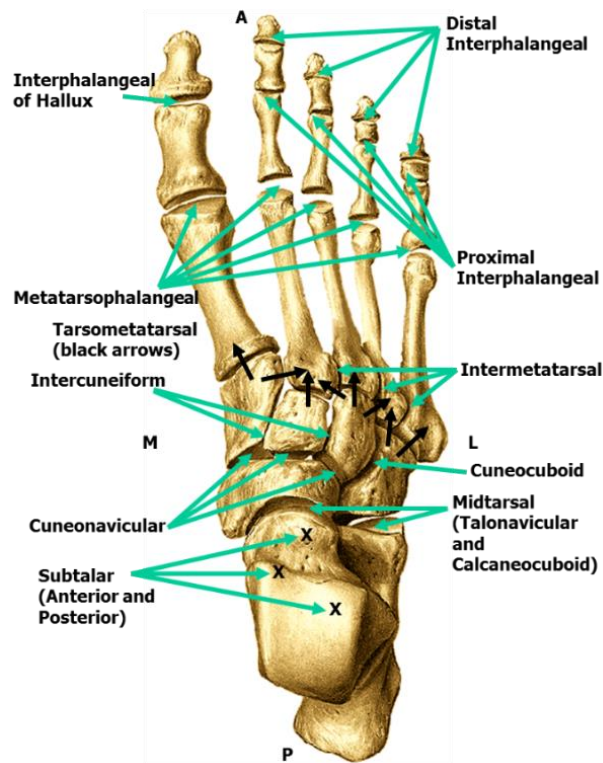


Figure 1.1.4 – Foot joints. [<http://d1yboe6750e2cu.cloudfront.net/i/38dc4e75f20e66de7b6c3de2adc2bf5e7410b8f2>]

### 1.1.5 Dorsal Muscles

Foot dorsal muscles (Figure 1.1.5) are mainly involved in toes motion and take place in the lower shank. Although they are not powerful muscles, the origin located in the shank allows them to produce more power than a hypothetical foot origin [4].

Foot dorsal muscles originate on the tibia and cross the ankle joint on their way to the foot, acting as levers. The ankle joint, that becomes the fulcrum, helps them to maintain a correct position along with the action of retinacula and tendinous sheaths. In the upper foot there are four main retinacula: *superior extensor retinaculum*, *inferior extensor retinaculum*, *peroneal retinaculum* and *flexor retinaculum* (Figure 1.1.5). Superior extensor retinaculum contains the long tendons of the foot extensor muscles. Inferior extensor retinaculum holds the foot extensor muscles. Peroneal retinacula contains the peroneus longus and brevis tendons. Finally, flexor retinaculum holds the flexor digitorum longus and the flexor hallucis longus tendons.

The main muscles underneath the foot dorsal skin (Figure 1.1.6) are *extensor digitorum brevis* and *extensor hallucis brevis* [4]. Their functions are totally explicated by their names. They cooperate with the *extensor digitorum longus* and the *extensor hallucis longus* respectively. Although they are not too powerful, they are useful to extend the fingers when the foot is already dorsiflexed.

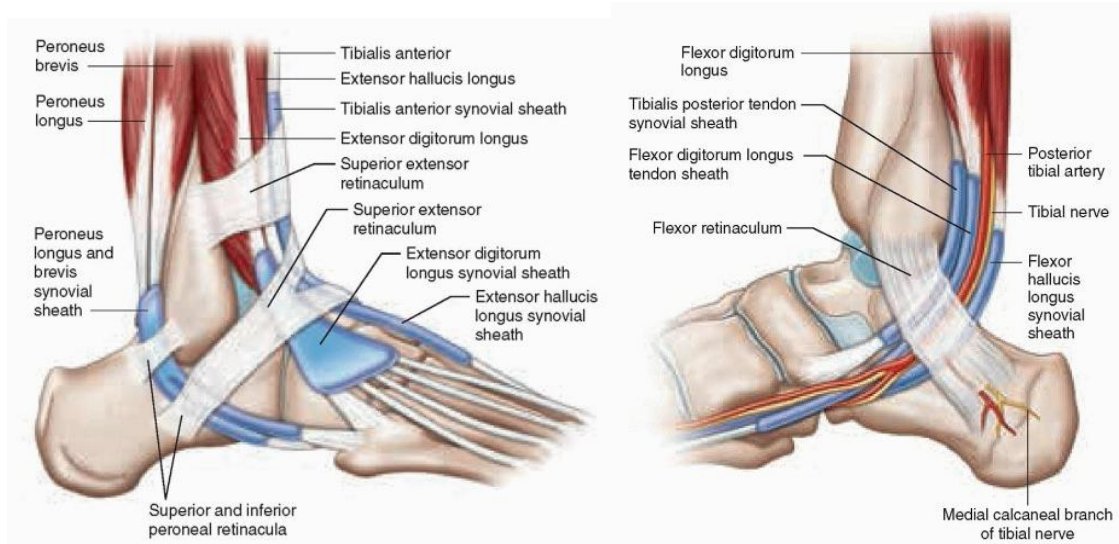


Figure 1.1.5 – On the left: medial view of the foot. It is possible to notice the superior and inferior extensor retinacula and peroneal retinacula. [<https://radiologykey.com/wp-content/uploads/2016/07/C8-FF7-7.gif>]. On the right: lateral view of the foot. The flexor retinaculum is shown. [<https://www.podiatryinthepines.com/storage/app/media/img-tarsal-tunnel.jpg>]

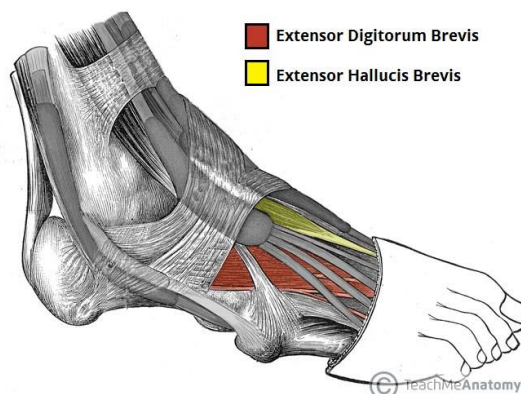


Figure 1.1.6 – Foot dorsal muscles. [<https://teachmeanatomy.info/wp-content/uploads/The-Dorsal-Layer-of-Muscles.jpg>]

### 1.1.6 Plantar Muscles and Plantar Aponeurosis

There are four layers of intrinsic muscles in the foot sole. They are constantly working during walking, running and jumping and allow these activities also on uneven terrain. The first layer's muscles help to flex, adduct and abduct the foot fingers, so they work as agonist muscles. The inner layers' muscles help to maintain the foot arches shapes and grant stability and flexibility both during activity and rest, so they work as stabilizer. Second to fourth layer muscles usually work together to maintain foot arches in their physiological shapes. Below, the plantar muscles and their functions are listed from the outer to the inner layer.

- **FIRST LAYER** (Figure 1.1.8A, next page)
  - *Abductor hallucis muscle* – It allows to flex and abduct the hallux.
  - *Flexor digitorum brevis muscle* – It is involved in foot finger flexion.
  - *Abductor digiti minimi muscle* – It allows to abduct and flex the foot little finger.
- **SECOND LAYER** (Figure 1.1.8B, next page)
  - *Quadratus plantae muscle* – It acts on flexor digitorum longus tendons stabilizing them.
  - *Flexor digitorum and hallucis longus tendons*.
  - *Lumbrical muscles* – They originate from the flexor digitorum longus tendons and are so-called because of their worm-like shapes. They allow toes to stand straight while they flex.
- **THIRD LAYER** (Figure 1.1.8B, next page)
  - *Flexor hallucis brevis muscle* – It helps the hallux to flex.
  - *Abductor hallucis muscle*.
  - *Flexor digiti minimi muscle* – It helps the little toe to flex.
- **FOURTH LAYER** (not shown) – The *dorsal interossei muscles* abduct the fingers, while the *plantar interossei muscles* adduce them.

A thick sheet of connective tissue, the so-called *plantar aponeurosis*, covers the midfoot plantar muscles [4]. While standing straight, the plantar aponeurosis takes up approximately 60% of the stress of weight-bearing. The ability of the plantar aponeurosis to absorb stress increases as it becomes taut with toe extension [5] [6]. This mechanism is called the *windlass effect* (Figure 1.1.7).

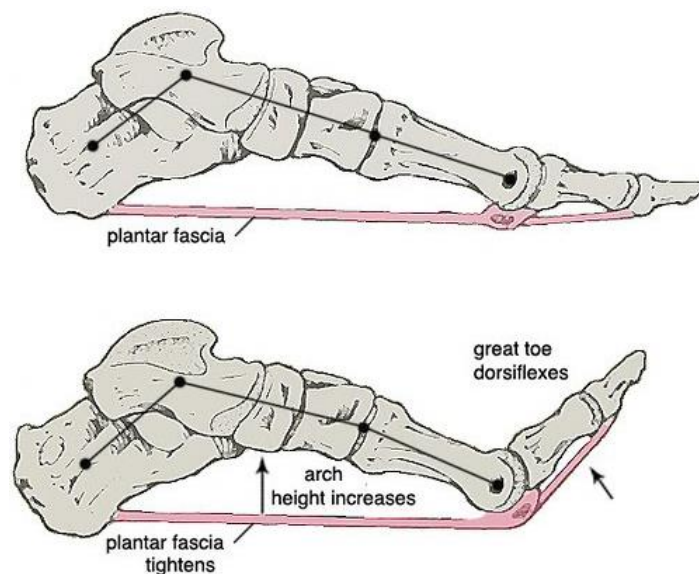


Figure 1.1.7 - Windlass effect explanation [2]



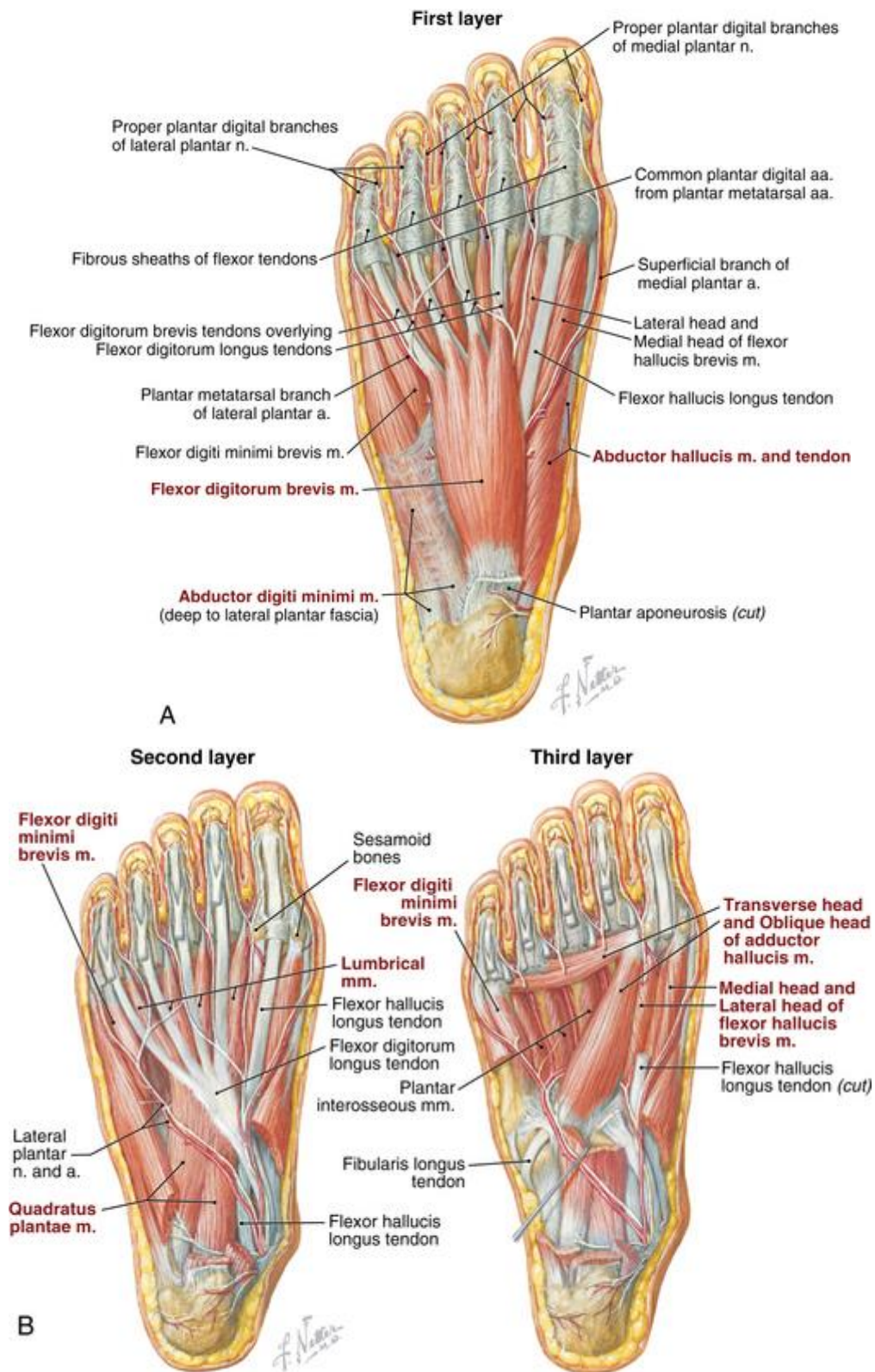


Figure 1.1.8 – A) First layer's structures. [[https://musculoskeletalkey.com/wp-content/uploads/2016/06/B9781455725311000171\\_f08-04a-9781455725311.jpg](https://musculoskeletalkey.com/wp-content/uploads/2016/06/B9781455725311000171_f08-04a-9781455725311.jpg)] B) Second and third layers' structures [[https://musculoskeletalkey.com/wp-content/uploads/2016/06/B9781455725311000171\\_f08-04b-9781455725311.jpg](https://musculoskeletalkey.com/wp-content/uploads/2016/06/B9781455725311000171_f08-04b-9781455725311.jpg)]

Obviously, all the muscles functions are lost when the subject undergoes a lower extremity amputation. Passive prostheses cannot replicate the muscles functions but they can possibly grant ligaments and bones' characteristics and confer elasticity to the passive structure.

### 1.1.7 Foot Biomechanics

Since the anatomical axes of the foot are not perpendicular to any cardinal body planes, foot movements are described by special terms as:

- *Dorsiflexion* (upwards) and *plantarflexion* (downward) – Motions performed within the *sagittal plane*;
- *Inversion* (or adduction) and *eversion* (abduction) – Motions performed within the *frontal plane*;
- *External rotation* and *internal rotation* – Motions performed within the *transverse plane* (or *horizontal plane*).

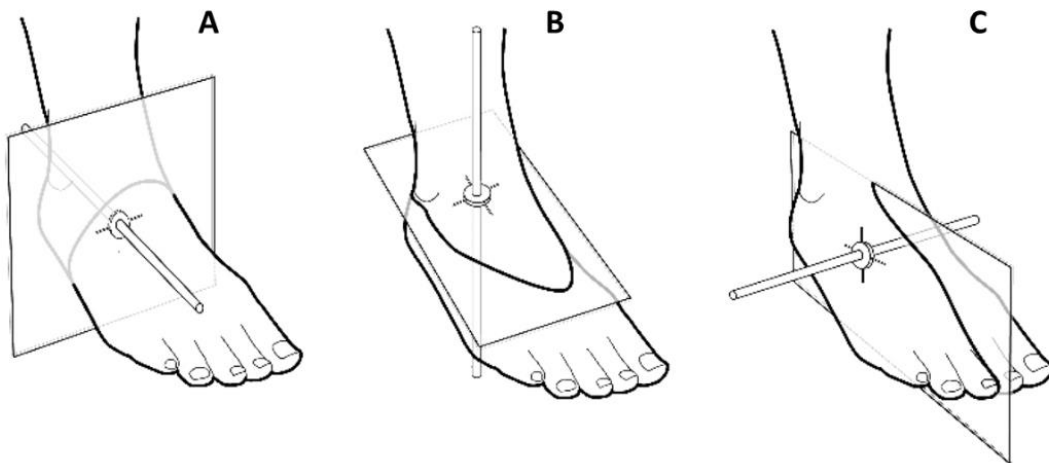


Figure 1.1.9 – Anatomic planes of the foot. A) Frontal plane with the relative frontal axes (or anterior-posterior axis). B) Transverse plane with the relative transverse axis (or inferior-superior axis). C) Sagittal plane with the relative sagittal axis (or medio-lateral axis). [<https://daniz53y71u1s.cloudfront.net/library/image1.jpg>]

Every anatomical plane has an associated anatomical axis (shown in Figure 1.1.9). The anatomical axes take the names of the anatomical planes which are perpendicular to. Generally, foot movements develop around their specific anatomical axis (as shown in Figure 1.1.10).

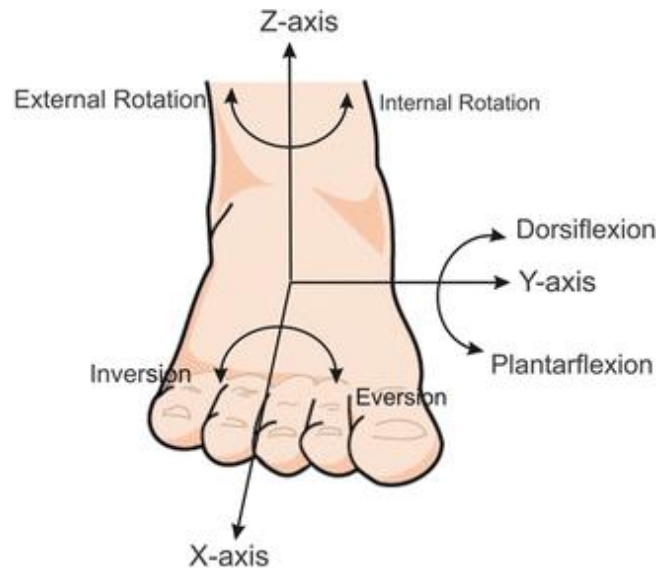


Figure 1.1.10 – Physiological movements of the foot. Inversion and eversion develop around the X-axis (frontal axis); dorsiflexion and plantarflexion develop around the Y-axis (sagittal axis); external and internal rotation develop around the Z-axis (transverse axis). [[https://media.springernature.com/original/springer-static/image/chp%3A10.1007%2F978-1-4939-1732-7\\_18/MediaObjects/31137\\_3\\_En\\_18\\_Fig2\\_HTML.gif](https://media.springernature.com/original/springer-static/image/chp%3A10.1007%2F978-1-4939-1732-7_18/MediaObjects/31137_3_En_18_Fig2_HTML.gif)]

Foot motion is *triplanar* but, in some cases, it can be modelled as uniplanar (in this study this assumption will be made). Triplanar movements can be described by two special terms specifically established:

- *Supination of the foot* – It is a simple rotation resulting in inversion, internal rotation (or adduction) and plantarflexion.
- *Pronation of the foot* – It is a simple rotation resulting from eversion, external rotation (or abduction) and dorsiflexion.

Sometimes, pronation and supination, are also used to describe eversion and inversion. [7]

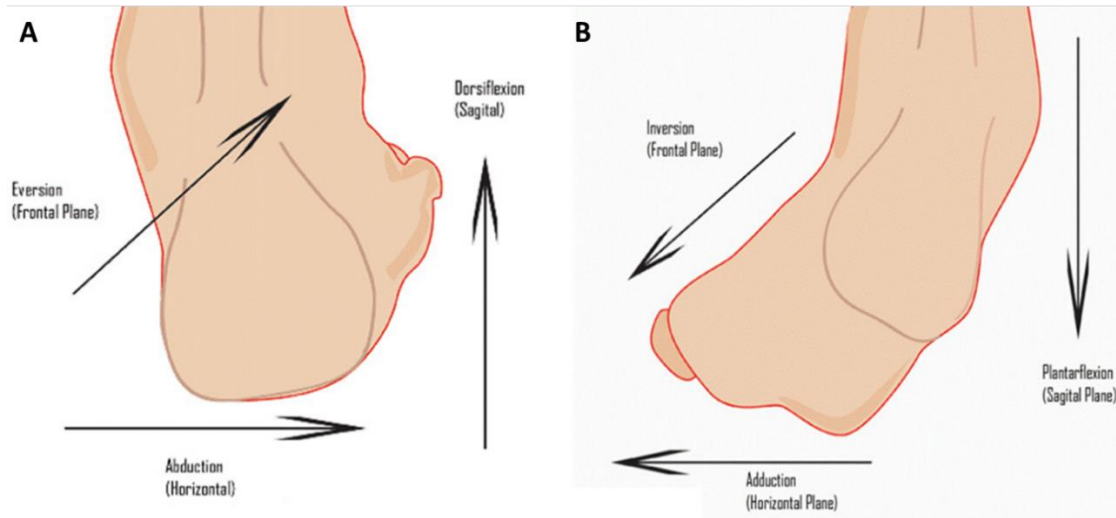


Figure 1.1.11 – A) Supination of the foot. B) Pronation of the foot. [<https://www.bestrunning-shoes.com/wp-content/uploads/2017/10/Best-running-shoes-for-overpronation-bying-guide.jpg>]

Because no muscles of the lower shank attach directly to the talus, foot pure dorsiflexion and plantarflexion are not allowed. In fact, motion on sagittal plane is influenced by simultaneous pronation or supination of the foot (Figure 1.1.11). Those movements are essential to grant the foot stability while walking and running on uneven terrain, but they are difficult to achieve with the Vari-Flex foot (or other ESAR feet) since it is connected to the shank pylon with a locked joint and it is made of a single carbon fibre sheet not articulated.

The next paragraph will describe the human gait. The foot is so important for it that one kind of terminology commonly used to describe the different gait phases directly refers to it.

## 1.2 Human Locomotion

Gait is a *manner of walking* [8]. This is the simplest definition of a fundamental every-day human activity. Going deeper, gait could be defined as a *series of rhythmical, alternating movements of trunks and limbs which results in the forward progression of the Centre of Gravity (COG)* [9].

The lower limb joints involved in human gait are:

- *Hip joint* – It can be considered as a spherical joint that allows 6 DOFs (*Degrees of Freedom*).
- *Knee joint* – It can be considered as a synovial hinge joint that allows 1 DOF.
- *Ankle joint* – It can be considered as a synovial hinge joint that allows 1 DOF.

The foot, that connects to the shank through the ankle joint, plays an important role in stability and forward propulsion during gait [2].

The lower extremities are frequently considered as a *closed kinematic chain* during walking. That means that foot relative motion influences the motion of the other bodies along the chain [5].

### 1.2.1 Gait Cycle

Gait cycle can be described by events or phases. The cycle starts with the *heel strike* and ends with the following heel strike of the ipsilateral limb. Two main phases can be distinguished: *stance* and *swing* phase.

Stance phase lasts approximately 60% of the entire gait cycle, while the swing phase lasts the remaining 40%. Only from 0% to 10% and from 50% to 60% of the gait cycle both feet are touching the ground (*double support phase*); for the remaining 80% the bodyweight is carried by a single foot (*single support phase*). Unlike running, while walking there never is a phase where both feet do not touch the ground referring to Mann et al. work (1980) [10].

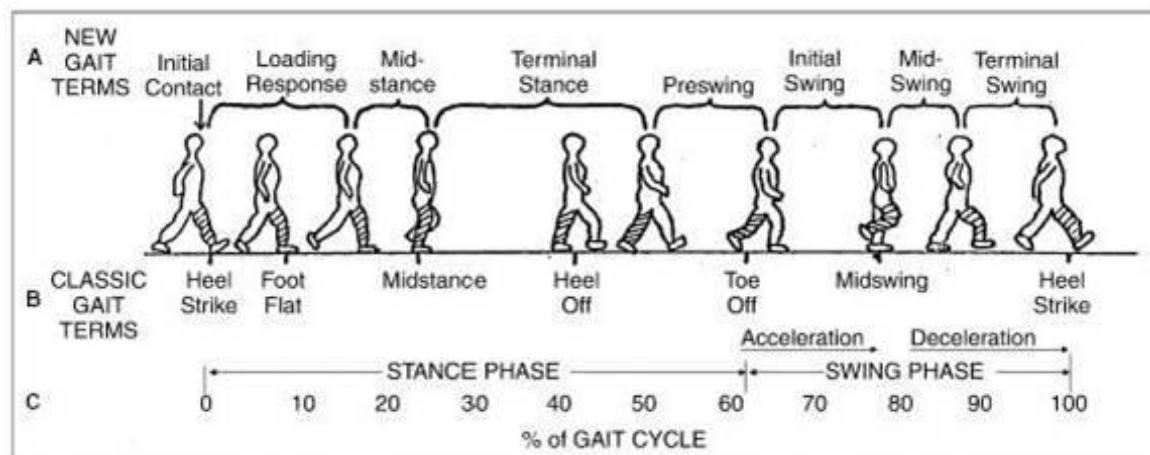


Figure 1.2.1 – Gait cycle terms and corresponding percentage of gait cycle [https://www.physio-pedia.com/images/b/b0/figure2.jpg].

The events and the phases that characterise gait cycle (shown in Figure 1.2.1) have different names depending on the terminology which refer to. There are two main terminologies: the *classic* one and the *new* one. The classic terminology highlights events that mainly concern the foot; while the new terminology highlights sub-phases, so it describes the gait from a wider point of view.

The classic gait terms are listed below.

1. *Heel strike* (0% gait cycle) – It is the precise moment when heel touches the ground and the double support phase starts. Ground reaction force (GRF) is focused in the hind foot. During heel strike the hip is flexed by 30° and the knee is full-extended; contralateral ankle plantar-flexes to push the body forward and ipsilateral knee flexion and ankle plantar-flexion begin. The tibialis anterior muscle plays an important role in ankle plantarflexion, the hamstring muscle allows the knee flexion.
2. *Foot flat* (8-10% gait cycle) – The foot absorbs the forces generated from the impact with the ground by rolling in pronation. A contraction of the adductor magnus and gluteus maximus muscles cause the hip to extend. The knee shows a 15°-20° flexion, while ankle plantar-flexion increases to 10-15°. GRF keep increasing until 15-20% of gait cycle, when it reaches a first maximum peak of amplitude that nearly corresponds to the body weight.
3. *Mid-stance* (20-25% gait cycle) – From this moment the forward propulsion phase begins. Going from foot flat to mid-stance (or from late loading response phase to midstance phase, if we consider the new terminology) the gluteus medium muscle causes a hip extension, the



knee reaches maximal flexion and then begins to extend, and the ankle reaches 5° dorsiflexion, which is caused by a contraction of the triceps surae muscles. During this phase, the weight-bearing is performed by single limb support. Going from midstance to heel-off, the GRF slowly moves from hind to mid and then to fore foot. Its amplitude decreases until 30% of gait cycle and then starts to re-increase to reach the second amplitude peak at 45-50% of gait cycle.

4. *Heel-Off* (40-45% gait cycle) – It is the instant when the hindfoot leaves the floor and terminal stance phase ends. From now until toe-off, bodyweight is shared between the metatarsal heads of the leading foot, while the contralateral foot approaches the ground. A hip hyperextension of 10° to 13° can be noted, then the hip goes into flexion during the pre-swing phase. After heel-off, the knee becomes flexed (0-5°) and the ankle gets supinated and plantarflexed. From heel-off to toe-off GRF amplitude keeps decreasing and reaches 0 N value at toe-off, since the foot is no more in touch with the ground.
5. *Toe-Off* (60-63% gait cycle) – At toe-off, the foot leaves definitively the ground, the pre-swing phase ends and the initial swing phase starts. The hip becomes less extended, while the knee is flexed by 35-40° and the ankle reaches 20° of plantarflexion. Referring to Schmid et al. study (2005) [11], in healthy subjects the toe leaves the ground around 63% of gait cycle.
6. *Mid-swing* (77-80% gait cycle) – At this instant the contralateral limb it's in the midstance condition. The hip flexes to 30°, the ankle becomes dorsiflexes, and the knee reaches a flexion of 60°. From now on the knee stars to extend thanks to the contraction of the quadriceps muscles.
7. *Heel strike* (100% gait cycle) – The ipsilateral heel touches the ground again and the cycle restarts.

The phases introduced by the new terminology better describe the swing phase as they subdivide it into three parts: the initial, mid and terminal swing phase. Since in the further study the swing phase will not be considered, the classic terms will be adopted to describe gait events. Also, the new gait terms describe a certain lapse of time and not only a precise moment. These new terms are described down below (N.B. Only the initial swing and terminal swing phases are detailed because stance phase and mid-swing phase have already been described before):

1. *Initial Contact* (0% of the gait cycle) – It corresponds to *heel strike*.
2. *Loading Response* (0-10% of the gait cycle) – It goes from *heel strike* to slightly after *foot flat*.
3. *Mid-stance* (10-25% of the gait cycle). It goes from slightly after *foot flat* to *midstance*.
4. *Terminal Stance* (25-40% of the gait cycle) – It goes from *midstance* to slightly after *heel-off*.
5. *Pre-swing* (40-60% of the gait cycle) – It goes from slightly after *heel-off* to *toe-off*.
6. *Initial Swing* (60-75% of gait cycle) – During this phase the hip extends to 10°. Then, iliopsoas muscle contraction causes the hip to flex of 20° with a lateral rotation; the knee flexes to 40-60°, and the ankle goes from 20° of plantar flexion to dorsiflexion, ending in neutral position (90° with respect to the shank).
7. *Mid-swing* (75-85% of the gait cycle).
8. *Terminal swing* (85-100% of the gait cycle) – The hip flexes to 30° and the tibialis anterioris causes ankle dorsiflexion. The knee from a 60° flexion extends approximately to 30°.

### 1.3 Foot Amputation Causes

Searching medical databases from the last 20 years, it was found that Lower Extremity Amputations (LEAs) can be consequences of (Table 1.3.1, next page) [12]:

- Diabetes mellitus – It has dysvascular disease as a major consequence.
- Traumatic events
- Osteosarcomas
- Infections

Among these causes, diabetes mellitus is the main responsible for LEAs in developed countries [13] [14] [15] [16] [17]. Therefore, having diabetes is associated with an increased risk of amputation. Epidemiological studies have shown that up to 75% of lower-extremity amputations are performed in patients with diabetes [13].

From 2005, the International Diabetes Federation (IDF) started to focus on the most severe diabetes complication that affects the gait: the diabetic foot disease. They published a “simplified and easy to digest” guideline to “prioritize health care practitioner’s early intervention” [18]. A study carried out by the IDF on 2018 [19] shows that personal, social and economic costs and the incidence of lower extremity amputations (LEAs) in subjected with diabetes increase with age, so the number of diabetes-related amputations will possibly increase in the next years since the global population is ageing. For these reasons foot prostheses improvement is important to ensure and improve the amputee’s comfort. Obviously, prosthetic approach is not the only one to be followed: it is also important to counter the causes of the disease.

Table 1.3.1 - Age-specific estimates of prevalence by sex, race and ethnicity, and Etiology (in thousands): year 2005, United States [12]. Highlighted in yellow there is the reported total amount of lower limb amputation. Highlighted in green there is the reported amount of lower limb amputation caused by dysvascular diseases related to diabetes.

Etiology, Sex, and Race and Ethnicity	All Ages	Under 65 Years				65 Years and Over		
		Total	Under 18	18-44	45-64	Total	65-74	75-100
All etiologies	1568	903	25	277	601	665	323	342
Sex								
Male	1026	668	16	218	433	358	199	159
Female	542	235	9	58	168	306	124	183
Race and ethnicity								
Nonwhite women	195	92	4	23	65	103	47	56
Nonwhite men	457	313	9	113	190	145	83	61
White women	347	143	5	35	104	203	76	127
White men	569	355	7	105	243	214	116	98
Dysvascular disease: total								
Total	846	375	2	52	321	471	228	242
Nonwhite women	151	59	*	8	50	92	42	50
Nonwhite men	185	101	*	17	84	84	50	34
White women	249	82	*	10	71	167	63	104
White men	261	133	*	17	116	128	73	54
Dysvascular disease with comorbidity of diabetes								
Total	592	191	*	18	174	400	162	239
Nonwhite women	106	31	*	3	28	75	28	47
Nonwhite men	146	60	*	6	54	86	44	42
White women	164	54	*	5	49	110	44	66
White men	176	47	*	4	43	129	45	84
Trauma								
Total	704	513	22	218	273	192	93	99
Nonwhite women	41	30	3	14	14	11	5	6
Nonwhite men	270	209	9	95	105	61	33	28
White women	92	57	4	23	30	35	13	22
White men	301	216	6	86	124	85	42	43
Cancer								
Total	18	15	*	7	7	3	2	*
Nonwhite women	3	2	*	1	*	*	*	*
Nonwhite men	3	3	*	1	*	*	*	*
White women	6	5	*	2	2	1	*	*
White men	7	6	*	2	3	*	*	*

NOTE. Totals may not equal sum because of rounding.

\*Represents less than 1000.

### 1.3.1 Diabetes

Diabetes is a *chronic disease that occurs when the pancreas is no longer able to make insulin, or when the body cannot make good use of the insulin it produces* [20].

The term *diabetes* was first introduced by Areteo from Cappadocia (81-133 A.D.). It derives from the ancient Greek verb *diabainein* that means “to go through”. This verb refers to the abnormal production of urine that occurs in patients with diabetes. The term *Mellitus* comes from an ancient Latin word that figuratively means “sweet as honey”. It refers to the sweet taste that blood and urine of patients diagnosed with diabetes have [21].

There are three main types of diabetes:

- Type I (also known as *Insulin-Dependent Diabetes Mellitus (IDDM)* or *juvenile diabetes*) – It most frequently occurs in children and adolescents. Patients affected by type I diabetes produce very little or no insulin.
- Type II (also known as *non-insulin-dependent diabetes mellitus (NIDDM)* or *adult-onset diabetes*) – It is more common in adults and it is the prevalent form of diabetes (90% of the total cases). People affected by type II diabetes cannot make good use of the insulin their body produces.
- Gestational diabetes (GDM) – This type of diabetes consists of high blood concentration of glucose during pregnancy and it is associated with complications to both mother and child. It usually disappears after pregnancy, but the mother and the child have a high probability to develop type II diabetes later.

### 1.3.2 Diabetic Foot

According to the World Health Organization (WHO) and to the International Working Group on the Diabetic Foot (IWGDF), diabetic foot is defined as *the foot of diabetic patients with ulceration, infection and/or destruction of the deep tissues, associated with neurological abnormalities and various degrees of peripheral vascular disease in the lower limb* [22].

People diagnosed with diabetes may also develop foot problems due to nerve damage (neuropathy) and poor circulation. The first problem, nerve damage, takes away the patient ability to feel pain and discomfort, while the further problem, poor circulation, reduces the subjects’ ability to heal and to resist to infections [23].

Neuropathy and dysvascular diseases cause a wide range of foot problems as:

- *Infections and ulcers sores* – Because of poor circulation and neuropathy, cuts or blisters on the foot can develop into infected ulcers unwilling to heal.
- *Corns and calluses* – Neuropathy makes impossible for impaired people to tell if the shoe is causing pressure and producing corns or calluses during walking.
- *Dry, cracked skin* – It can lead to sores formation.
- *Nail disorders* – As for corns and calluses, ingrown toenails and fungal infection may not be noticed because of loss of feeling due to neuropathy.
- *Hammertoes and bunions* – Nerve damage also affects muscles tone. Therefore, there is a loss of tone in the feet that leads to deformity. If these deformities are left untreated, they can bring to ulcers formation.
- *Charcot foot* – It is the result of the combined effect of an undetected broken bone and the loss of feeling due to neuropathy. If there is a broken bone and the patient cannot feel the

pain because of neuropathy, he continues to walk over the broken bone, making the situation worse and worse. The consequence is destruction of foot soft tissues. At this point, the only solution is foot amputation.

- *Poor blood flow* – Diabetes may also cause narrowing of under the knee blood vessels. This dysvascular disease prevents the wound from healing possibly causing tissue death.

These dysfunctions, when combined with each other, can turn into more serious complication as infections, ulcers and gangrene. These three factors, if left untreated, may lead to tissue death, culminating in foot total or partial amputation [24]. In Figure 1.3.1 there is an overview of the diseases caused by diabetes, their consequences and relationships.

Since complications due to diabetes mellitus pathology may lead to foot and lower extremity amputations, in the next chapters are presented the different lower limb prosthetic solutions available on commerce.

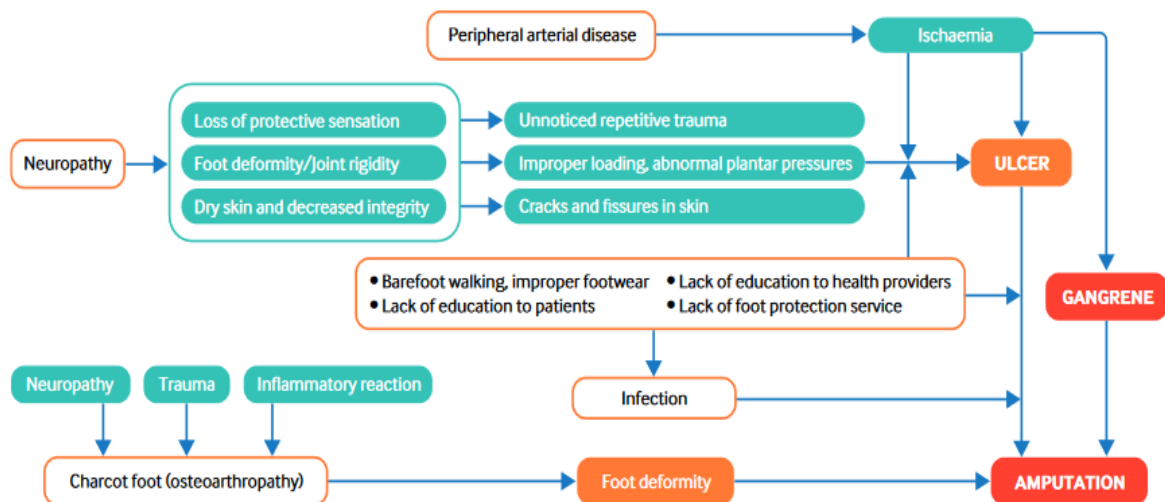


Figure 1.3.1 Risk factors and mechanism that may lead to foot ulcer and amputation [25].

## 1.4 Lower Limb Prosthetics

The American Academy of Physical Medicine and Rehabilitation define a prosthesis as *an artificial substitute for a missing body part that is used to restore the function of that body part or for cosmetic purposes* [26].

### 1.4.1 Amputation's Levels

There are different types of lower limb prostheses and their names come from the associated amputation level. Lower limb amputations main categories are shown in Figure 1.4.1 and Figure 1.4.2 (both in next page), while their names are listed below (starting from the foot and moving to the hip).

- *Foot amputation*. There are different types of foot amputation, such as:
  - *Hindfoot amputation* (such as *Boyd* or *Pirogof* amputation)
  - *Chopart* amputation
  - *Lisfranc* amputation
  - *Transmetatarsal* amputation
  - *Toes disarticulation or amputation*
- *Ankle disarticulation* (or *Symes foot amputation*)
- *Transtibial* amputation

- *Short below knee*
- *Standard below knee*
- *Knee disarticulation*
- *Transfemoral amputation*
  - *Very short above knee*
  - *Short above knee*
  - *Medium above knee*
  - *Long above hip*
- *Hip disarticulation / Hemipelvectomy*

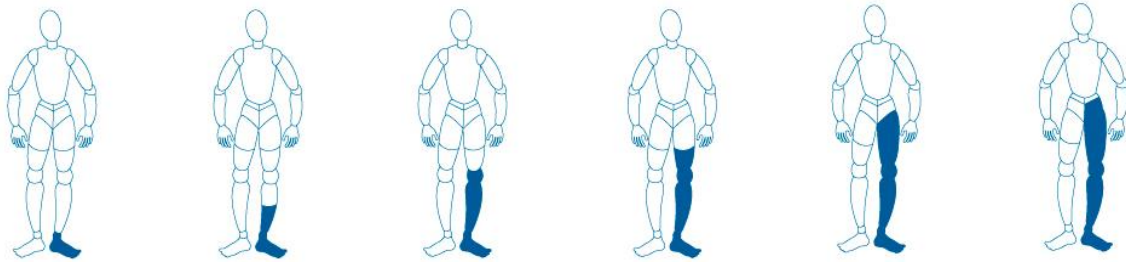


Figure 1.4.1 - Lower limb amputation's levels. Going from left to right: ankle/foot disarticulation, transtibial amputation, knee disarticulation, transfemoral amputation, hip disarticulation, hemipelvectomy. [<http://chirurgiadelmoncone.org/L/amputazione.html>]



Figure 1.4.2 – Different types of foot amputation. Going from left to right: toes disarticulation or amputation, Transmetatarsal amputation, Lisfranc amputation, Chopart amputation, Pirogof amputation, Syme amputation. [<http://chirurgiadelmoncone.org/L/amputazione.html>]

## 1.4.2 Parts of Lower Limb Prosthesis

Possible lower limb prostheses' components are (Figure 1.4.3, on the right):

- Hip joint
- Socket
- Thigh piece
- Knee joint
- Shank piece (or pylon)
- Ankle joint
- Foot device

Based on the severity of the amputation, we can find all these components on the substitutive device or only some of them. The devices that compose the prostheses utilized for different level of amputation are listed below (the correspondent prostheses are shown in Figure 1.4.4, next page):

- *Foot amputation*
  - Stump socket
  - Ankle joint (eventually)

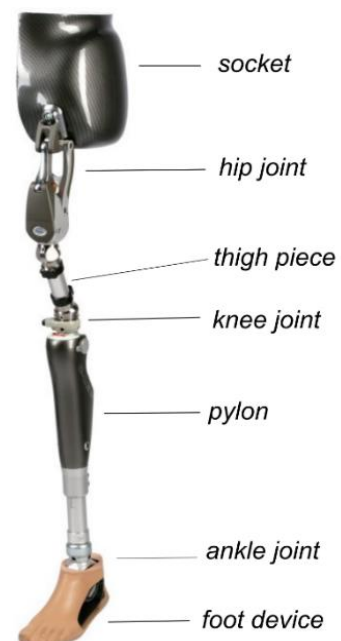


Figure 1.4.3 – Lower limb prostheses' components.

- Foot device (with mainly cosmetic functions)
- *Ankle disarticulation / Transtibial amputation* – The associated prostheses are commonly known as *below-knee prosthesis*
  - Shank socket (only in transtibial amputation's prosthesis)
  - Pylon
  - Ankle joint
  - Foot device
- *Knee disarticulation / Transfemoral amputation* – The associated prostheses are commonly known as *above-knee prosthesis*.
  - Thigh socket
  - Thigh piece (only in transfemoral amputation)
  - Knee joint
  - Pylon
  - Ankle joint
  - Foot device

Lower limb prostheses developed by Fondazione IIT are above-knee prostheses for transfemoral amputee. The prosthetic foot, that is the object of this Thesis, would possibly be a part of it.

- *Hip disarticulation / Hemipelvectomy*
  - Hip bandage/socket
  - Hip joint
  - Thigh piece
  - Knee joint
  - Pylon
  - Ankle joint (little used in this kind of prosthesis)
  - Foot device



Figure 1.4.4 – From left to right: prosthesis' foot component, below-knee prosthesis, above-knee prosthesis, hip disarticulation/hemipelvectomy prosthesis.

## 1.5 Foot Prosthetics

### 1.5.1 Role of the Foot Prosthetics

Foot prostheses must grant specific functional features for each different gait cycle phase and while the subject is standing straight:

- *Standing* – The prosthesis must permit the subject to balance COM's (Centre of Mass) oscillations.
- *Heel strike* – The prosthetic feet must absorb the Ground Reaction Forces (GRF) in order to lower the interarticular forces acting on the knee and the hip and prevent joint injuries like osteoarthritis.
- *Stance phase* – During this phase, the bodyweight must transfer from heel to toe. This function is normally controlled by plantar flexor muscles of the ankle joint, which are lost after the amputation. The analysis of this phase will be crucial for this Thesis work.
- *Push-off* – During the terminal stance phase, the foot must return the energy stored during the heel strike to promote the forward propulsion of the body. This role is normally promoted by the flexor muscles of the ankle joint. During push-off is also important the right positioning of the mechanical ankle joint (if present).

Foot prostheses must also grant stability all over the gait cycle and must assure a physiologic ankle joint Range of Motion (ROM).

### 1.5.2 Prosthetics Feet Available on the Market

Many types of prosthetic feet are available on the market [27]. They could be custom or not, but each one of them can be addressed in one of the categories listed below:

- *Rigid foot*
  - *SACH (Solid Ankle Cushioned Heel) foot*
  - *Dynamic foot*
- *Articulated foot*
  - *Single Axis foot*
  - *Multiple Axis foot*
- *ESAR (Energy Storage and Return) foot*
- *Sport Purpose Foot*

#### 1.5.2.1 Rigid Foot

Rigid feet are so-called because they have a rigid wooden, plastic or metallic keel covering them. This type of prosthetic foot is cheap, durable and almost maintenance-free. They can store (absorb) energy during heel-strike, but they are not very effective to return it during the push-off phase, when the body needs to accelerate forward. As said before, the rigid feet (shown in Figure 1.5.1, next page) may be divided into two categories: *SACH* feet and *dynamic* feet.

*SACH* feet have a rigid keel that covers the internal components. These inner components, which are usually made by plastic polymers, form the *Cushioned Heel* and they are meant to absorb the forces exchanged with the ground during heel-strike and to help the foot forward roll-over during the stance phase (from *heel-strike* to *toe-off*).

For what concern the structure, *dynamic* feet are like the SACH feet, but the firsts are made up by segments showing different stiffnesses. This improvement is meant to grant improved flexibility to the foot, also allowing the subject to walk on uneven terrain. For this reason, this kind of prosthetic foot is recommended for quite active subjects.



Figure 1.5.1 – Examples of rigid feet. On the left there is an example of SACH foot. On the right is represented a dynamic foot. [27]

### 1.5.2.2 Articulated Foot

Articulated prosthetic feet (Figure 1.5.2) present a mechanical joint that connects them to the shank and allows them to move in a single direction or in multiple directions. Referring to the number of directions in which they are free to move, they can be distinguished in *mono-axial* feet and *pluri-axial* feet. The difference is, as their names say, they may allow movements around one axis only or around multiple axes. In the case of the *mono-axial* feet, the movements allowed are foot plantar-flexion and dorsiflexion. Specifically, the dorsiflexion is limited by a rigid brake and it is controlled by a rubber damper. This kind of foot is usually used in above-the-knee prostheses.

Articulated feet are more comfortable than rigid ones because they show more physiological behaviour. Of course, *pluri-axial* feet have an even more natural response. In fact, they also permit movements within transverse and frontal planes.

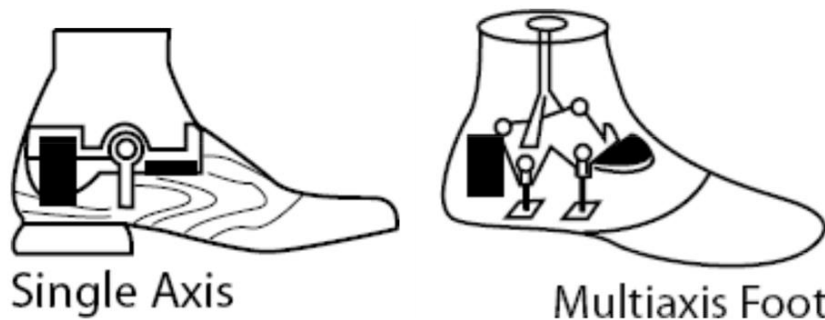


Figure 1.5.2 – Examples of articulated prosthetic feet. [27]

### 1.5.2.3 ESAR Foot

The *ESAR* feet (Figure 1.5.3, next page) store the energy absorbed during the initial contact with the ground and return it during the push-off phase. They confer better symmetry to the gait and they improve the subject's comfort and reactivity; also, they reduce the ground reaction forces generated on the contralateral heel when it strikes the ground.

Even if *ESAR* feet are the best to copy the foot physiological function of energy storage and return, they couldn't perform as well as the human foot. In fact, while the human foot returns the 240% of the energy stored, a prosthetic *ESAR* foot can approximatively return only 80% of stored energy. SACH feet are even worse: they only return 30% of stored energy. What causes this difference is the absence of active components in the foot prosthesis: human foot has plantar-dorsiflexor muscles that



help the foot to store and return energy during gait, while a passive foot prosthesis with no ankle active component does not have this faculty.



Figure 1.5.3 – Examples of ESAR feet. On the right there is the Vari-Flex® foot, the one that will be analysed in this work.

#### 1.5.2.4 Sport Purpose Foot

Sport purpose feet (Figure 1.5.4) are ESAR feet that have undergone an extreme optimization since they are meant for subjects that want to practice high-level sports (like sprint, high-jump, long-jump and similar disciplines). They are not meant for every-day activities.



Figure 1.5.4 – Examples of sport purpose foot for running.

### 1.5.3 Foot Prosthesis Issues and Their Relationships with Prosthetic Foot Stiffness

Since foot prostheses do not have a completely physiological behaviour, they can cause various problems for the amputee. Therefore, it is important to investigate the elastic properties of the prosthesis because a considerable number of studies address the prosthetic foot stiffness as one of the most important parameters affecting the foot behaviour [28] [29] [30] [31] [32] [33]. Even in this Thesis' work stiffness will be the main player.

Most of these studies are conducted on below-the-knee amputees, but the foot prosthesis issues are also shared with above-the-knee amputees since the foot components are nearly the same. A list and a resuming scheme (Figure 1.5.5, next page) of the most common issues of prosthetic feet found by Adameczyk et al. [28], Klodd et al. [29], Zelik et al. [30], Raschke et al. [31] and Fey et al. [32] [33] are presented below:

- *Osteoarthritis*
- *Metabolic cost*
- *Stability*
- *Contralateral limb interarticular forces*
- *Comfort*

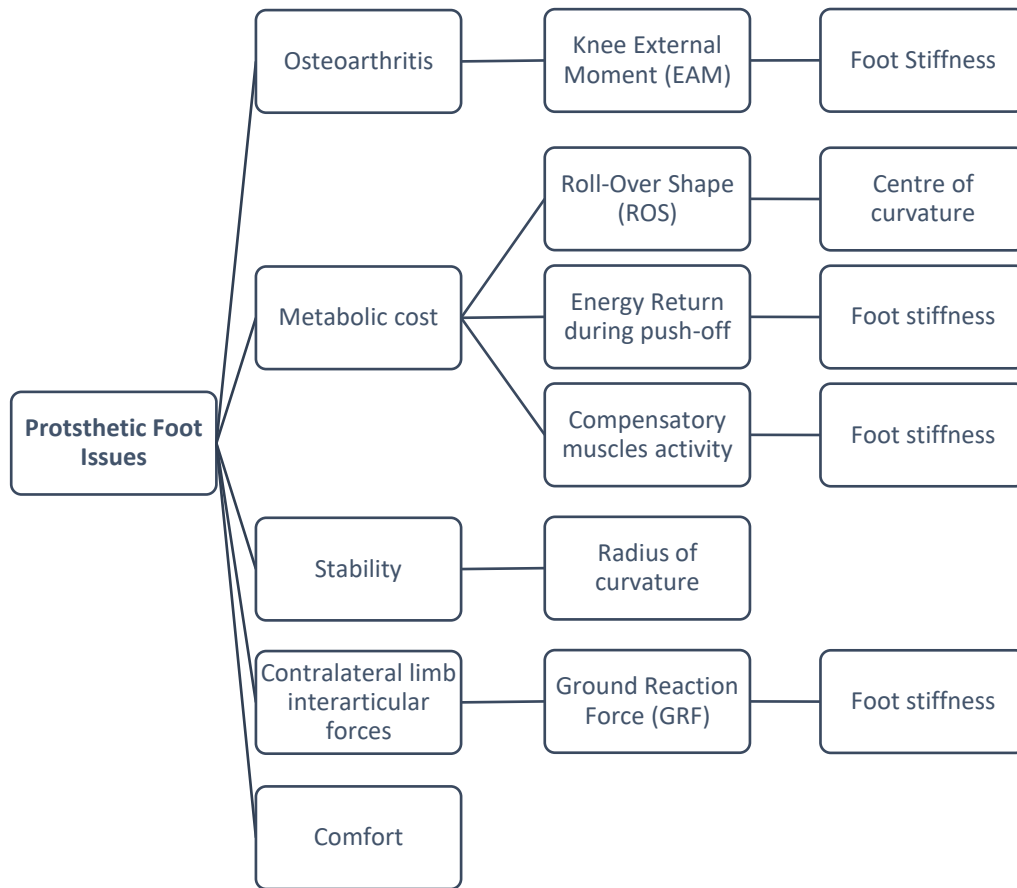


Figure 1.5.5 – Overview of the foot prosthetic issues and the parameters and characteristics who are related with.

These issues will be further analysed in the following paragraphs.

### 1.5.3.1 Osteoarthritis and Contralateral Limb Interarticular Forces

Osteoarthritis is the most common form of arthritis and it usually affects the joints that bear most of our body weight, such as hip, knee and ankle. When a joint develops osteoarthritis, part of the cartilage becomes rougher and thins out. Therefore, the joint does not move as smoothly as it should and this condition can cause pain to the subject [34].

Especially, knee osteoarthritis (OA) of the intact limb is one of the secondary impairments due to monolateral limb amputation [35]. Transtibial amputees (TTAs) are five times less likely to develop knee pain in their amputated limb than a control population [36]. This is due to the TTAs' attitude to load their intact limb to a greater extent than their prosthetic limb during gait.

D. C. Morgenroth et al. [36] in their study found an interesting parameter, the first peak of the knee External Adduction Moment (EAM), that is highly associated with the development of osteoarthritis in the contralateral limb. Knee EAM is negatively correlated to prosthetic foot-ankle push-off work that (as said in paragraph 1.5.2.3) it is much lower in amputees than in healthy subjects. The study shows how foot-ankle push-off work and intact limb first peak knee EAM are related (Figure 1.5.6, next page).

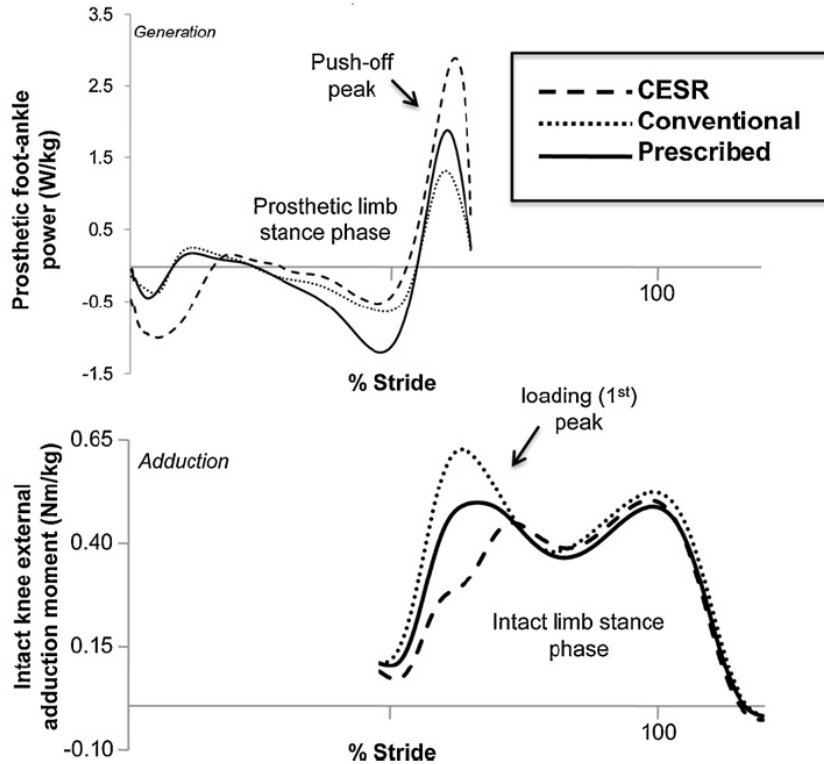


Figure 1.5.6 – In Morgenroth et al. study were tested different foot: a dynamic (conventional) foot, an ESAR foot (prescribed) and a CESR (Controlled Energy Storage and Return) foot designed by them. The image shows the correlation between prosthetic foot-ankle push-off power and intact knee external adduction moment for each type of foot. As it can be seen, as the foot-ankle push-off power increases, intact knee EAM decreases. A decreased intact knee EAM means a lower load on the intact knee, resulting in a lower probability for the amputee subject to develop osteoarthritis [36].

### 1.5.3.2 Metabolic Cost

Metabolic cost is the amount of energy consumed as the result of performing a given work task; usually expressed in calories [37].

The metabolic cost of walking with a prosthetic foot is affected by the Roll-Over Shape (ROS) of the prosthetic foot [38] [39] [40] [41] and the artificial foot capability of returning energy during the push-off. Therefore, these two characteristics will further affect the necessary compensatory activity of the residual muscles, both in the ipsilateral and in the contralateral limb.

Curtze et al. [38] found that the *centre of curvature's position*, which is the centre of the osculating circle referred to the ROS curve (Figure 1.5.7, next page), affects the system's mechanical response. ROS curve's centre of curvature can be positioned in three different configurations: *flexed*, *neutral* or *extended* (Figure 1.5.7, next page). These configurations are determined during the prosthesis' alignment. Therefore, also the artificial foot alignment affects the metabolic cost [41].

Referring to Adamczyk et al. [39] study, also the *radius of curvature* affects the net metabolic cost of walking. They found that rolling feet with a radius of curvature 0.3 L (where L is the leg length) appear energetically advantageous for human walking (Figure 1.5.8, next page).

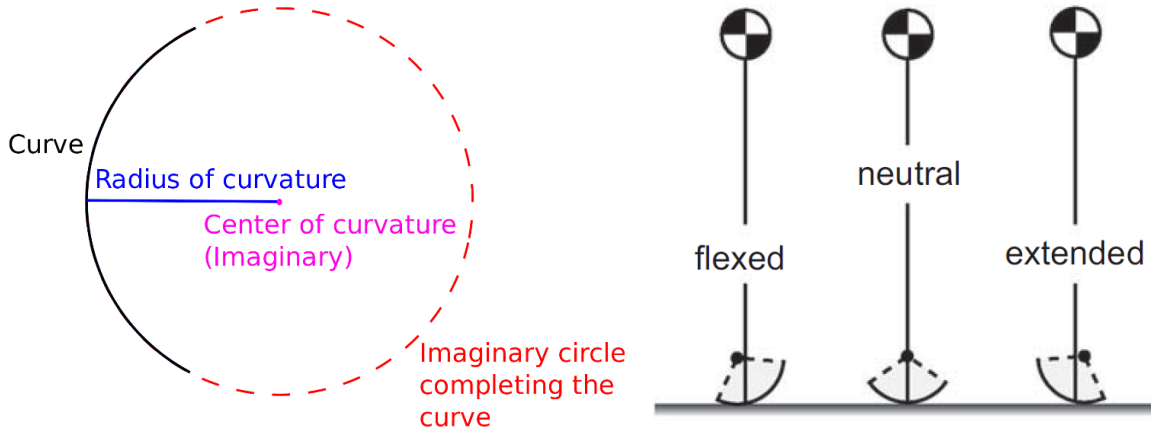


Figure 1.5.7 – Left figure: representation of the radius and the centre of curvature. The black curve is the imaginary ROS curve, with its own radius of curvature and the relative centre of curvature. The dashed circle in red is the ROS curve's osculating circle. [https://en.wikipedia.org/wiki/Center\_of\_curvature#/media/File:Radius\_of\_curvature.svg]. Right figure: different configurations of foot centre of curvature. [38]

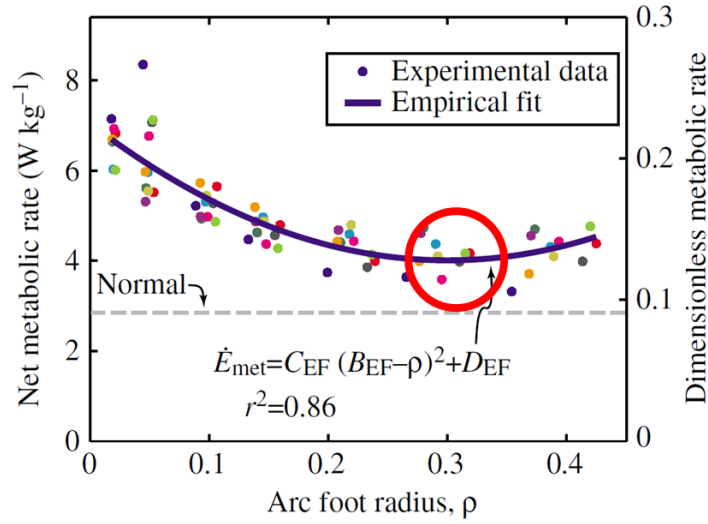


Figure 1.5.8 – The figure shows the relationship between the net metabolic rate and the normalized (over leg length,  $L$ ) arc foot radius. The curve shows a minimum where the arc foot radius is approximately equal to  $0.3 L$ . [39]

### 1.5.3.3 Stability and Comfort

The centre of curvature *extended* configuration enhances the energy return during the push-off phase, while the *flexed* configuration improves shock-absorbing during *initial contact*. As discussed before, these two phases play a fundamental role in human gait: during the initial contact with the ground the foot must store the energy and later return it to allow the forward propulsion of the body during push-off. Therefore, the desired goal is to confer to the prosthetic foot different curvatures in order to optimize both the heel-strike phase and the forward propulsion phase. Consequently, the artificial feet should present different curvatures all over different gait phases.

Nevertheless, Curtze et al. [38] and Hansen et al. [40], respectively found that: the higher radius of curvature is, the better stability is achieved over gait cycle; the radius of curvature does not depend on the walking speed. Curtze et al. also highlighted a connection between radius of curvature and COP (Centre of Pressure) displacement as COP moves more gradually from the heel to the toe in artificial feet showing a more constant radius of curvature (Figure 1.5.9, next page).

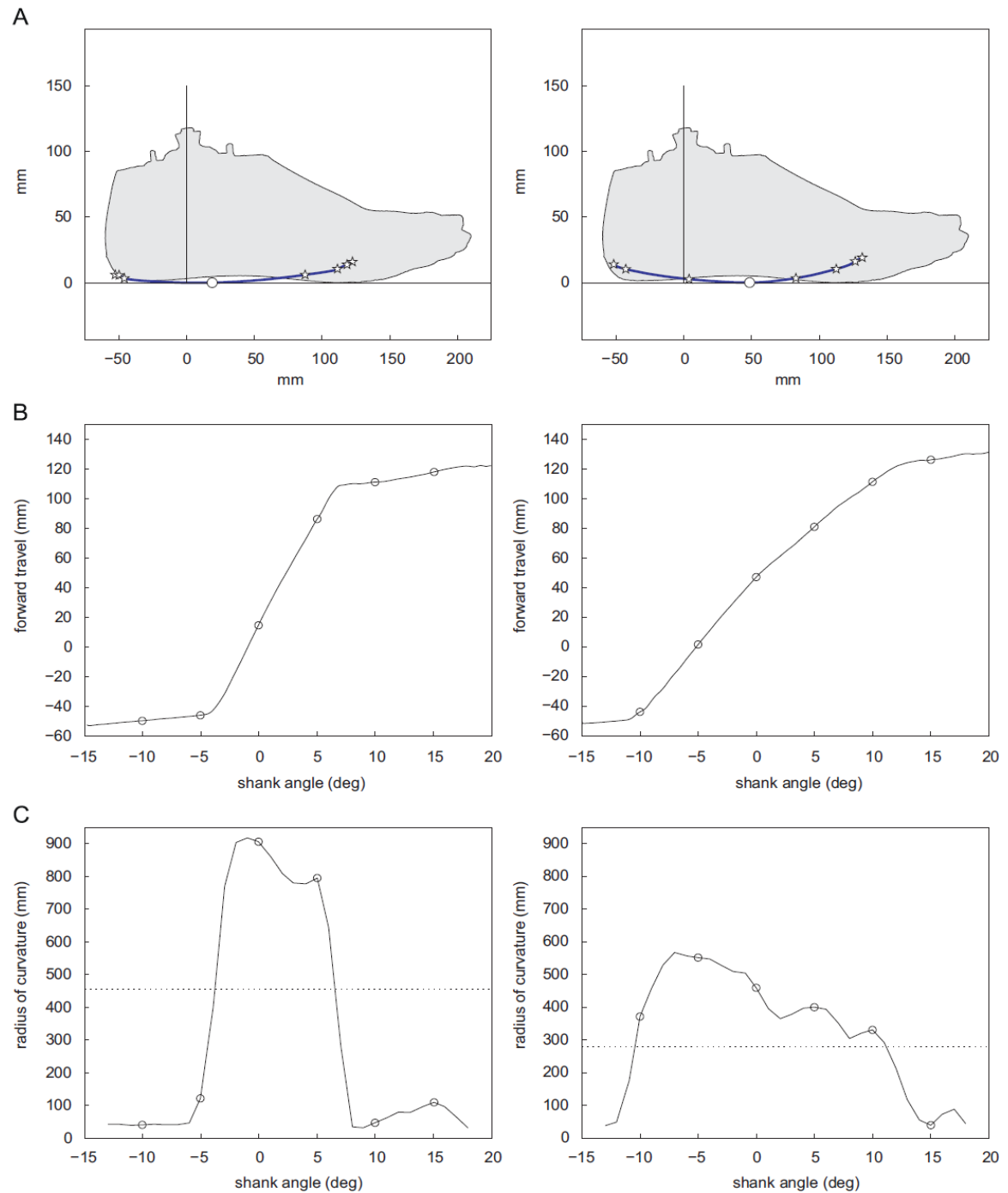


Figure 1.5.9 – A) ROS of the two feet tested by Curtze et al. The figure on the left is referred to an Esprit foot, while the figure on the right is the ROS of a Vari-Flex® foot. B) COP forward travels of the Esprit® foot (left) and the Vari-Flex® foot (right). C) Radii of curvature of the Esprit foot (left) and Vari-Flex® foot (right) [38].

### 1.5.3.4 Effects of Different Prosthetic Foot Stiffnesses

Table 1.5.1 (next page) illustrates the effects that stiffness has on prosthetic foot characteristics. To realize this summary, I have considered the works of Adamczyk et al. [28], Klodd et al. [29], Zelik et al. [30], Raschke et al. [31] and Fey et al. [32] [33].

Table 1.5.1 – Effects that stiffness variations on different parts of foot have on biomechanical outcomes.

	Hindfoot	Forefoot
Increased stiffness	<b>What increases:</b> <ul style="list-style-type: none"> <li>• Energy return [28]</li> <li>• GRF on residual limb during heel strike [28]</li> <li>• Knee flexional angle during stance phase [28]</li> </ul>	<b>What increases:</b> <ul style="list-style-type: none"> <li>• Interarticular forces on sound limb during heel strike [28]</li> <li>• Knee extensional angle during mid-stance [28]</li> <li>• Comfort [29]</li> </ul> <b>What decreases:</b> <ul style="list-style-type: none"> <li>• Prosthetic limb motor work on COM [28] [30]</li> <li>• Contact force on sound knee [33]</li> </ul>
	<b>What increases:</b> <ul style="list-style-type: none"> <li>• GRF on sound limb during heel strike [32]</li> <li>• Knee flexional moment [32]</li> <li>• Moment on the sagittal plane during push off [31]</li> </ul>	
Decreased stiffness		<b>What increases:</b> <ul style="list-style-type: none"> <li>• Contact force on sound limb during push off [29]</li> <li>• Stored and returned energy [29] [30]</li> <li>• Mechanical efficiency [29]</li> <li>• Work on prosthetic ankle joint [30]</li> </ul> <b>What decreases:</b> <ul style="list-style-type: none"> <li>• Metabolic cost [33]</li> </ul>
	<b>What increases:</b> <ul style="list-style-type: none"> <li>• GRF on residual limb during mid-stance phase [32]</li> <li>• Ankle joint angles [32]</li> <li>• Knee flexional angle during swing [32]</li> <li>• Knee flexional moment during push off [32]</li> <li>• Sound hip extensional moment [32]</li> <li>• Muscle activity in residual limb [32]</li> <li>• Sound knee extensional moment during heel strike [32]</li> <li>• Stability on uneven terrains [31]</li> </ul> <b>What decreases:</b> <ul style="list-style-type: none"> <li>• GRF on residual limb during loading phase [32]</li> <li>• Plantarflexion moment [32]</li> <li>• Sound knee flexion moment [32]</li> </ul>	

Looking at the previous table, it is possible to assert that choosing the optimal foot stiffness is a complex design task. Every stiffness variation in different parts of the foot leads to different prosthesis behaviour. That is why there are so many different foot prostheses on the market: each one of

them optimizes a specific parameter and lacks on others. It is the orthopaedic technician that must decide which is the optimal prosthesis for the amputee and tune it to fit it to the subject.

Because of these preliminary fundamental results, the presented study will focus on foot stiffness to reproduce the quasi-static mechanical behaviour of the Vari-Flex® foot (Chapter 3). In order to achieve this, it will be necessary to properly define the stiffness of the multibody prosthetic foot model (Chapter 2). A tuning procedure of stiffness has been done to optimize the results in quasi-static loading condition, but it had not brought to the expected results. The reasons behind this issue will be further discussed in Chapter 7. The last part of the study will be conducted on a multibody model simulating gait stance phase (Chapter 5). Moreover, the accuracy and precision of the model will be evaluated comparing deflections computed by the model with the ones obtained from experimental data acquisitions (Chapter 4).





## 2. Multibody Model Implementation

---

In multibody models each body element is treated as a rigid unit, incapable of mechanically induced distortions. Finite-Element Methods (FEM) are normally used to model and analyse flexible bodies. However, FEM-based approaches could be expensive and often require special treatment to apply to multi-physics domain with elaborate control systems. This project is intended to reduce time costs required to simulate prosthetic foot dynamical properties during walking and obtain acceptable results when compared to experimental acquisitions. Lumped parameters/multibody model and FEM model will be compared in quasi-static loading conditions.

The multibody model implemented during this Thesis may be considered as a lumped parameters (LP) model, since the material elastic properties are concentrated in the joints, while the mass properties are referred to the rigid segments. A theoretical study by Leonard et al. (1980) [42] compared from a theoretical point of view the FEM and the LP methods. In this study, these methods were used to model oceanic cables. They found no significant differences between the two methods from a theoretical point of view but, they did not “intended to program both methods and compare results for a given sets of problem”. In other words, they tested the mathematical feasibility of both analyses, but they did not program some models to compute physical results, which is what will be further done in this study.

This chapter will describe the methods and the different software used to create a multibody model of the Vari-Flex® foot by Ossür. Mathematical equations used to set the starting values for stiffness will also be described. The model simulates what happens to the foot over stance phase.

The idea to realize a multibody/lumped parameters (LP) model is supported by other studies found in the literature [33] [43] [44]. These studies utilized multibody lumped parameters models to simulate the dynamic behaviour of different objects such as ESAR foot [33], prosthetic foot for sport purpose [43] and neck whiplash phenomenon [44].

### 2.1 Simscape Multibody

*Information and examples contained in this paragraph are mainly taken from “Modeling Flexible Bodies with Simscape Multibody Software” by S. Miller et al. [45] and “Simscape Multibody Getting Started Guide” by MathWorks [46]. The functions of the Simscape blocks cited in this paragraph are detailed in Appendix B first paragraph: Simulink/Simscape’s blocks legend.*

Simscape Multibody is a Simulink®’s (property of The MathWorks, Inc.) library providing a multibody simulation environment for 3D mechanical systems. To support multibody modelling, there are specific Simulink®’s blocks: they can represent bodies, joints constraints, force elements and sensors. These blocks allows Simulink® to implement and solve the equations of motion for complex mechanical systems.

#### 2.1.1 Flexible Bodies Modelling

Simscape Multibody allows to model flexible bodies with a lumped parameters approach. Therefore, each flexible body can be modelled as a group of connected discrete flexible units. Each one of them is made up two or more rigid mass elements coupled by joint with internal springs and dampers. Joints are what provide the degrees of freedom required for deformation to occur: if they have rota-

tional degrees of freedom, they will enable bending and torsion, while those with translational degrees of freedom enable axial deformation and shear. The inertial properties of the bodies are contained in rigid mass elements (*Solid* block), while materials' viscoelastic properties are provided by *Joint* blocks. Joints' elastic and damping properties must be inserted by user and could be calculated starting from model geometry and material properties. Bodies' inertial properties are automatically computed by the software considering geometry and density.

In multibody models created for this Thesis, connections between two following segments are realised with *rotational* joint. Therefore, the software will solve for each segment the forced torsional damped harmonic oscillator's equation of motions:

$$I \frac{d^2\theta}{dt^2} + b_R \frac{d\theta}{dt} + k_R \theta = \tau$$

Equation 2.1.1– Forced torsional damped harmonic oscillator's equation of motion.

Where:

$\theta$  is the relative orientation between two following segments

$I$  is the moment of inertia of the mass element about the axis of rotation

$b_R$  is the rotational damping coefficient of the joint

$k_R$  is the rotational spring coefficient of the joint

$\tau$  is the net external torque acting on the rotating mass elements

Simscape Multibody models give correct results for *small*, *linear* and *elastic* deformations. In a prosthetic foot these hypotheses are not verified. Therefore, it will be necessary to evaluate the errors committed by the model.

## 2.2 Stiffness Issue

To see if Simscape models return correct solution using the stiffness formulation proposed by Fey et al. [33] and Miller et al. [45] (Equation 2.2.6, p. 30), a simple simulation of a wedged beam loaded at the free end with a ramp force going from 0 N to 1000 N<sup>1</sup> has been realized. Applying the external force in the previous described way, it is possible to simulate a quasi-static condition of loading. Since the overall model behaves as a forced torsional damped harmonic oscillator, the beam would have shown a strong oscillatory behaviour (response to a step input) if it had been instantaneously loaded with a considerable non-null force. Instead, applying a force that slowly increases over time, the system switches between consequent quasi-static conditions of loading.

### 2.2.1 Theoretical Wedged Beam Subjected to Bending

From Structural Mechanics theories it is possible to describe the behaviour of a wedged beam loaded with a bending force at the free end (Figure 2.2.1, next page). The mathematical equations describing the phenomenon are presented in the next page.

---

<sup>1</sup> Simulink®'s scheme of a 5-segments wedged beam is reported in Appendix B's second paragraph: 5-Segments Wedged Beam Model – 'bar\_model\_5.slx'. The relative MATLAB® script can be found in Appendix A's first paragraph: Theoretical wedged beam model – 'bar\_model\_theoretical.m'.

The vertical reaction force ( $R_A$ ) and torque ( $T_A$ ) acting on the weld joint can be respectively expressed as:

$$|R_A| = P$$

Equation 2.2.1 – Stress sensed at the weld joint

$$|T_A| = PL$$

Equation 2.2.2 – Momentum sensed at the weld joint

Where:

$P$  is the force applied at the loaded end

$L$  is the beam's total length.

Beam's deflection along vertical direction at a certain distance  $x$  from the weld joint can be expressed as:

$$f(x) = -\frac{PL^3}{2EJ} \left( \frac{x^2}{L^2} - \frac{x^3}{3L^3} \right)$$

Equation 2.2.3 – Theoretical beam's vertical deflection

Where:

$E$  is the material Young modulus

$J$  is the cross-sectional moment on inertia.

It is important to remember that the deflection is considered positive when the beam moves up from the former equilibrium position.

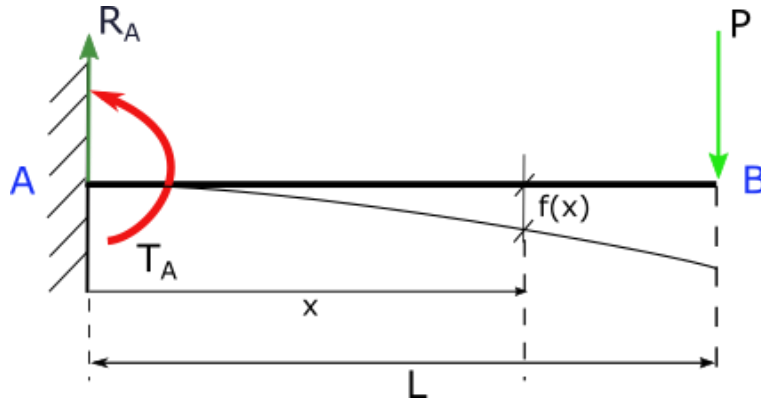


Figure 2.2.1 – Schematic representation of a wedged beam subjected to bending.

Cross-sectional moment depends on sectional area and, for a beam with a rectangular section, can be expressed as:

$$J = \frac{WT^3}{12}$$

Equation 2.2.4 – Cross-sectional moment of inertia for a beam with a rectangular section

Where  $W$  is the beam's width (along the out-of-plane axis) and  $T$  is the beam's thickness (along the vertical in-plane axis).

Consequently, the beam vertical deformation at the free end can be expressed as:

$$f_b = \frac{PL^3}{3EJ}$$

Equation 2.2.5 – Beam's maximum deflection at the loaded end

All these considerations are verified for a slender beam, with a rectangular section, made up of an isotropic material. If these hypotheses are not verified, the deformation will not be small, linear and elastic and the model will introduce errors.

### 2.2.1.1 Simulation's Configuration

Considering the theoretical formulas, it has been realized a MATLAB® script (presented in appendix A's first paragraph: *Theoretical wedged beam model* – 'bar\_model\_theoretical.m') to pass the material parameters and the geometric characteristics of the wedged beam to the Simulink® model.

Meanwhile, five different models of wedged beams have been realized in Simulink®: each one of them differs from the others for the number of segments the beam is divided into. Specifically, Simulink®'s schemes realized are:

- 1-segment wedged beam
- 2-segments wedged beam
- 5-segments wedged beam
- 10-segments wedged beam
- 20-segments wedged beam

The reason why different models were made is checking if the stiffness formulation proposed by Fey et al. [33] and Miller et al. [45] (Equation 2.2.6) allowed to reach force, torque and deflection' theoretical results with different models of beam. More accurate results are expected when the number of segments modelling the beam are higher. Instead, significant variations in force and torque sensed on the weld joint are not expected, since those should be independent from the number of segments.

$$k_i = \frac{EJ}{l_i}$$

Equation 2.2.6 – Formulation of the  $i^{th}$  joint's stiffness as proposed by Fey et al. and Miller et al. [33] [45]

Where (referring to Figure 2.2.2):.

$k_i$  is the rotational stiffness of the  $i^{th}$  joint;

$l_i$  is the length of the  $i^{th}$  segment.

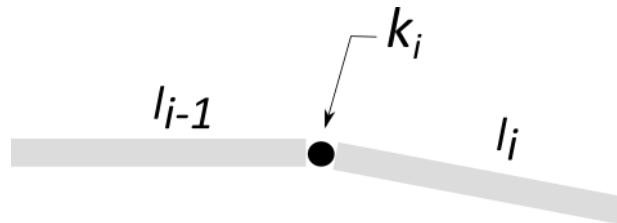


Figure 2.2.2 - How  $k_i$  and  $l_i$  are considered in the multibody scheme.

The material and geometrical properties chosen for the simulation are listed in Table 2.2.1 (next page), while the simulation parameters are listed in Table 2.2.2 (next page). The material considered for the simulation was T700S composite carbon fibre by Toray Composite Material America Inc.

## 2. Multibody Model Implementation

Table 2.2.1 - Material and geometrical properties of the simulated wedged beam

Property (abbr.)	MATLAB's variable name	Value	Unit of measurement
Total beam length ( $L$ )	L	1	[m]
Beam thickness ( $T$ )	H	0.1	[m]
Beam width ( $W$ )	W	0.1	[m]
External force ( $P$ )	fmax	1000	[N]
Density ( $\rho$ )	rho	1.8	[g · cm <sup>-3</sup> ]
Young Modulus [ $E$ ]	E	134	[GPa]
Damping coefficient [ $\beta$ ]	b	0.001	[N · m · s · rad <sup>-1</sup> ]

Table 2.2.2 – Simulation's parameters

Parameter	MATLAB's variable name	Value	Unit of measurement
Sampling frequency	fs	1000	[Hz]
Time duration	T	1	[s]

From material and geometrical properties, applying Equation 2.2.4 and Equation 2.2.6, the stiffnesses and cross-sectional moment values (listed in Table 2.2.3) have been obtained.

Table 2.2.3 – Stiffnesses and cross-sectional moment values obtained from Equation 2.2.4 and Equation 2.2.6

Property (abbr.)	MATLAB's variable name	Value	Unit of measurement
Cross-sectional moment of inertia	J	0.05	[m <sup>4</sup> ]
1-segment beam joints' rotational stiffness	k1	1.11e6	[N · m · rad <sup>-1</sup> ]
2-segments beam joints' rotational stiffness	k2	2.23e6	[N · m · rad <sup>-1</sup> ]
5-segments beam joints' rotational stiffness	k5	5.58e6	[N · m · rad <sup>-1</sup> ]
10-segments beam joints' rotational stiffness	k10	1.11e7	[N · m · rad <sup>-1</sup> ]
20-segments beam joints' rotational stiffness	k20	2.23e7	[N · m · rad <sup>-1</sup> ]

### 2.2.1.2 Simulation Results

Simulation shown the predicted results since the simulated beam deflection, as the number of segments increases, deviates less and less from the theoretical shape (Figure 2.2.5 and Figure 2.2.6, next page). Nevertheless, even the 20-segments model does not give precise results if we consider the

deflection at the bar free end. Furthermore, force and torque sensed at the weld end do not differ within the different models (Figure 2.2.3 and Figure 2.2.4).

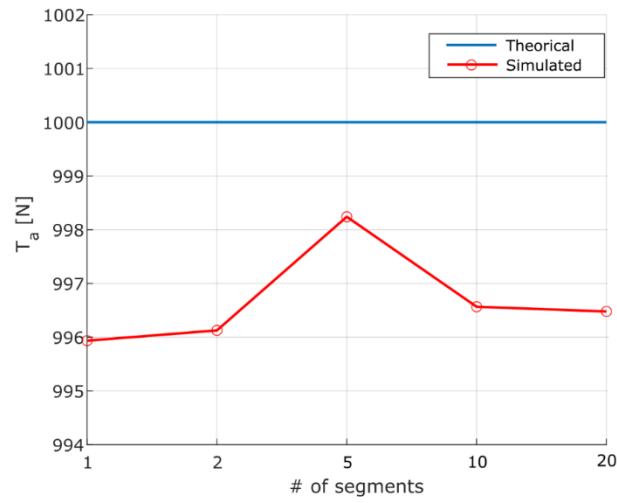


Figure 2.2.3 – The blue line represents the theoretical force sensed at the weld joint. The red line is the force sensed in simulations with 1, 2, 5, 10 and 20 segments.

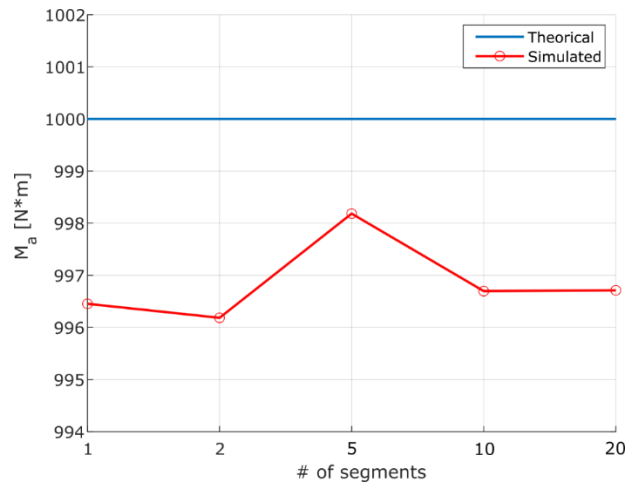


Figure 2.2.4 – The blue line represents the theoretical torque sensed at the weld joint. The red line is the torque sensed in simulations with 1, 2, 5, 10 and 20 segments.

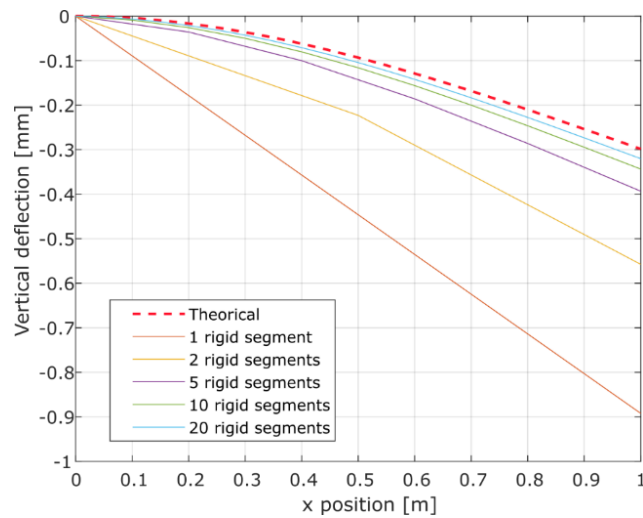


Figure 2.2.5 - Vertical deflection achieved by the different models. The dashed thicker line is the theoretical result, while the other lines represent the deflection obtained by the simulated models.

Probably, the force and torque computed from the simulated models differ from the theoretical values because when the external force magnitude increases, some vibrations occur. These vibrations may affect the results and justify the divergence (that still is less than 0.5%).

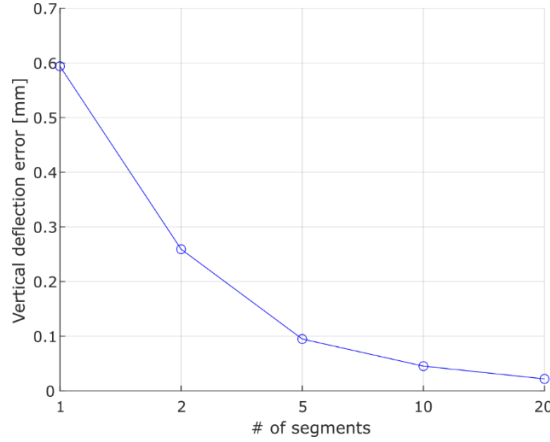


Figure 2.2.6 – The blue dots represent the error that each simulated model present with respect to the theoretical maximum deflection at the beam's loaded end.

Nevertheless, the aim of this modelling was knowing if it was possible to achieve the elastic line theoretical results (or at least the free end theoretical deflection) working on the stiffness formula. The idea was to achieve the theoretical free end deflection irrespective of the number of segments approximating the beam. This problem will be further address in the next paragraph.

### 2.2.2 Analytical Stiffness Value

In this paragraph I will present the analytical solution that I have found to better address the stiffness issue described in the former paragraph. As said before, I wanted to achieve a stiffness formula that allows to exactly obtain the theoretical deflection at the loaded end using models with different number of segments. To do so, I have started solving the analytical equation for 1-segment, 2-segments and 3-segments wedged beam models; then, I have tried to extrapolate a relationship between the analytical stiffness values found.

The hypotheses made to simplify the solution are shown below:

- The material which the beam is composed shows a linear, elastic behaviour.
- Displacements are considered *small*.
- Every revolute joint has the same rotational stiffness value.
- Rigid segments are the same length.

In the next paragraphs are reported all the mathematical formulas considered for the solution and the relationship found between rotational stiffness and number of segments which the beam is divided into.

#### 2.2.2.1 1-Rigid-Segment Wedged Beam Analytical Model

Under the assumption of a purely elastic material it is possible to affirm that reaction torque acting on the weld joint ( $T_A$ ) and segments relative rotation ( $\theta$ ) are linearly dependent. The linear coefficient which relates them is the rotational stiffness ( $k_R$ ).

$$k_R = \frac{T}{\theta}$$

Equation 2.2.7 - Rotational stiffness expression for a 1-segment beam loaded at the free end.

Considering Equation 2.2.2, it is possible to rewrite Equation 2.2.7 to obtain Equation 2.2.8.

$$k_R = \frac{PL}{\theta}$$

Equation 2.2.8 – Rotational stiffness expression deriving from Equation 2.2.2 and Equation 2.2.7.

If the small displacements hypothesis is verified, the angular coordinate  $\theta$  could be expressed as:

$$\theta = \frac{dy}{L}$$

Equation 2.2.9 . Relation between angular and linear coordinates under the condition of small displacements.

Then, rotational stiffness can be rewritten as:

$$k_R = \frac{PL^2}{dy}$$

Equation 2.2.10 - Rotational stiffness obtained considering eq. Equation 2.2.2, Equation 2.2.8 and Equation 2.2.9.

Merging Equation 2.2.5 ( $f_b$  is the equivalent of  $dy$ ) and Equation 2.2.10 it is possible to finally reach the stiffness equation (Equation 2.2.11) for a 1-rigid-segment wedged beam (Figure 2.2.7).

$$k_R(1) = \frac{3EJ}{L}$$

Equation 2.2.11 – Analytical rotational stiffness equation for a 1-rigid-segment model of wedged beam.

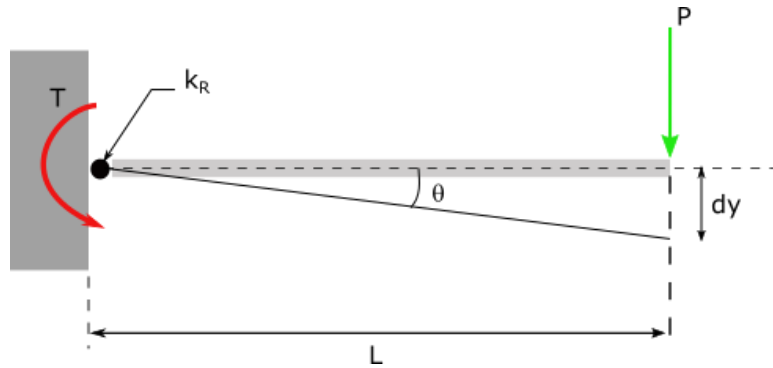


Figure 2.2.7 – Representation of a 1-rigid-segment model of wedged beam loaded with a bending force at the free end.

### 2.2.2.2 2-Rigid-Segments Wedged Beam Analytical Model

If rigid segments are the same length ( $l_1 = l_2 = l_i = \frac{L}{n}$ , where  $n = \text{number of segments}$ ) and material has pure elastic behaviour, the mechanical system (Figure 2.2.8) can be described with a system of two linear equations (Equation 2.2.12 (a) and (b)).

$$\begin{cases} k_{R,1}\theta_1 = P(l_1 + l_2) = 2P\frac{L}{2} & (a) \\ k_{R,2}\theta_2 = Pl_2 = P\frac{L}{2} & (b) \end{cases}$$

Equation 2.2.12 – System of two linear equation that describes the 2-rigid-segments model of wedged beam.

Utilizing the hypothesis that joints have the same rotational stiffness values ( $k_{R,1} = k_{R,2}$ ) and dividing Equation 2.2.12 (a) by Equation 2.2.12 (b), it is possible to find the relationship between  $\theta_1$  and  $\theta_2$  (Equation 2.2.13, next page).



$$\frac{\theta_1}{\theta_2} = \frac{l_1 + l_2}{l_2} = A = 2 \rightarrow \theta_1 = A\theta_2$$

Equation 2.2.13 – Relation between relative rotations  $\theta_1$  and  $\theta_2$ .

If small displacements hypothesis is verified, the sinus of the angle could be replaced by the angle itself and the beam total deflection is:

$$dy = l_1 \sin \theta_1 + l_2 \sin(\theta_1 + \theta_2) \approx l_1 \theta_1 + l_2(\theta_1 + \theta_2)$$

Equation 2.2.14 – Total beam deflection expression for a 2-rigid-segment model of beam.

Substituting  $\theta_1$  expression (Equation 2.2.13) in Equation 2.2.14, it is possible to obtain the analytical value of  $\theta_2$ .

$$dy = \frac{L}{2} A \theta_2 + \frac{L}{2} (A \theta_2 + \theta_2) = \frac{L}{2} (2A \theta_2 + \theta_2) = 5 \frac{L}{2} \theta_2 \rightarrow \theta_2 = \frac{2dy}{5L}$$

Equation 2.2.15 -  $\theta_2$  expression for a 2-rigid-segments model of beam.

Substituting  $\theta_2$  expression Equation 2.2.12 (b) and remembering that, as hypothesis, all joints have the same rotational stiffness, it is possible to obtain the rotational stiffness formula for a 2-rigid-segments model of beam (Equation 2.2.16):

$$k_{R,1} = k_{R,2} = k_R(2) = \frac{F L}{\theta_2 2} = \frac{5 FL^2}{4 dy} = \frac{5 3EJ}{4 L}$$

Equation 2.2.16 – Rotational stiffness' analytical value for a 2-rigid-segments model of wedged beam.

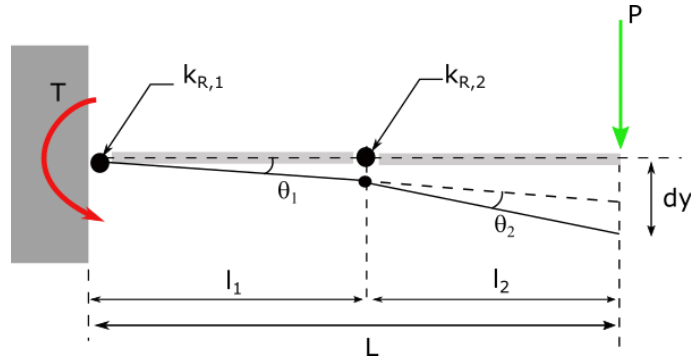


Figure 2.2.8 - Representation of a 2-rigid-segments model wedged beam loaded with a bending force at the free end.

### 2.2.2.3 3-Rigid-Segments Wedged Beam Analytical Model

If rigid segments are the same length:

$$l_1 = l_2 = l_3 = l_i = \frac{L}{n} \quad \text{where } n = \text{number of segments}$$

And material has pure elastic behaviour, the mechanical system (Figure 2.2.9) can now be described with a system of three linear equations.

$$\begin{cases} k_{R,1} \theta_1 = P(l_1 + l_2 + l_3) = 3P \frac{L}{3} & (a) \\ k_{R,2} \theta_2 = P(l_2 + l_3) = 2P \frac{L}{3} & (b) \\ k_{R,3} \theta_3 = Pl_3 = P \frac{L}{3} & (c) \end{cases}$$

Equation 2.2.17 - System of three linear equation that describes the 3-rigid-segments model of wedged beam.

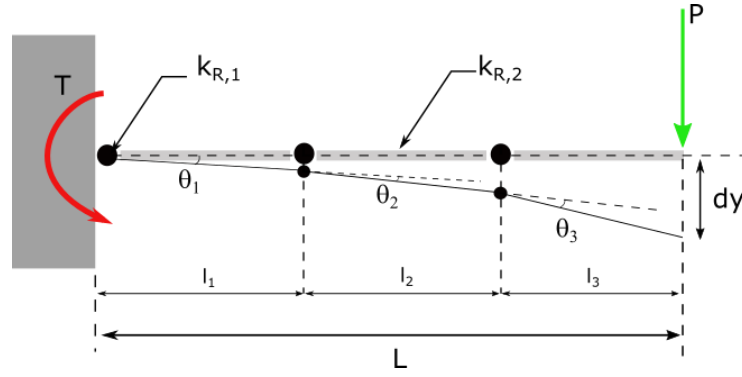


Figure 2.2.9 – Representation of a 3-rigid-segments model of wedged beam loaded with a bending force at the free end.

Since it has been assumed that joints have the same value for rotational stiffness, it is possible to find two relationships between the angles describing the problem (Equation 2.2.18 and Equation 2.2.19).  $A$  is the adimensional coefficient that relates  $\theta_1$  with  $\theta_3$ , while  $B$  relates  $\theta_2$  with  $\theta_3$ .

$$A = \frac{\theta_1}{\theta_3} = \frac{l_1 + l_2 + l_3}{l_3} = 3 \rightarrow \theta_1 = A\theta_3$$

Equation 2.2.18 - Relationship between  $\theta_1$  and  $\theta_3$ .

$$B = \frac{\theta_2}{\theta_3} = \frac{l_2 + l_3}{l_3} = 2 \rightarrow \theta_2 = B\theta_3$$

Equation 2.2.19 – Relationship between  $\theta_2$  and  $\theta_3$ .

In a 3-rigid-segments model, the deflection could be expressed as:

$$dy = l_1 \sin \theta_1 + l_2 \sin(\theta_1 + \theta_2) + l_3 \sin(\theta_1 + \theta_2 + \theta_3) \approx l_1 \theta_1 + l_2(\theta_1 + \theta_2) + l_3(\theta_1 + \theta_2 + \theta_3)$$

Equation 2.2.20 – Total beam's deflection expression for a 3-rigid-segment model of beam.

Replacing equations Equation 2.2.18 and Equation 2.2.19 in Equation 2.2.20, beam's deflection can be written as:

$$dy = \frac{L}{3} A\theta_3 + \frac{L}{3} (A\theta_3 + B\theta_3) + \frac{L}{3} (A\theta_3 + B\theta_3 + \theta_3) = \frac{L}{3} \theta_3 (3A + 2B + 1) = \frac{14}{3} L\theta_3$$

Equation 2.2.21 – Total beam's deflection referred to  $\theta_3$  and  $L$ .

From Equation 2.2.21, it is possible to express the value of  $\theta_3$  as:

$$\theta_3 = \frac{3}{14} \frac{dy}{L}$$

Equation 2.2.22 –  $\theta_3$  expression.

Considering Equation 2.2.17(c), rotational stiffness for a 3-rigid-segments beam can be expressed as:

$$k_{R,1} = k_{R,2} = k_{R,3} = k_R(3) = \frac{P L}{\theta_3} = \frac{14 PL^2}{9 dy} = \frac{14 3EJ}{9 L}$$

Equation 2.2.23 – Rotational stiffness' analytical value for a 3-rigid-segments model of wedged beam.

#### 2.2.2.4 N-Rigid-Segments Wedged Beam Analytical Model

Starting from the rotational stiffness values found in previous wedged beam models, a general solution for a N-rigid-segments system has been computed. It has been noticed that the stiffness formulas

found differ by the numerical coefficient that multiplies  $3EJ/L$ . Therefore, it was necessary to find a relationship between the three numerical coefficients found solving the previous models (reported in Equation 2.2.24).

$$k_R(1) = 1 \frac{3EI}{L}; \quad k_R(2) = \frac{5}{4} \frac{3EJ}{L}; \quad k_R(3) = \frac{14}{9} \frac{3EJ}{L} \rightarrow k_R(N) = c(N) \frac{3EJ}{L}$$

Equation 2.2.24 – Rotational stiffness' multiplying coefficients for 1-rigid-segment, 2-rigid-segments, 3-rigid-segments and N-rigid-segments wedged beam's models.

To do so, numerator and denominator must be analysed separately. What I came up with is shown in Equation 2.2.25.

$$c(N) = \frac{K(N)}{N^2} \quad \text{where} \quad \begin{cases} N = \text{number of segments} \\ K(N) = \sum_{i=1}^N i^2 \end{cases}$$

Equation 2.2.25 – Numerical coefficients multiplying  $3EJ/L$  in a N-rigid-segments wedged beam model.

Therefore, rotational stiffness for a N-rigid-segments wedged beam model can be expressed as:

$$k_R(N) = c(N) \frac{3EJ}{L}$$

Equation 2.2.26 – Rotational stiffness expression for a N-rigid-segments wedged beam model.

### 2.2.2.5 Simulations' Results Obtained with Analytical Formula for Rotational Stiffness<sup>2</sup>

With this new rotational stiffness formula, all the models shown the same deflection at the beam's end, with a maximum error that is less than  $1 \mu m$ , possibly due to approximations made by the solver. The results are shown in Figure 2.2.10 and Figure 2.2.11 in the following page.

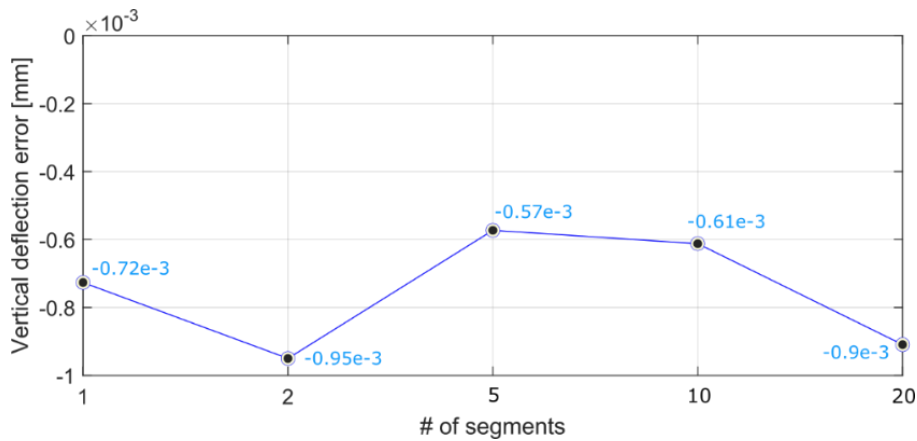


Figure 2.2.10 – Maximum deflection's error found using the analytical formula for rotational stiffness.

<sup>2</sup> Simulations were configured as described in paragraph 2.2.1.1. MATLAB®'s script is reported in Appendix A's second paragraph (Analytical wedged beam model - 'bar.m'), while the Simulink®'s scheme is the same utilized in theoretical

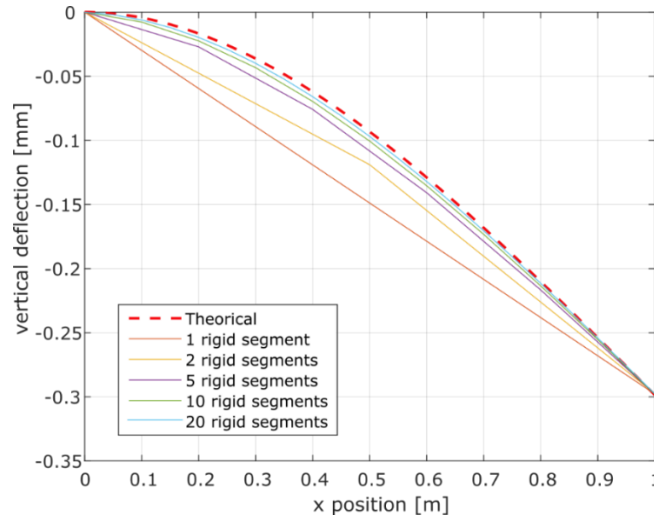


Figure 2.2.11 – Wedged beam's elastic line obtained with the analytical rotational stiffness' formula.

## 2.3 Highlander® Multibody Model – Preliminary Study

Once solved the stiffness' issue, the Highlander® (by Freedom Innovations Inc.) multibody model proposed by Fey et al. in their article [33] has been realized. The purpose of creating this model was to become familiar with the software, to see if it was possible to realise a complete prosthetic foot model and to test the software's limits in modelling since Fey et al. used a different software to realize the multibody model. Also, this testing model will help to define which are the required inputs to run simulations on Vari-Flex® prosthetic foot multibody model.

### 2.3.1 Realising the Geometrical Model

To build the Highlander® model, the first step is to reproduce its geometry: referring to Figure 2.3.1, the prosthetic foot joint coordinates has been obtained using WebPlotDigitizer [47], a free-source tool available online that allows to extrapolate image coordinates after axes' calibration procedure.

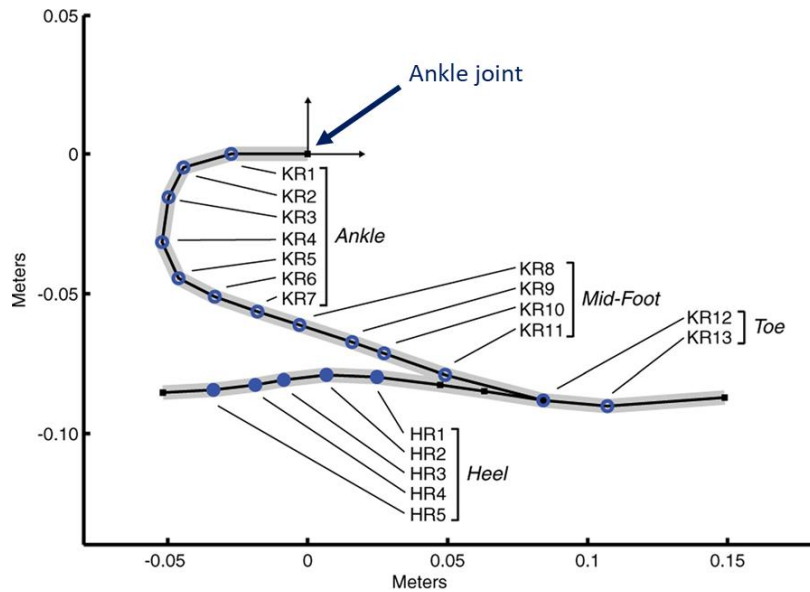


Figure 2.3.1 – Schematic representation of the Highlander® lumped parameters model realized by Fey et al. [33]. The revolute joints highlighted with blue circles have viscoelastic properties, while the others have been considered as locked joints: they are pulled by the other segments, but do not allow relative rotations. The ankle joint is the origin of the reference system and it is fixed in space.

From the coordinates, the relative orientation within each two connected segments could be computed. Since in a Simscape Multibody model the position of each link is defined through its relative orientation with respect to the former link, this latter data is fundamental. Along with the orientation, it is possible to obtain the length of each link composing the model. The width and the thickness of the segments was not reported, so reasonable values were given to them:  $0.06\text{ m}$  width and  $0.01\text{ m}$  thickness. Each link had the same width and thickness so, segments differ only by their length.

The physical Highlander® model realised by Fey et al. was made of Rilsan™ D80 (Nylon 11, Arkema, Inc), with Young modulus ( $E$ ) value equal to  $1.4\text{ GPa}$  and density ( $\rho$ ) value equal to  $0.47\text{ g} \cdot \text{cm}^{-3}$ . The damping coefficient of the material considered by Fey et al. was determined in a previous work of them [32] and it is set at  $5.73\text{ N} \cdot \text{m} \cdot \text{s} \cdot \text{rad}^{-1}$ .

It was possible to compute the inertial and viscoelastic properties of the foot from described information. The Highlander® multibody model resulting from presented data is shown in Figure 2.3.2. The Simulink® script can be found in Appendix B's third paragraph: Highlander® multibody model – 'sim\_highlander\_v6.slx'.

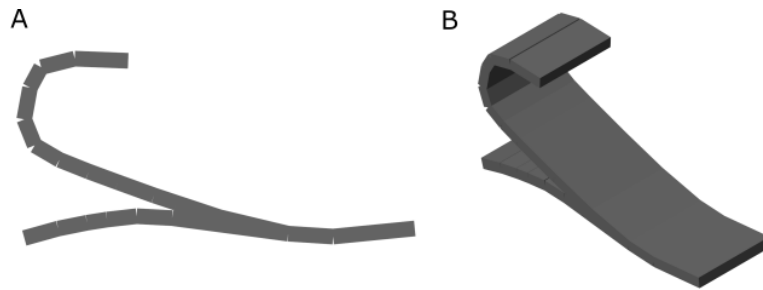


Figure 2.3.2 – A) Lateral view of the Highlander® model realized with Simscape. B) Isometric view of the same model.

### 2.3.2 Model Actuation

To simulate the foot rigid movement around the ankle occurring over gait, the foot model is controlled with the physiological foot flex-extension angle (shown in Figure 2.3.3). Angle information can be found in Bovi et al. study [48], which consisted of gait data collection from 40 healthy subjects. They categorised data according to subjects' age and gait speed. Reported data refers to “Adult – Natural (speed)” category.

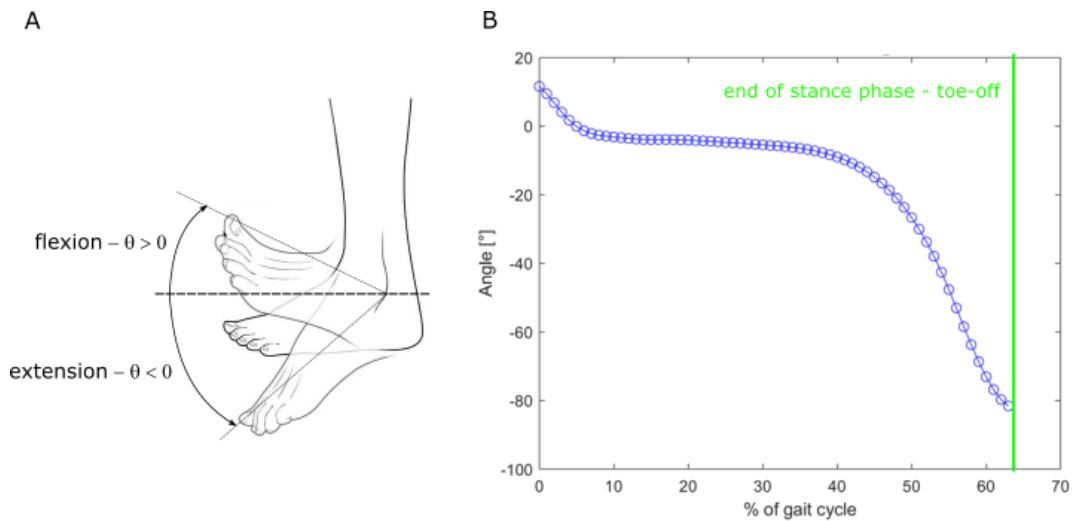


Figure 2.3.3 – A) Definition of foot flex extension angle: is the angle that the anterior-posterior axis of the foot and the line that connects the big toe and the ankle form. B) Trend of the foot flex-extension angle in healthy people over stance phase.

### 2.3.2.1 Applying Vertical Ground Reaction Forces to the Model

Other input data are vertical ground reaction forces (vGRF) and COP displacement (Figure 2.3.4). vGRF data is taken from Bovi et al. study [48], while COP information comes from Schmid et al. work [11], conducted on trans-femoral amputees. vGRF and COP displacement trends over gait cycle are respectively shown in Figure 2.3.5 and Figure 2.3.6 (next page).

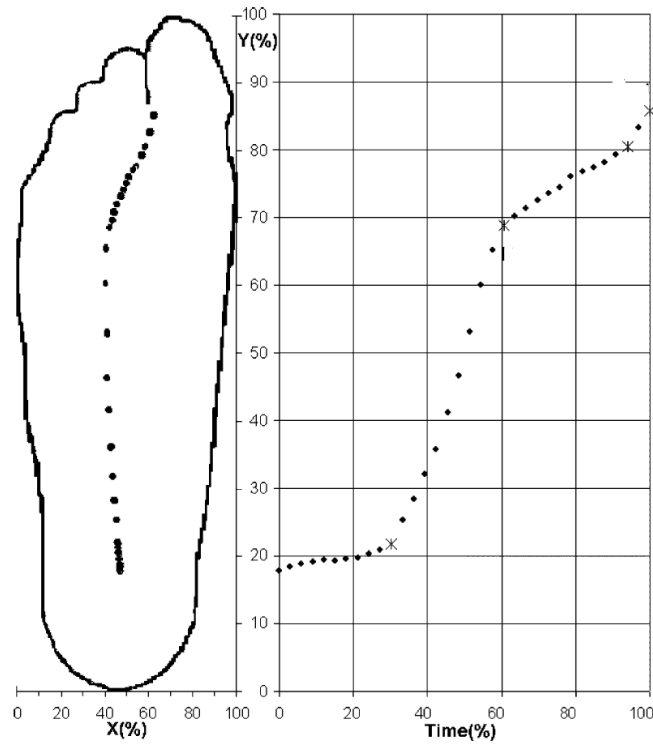


Figure 2.3.4 – COP amputee displacement. The graph particularly represents the COP displacement along anterior-posterior direction, as the figure on the left explains. The time axis is referred to the stance phase only [11].

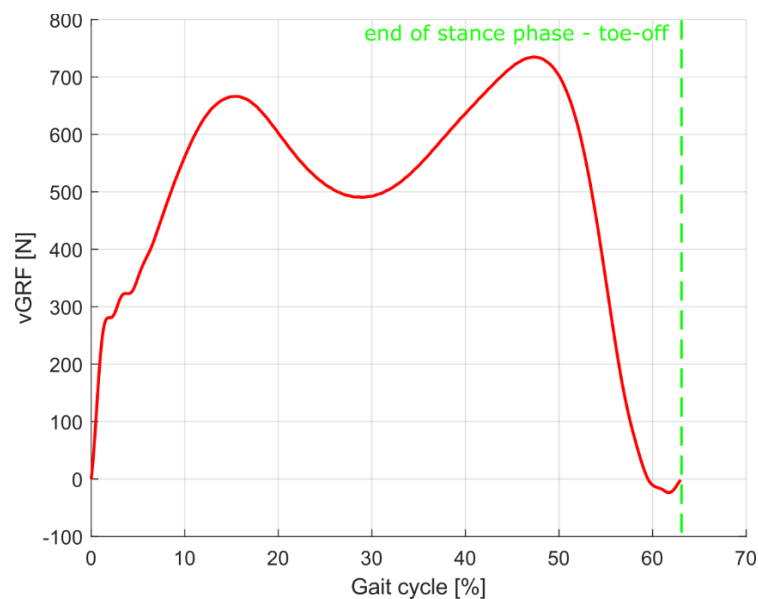


Figure 2.3.5 – Vertical ground reaction force trend over stance phase.

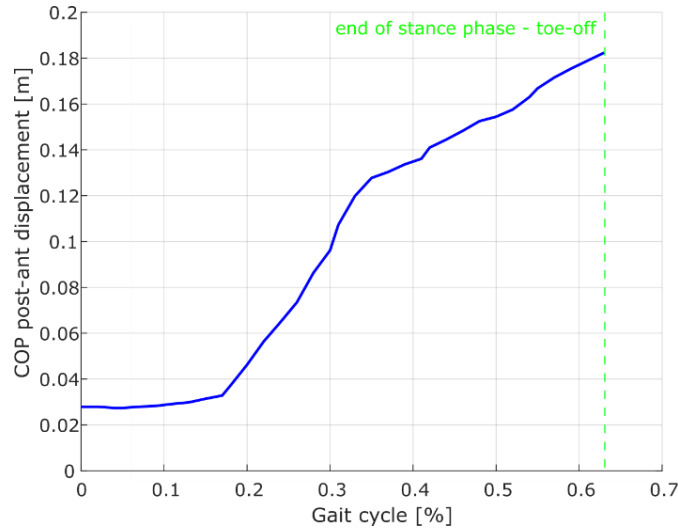


Figure 2.3.6 – COP posterior-anterior displacement referred to the Highlander foot length.

Information is not consistent: COP and GRFs data refers to two different categories of subjects (healthy and amputated). For now, this will not be a problem since the only aim of this model is not to compute physiologically significant parameters, but to see if it is possible to simulate a prosthetic foot while walking and to learn how the Simscape blocks work. Later, gait signals on a healthy subject wearing a prosthesis adapter will be acquired. Acquisition protocol, adapter description and final gait data will be presented in Chapter 4.

COP displacement and vGRF information had to be combined to know where and when applying the vGRF forces to the foot. Furthermore, it has been assumed that vGRF could only act on segments' midpoints to simplify the problem (further explanations in Figure 2.3.8, next page), as the main purpose of this study is to produce a simplified model of a prosthetic foot. To better understand how COP displacement, foot flex-extension angle and vGRF are related, a scheme representing the model inputs is shown in Figure 2.3.7.

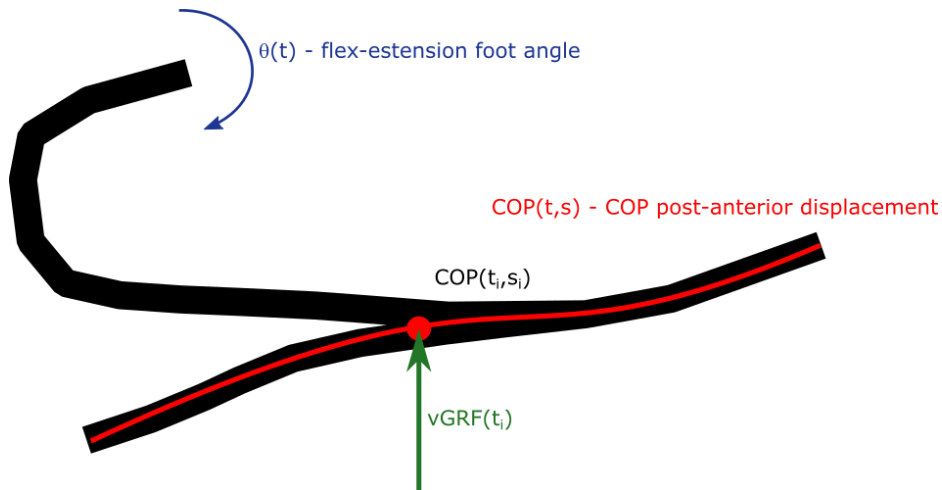


Figure 2.3.7 – How inputs are given to the model. Foot flex-extension angle and vertical ground reaction force depend only on time, while COP posterior-anterior displacement is a function of both time and space.

Managing time-varying data is not a problem in Simulink® since the software is intended to handle this kind of inputs and outputs. The problem is giving to the software the instruction to load the correct segment (which is the one containing the COP) with the correct force at the correct time. It is possible to do so with a few lines of MATLAB®'s code. The discretized resulting positions of COP are shown in Figure 2.3.8 (next page).

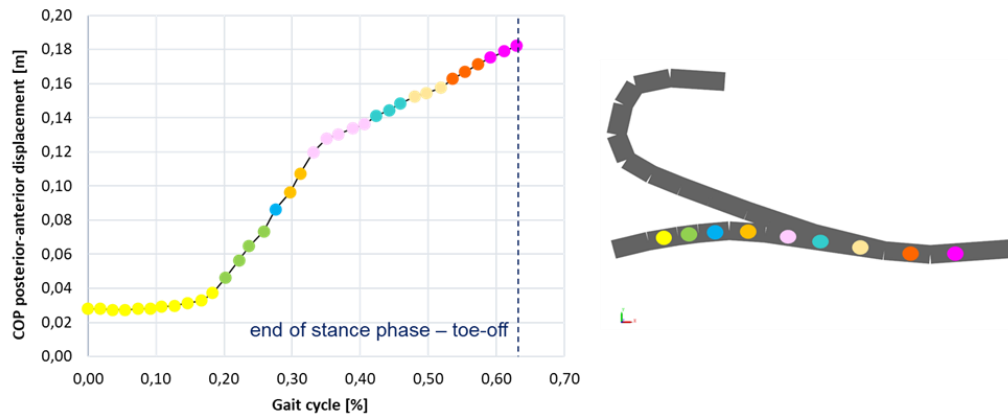


Figure 2.3.8 – The graph on the left shows the COP motion from hindfoot to forefoot over stance phase. Dots of same colour are related to the same segment's midpoint highlighted in the figure on the right.

Since there is no further information about vGRF, COP displacement, mechanical response or geometry of the Highlander foot, it wasn't possible to test the software on this model. Therefore, the analysis of the potentiality of Simscape modelling has been carried out and the multibody model validation has been postponed for when the Vari-Flex® multibody model would have been defined.

### 2.3.3 Insertion of the Highlander® Foot in a Lower Limb Multibody Model

It is possible to link the multilink model of the foot to a multibody system of the entire human body. This kind of “composite” model has been realized to further investigate the potentiality of Simulink®.

A lower limb model with thigh and leg segments controlled with hip, knee and ankle joints' kinematics has been realized. The foot segment was realized with the highlander model realized. Thigh and shank' anthropometric data was taken from a Winter's study [49]. Considered data are reported in Figure 2.3.9 and Figure 2.3.10 (next page). Instead, joints kinematic information was taken from Bovi et al. study [48]. Joints' kinematics data is shown in Figure 2.3.11 (next page) and it refers to an “Adult – Normal” subject's stance phase. The multibody model ran in simulations is presented in Figure 2.3.12 (next page).

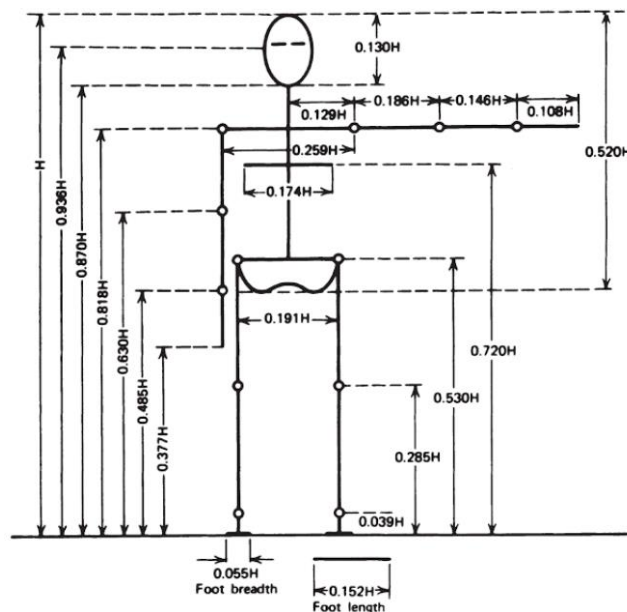


Figure 2.3.9 – Segments' lengths referred to total body height,  $H$ . [49]



## 2. Multibody Model Implementation

Segment	Definition	Segment Weight/Total Body Weight	Center of Mass/ Segment Length		Radius of Gyration/ Segment Length			Density
			Proximal	Distal	C of G	Proximal	Distal	
Hand	Wrist axis/knuckle II middle finger	0.006 M	0.506	0.494 P	0.297	0.587	0.577 M	1.16
Forearm	Elbow axis/ulnar styloid	0.016 M	0.430	0.570 P	0.303	0.526	0.647 M	1.13
Upper arm	Glenohumeral axis/elbow axis	0.028 M	0.436	0.564 P	0.322	0.542	0.645 M	1.07
Forearm and hand	Elbow axis/ulnar styloid	0.022 M	0.682	0.318 P	0.468	0.827	0.565 P	1.14
Total arm	Glenohumeral joint/ulnar styloid	0.050 M	0.530	0.470 P	0.368	0.645	0.596 P	1.11
Foot	Lateral malleolus/head metatarsal II	0.0145 M	0.50	0.50 P	0.475	0.690	0.690 P	1.10
Leg	Femoral condyles/medial malleolus	0.0465 M	0.433	0.567 P	0.302	0.528	0.643 M	1.09
Thigh	Greater trochanter/femoral condyles	0.100 M	0.433	0.567 P	0.323	0.540	0.653 M	1.05
Foot and leg	Femoral condyles/medial malleolus	0.061 M	0.606	0.394 P	0.416	0.735	0.572 P	1.09
Total leg	Greater trochanter/medial malleolus	0.161 M	0.447	0.553 P	0.326	0.560	0.650 P	1.06
Head and neck	C7–T1 and 1st rib/ear canal	0.081 M	1.000	— PC	0.495	0.116	— PC	1.11
Shoulder mass	Sternoclavicular joint/glenohumeral axis	—	0.712	0.288	—	—	—	1.04
Thorax	C7–T1/T12–L1 and diaphragm*	0.216 PC	0.82	0.18	—	—	—	0.92
Abdomen	T12–L1/L4–L5*	0.139 LC	0.44	0.56	—	—	—	—
Pelvis	L4–L5/greater trochanter*	0.142 LC	0.105	0.895	—	—	—	—
Thorax and abdomen	C7–T1/L4–L5*	0.355 LC	0.63	0.37	—	—	—	—
Abdomen and pelvis	T12–L1/greater trochanter*	0.281 PC	0.27	0.73	—	—	—	1.01
Trunk	Greater trochanter/glenohumeral joint*	0.497 M	0.50	0.50	—	—	—	1.03
Trunk head neck	Greater trochanter/glenohumeral joint*	0.578 MC	0.66	0.34 P	0.503	0.830	0.607 M	—
Head, arms, and trunk (HAT)	Greater trochanter/glenohumeral joint*	0.678 MC	0.626	0.374 PC	0.496	0.798	0.621 PC	—
HAT	Greater trochanter/mid rib	0.678	1.142	—	0.903	1.456	—	—

\*NOTE: These segments are presented relative to the length between the greater trochanter and the glenohumeral joint.

Figure 2.3.10 – Other segments information as densities, masses, centre of mass (COM)'s position and radius of gyration. Masses are referred to total body weight (M). COM's position and radius of gyration are expressed as a percentage of the segment's length. Finally, density is expressed in g/cm<sup>3</sup>. [49]

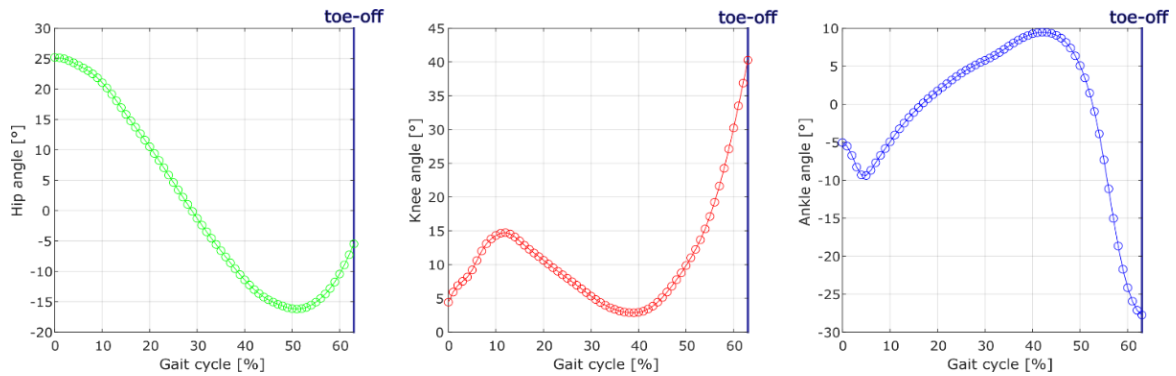


Figure 2.3.11 – From left to right: hip joint's flex-extension angle; knee joint's flex-extension angle; hip joint's flex-extension angle. Data taken from Bovi et al. study [48].

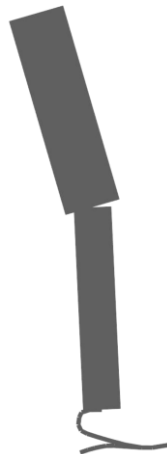


Figure 2.3.12 – Representation of the lower limb multibody model simulated. The foot segment is realized with the Highlander® multilink model.

This kind of implementation could be useful to further investigate the interarticular forces acting on different joints during gait stance phase.

## 2.4 Vari-Flex® Segmentation

For the Highlander foot, the segmentation was already done by Fey et al. (2012) [33], while I had to figure out how to segment the Vari-Flex® foot starting from its CAD model. In this chapter the procedure to realize the segmentation of a prosthetic foot will be discussed using the Vari-Flex® foot as example. This kind of segmentation is semi-automated and it can possibly be applied to different ESAR foot. The segmentation's process is schematically resumed in Figure 2.4.1 (next page).

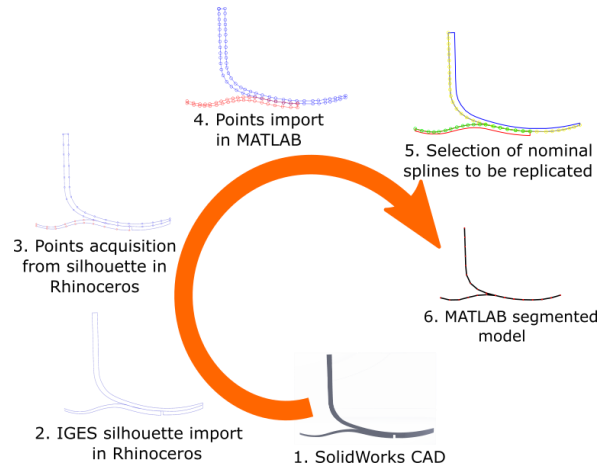


Figure 2.4.1 – Schematic representation of the segmentation process. The software I have used are SolidWorks®, Rhinoceros® and MATLAB®.

### 2.4.1 Points Import in MATLAB®

Starting from the Solidworks® CAD model of the Vari-Flex® foot (Figure 2.4.2), I have saved it as an IGES file. This file extension allows to import in Rhinoceros® the lines and the surfaces composing the model (Figure 2.4.3).

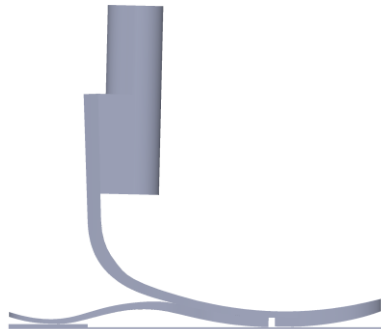


Figure 2.4.2 – Solidworks® CAD model of the Vari-Flex® foot.

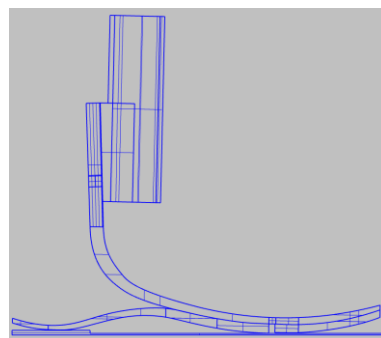


Figure 2.4.3 – Rhinoceros® IGES model of the Vari-Flex® foot.

In Rhinoceros®, all the lines except those who outline the silhouette of the two laminas forming the Vari-Flex® heel and keel sections (Figure 2.4.4) have been deleted. The little insole present under the toe section will not be considered for the further implementation.

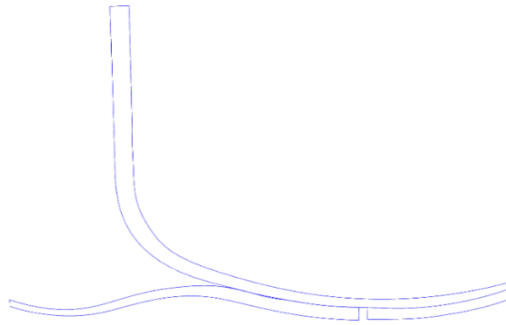


Figure 2.4.4 – Silhouette of the two laminas forming the elastic structure of the Vari-Flex foot.

Then, some arbitrary points on the Vari-Flex® silhouette have been taken. These points must be created following the order shown in Figure 2.4.5 to correctly perform the further segmentation process.

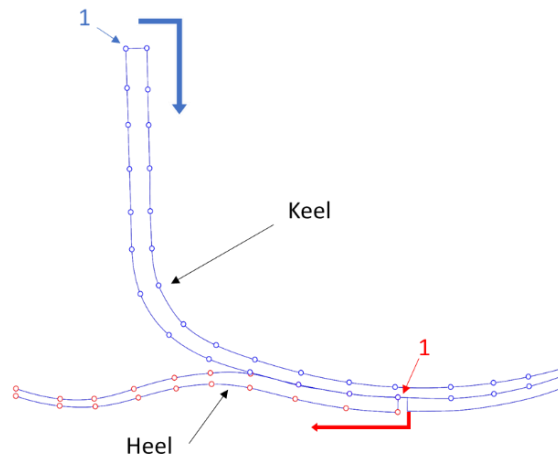


Figure 2.4.5 – Order in which the points must be created to perform the further segmentation steps. The points must be created starting from position 1 and following the arrows. Blue number and arrow refer to the keel spline, while the red ones refer to the heel spline.

To create the points, it is recommended the use of the command *Points* with options *Near*, *End* and *Point* activated. The result is shown in Figure 2.4.6.

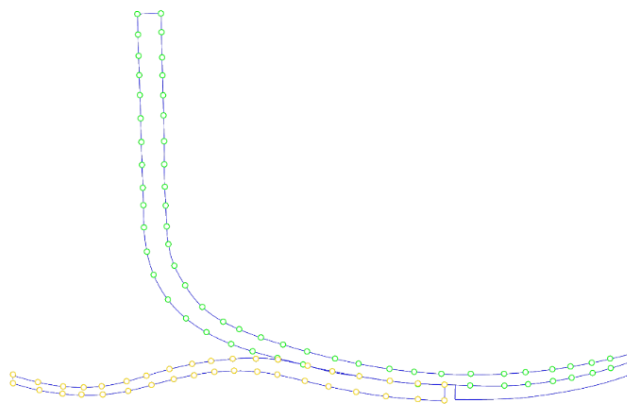


Figure 2.4.6 – Points taken on the Vari-Flex's silhouette. The green points form the keel silhouette, while the yellow points form the heel silhouette.

To import the coordinates of the points in MATLAB®, it is necessary to select the two levels containing the points. Then, save them in Point format. This command generates a .txt file, that can be easily imported in MATLAB® (Figure 2.4.7).

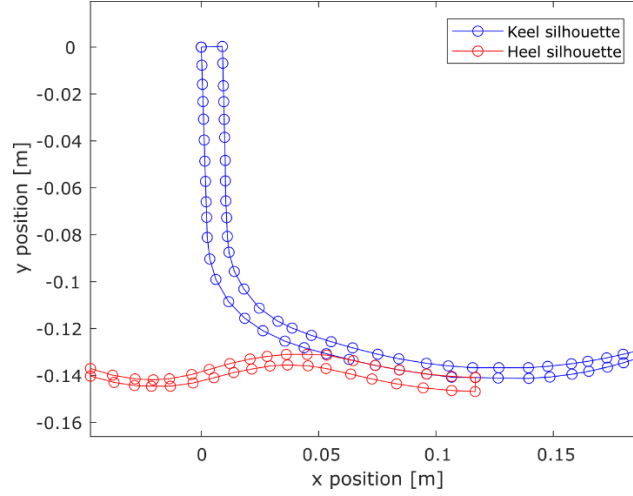


Figure 2.4.7 – Vari-Flex®'s silhouette points imported in MATLAB®.

### 2.4.2 Segmentation Methods

From these points, two splines to be segmented have been chosen. From their segmentation, the construction of the multibody model will start (Figure 2.4.8, next page).

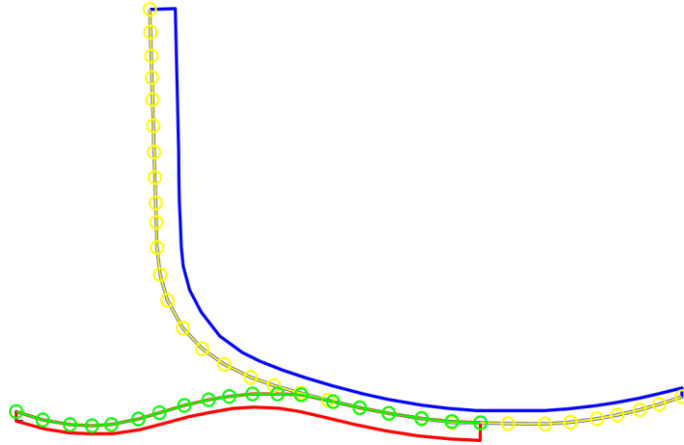


Figure 2.4.8 – The splines that will be further considered to segment the foot model are highlighted in green (heel spline) and yellow (keel spline).

Vari-Flex® has been divided in segments with equal length following the segmentation idea applied to the beam model. To do so, two methods have been implemented: the first considers the relationship between cumulative spline length and relative orientation between two following points; the second accounts the relationship between the points' x and y coordinates and cumulative spline length. So, basically, the two methods carry same information but, the first considers polar coordinates, while the second considers Cartesian coordinates. The two methods will be further explained in the further paragraphs.

#### 2.4.2.1 Polar Coordinates Segmentation Method (PCSM)

This segmentation method is based on the relationship that exist between cumulative spline length (CSL) and relative orientation (RO) between two following segments. CSL is computed as the sum of the lengths of the straight segments that form the spline, while RO is the angle included between

two following segments. The idea is to find an approximant function of this relationship to compute the coordinates of new points lying along the spline and which are separated by a fixed distance. Those points will give the final segmented splines.

It is possible to compute the nominal function that relates CSL and RO in correspondence of the nominal spline points. Since the model must be divided into an arbitrary number of segments, it was necessary to find an approximant function of the nominal relationship between CSL and RO in order to extract the relative orientation between two arbitrary points along the spline. Then, with relative orientation info it will be possible to compute the Cartesian coordinates of the points that will approximate the nominal spline.

The mathematical equations that relates the distances between two points and their relative orientation in Cartesian coordinates are presented below:

$$\begin{cases} x_{keel,i} = x_{keel,i-1} + l_{keel} \cdot \cos(\theta_{keel,i}) \\ y_{keel,i} = y_{keel,i-1} + l_{keel} \cdot \sin(\theta_{keel,i}) \end{cases}$$

*Equation 2.4.1 – Relationship between approximant segment distance, points coordinates and relative orientation between two following points for the keel spline.*

$$\begin{cases} x_{heel,i} = x_{heel,i-1} - l_{heel} \cdot \cos\left(\theta_{heel,i} + \frac{\pi}{2}\right) \\ y_{heel,i} = y_{heel,i-1} + l_{heel} \cdot \sin\left(\theta_{heel,i} + \frac{\pi}{2}\right) \end{cases}$$

*Equation 2.4.2 – Relationship between approximant segment distance, points coordinates and relative orientation between two following points for the heel spline.*

Where:

- $x_{keel,i}$  is the  $i^{th}$  point x-coordinate of the keel spline ( $x_{keel,i-1}$  is the previous point x-coordinate).
- $y_{keel,i}$  is the  $i^{th}$  point y-coordinate of the keel spline ( $y_{keel,i-1}$  is the previous point y-coordinate).
- $l_{keel}$  is the distance between  $i^{th}$  and  $(i-1)^{th}$  keel points and is computed as:

$$l_{keel} = \frac{\text{cumulative\_keel\_spline\_length}}{n_{keel}}$$

Where  $n_{keel}$  is the number of segments in which the keel spline is chosen to divide into.

- $\theta_{heel,i}$  is the relative orientation between  $i^{th}$  and  $(i-1)^{th}$  heel points. It is function of *cumulative\_heel\_spline\_length*.
- $x_{heel,i}$  is the  $i^{th}$  point x-coordinate of the heel spline ( $x_{heel,i-1}$  is the previous point x-coordinate).
- $y_{heel,i}$  is the  $i^{th}$  point y-coordinate of the heel spline ( $y_{heel,i-1}$  is the previous point y-coordinate).
- $l_{heel}$  is the distance between  $i^{th}$  and  $(i-1)^{th}$  heel points and is computed as:

$$l_{heel} = \frac{\text{cumulative\_heel\_spline\_length}}{n_{heel}}$$

Where  $n_{heel}$  is the number of segments in which the heel spline is chosen to divide into.

- $\theta_{keel,i}$  is the relative orientation between  $i^{th}$  and  $(i-1)^{th}$  keel points. It is function of *cumulative\_keel\_spline\_length*.

The selected notations are better explained in Figure 2.4.9.

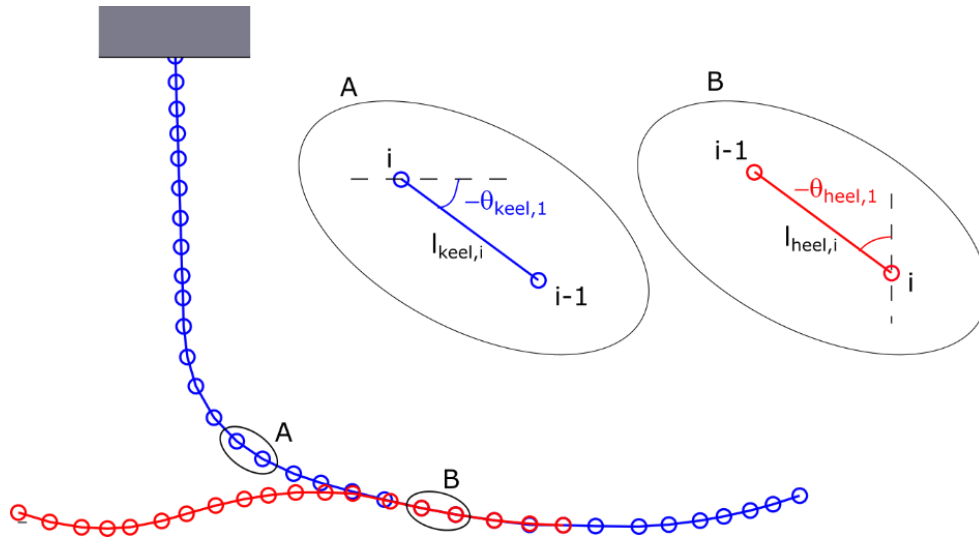


Figure 2.4.9 – Relevant measures for polar-coordinates-based segmentation.

Once an approximant function of the relationships between RO and CSL is found, with the use of Equation 2.4.1 and Equation 2.4.2 it is possible to find the coordinates of the new points that will describe the keel and heel splines.

In Figure 2.4.10 is presented the relationship between relative orientation and cumulative spline length for heel and keel splines (black line) and the approximant function found using MATLAB®'s function `interp1`. The approximant function (green line) is computed considering the cumulative spline length, but with different steps. These new steps are equal to  $l_{heel}$  or  $l_{keel}$  depending on which spline is currently analysed.

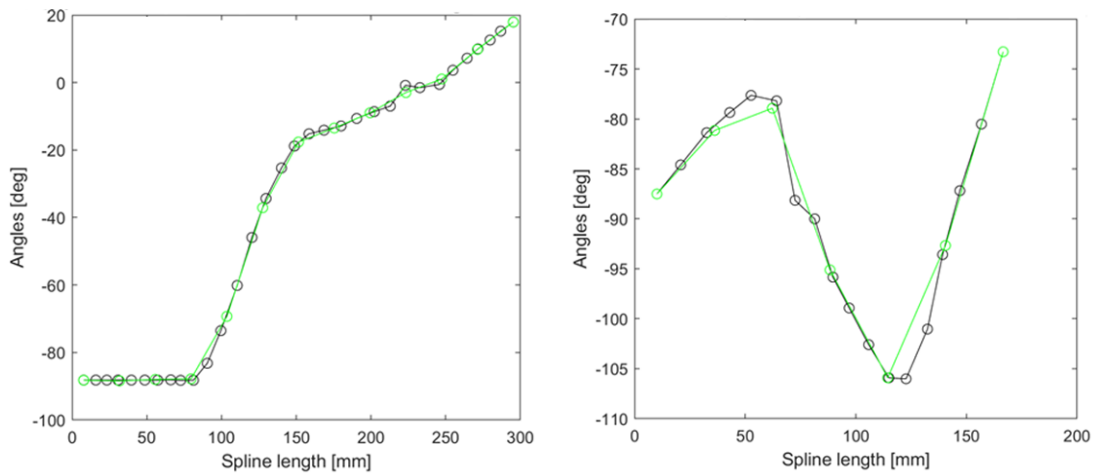


Figure 2.4.10 – Relationship between points' relative orientation and cumulative spline length. The former relationship of the nominal splines is coloured in black, while the approximant function found is coloured in green. The graphic on the left is referred to the keel spline, while the one on the right refers to the heel spline.

The user, then, must insert into MATLAB® Command Window the number of desired segments to divide the spline into. The number of points forming the spline, consequently, will be the number of segments plus one.

Using the coordinates calculated with Equation 2.4.1 and Equation 2.4.2 it is possible to obtain the reconstructed splines shown in Figure 2.4.11. It is easy to notice that the reconstructed splines introduce geometrical error into the model. This is the reason why the second segmentation method has been implemented.

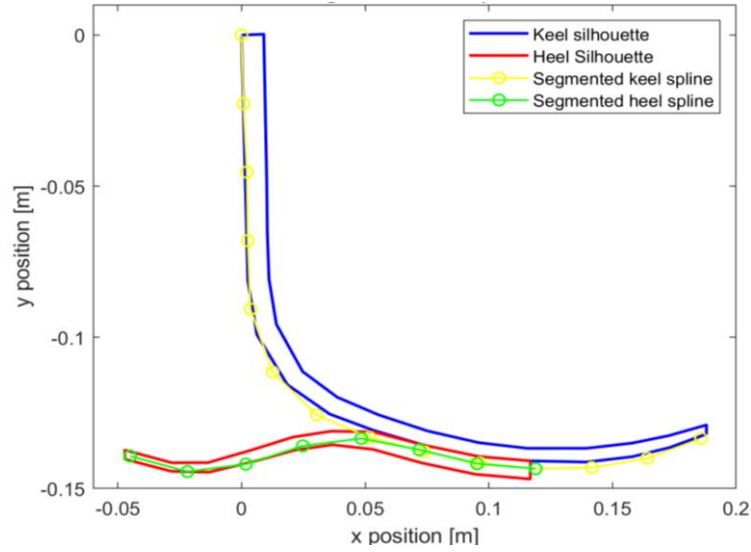


Figure 2.4.11 – Reconstructed splines using polar coordinates segmentation method.

#### 2.4.2.2 Cartesian Coordinates Segmentation Method (CSSM)

The complete script which perform this kind of segmentation is presented in Appendix A – 3<sup>rd</sup> paragraph: Cartesian Coordinates Segmentation Method – ‘segmentation\_auto\_DEF.m’

The aim of this new logic of segmentation is to produce less or none geometrical error in the segmented model when compared to the nominal one.

This method considers the relationship between x and y coordinates of the splines’ points and the cumulative spline length (better explained in Figure 2.4.12). The new points’ coordinates will be no more computed using Equation 2.4.1 and Equation 2.4.2 but they will be directly calculated from the approximant function.

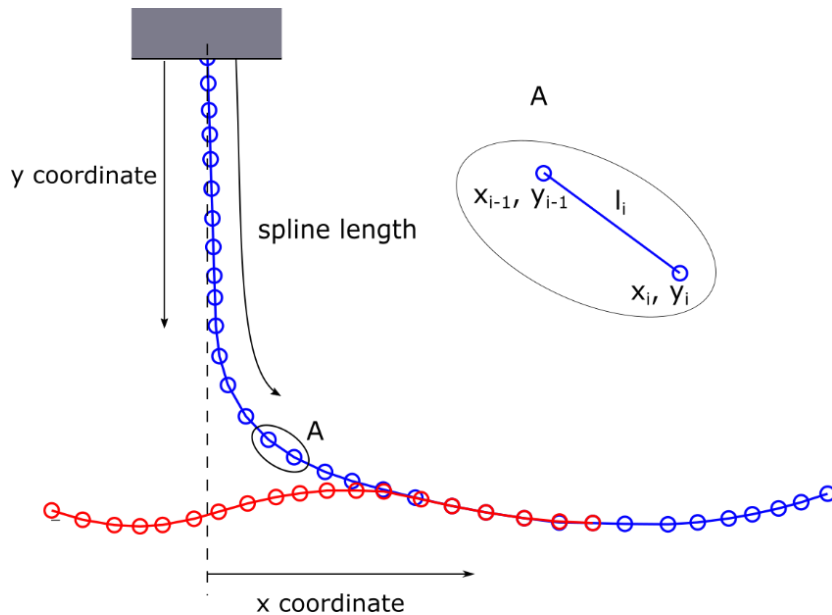


Figure 2.4.12 - Relevant variables for cartesian-coordinates-based segmentation

As it is possible to notice from Figure 2.4.14 (next page), this relationship can be approximated with a function that introduces a smaller error and allows to segment the nominal splines in a more satisfactory way (Figure 2.4.13).

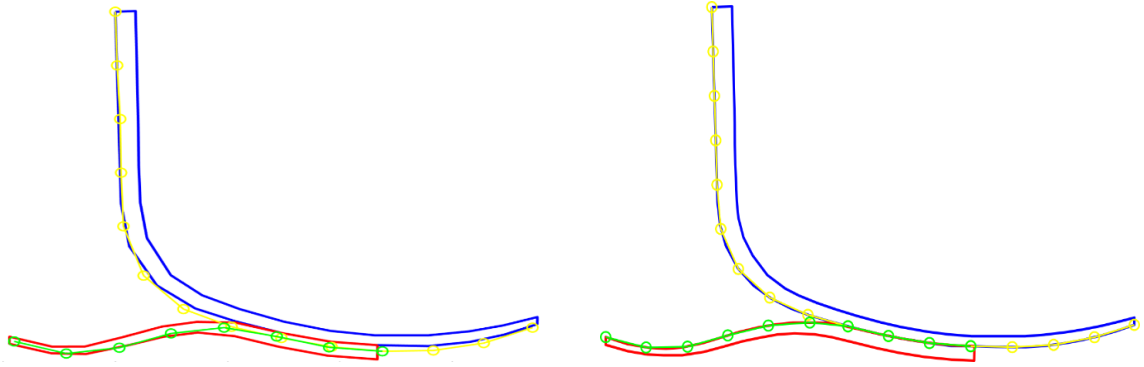


Figure 2.4.13 – Comparison between the two segmentation methods. The one on the left (PCSM) introduces a significant geometrical error, especially where the two splines touch and on the heel. The segmentation on the right (CSSM) better approximates the nominal curves.

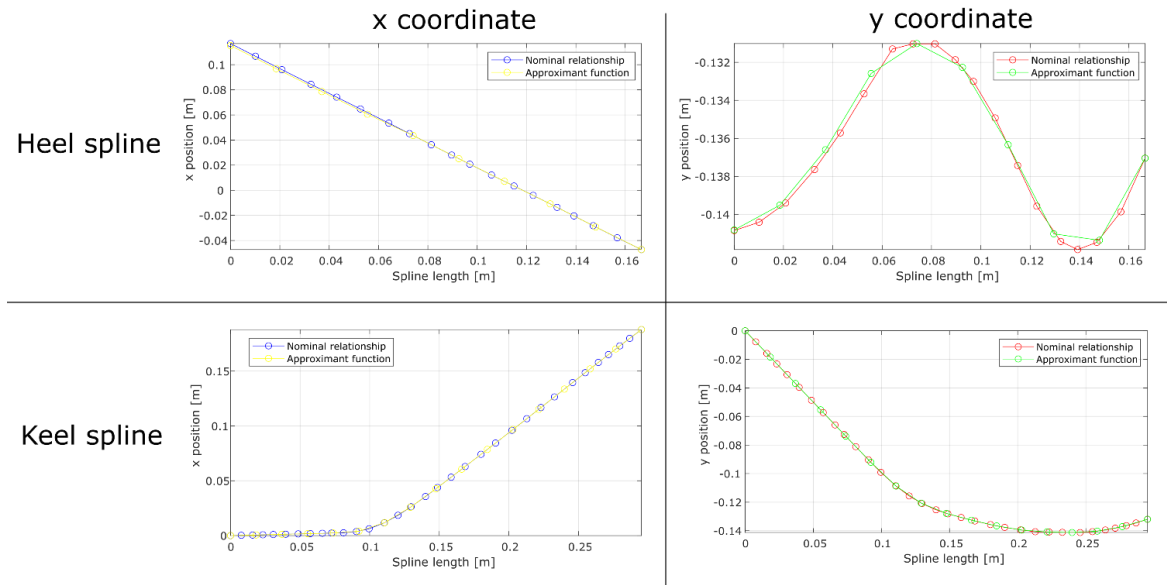


Figure 2.4.14 – Comparison of the nominal relationship between x and y coordinates and the cumulative spline length and the approximant function. Going from left to right and from up to down, the figures refers to heel spline x coordinate, heel spline y coordinate, keel spline x coordinate and keel spline y coordinate relationships with the cumulative spline length.

### 2.4.3 Semi-Automated Segmentation Script (CSSM)

The complete script can be found at Appendix A's third paragraph: Cartesian Coordinates Segmentation Method – 'segmentation\_auto\_DEF.m'

This MATLAB®'s script perform the Cartesian Coordinates Segmentation Method discussed above. In this paragraph only the most relevant parts of the script will be detailed:

- Silhouette points' coordinates import
- Points' coordinates management
- Keel and heel segmentation

Finally, the necessary inputs to correctly run the script and the outputs that it will return and save in a specific MATLAB® file (\*.m) will be resumed.



The segmentation process could be considered as “semi-automated” since the user must insert some parameters from keyboard and he should possibly change the script when using different .txt files.

#### 2.4.3.1 Coordinates Import and Management

First, the origin of the reference system has been shifted where there is the upper point of the keel silhouette (Figure 2.4.15), that will be also the first point of the keel spline. This point coordinates are named `x_corr` and `y_corr` in the script presented below. `coord_keel` and `coord_heel` are, respectively, the new coordinates of the keel and heel silhouette referred to the new reference system.

```
x_corr=coord_keel(1,1);
y_corr=coord_keel(1,2);

coord_keel=[coord_keel(:,1)-x_corr coord_keel(:,2)-y_corr];
coord_heel=[coord_heel(:,1)-x_corr coord_heel(:,2)-y_corr];
```

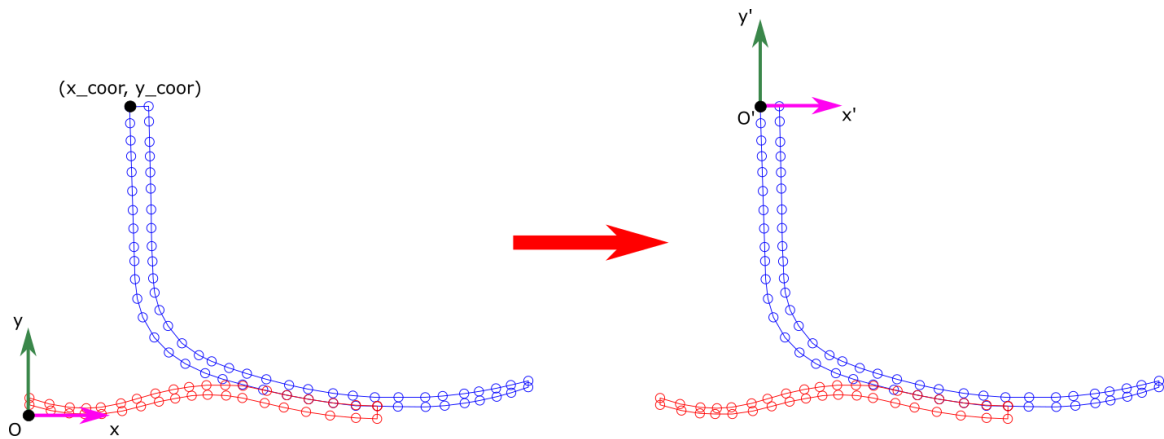


Figure 2.4.15 – On the left, the original reference system and the new desired origin are shown. On the right the new reference system derived from the coordinates shift is presented.

#### 2.4.3.2 Selection of the Nominal Splines.

From the silhouette points only two splines have been considered. To do so, the ID numbers of the points that were forming the nominal splines (already shown in Figure 2.4.15) must be manually inserted in the script.

```
start_keel=1;
end_keel=33
start_heel=1;
end_heel=19
coord_keel=coord_keel_sil(start_keel:end_keel,:);
coord_heel=coord_heel_sil(start_heel:end_heel,:);
```

The most internal splines have been selected instead of the outer ones because they will be more convenient to design the multibody model (described in paragraph 2.5).

#### 2.4.3.3 Segmentation Process

The script architecture regarding the segmentation process is formally divided in keel segmentation and heel segmentation.

The first task executed by the script is the keel segmentation. To do so, it is necessary to compute the keel spline cumulative length (`cum_len_sr_keel`), which is necessary information to do all the consequent tasks. The cumulative spline length is obtained doing a cumulative sum over the distances of the keel spline points (`len_sr_keel`).

```
j=1;
for i=2:length(coord_keel)
    len_sr_keel(j)=sqrt(sum((coord_keel(i,:)-coord_keel(i-1,:)).^2));
    j=j+1;
end
cum_len_sr_keel=[0 cumsum(len_sr_keel)]
```

Then, the user must insert from the Command Window the number of segments desired to segment the keel spline.

```
prompt='\nType the number of rigid segments in which you want to di-
vide the keel spline: ';
Nkeel=input(prompt);
```

Command Window

```
fx Type the number of rigid segments in which you want to divide the keel spline: |
```

Now the script performs the two fundamental segmentation processes on the keel spline: interpolation of nominal spline coordinates over the cumulative spline length and calculation of new spline coordinates from the relationship found. To do both the tasks, there is a useful function already implemented in MATLAB® named `interp1`.

```
method='linear';
coord_keel_fit(:,1)=interp1(cum_len_sr_keel,coord_keel(:,1),lin-
space(0,cum_len_sr_keel(end),Nkeel+1),method);
coord_keel_fit(:,2)=interp1(cum_len_sr_keel,coord_keel(:,2),lin-
space(0,cum_len_sr_keel(end),Nkeel+1),method);
```

X-coordinates and y-coordinates interpolations are performed in two different steps. The result is shown in Figure 2.4.16 (next page). The interpolation method chosen is “linear” because even if it is the simplest interpolation method among all the ones granting continuity proposed by MATLAB®, it does not present any significant difference with respect to the others and it is also the fastest to run among them, as reported in MATLAB® documentation online [50].

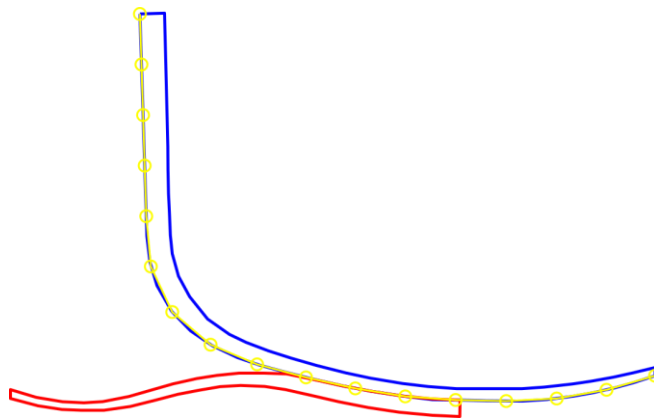


Figure 2.4.16 – Segmented keel spline.

Heel segmentation process is similar, but the user must insert from the Command Window additional information (as well as the desired number of heel segments – `Nheel`): the number of segments that the two splines have in common (`common_sr`) and the ID number of the keel point which the heel spline is attached to (`start_heel`). To do so, the user could help himself watching figure 3 (Figure 2.4.17), as suggested by the Command Window prompt. Those parameters are schematized in Figure 2.4.18 (next page).

```
prompt='\nType the number of rigid segments which you want to divide
the heel spline into: ';
Nheel=input(prompt);
prompt='\n\nWATCH FIGURE 3 - Type the number of segments that are
shared by the keel spline and the heel spline: ';
common_sr=input(prompt);
```

```
prompt='\n\nWATCH FIGURE 3 - Type the keel point ID number that links
keel and heel spline: ';
start_heel=input(prompt);
```

Command Window

`fx` Type the number of rigid segments in which you want to divide the heel spline:

Command Window

`fx` WATCH FIGURE 3 - Type the number of segments that are shared by the keel spline and the heel spline:

Command Window

`fx` WATCH FIGURE 3 - Type the keel point ID number that links keel and heel spline:

The ID number of the heel junction is necessary to correctly reconstruct the selected splines, while the number of segments shared by heel and keel splines is useful for the further construction of the multibody model: with this information, it is possible to make these segments equally long, both for heel spline and keel spline. So, it will be possible to group them in a single body.

Once these parameters are given to the script, it will proceed with the actual heel segmentation process following the same logic that rules the keel segmentation process. This time there will also be few code lines that make the segments shared by heel and keel splines of the same length. This result is achieved by making the heel segments of the same length of the keel segments.

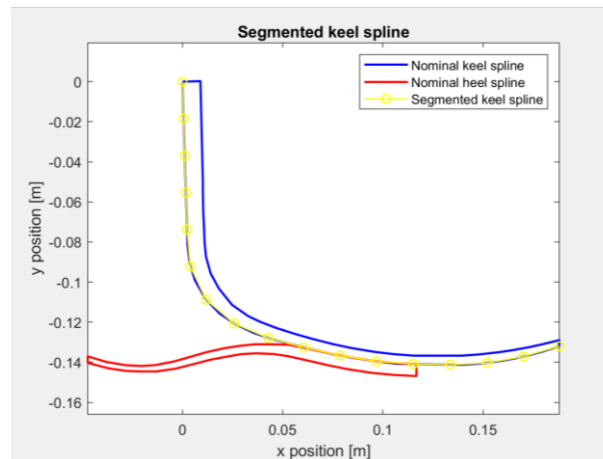


Figure 2.4.17 – ‘Figure 3’ generated by the segmentation script. It helps the user to decide how many segments keel and heel spline have in common and which is the ID number of the heel junction point.

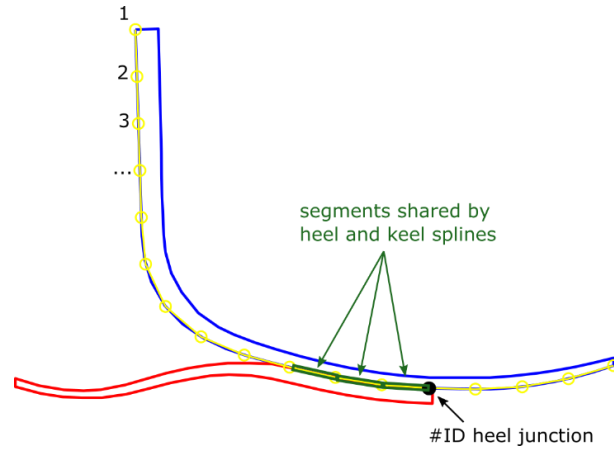


Figure 2.4.18 – Basic information to give to MATLAB® Command Window (together with heel segments number) to perform the heel segmentation.

```
j=1;
for i=2:length(coord_heel)
    len_sr_heel(j)=sqrt(sum((coord_heel(i,:)-coord_heel(i-1,:)).^2));
    j=j+1;
end
cum_len_sr_heel=[0 cumsum(len_sr_heel)];
L_heel=sum(len_sr_heel);

coord_heel_fit(:,1)=interp1(cum_len_sr_heel,coord_heel(:,1),lin-
space(0,cum_len_sr_heel(end),Nheel+1),method);
coord_heel_fit(:,2)=interp1(cum_len_sr_heel,coord_heel(:,2),lin-
space(0,cum_len_sr_heel(end),Nheel+1),method);
j=1;
for i=1:common_sr+1
    if i==1
        coord_heel_fit(j,:)=coord_keel_fit(start_heel,:);
        j=j+1;
    else
        coord_heel_fit(j,:)=coord_keel_fit(start_heel-i+1,:);
        j=j+1;
    end
end
end
```

At the end of the segmentation process, the script will save splines' x and y coordinates, the number of heel and keel segments, the ID number of the heel junction and the number of segments shared by the two splines in a file called "foot\_info\_*number of keel segments*\*\_*number of heel segments*.m".

```
foot_coord=[coord_keel_fit; coord_heel_fit];
str=sprintf('foot_info_%s_%s',string(Nkeel),string(Nheel));
save(str,'foot_coord','Nkeel','Nheel','start_heel','common_sr')
```

#### 2.4.4 Final Segmented Model

From the computed Vari-Flex® segmentations it is possible to realize various models. The aim is to obtain a model made up of a reasonable number of rigid segments (less than 30). When the number

of segments increase too much the risk is to approximate FEA using a multibody software. Plus, the heel spline and keel spline intersection point had to be not too far from where the real junction point is and the length of the first heel spline segment should not differ too much from the one of the corresponding segment on keel spline.

To achieve this, many Vari-Flex® segmented model were realised. Those who were not fulfilling the previous requirements had been rejected. Fortunately, these objectives were easily to check by view. Figure 2.4.19 shows the fulfilling segmented models, while Figure 2.4.20 shows an example of a model considered not satisfactory.

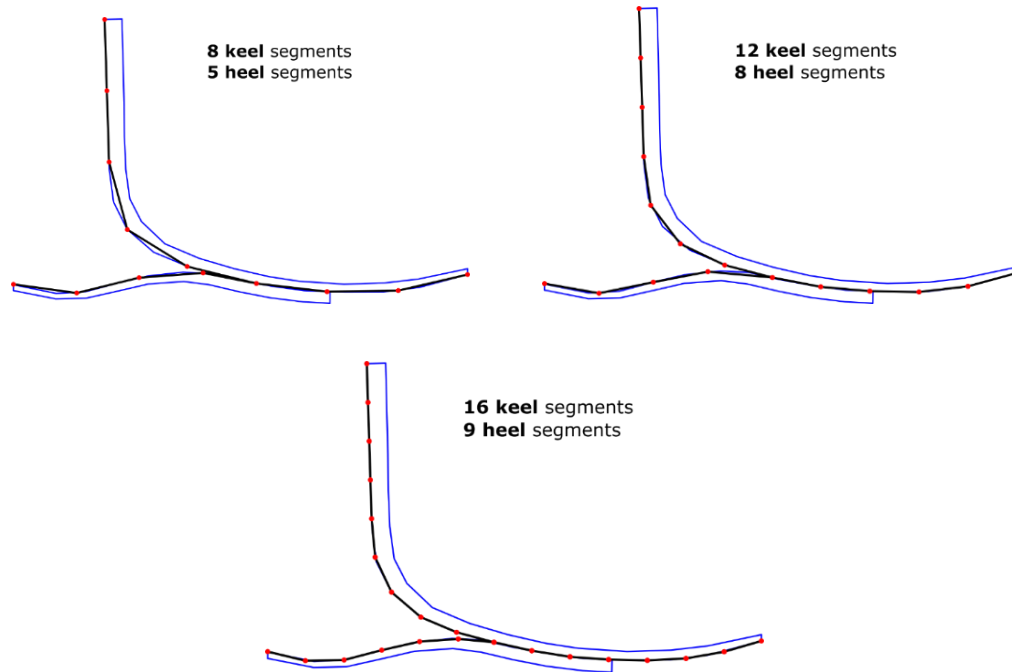


Figure 2.4.19 – Example of segmented multibody models that respect the requirements described before. Especially, the third model here presented will be the one used to conduct the further analysis.

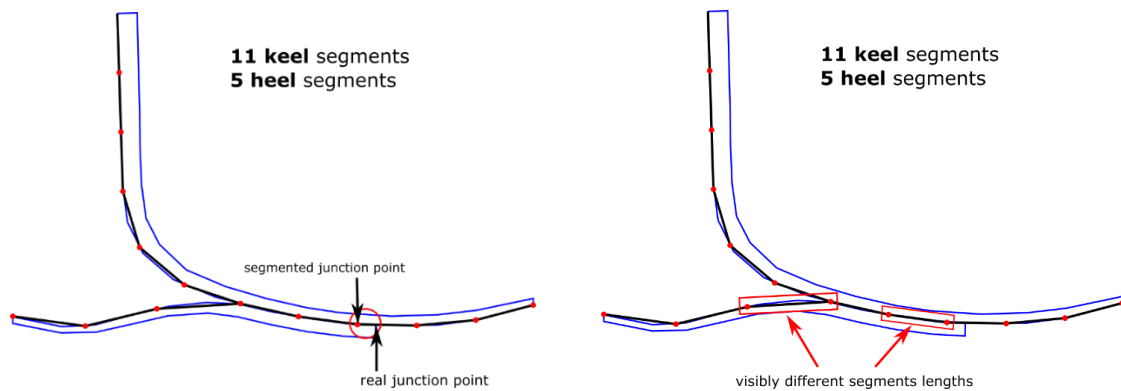


Figure 2.4.20 – Example of a segmented model that does not fulfil the requirements.

From the three models shown in Figure 2.4.19, the third one has been chosen to perform the further analysis. The model is composed of 16 keel segments and 9 heel segments, it better reproduces the shape of the two splines, the junction point is very close to the real one and its keel and heel segments have roughly the same length. Moreover, it better follow the curves of the Vari-Flex® model.

The next paragraph is committed to explain how the Vari-Flex® multibody model has been realized in Simulink® starting from the current segmentation.

## 2.5 Vari-Flex® Multibody Model

In this paragraph the geometrical and elastic features of the Vari-Flex® multibody model will be discussed. Especially, this model (inserted in different simulated testing environments) will be used to analyse the quasi-static and dynamic behaviour of the Vari-Flex® prosthetic foot. These two analyses will be addressed, respectively, in Chapter 3 and Chapter 5.

Once the Vari-Flex® multibody scheme is realized, simulation of quasi-static compression tests will be performed with it. The tests will simulate foot compression while the Vari-Flex® is kept at certain angles with respect to the vertical axis perpendicular to compression plate. Since contacts will not be modelled, in the simulations there will not be a physical plate that will transmit a contact force to the model, but an external concentrated force will be applied to the Vari-Flex® in arbitrary points. This process will be treated in paragraph 3.1.

Since rotational stiffness and damping values given to the model joints are computed utilizing Equation 2.2.25 and Equation 2.2.26 deducted for a loaded wedged bar in paragraph 2.2, the simulated quasi-static tests will probably not show the same results of the experimental ones. For this reason, a stiffness and damping parameters tuning has been later performed. The tuning modality will be further discussed in paragraph 3.2.

Once the model is tuned, it will be used to simulate the stance phase of the gait cycle (this phase will be discussed in Chapter 5). Once again, since contacts between bodies are not modelled, the external forces applied to the model and their application points will be given as model inputs. Biomechanical gait data have been acquired for this reason (data acquisition and processing will be better discussed in Chapter 4).

### 2.5.1 Model Realization in Simulink®/MATLAB®

*Vari-Flex® Simulink® scheme is shown in Appendix B – fourth paragraph: Vari-Flex® multibody model - 'sim\_vari\_flex\_16\_9\_geom.slx'.*

To realize the Vari-Flex® multibody model the same approach followed for the beam and the Highlander® multibody models has been adopted: all the inertial properties were concentrated in *Solid* blocks, while the viscoelastic properties are related to the joint elements. Once again, the selected joints are *revolute* ones; therefore, they allow a single rotational degree of freedom between two following rigid segments. In this paragraph it will better explained how the Simscape blocks must be programmed.

#### 2.5.1.1 Rigid and Flexible Bodies

Referring to the Vari-Flex® model shown in Figure 2.5.1 (next page), it is possible to recognize the different parts composing the prosthetic foot.

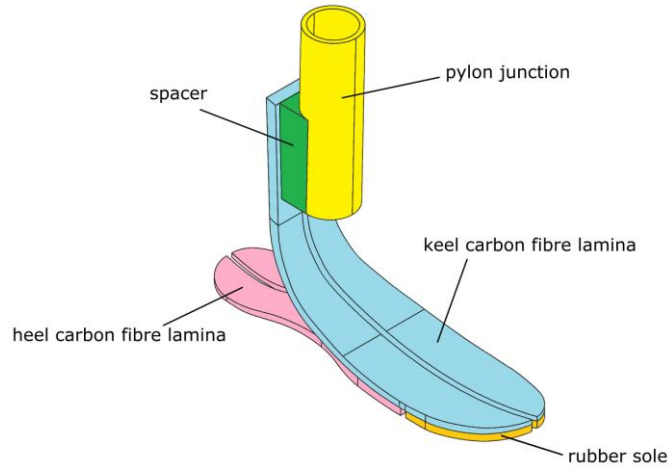


Figure 2.5.1 – Vari-Flex® parts detailed. The rubber sole will be not considered in the multibody model.

Each part of the model can be considered as a rigid or an elastic element. The parts considered as elastic bodies in the multibody model are:

- *Keel carbon fibre lamina*
- *Heel carbon fibre lamina*

While the rigid bodies are:

- *Spacer*
- *Pylon junction*

These parts are considered as rigid bodies since they have reduced flexing capabilities with respect to the two carbon fibre laminas. As said before, the rubber sole will not be modelled.

Referring to the model realization with Simulink®, rigid bodies are connected to each other with *Rigid Transform* blocks (as presented in Figure 2.5.2). These blocks do not allow any relative rotation or translation between the two connected bodies but, permit to define an angular orientation value between the two segments that will be kept during the simulation. For flexible bodies, instead, *Rotational Joints* have been used, as it has been already done for Highlander® foot modelling (example in Figure 2.5.3). These joints permit one rotational degree of freedom.

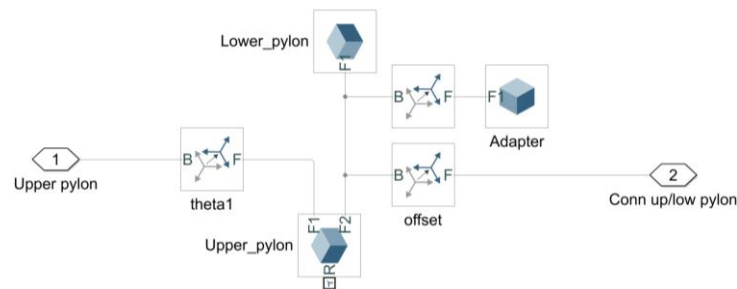


Figure 2.5.2 – Details of pylon junction modeling – rigid body.

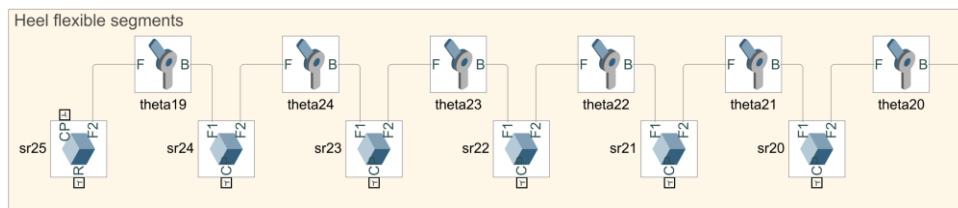


Figure 2.5.3 – Details of heel lamina modeling – flexible body.

The only exception made when building flexible bodies is the first segments forming the keel lamina: the rigid segments are joined using *Rigid Transform* blocks instead of *Revolute Joints* blocks. In fact, these segments could not undergo large deformations due to external constraints as the pylon junction's cylinder can be.

### 2.5.1.2 Geometrical and Material's Parameters

Once realized the Simulink®'s model, it is necessary provide it with geometrical and material's parameters of Vari-Flex® foot. To do so, it has been written a MATLAB® script. The fundamental parameters describing the model are:

- For flexible laminas
  - Segments length ( $L_i$ ) – taken from segmentation data.
  - Segments width ( $W_i$ ) – taken from Vari-Flex® CAD.
  - Segments thickness ( $H_i$ ) – taken from Vari-Flex® CAD.
  - Carbon fibre's density ( $\rho = 1.80 \text{ g/cm}^3$ ) – T700S (TORAY, Toray Composite Materials America, Inc.).
  - Carbon fibre's Young Modulus ( $E = 55 \div 75 \text{ GPa}$ ) – taken from L. Cavallaro et al. study (Master's Degree Thesis) of a FEM model of the Vari-Flex® foot [51].
  - Rotational stiffnesses value ( $k_{R,i}$ ) – calculated from Equation 2.2.25 and Equation 2.2.26.
  - Rotational damping values ( $\beta_{R,i}$ ) – assumed near to 0 since carbon fibres have low damping ratio.
- For spacer and pylon junction (parameters are directly inserted in Simulink's blocks, they are not written in the MATLAB script)
  - Cylinder length ( $L_C$ ) – taken from Vari-Flex® CAD.
  - Cylinder's internal radius ( $r_{min}$ ).
  - Cylinder's external radius ( $r_{max}$ ).
  - Spacer geometry – directly given from its CAD® model.

### 2.5.2 Final Multibody Models

Two different models of Vari-Flex® foot (shown in Figure 2.5.4) have been realized using previously listed data:

- *Simple* model
- *Complex* model

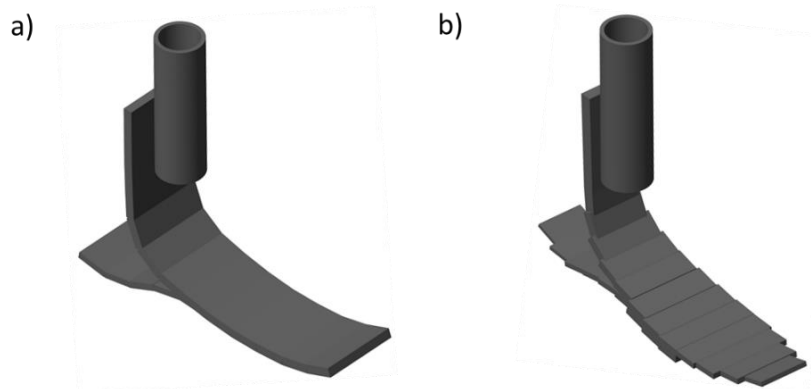


Figure 2.5.4 – a) Simple multibody model. b) Complex multibody model.



The two models are essentially the same but, while the *Simple* model has segments of the same length, width and thickness, the *Complex* model's segments more accurately reproduce the real Vari-Flex® shape. The advantage of the simpler one is that there is no need to measure the different segments' width and thickness from the CAD model.

The test executed on both models to decide which one had the best results will be described in Paragraph 3.2.



### 3. Quasi-Static Simulations & Multibody Model Tuning

In this chapter the methods used to reproduce the quasi-static compression tests executed on a Vari-Flex® foot by L.Cavallaro et al. [51] will be described. During this latter study it is also been developed a FEA model of the Vari-Flex® foot. L.Cavallaro (now working for Fondazione IIT's Rehab Technologies Department) has recently improved the model based on FEA that is able to reproduce the Vari-Flex®'s force-deflection curve in quasi-static condition. Data shown in paragraph 3.1.3 are obtained from the improved model.

The purpose of the multibody model simulations is to characterize the model's viscoelastic properties. Since it is not expected that analytical rotational stiffnesses values (computed from Equation 2.2.25 and Equation 2.2.26) will make the model perfectly simulate the quasi-static behaviour of the prosthetic foot, the rotational stiffness and damping values has been tuned to reproduce the force-deflection curve obtained with experimental tests and FEA.

After this tuning phase the tuned multibody model will be used to simulate a complete stance phase: from heel-strike to toe-off.

In the further paragraphs the experimental mechanical conditions are briefly described and the force-deflection curves obtained from both the mechanical tests and FEA are presented. Then, it will be explained how reproduce quasi-static test with Vari-Flex® multibody model and how the MATLAB®'s tool used for the tuning works. Finally, tuning process settings will be discussed.

#### 3.1 Experimental Quasi-Static Tests and FEM Simulations

##### 3.1.1 Equipment for Experimental Quasi-static Tests

*Information described in this Paragraph is taken from L. Cavallaro's Master Thesis [51].*

The quasi-static mechanical tests on the Vari-Flex® foot were carried out at DIMEAS' (Dipartimento di Ingegneria Meccanica e Aerospaziale) Laboratory of Mechanics, part of the Politecnico di Torino. Here there is a fatigue testing machine Instron 8801 (Figure 3.1.1, on the right). This testing machine has a hydraulic compression system capable of supply up to 100 kN for 150 mm of stroke. The hydraulic system is powered with 207 bar and instrumented with a Dynacell loading cell.

The loading platform is secured to the lower part of the machine with a vise. In the upper part, instead, there is a crescent-shaped (Figure 3.1.2, next page) metallic support that allows to test the Vari-Flex® at different angles with respect to the vertical. This special support is secured to the upper part of the machine with a vise, while the Vari-Flex® is screwed on it. The support with the prosthetic foot mounted on it is shown in Figure 3.1.3 in the following page.



Figure 3.1.1 – Fatigue testing machine Instron 8801. [51]

The machinery is controlled in position: the speed of movement of one of the machine's arms (upper or lower) must be set. The testing machine stops when it reaches a predefined force value.



Figure 3.1.2 – Details of the crescent-shaped special support designed by L.Cavallaro et al. [51]



Figure 3.1.3 – Crescent-shaped support with the Vari-Flex® screwed on it. [51]

### 3.1.2 Testing Conditions

With the experimental set up described in the previous paragraph the Vari-Flex® has been originally tested in 6 different configurations [51] (resumed in Table 3.1.1). The loading speed is referred to the lower loading support.

Table 3.1.1 – Quasi-static testing condition's resume [51]

Trial	Loading speed [mm/min]	Force limit [N]
20° heel touch	5	750
10° heel touch	1	1200
0° foot flat	1	2000
10° toe touch	5	1200
20° toe touch	6	1450
30° toe touch	5	1000

Recently, these tests were replied by Fondazione IIT's Rehab Technologies Department with the same experimental set up: those data has been used for the further work implementation. The new

testing conditions do not consider foot  $30^\circ$  toe touch test and *foot flat* test<sup>3</sup> and are resumed in Table 3.1.2, while a schematic representation of them is shown in Figure 3.1.4.

Table 3.1.2 – New quasi-static testing condition's resume.

Trial	Loading speed [mm/min]	Force limit [N]
$20^\circ$ heel touch	10	400
$10^\circ$ heel touch	10	800
$10^\circ$ toe touch	10	800
$20^\circ$ toe touch	10	400

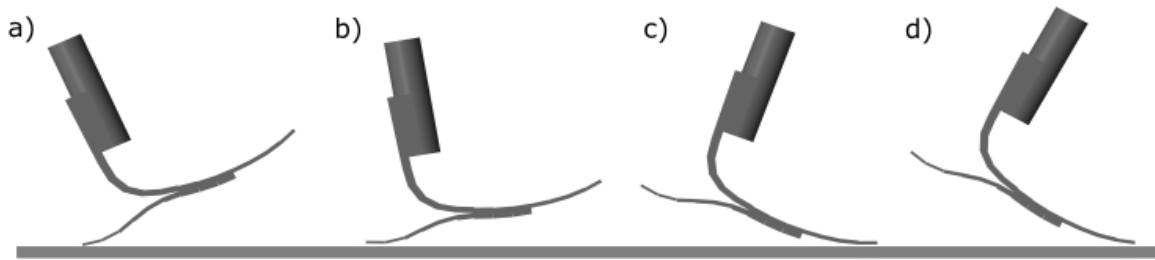


Figure 3.1.4 – a)  $20^\circ$  Heel touch configuration. b)  $10^\circ$  Heel touch configuration. c)  $10^\circ$  Toe touch configuration. d)  $20^\circ$  Toe touch configuration.

### 3.1.3 Experimental and FEM Force-Deflection Graph

In this paragraph the force-deflection diagram found for each trial condition are presented.

From the figures below (from Figure 3.1.5 to Figure 3.1.8) it can be noticed how FEM simulation can approximate the non-linear behaviour of the force-deflection relationship.

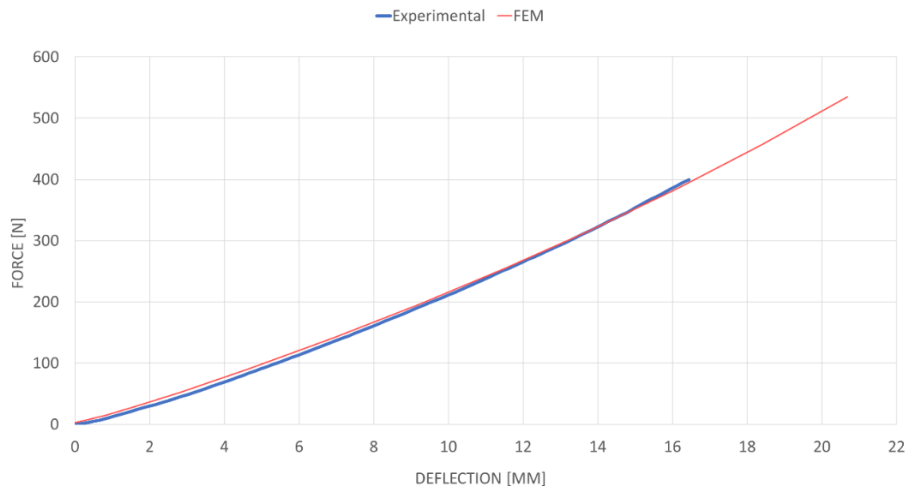


Figure 3.1.5 – Force-deflection diagram for  $20^\circ$  toe touch loading condition.

<sup>3</sup>  $30^\circ$  toe touch testing conditions was not considered because the experiments were recently remade by L. Cavallaro and he did not test anymore this condition. Hence, the data related to it were not available. For *foot flat* condition the problem is related to the model here used: It is not possible to determine which points must be loaded to simulate this loading condition.

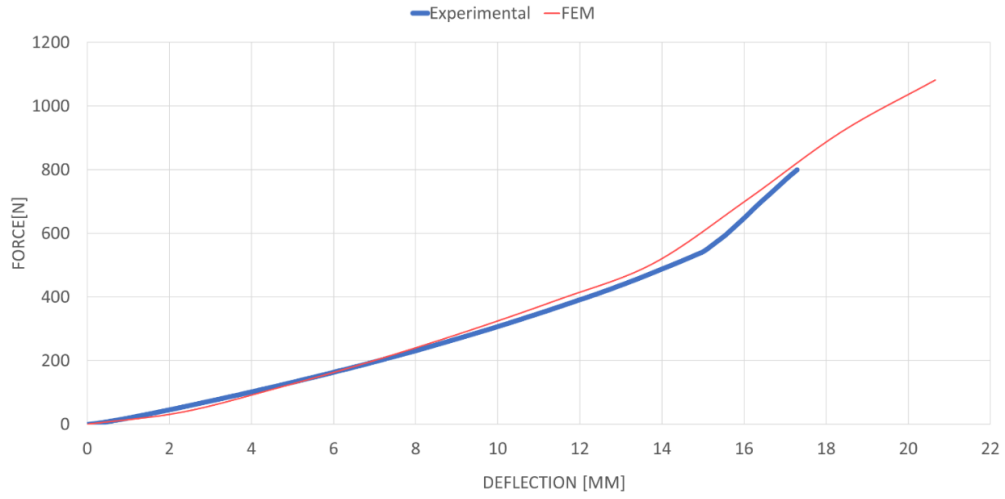


Figure 3.1.6 – Force-deflection diagram for 10° toe touch loading condition.

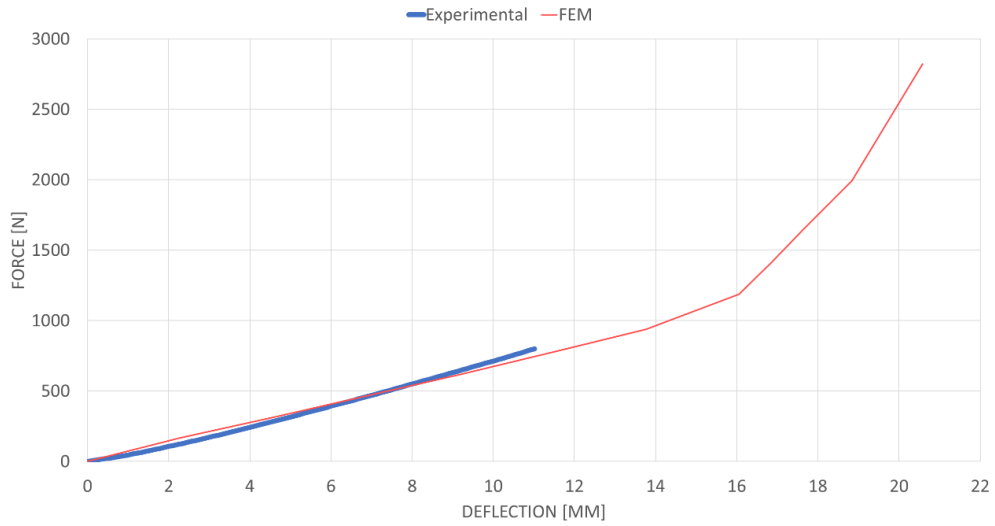


Figure 3.1.7 – Force-deflection diagram for 10° heel touch loading condition.

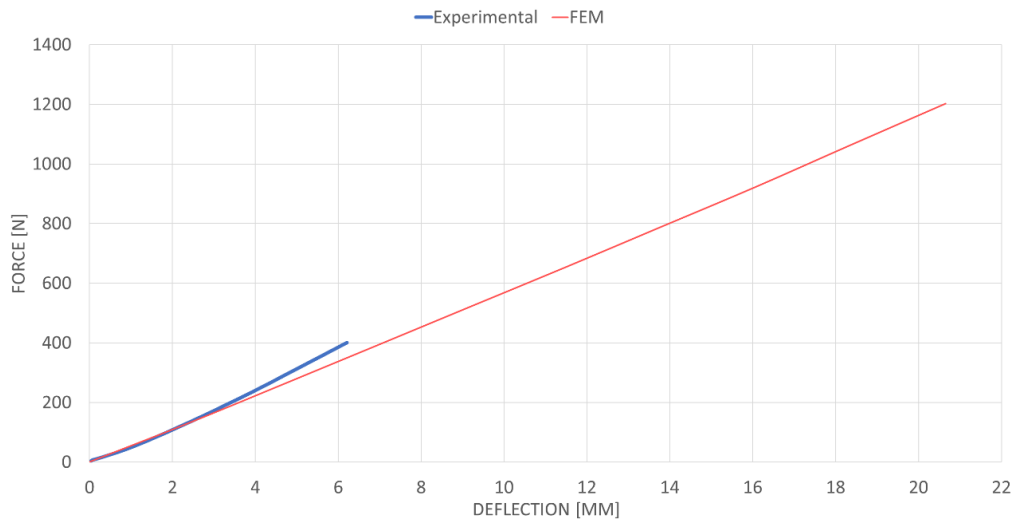


Figure 3.1.8 – Force-deflection diagram for 20° heel touch loading condition.

These are the experimental and computational results the model is expected to achieve. The experimental results will also be considered as the objective function for further stiffness tuning.

## 3.2 Simulation of Quasi-Static Test with Vari-Flex® Multibody Model

### 3.2.1 Set Up of Quasi-Static Simulations in MATLAB/Simulink

The Simulink scheme can be found at Appendix B – fifth paragraph: Quasi-Static Simulation 20 Heel Vari-Flex® Model – ‘sim\_vari\_flex\_mech\_test\_heel\_20.slx’. The MATLAB® script associated to it can be found at Appendix A – fourth paragraph: Quasi-Static Simulation (with Geometrical Information) – ‘load\_test\_geom.m’

In these simulations, the foot must be tilted to a certain angle (the heel or the toe must be tilted of 10 or 20 degrees with respect to the loading plate) and the force must be applied to the lowest foot’s point in order to reproduce the effect of the contact between loading plate and Vari-Flex®. To achieve this, it is possible to control the pylon angle with a *Rigid transform* block and connected an *External force and torque* block to the lowest point.

Since not all the Simulink®’s schemes associated to each loading condition are shown in Appendix B, in Figure 3.2.1 the points where the force is applied during the quasi-static test simulation are pointed out with arrows.

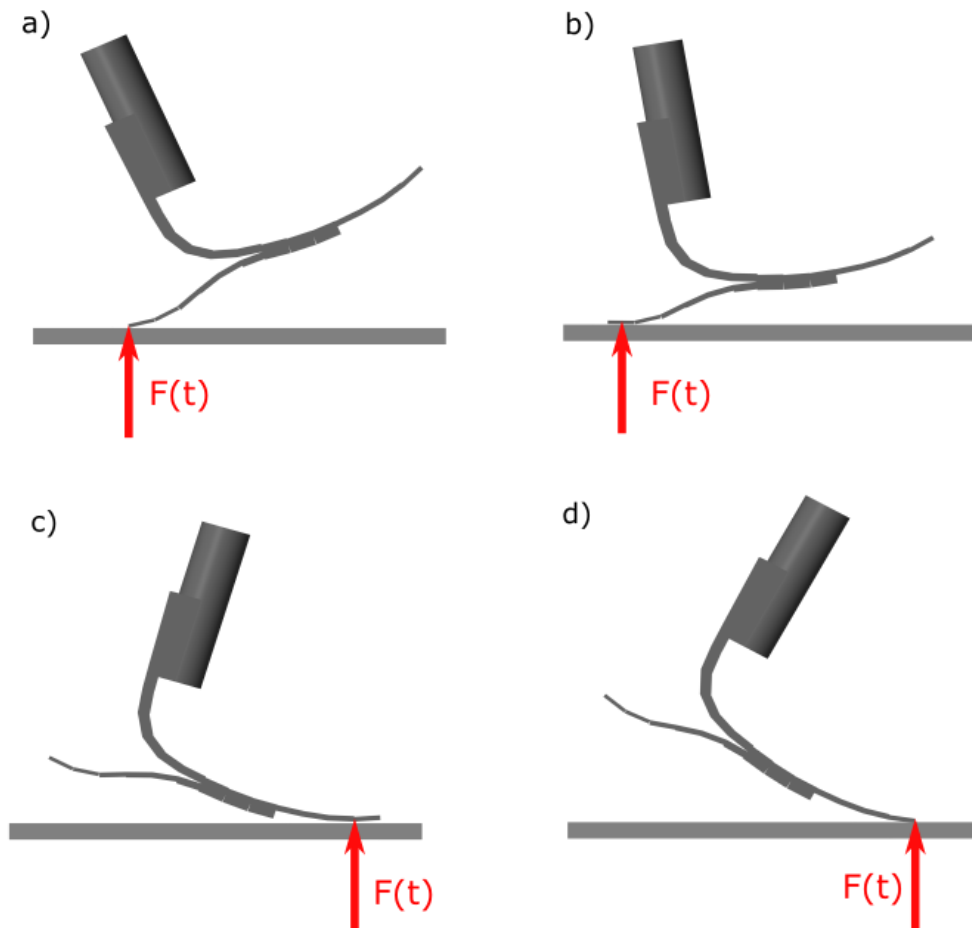


Figure 3.2.1 – Schematization of the external force’s application point in the different configurations: a) 20° heel touch; b) 10° heel touch; c) 10° toe touch; d) 20° toe touch.

To replicate a quasi-static condition of loading, the same force profiles acquired from the mechanical tests have been used. When the foot was tilted of 10 degrees (toe or heel touch), the maximum experimental force reached was 800 N; instead, when the foot was tilted of 20 degrees (toe or heel

touch), the maximum experimental force was equal to 400 N. Those force profiles are shown in Figure 3.2.2 (next page).

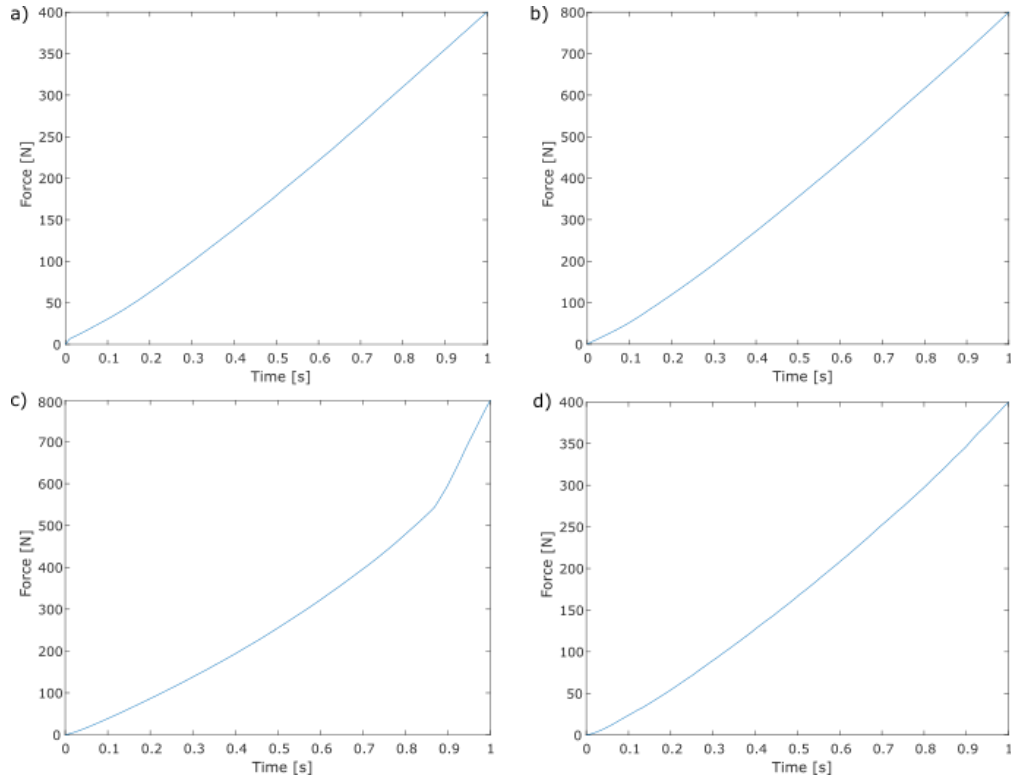


Figure 3.2.2 – External forces profiles: a) 20° heel touch; b) 10° heel touch; c) 10° toe touch; d) 20° toe touch.

### 3.2.2 Selection of the Multibody Model to Be Tested

Before proceeding with the simulation of the quasi-static loading test and the further tuning of rotational stiffness and damping values, it necessary to decide which model among those discussed in paragraph 2.5.2 (Figure 2.5.4) gives the better preliminary results. To evaluate this, the resulting force-deflection curve has been considered. This was the only criterion adopted to select the most performing model, since both the model can perform a quasi-static simulation in almost 20 seconds, so there is no difference in terms of simulation time.

The preliminary test has been performed on all the testing conditions, using the same loading strategy discussed in the previous paragraph (3.2.1). Model's parameters are resumed in Table 3.2.1.

Table 3.2.1 – Model's parameter for quasi-static simulations.

Parameter	Abbreviation	Measurement unit	Value
Young modulus	E	GPa	134 <sup>4</sup>
Density	$\rho$	$g \cdot cm^{-3}$	1.8 <sup>6</sup>
Joint's rotational damping	$\beta_{R,i}$	$N \cdot m \cdot s \cdot rad^{-1}$	0.01
Joint's rotational stiffness	$k_{R,i}$	$N \cdot m \cdot rad^{-1}$	Analytical (from Equation 2.2.25 and Equation 2.2.26)
Segment's thickness	$H_i$	m	0.007 (keel spline – Simple model)

<sup>4</sup> T700S composite (TORAY, Toray Composite Materials America, Inc.)



			0.005 (heel spline – <i>Simple</i> model) Deducted from CAD ( <i>Complex</i> model) *
Segment's length	$L_i$	$m$	Calculated from <i>segmentation_info</i>
Segment's width	$W_i$	$m$	0.06 ( <i>Simple</i> model) Deducted from CAD ( <i>Complex</i> model) *
Sampling frequency	$f_s$	$Hz$	100

\* Resumed in Table 3.2.2

Table 3.2.2 – Complex model segments' thickness and width.

Segment no.**	<b>1</b>	<b>2</b>	<b>3</b>	<b>4</b>	<b>5</b>	<b>6</b>	<b>7</b>	<b>8</b>	<b>9</b>
Width [mm]	38.2	38.2	38.2	38.2	38.2	42	48	53	55
Thickness [mm]	8.8	8.8	8.7	8.7	8.5	7.8	6.8	6.2	6
Segment no.**	<b>10</b>	<b>11</b>	<b>12</b>	<b>13</b>	<b>14</b>	<b>15</b>	<b>16</b>	<b>17</b>	<b>18</b>
Width [mm]	60	63.8	66	66	62	50	38	66	63.8
Thickness [m]	5.2	4.7	4.5	4.3	4.2	4.1	3.5	6.1	6.1
Segment no.**	<b>19</b>	<b>20</b>	<b>21</b>	<b>22</b>	<b>23</b>	<b>24</b>	<b>25</b>		
Width [mm]	6.	53	52.4	50	50	45	35		
Thickness [mm]	6.1	5.4	4.2	4.1	3.6	2.8	2.7		

\*\* Starting from the top of the lamina to the toe and from the connection between the two laminas to the heel.

The results obtained from these quasi-static simulations are shown from Figure 3.2.3 to Figure 3.2.6 on the following pages. The computational results significantly differ from the experimental ones because the model has been initially tested using a Young modulus value (134 *GPa*) that is not precise for Vari-Flex® foot. In fact, this value is associated with commercial carbon fibre composite. Analysing the literature regarding carbon fibre composites [52], it appears that the Young modulus of these materials could vary with respect to the fibre orientation and the specimen volume.

During his Thesis, L. Cavallaro et al. made an accurate study of this effect to tune his FEA model. Therefore, after these preliminary tests, the simulations have been re-run using the Young modulus ranged proposed by L.Cavallaro et al. (55 – 75 *GPa*) [51]. The results of these further simulations will be discussed in paragraph 3.2.3.

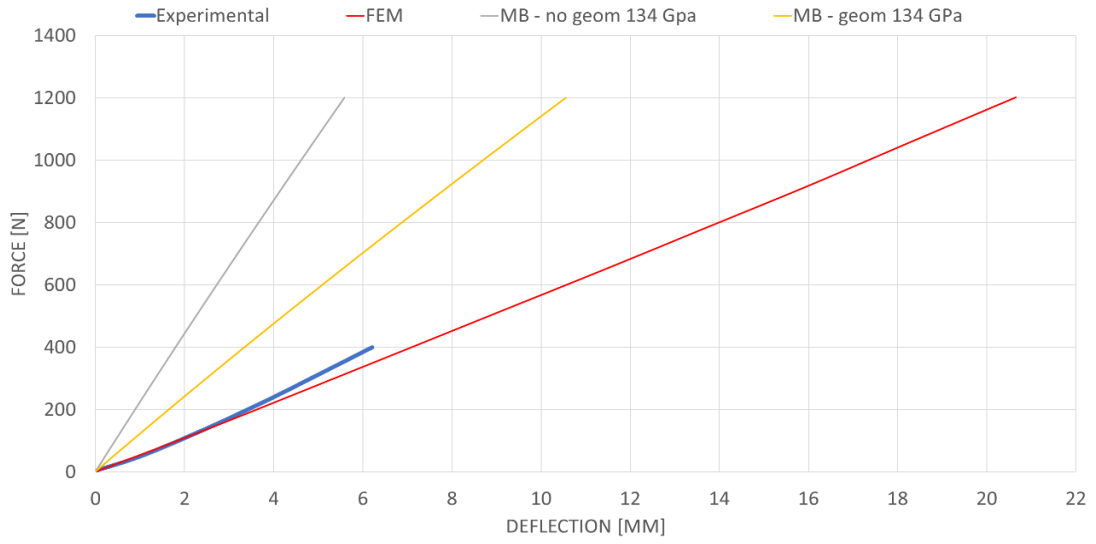


Figure 3.2.3 – Results of preliminary tests at 20° heel touch.

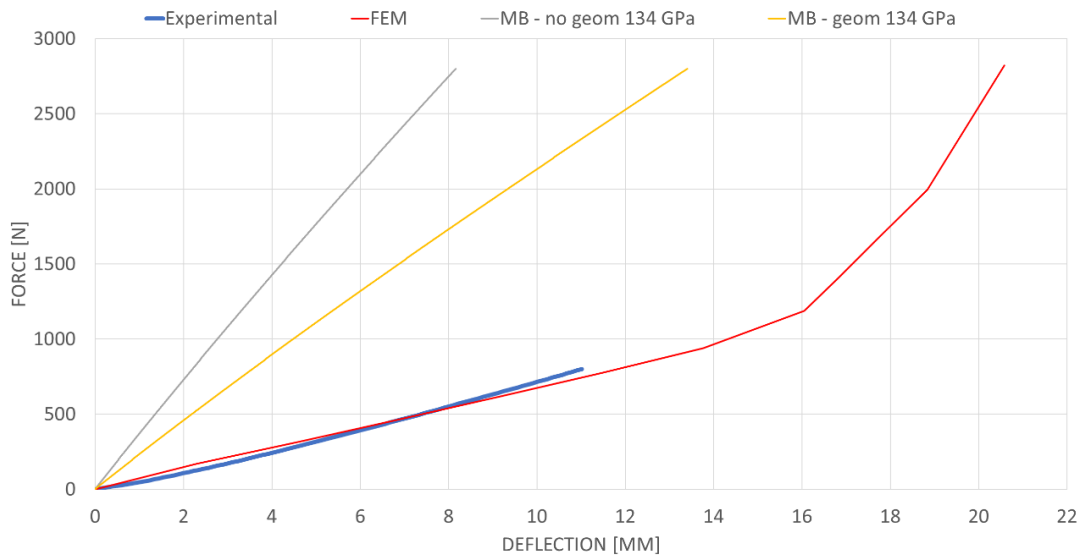


Figure 3.2.4 - Results of preliminary tests at 10° heel touch.

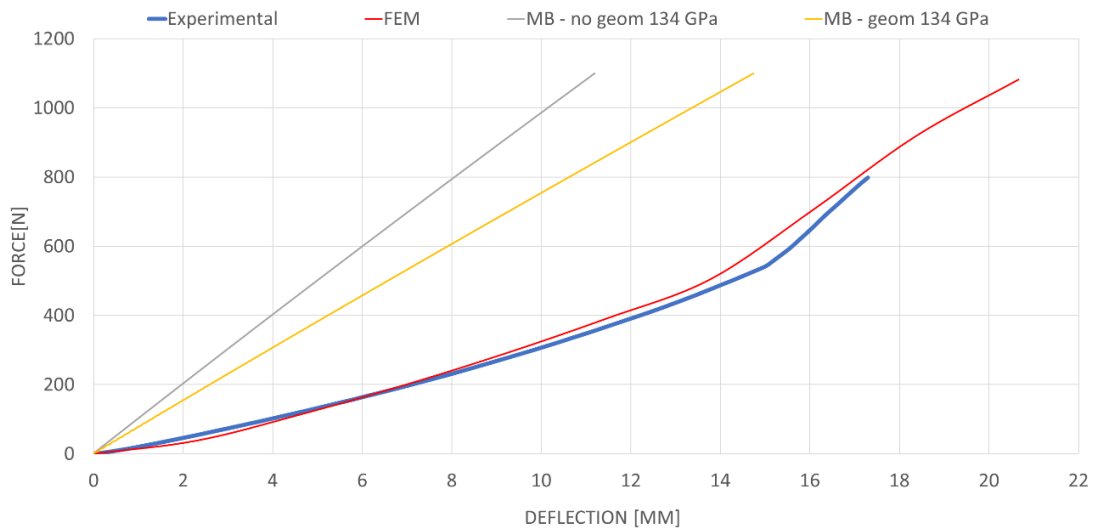


Figure 3.2.5 – Results of preliminary tests at 10° toe touch.

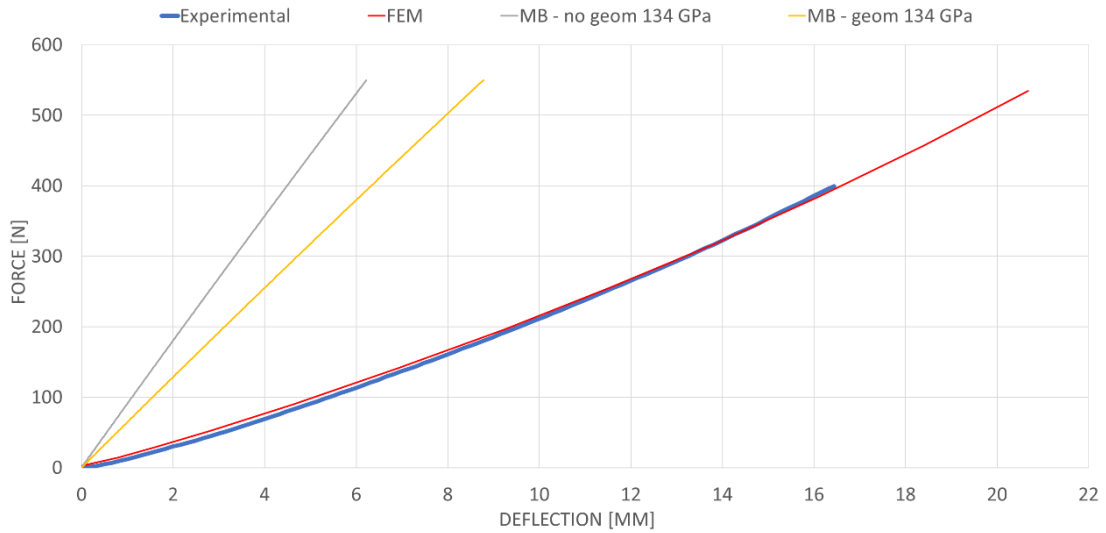


Figure 3.2.6 - Results of preliminary tests at 20° toe touch.

From the graphs, it is easy to notice that the *Complex* multibody model commits fewer errors, so it will definitively be used to run the further simulations. As anticipated, the force deflection curves obtained from these preliminary simulations are not significant and will not be considered: the Young modulus used is too different from the one proposed by L. Cavallaro et al. [51].

Now the geometrical model that will be used for further simulations has been chosen. The next step is investigating the Young modulus range proposed by L. Cavallaro et al. (55 – 75 *GPa*) [51] to decide which Young modulus' value gives the best results. Then, the value that introduces the fewest errors in quasi-static loading conditions will be used to calculate the starting rotational stiffness.

### 3.2.3 Selection of the Starting Young Modulus' Value

The process used to investigate the proposed Young modulus' range is like the one used to choose the best multibody model: quasi-static simulation must be run in all the tilted conditions changing the Young modulus' value by steps of 5 *GPa*. Therefore, the Young modulus' values investigated are:

- 55 *GPa*
- 60 *GPa*
- 65 *GPa*
- 70 *GPa*
- 75 *GPa*

The results obtained are shown in from Figure 3.2.8 to Figure 3.2.11.

From these results the error area between the computational results and the experimental ones (as shown in Figure 3.2.7, next page) has been calculated. Since the force applied to the model is equal to the one acquired from the experimental tests, the error is computed in terms of deflection. Therefore, the error will be defined as the difference between the deflection computed by the MB model and the one obtained by experimental data at each sampled force value.

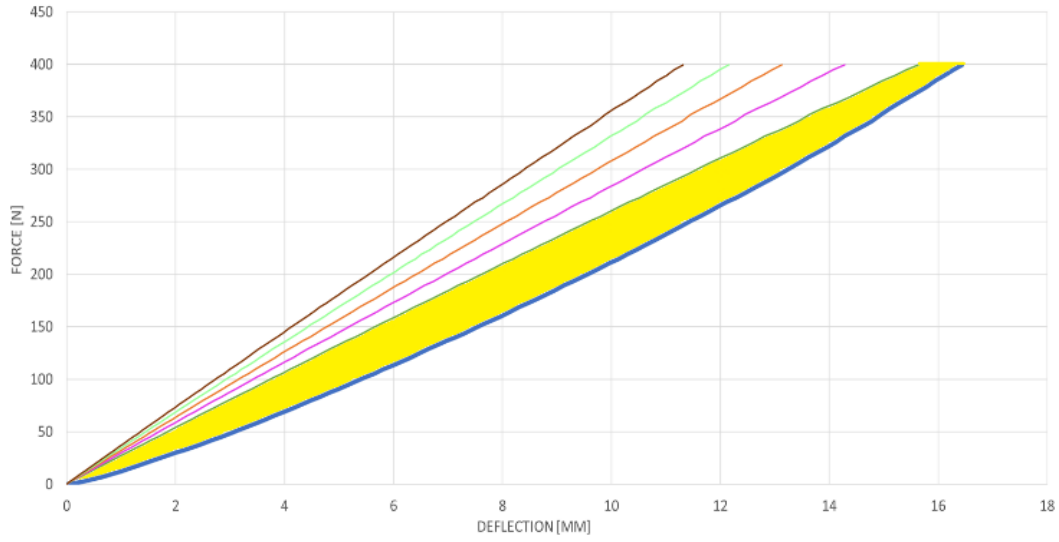


Figure 3.2.7 – Example of the error area between computational force-deflection curve and experimental one.

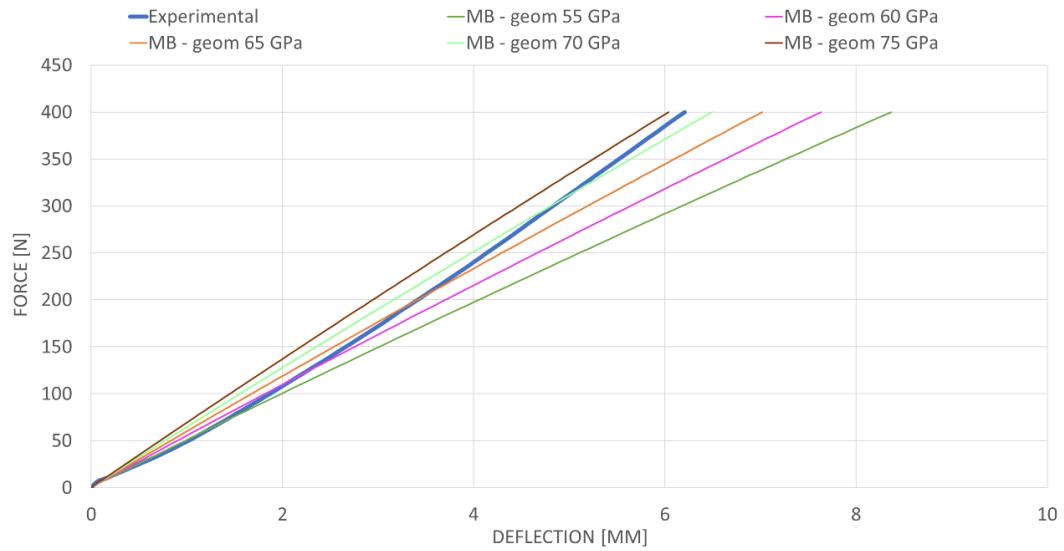


Figure 3.2.8 - Results of Young modulus tests at 20° heel touch.

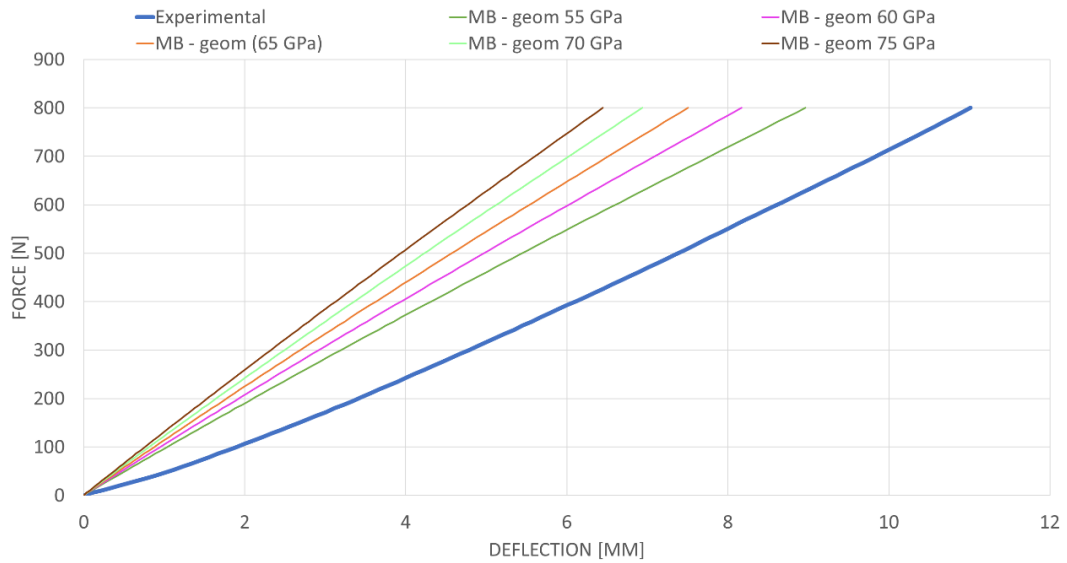


Figure 3.2.9 - Results of Young modulus tests at 10° heel touch.

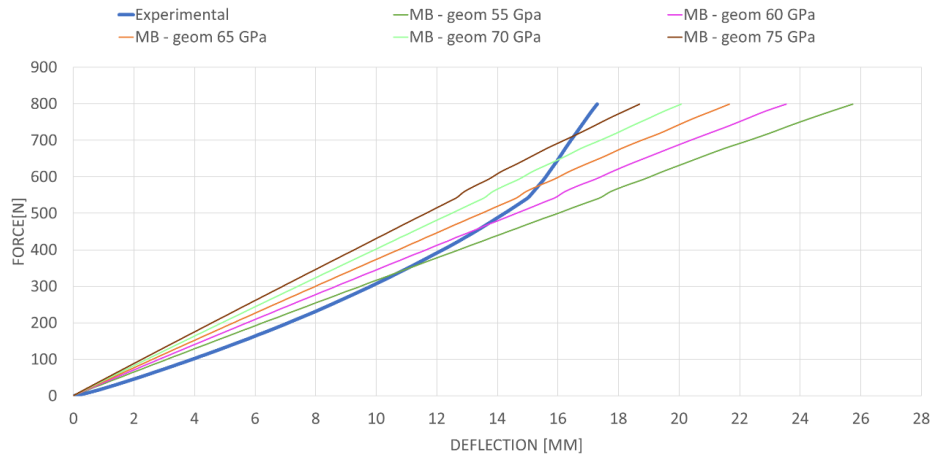


Figure 3.2.10 – Results of Young modulus tests at 10° toe touch.

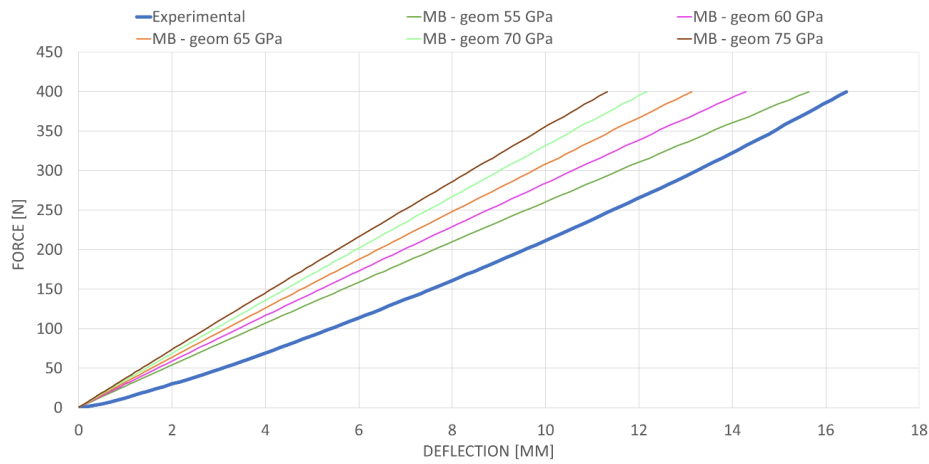


Figure 3.2.11 – Results of Young modulus tests at 20° toe touch.

The graph below (Figure 3.2.12) shows the errors committed at different loading configurations using different Young modulus values.

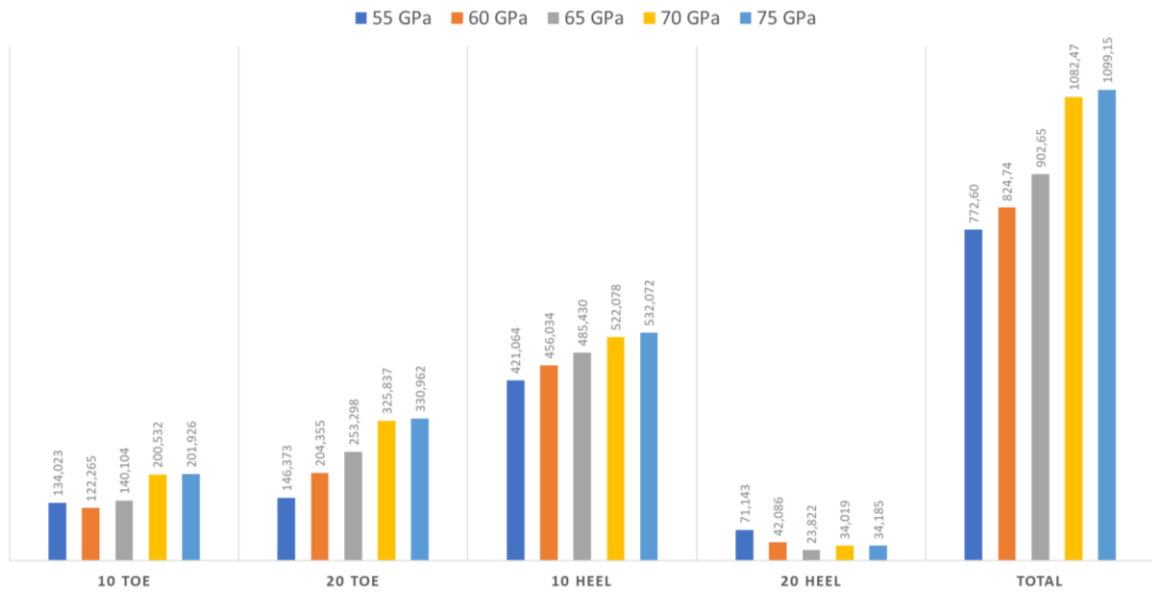


Figure 3.2.12 – Total error area for different Young modulus' values. The results are presented for each loading conditions and then summed up and reported in "TOTAL" graphic.

Considering Figure 3.2.12 (previous page) it is possible to notice that the loading test characterized by the smallest errors is the 20° heel touch test and that the Young modulus value that has the smallest overall error is 55 GPa. Nevertheless, the use of this value implies a higher error in 20° heel touch test. Anyway, it has been decided to use a Young modulus of 55 GPa to calculate the starting rotational stiffnesses values.

### 3.3 Parameters Estimation MATLAB®'s Tool

The MathWorks Inc. released a *Getting Started Guide* and a *User's Guide* related to Simulink®'s Design Optimization toolbox. All the details about this software can be found on these guides on MathWorks's website [53] [54].

Before describing the tuning processes, it is necessary to present the Simulink®'s toolbox utilized for this purpose. *Parameters estimation* is a toolbox with a graphic interface contained in Simulink® Design Optimization. It can be used to “fit the model to test data and tune it to meet requirements” [54]. That is exactly what should be done with rotational stiffness and damping values: they must be tuned to reproduce the experimental behaviour of the prosthetic foot.

To utilize this toolbox is necessary having experimental data describing the real model response. Experimental data will be compared to the selected model response in order to optimize the desired parameters. On MathWorks website there are a lot of example regarding first-order and second-order lumped parameters systems.

As said before, the toolbox has a Graphic User Interface (GUI) that shows the selected parameters to be optimized, the optimization results and the experiments considered. The optimization parameters, experimental data and model output data can be also plotted, as it is shown in Figure 3.3.1.

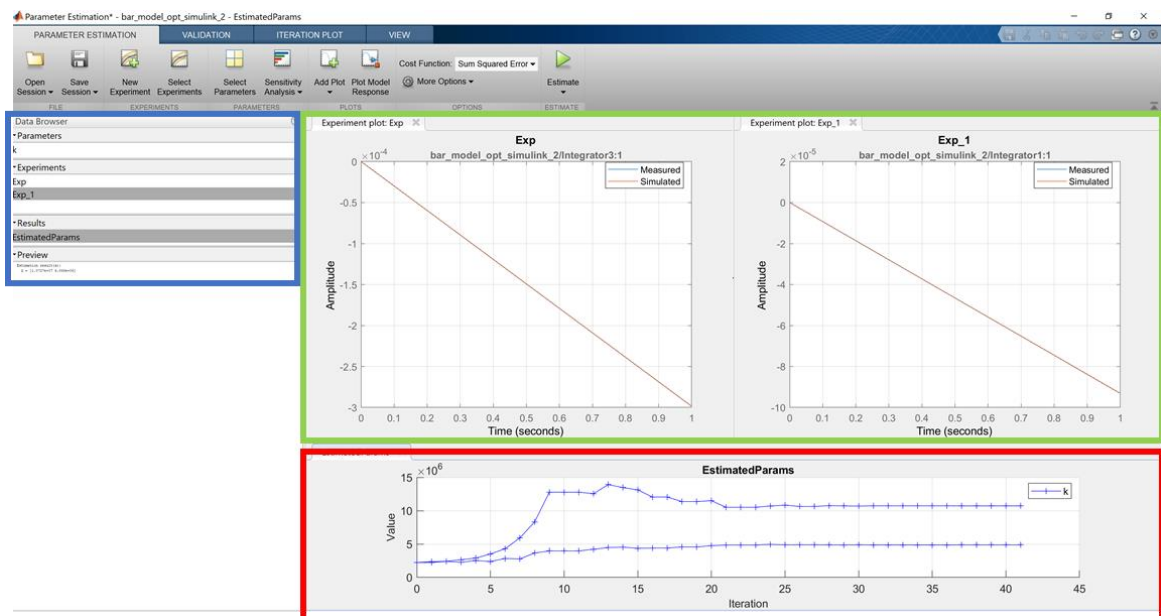


Figure 3.3.1 – Parameters Estimation's Graphic User Interface (GUI).

Referring to the previous figure, the section framed in blue contains the Parameters, Experiments and Results information. It works like MATLAB® Workspace: double-clicking on the parameters or results, they will be shown in “Preview” section; double-clicking on the experiments it is possible to configure them. The section framed in green show the plot of experimental and model data overlapping. The section framed in red shows the estimated parameters variations referred to the number of iterations made by the optimization algorithm. Both plots are refreshed at the end of each iteration.

### 3.3.1 Main Functionalities

The main functionalities of this toolbox are:

1. Possibility to configure some *experiments* to tune the selected parameters and others to validate them. All the experiments consider an experimental *time-dependent* function and the model response. Experimental data will be used as objective function.
2. Selection of the *parameters to be optimized*. These parameters can be considered as global or local ones. The difference between them is that local parameters will be tuned considering only the experiment which are related to, while the global parameters will be tuned considering all the experiments created in the environment. In Figure 3.3.2 is shown where to declare the different types of parameters.
3. When setting an *experiment*, it is also possible to configure its *initial state*. For example, if we are considering the lumped parameter model of a ball bouncing on a plate, it is possible to configure the height from which the ball is released.
4. Once the optimization process is ended, it is possible to perform a *sensitivity analysis* on the model outputs to see which one(s) has (have) the higher impact on the model's outcomes.

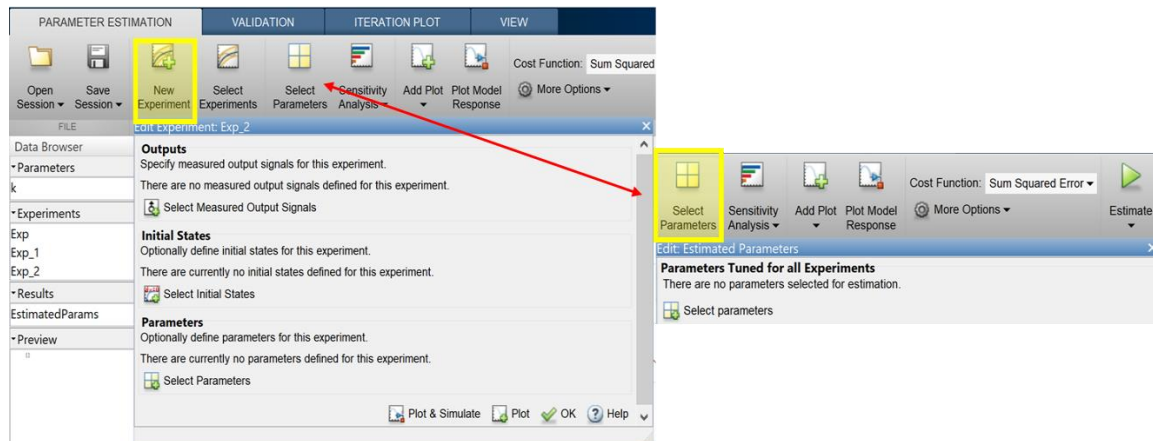


Figure 3.3.2 – In ‘New Experiment – Edit Experiment’ section (on the left) it is possible to configure the local parameter that are specific for the experiment. In ‘Select Parameters – Edit Estimated Parameters’ section (on the right) it is possible to declare the parameters that have to be tuned considering all the loaded experiments.

The tuning process can be done on one model at a time, it is not possible to use different models to tune the same parameters. This will be a limitation when tuning the different quasi-static configurations of the Vari-Flex®.

### 3.3.2 Optimization Methods

Now that the basic features of the toolbox have been explained, it is necessary to briefly describe the optimization methods that are already implemented in it. There are mainly four optimization methods but each method has different variants implemented selectable by the user (GUI windows shown in Figure 3.3.3, next page). The methods can be separated in linear/non-linear methods and gradient-based or gradient-free methods but all these methods search the local minimum of their objective function: that is why it could be important to vary the initial values of the parameters. Those methods are:

- Gradient-based
  - *Gradient Descent (GD)* method
  - *Non-Linear Least Square (NLLS)* method

- Gradient-free
  - *Pattern Search (PS)* method
  - *Simplex Search (SS)* method

GD and NLLS methods consider the derivatives (gradient-based) of the fitness function to solve the optimization problem. The difference is that GD is a linear method, while NLLS is non-linear (as his name suggests). On the other hand, PS and SS are methods called gradient-free, so they may investigate functions that are not continuous or derivable. While SS is a linear method of research among the solutions field, PS methods implement a non-linear algorithm of research.

To perform the further model optimizations, the SS method has been used. This method relies to the Nelder-Mead optimization algorithm, so a wider field of solutions will be investigated, since it has less constraints than the other methods. Nevertheless, Nelder-Mead method is “fast and widely used in local minimum optimization”, as reported by N. Pham et al. [54].

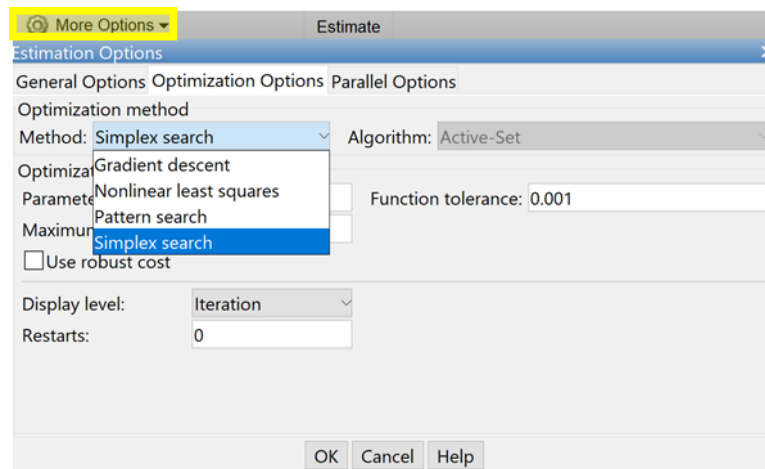


Figure 3.3.3 – ‘Estimation Options’ GUI. The menu were to find them is highlighted in yellow.

## 3.4 Tuning Process

Before tuning the Vari-Flex multibody model, some preliminary tests have been executed to familiarize with the tool and to see how it works. These tests have been conducted on a 2-segments beam model. The tuning set up will be discussed in the further paragraph (3.4.1). Then, the tuning process applied to the Vari-Flex multibody model will be described (paragraph 3.4.2). The aim of the Vari-Flex tuning, as discussed before, is varying stiffness and damping analytical values in order to reproduces the quasi-static mechanical tests’ outcomes.

### 3.4.1 Preliminary Test on a 2-Segments Beam Model

The MATLAB® script can be found at Appendix A – sixth paragraph: 2-Segments Beam Model to Be Tuned – ‘bar\_optimization.m’. While the Simulink® scheme is shown at Appendix B – fifth paragraph: 2-Segments Beam Model to Be Tuned – ‘bar\_model\_opt\_2.slx’.

#### 3.4.1.1 Simulation parameters

The 2-segments beam model has been created in Simulink® using Simscape’s blocks. Its mechanical schematic representation is shown in Figure 3.4.1 (next page).



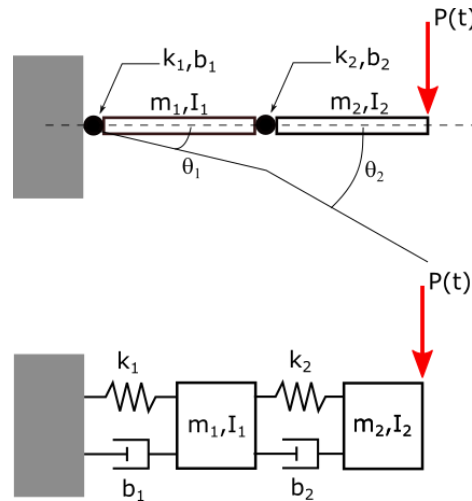


Figure 3.4.1 – Schematic representation of a 2-segments beam model loaded with a vertical force at the free end.

The model is tested in quasi-static loading condition since a vertical force  $[P(t)]$  slowly increases from 0 N to its maximum value ( $fmax = 1000$  N) during the simulation. It is important to say that the beam initial condition is its undeformed state of rest.

The other simulation parameters are resumed in Table 3.4.1.

Table 3.4.1 – 2-segments beam initial tuning parameters.

Parameter's name	Abbreviation	Measurement unit	Value
Density	$\rho$	$g/cm^3$	1.80 <sup>5</sup>
Joints' initial rotational damping	$\beta$	$N \cdot m \cdot s \cdot rad^{-1}$	0.01
Joints' initial rotational stiffness	$k_{R,i}$	$N \cdot m \cdot rad^{-1}$	Analythical (from Equation 2.2.25 and Equation 2.2.26)
Young modulus	$E$	$GPa$	134 <sup>7</sup>
Total beam length	$L$	$m$	1
Segment width	$W$	$m$	0.1
Segment thickness	$H$	$m$	0.1
Sampling frequency	$f_s$	$Hz$	1000
Simulation duration	$T$	$s$	1
Number of segments	$n$	-	2
Maximal vertical force	$fmax$	$N$	1000

N.B.: The two joints had the same initial stiffness values since the two segments have the same length and cross-sectional area.

### 3.4.1.2 Parameters Estimation Tool's Settings

For the 2-segments beam model it has been decided to tune only the stiffness values of the viscoelastic joints, to simplify the tuning process since the only purpose of this simulation is to familiarize with the tool.

<sup>5</sup> T700S composite (TORAY, Toray Composite Materials America, Inc.)

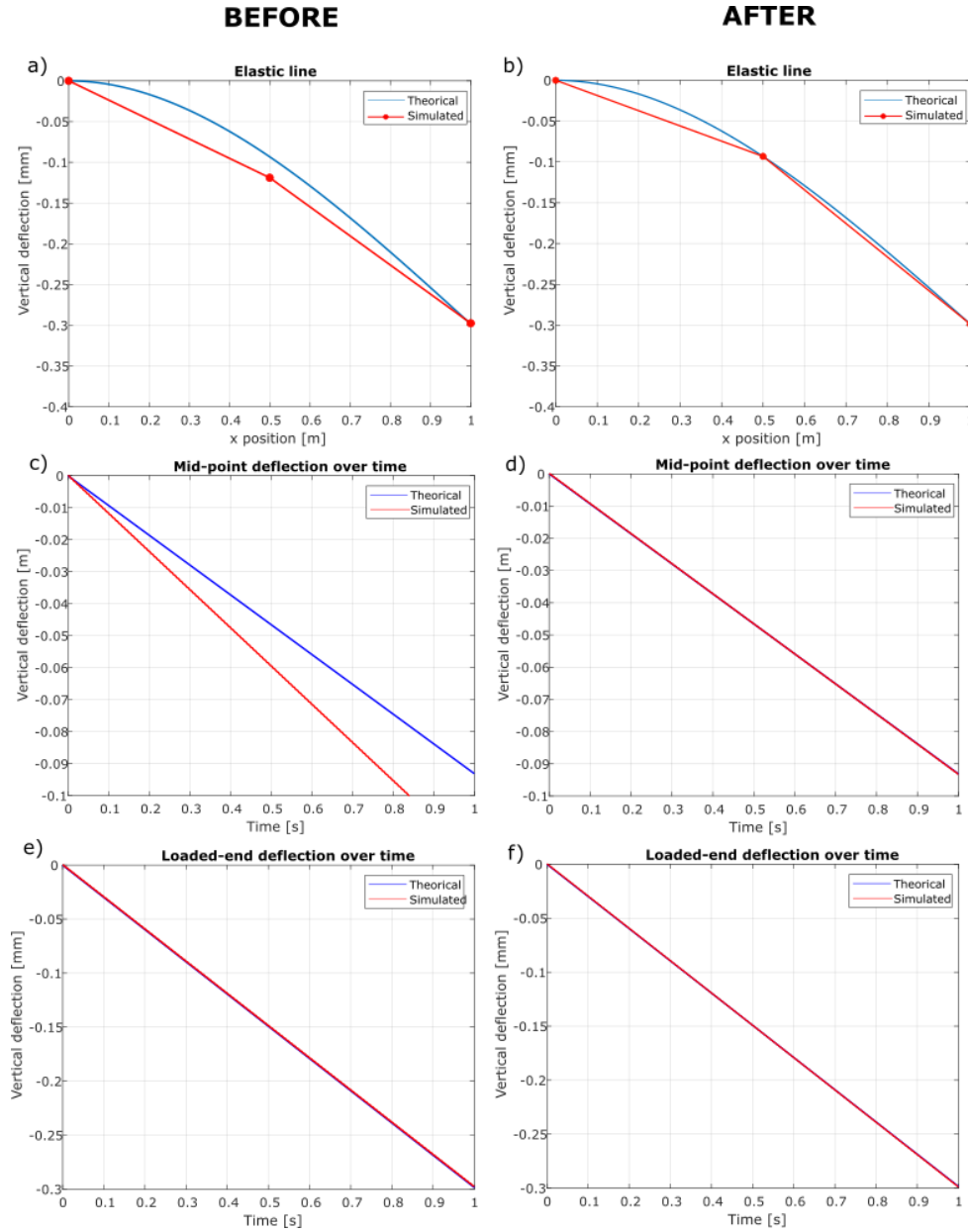


Figure 3.4.2 - a) Elastic line before tuning. b) Elastic line after tuning. c) Mid-point deflection before tuning; d) Midpoint deflection after tuning. e) Loaded-end deflection before tuning. f) Loaded-end deflection after tuning.

The target of this tuning process is getting closer the segments' ends to the theoretical beam's elastic line. To do so, two different experiments with two different objective functions have been realised:

- *First experiment* – the objective function is the beam's midpoint deflection over time.
- *Second experiment* – the objective function is the beam's free-end deflection over time.

With a *Transform sensor* block it is possible to acquire same information from the model.

As optimization method, the non-linear and gradient-free *Simplex method* has been chosen. The cost function selected utilize the *sum squared error* to evaluate the difference between objective function and model response. The maximum number of iterations set was 200.

The results of this preliminary test are shown in the further Figures. Figure 3.4.3 (next page) shows joints' stiffnesses variations over the tuning process (number of iterations), while Figure 3.4.2 shows the model outcomes before and after the tuning process.

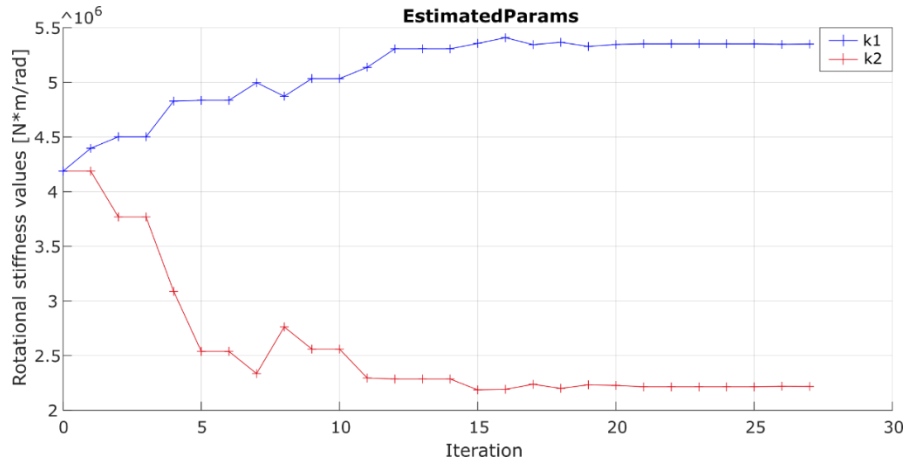


Figure 3.4.3 – Estimated stiffness variations over tuning iterations.

### 3.4.2 Vari-Flex Stiffness and Damping Tuning

To tune the Vari-Flex model in quasi-static conditions, it is necessary to use a different logic from the one used to tune the 2-segments beam model because the model must be characterized in different inclination conditions and with different external forces applied.

To do so, it is necessary to tune the model representing the different mechanical test conditions separately and then to calculate the average between the stiffnesses and the damping ratio estimated in each loading condition. It has been also tried to change the tuning settings and test them on ‘20° toe’ trial, but this did not change the resulting force-deflection curve. Therefore, the stiffness and damping values obtained from the first tuning process have been considered for further implementations.

Settings and parameters adopted for tuning the Vari-Flex® model in quasi-static conditions will be explained in the further Paragraph. The results will be shown in paragraph 6.1.1.

#### 3.4.2.1 Simulation Parameters

The material and simulation parameters utilized for the Vari-Flex® model are resumed in Table 3.4.2

Table 3.4.2 – Initial parameters for Vari-Flex® model.

Parameter's name	Abbreviation	Measurement unit	Value
Density	$\rho$	$g \cdot cm^{-3}$	1.80 <sup>6</sup>
Joints' initial rotational damping	$\beta_{R,i}$	$N \cdot m \cdot s \cdot rad^{-1}$	0.01
Joints' initial rotational stiffness	$k_{R,i}$	$N \cdot m \cdot rad^{-1}$	Analytical (from Equation 2.2.25 and Equation 2.2.26)
Young modulus	$E$	GPa	55
Segment length	$L_i$	m	Calculated from <i>segmentation_info</i>
Segment width	$W_i$	m	Taken from CAD model
Segment thickness	$H_i$	m	Taken from CAD model
Sampling frequency	$f_s$	Hz	1000
Simulation duration	$T$	s	1

<sup>6</sup> T700S composite (TORAY, Toray Composite Materials America, Inc.)

Number of segments	$n$	-	25
Maximal vertical force	$f_{max}$	$N$	800 (10° toe; 10° heel) 400 (20° toe; 20° heel)

### 3.4.2.2 Tuning Settings

As said before, it has been tried to tune the model setting the *Parameters Estimation* tool in different ways. The settings utilized are reported in Table 3.4.3.

It is necessary pointing out what is the difference between *linear* and *experimental* force profile:

- *Linear* force profile – the external force magnitude increases from 0  $N$  to the maximum value with a linear trend.
- *Experimental* force profile – the external force magnitude increases from 0  $N$  to the maximum value following its experimental trend (Figure 3.2.2).

N.B.: An example of *linear* and *experimental* trend for 20° heel touch loading conditions is shown in Figure 3.4.4.

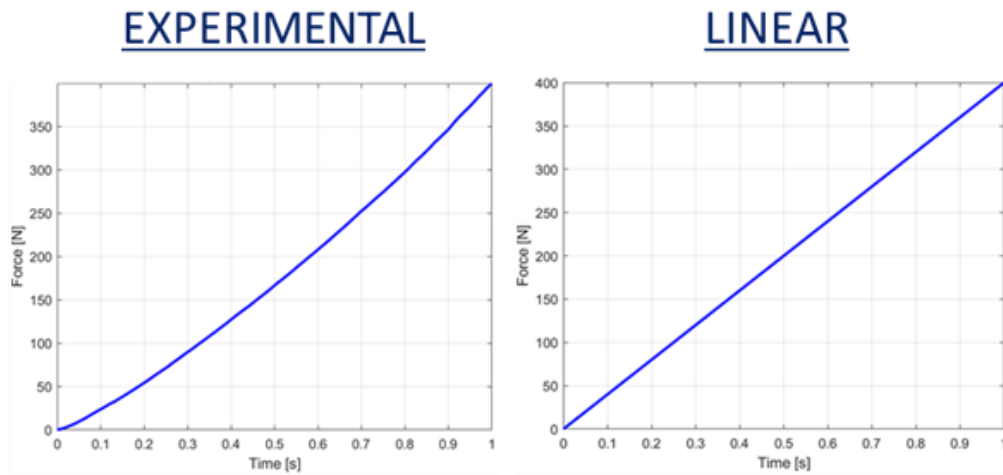


Figure 3.4.4 – Example of ‘experimental’ and ‘linear’ force profiles.

Table 3.4.3 – Tuning process settings.

Tuning run no.	1	2	3	4
Applied force profile	Linear	Experimental	Experimental	Experimental
Stiffness tuning	1 <sup>st</sup> run	1 <sup>st</sup> run	Same run	Same run
Damping tuning	2 <sup>nd</sup> run	2 <sup>nd</sup> run		
Starting stiffness values [ $N \cdot m \cdot rad^{-1}$ ]	Analytical (from Equation 2.2.25 and Equation 2.2.26)	Analytical (from Equation 2.2.25 and Equation 2.2.26)	Analytical (from Equation 2.2.25 and Equation 2.2.26)	Analytical (from Equation 2.2.25 and Equation 2.2.26)
Starting damping val- ues [ $N \cdot m \cdot s \cdot$ $rad^{-1}$ ]	0.01	20	20	20
Optimization method	Simplex search	Simplex search	Simplex search	Simplex search
Max No. of iterations	200	200	400	400

## 4. Gait Data Acquisition

---

To test the model in dynamic conditions, it is necessary to acquire gait data (as Ground Reaction Forces and Vari-Flex® cinematic information). Those data was acquired at IIT's Rehab Technologies Department in Genova, where there is a lab room completely dedicated to gait analysis.

In this chapter the equipment used, the acquisition protocol followed to acquire gait data and the adopted data processing algorithm will be discussed. Finally, elaborated data will be presented. COP posterior-anterior displacement and GRF data will be utilized as dynamic model inputs, while cinematic information could be used as reference for comparison to test the model's reliability when computing laminas' deflections.

### 4.1 Equipment

In this paragraph the equipment used to acquire dynamic and kinetic data about the stance phase of a subject with an above-the-knee amputation will be described. Since it was not possible recruiting amputees, a special adapter implemented by IIT's Rehab Technologies Department has been used to allow the subject to use the prosthetic knee and the Vari-Flex®.

#### 4.1.1 Prosthetic Equipment and Adapter

As shown in Figure 4.1.1, the subject is wearing the adapter that allows him to wear the lower limb prosthesis and use it to walk. The adapter is composed by a rigid structure and three belts in order to keep the subject's lower limb strictly in contact with it. Below, there is a metal plate with bolted joints that allows to attach the knee prosthesis to the adapter. The prosthetic knee is the Power Knee® by Össur. The shank pylon which the Vari-Flex® is attached to is already included in the knee prosthesis. Finally, the Vari-Flex® is connected to the Power Knee® with a carbon fibre tube instead of the standard pyramidal joint. Since prosthetic knee and foot did not fit subject's height, he had to wear a raised shoe to permit a correct prosthesis' alignment in frontal and sagittal plane.

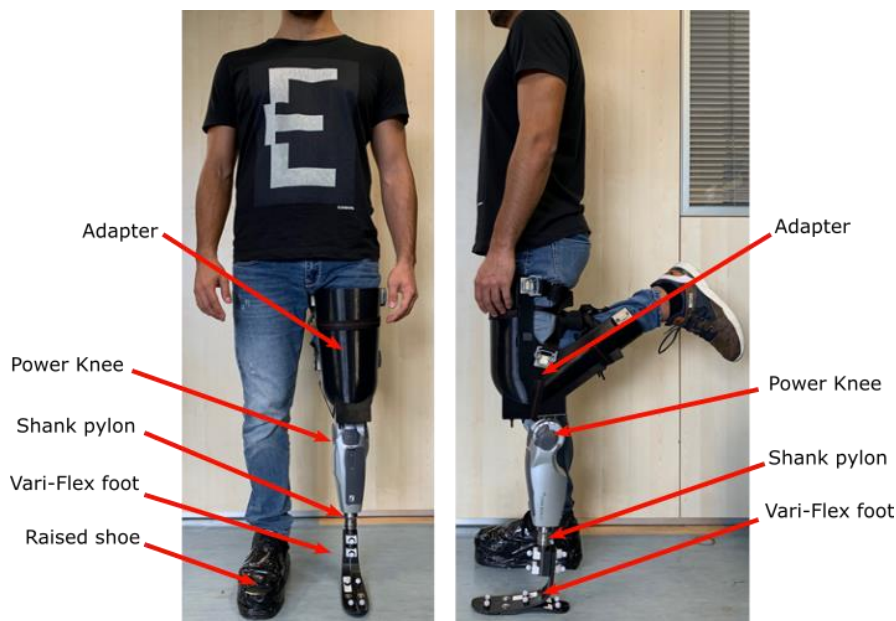


Figure 4.1.1 – Subject wearing the adapter with Power Knee and Vari-Flex mounted.

#### 4.1.1.1 Adapter's Pros and Cons

It is necessary to briefly describe the advantages and the disadvantages that come with the using of the adapter. The advantages are that:

- It permits to test prosthetic feet and knees on healthy subjects.
- It permits to preserve the hip functionality.

The disadvantages that the adapter shows are that:

- It is not easy to wear. The tester should be helped to tighten the bands.
- It could produce relative movements between thigh and lower limb prosthesis.
- It can cause discomfort to the tester since the knee is flexed at an unnatural angle.

#### 4.1.2 Sensors and Instrumentation

To measure kinetic quantities (i.e. Vari-Flex® deflection over gait) some markers have been placed on the Vari-Flex® foot and they have been monitored with a stereophotogrammetrical Vicon system with six cameras. Instead, to measure dynamic quantities of interest (i.e. Ground Reaction Force and COP displacement), a system composed of two force plates placed under a treadmill has been used. A schematic representation of the instrumentation is shown in Figure 4.1.2.

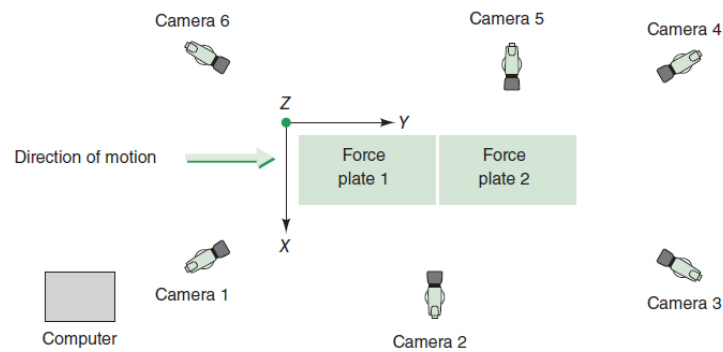


Figure 4.1.2 – Schematic representation of the experimental set up [51].

Both the kinetic and dynamic quantities are acquired and saved with Vicon Nexus®, a dedicated software by Vicon.

##### 4.1.2.1 Vicon System

The Vicon stereophotogrammetrical system available at the *IIT's Rehab Technologies Department* is composed of six Vicon Vero® cameras (Figure 4.1.3) acquiring at 100 Hz. This sampling frequency allows to catch kinetic phenomena occurring during gait because a normal gait cycle has a normal characteristic frequency of nearly 1 Hz (the complete gait cycle of a human lasts about 1 second [10]). The cameras acquire in infrared.



Figure 4.1.3 – Vicon Vero® camera.

### 4.1.2.2 Force Plates

The two force plates by AMTI available are mounted under a treadmill placed at the centre of the room (Figure 4.1.4, next page). The treadmill is equipped with lateral bar that could help the subject to keep the balance while walking. The force plates acquire at a frequency rate of 1000 *Hz*. These force plates permits to acquire the Ground Reaction Forces (GRFs) and calculate from them the COP displacements along X, Y and Z axes.

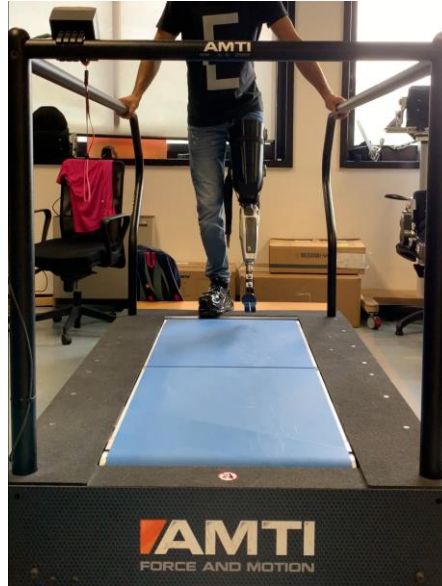


Figure 4.1.4 – AMTI treadmill. The two force plates are mounted under the blue sliding mat.

### 4.1.2.3 Markers Positioning

The Vari-Flex® prosthetic foot is instrumented with 10 passive markers (their positioning is detailed in Figure 4.1.5). Four passive markers are placed in a non-flexible zone: the carbon fibre tube that allows to connect the Vari-Flex® to the shank pylon. Displacement information acquired with these markers will be used to define the pylon angle with respect to an ideal line perpendicular to the ground (Figure 4.1.6, next page). These markers will also be used as reference points to calculate the relative displacements of the markers placed in flexible zones. The other six markers are placed in flexible zones. These ones will be used to calculate the hindfoot, midfoot and forefoot deflections over stance phase.

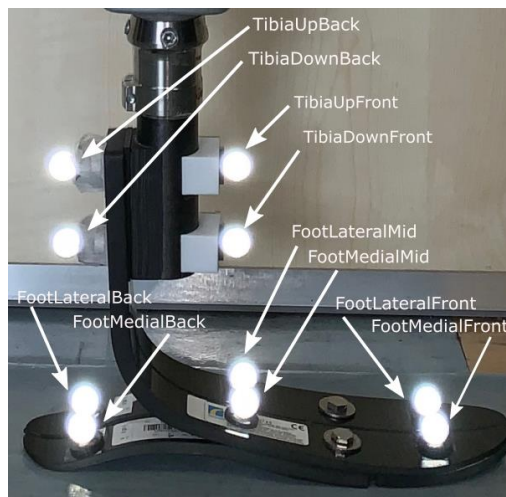


Figure 4.1.5 – Experimental marker set with markers' names.



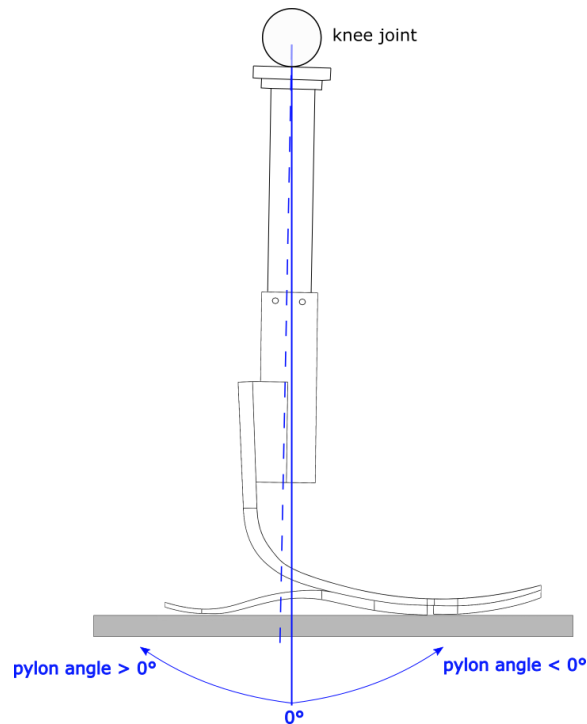


Figure 4.1.6 – Schematic representation of the pylon angle with respect to an ideal line perpendicular to the ground.

The markers are named after their position (Figure 4.1.5, previous page):

- *Non-flexible-zones markers*
  - TibiaUpFront
  - TibiaUpBack
  - TibiaDownFront
  - TibiaDownBack
- *Flexible-zones markers*
  - FootLateralBack
  - FootLateralMid
  - FootLateralFront
  - FootMedialBack
  - FootMedialMid
  - FootMedialFront

## 4.2 Gait Protocol

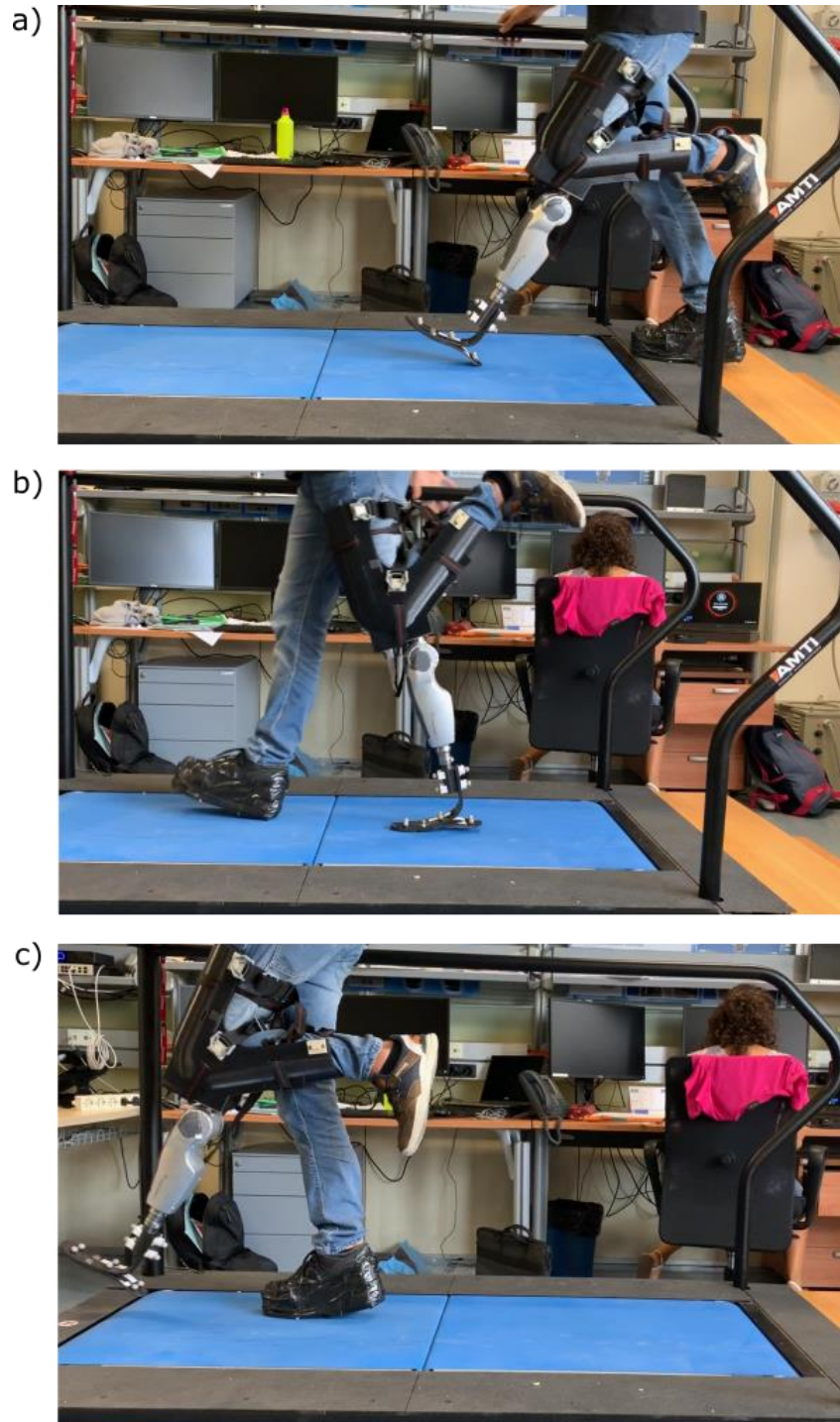
The gait protocol consists in a complete step with the prosthetic leg on the first force plate. The treadmill has not been activated and the prosthetic knee joint has been kept locked. It has been decided to keep the knee locked during the trials because the subject was not trained to walk with an active knee prosthesis and he affirmed that he was more comfortable walking with a locked knee.

It is important to point out that the subject could help himself keep the balance with the treadmill lateral bars and that he was not specifically trained to walk with the adapter, but he has already used it before to do similar tasks.

Since the study's aim was not to measure kinetic or dynamic quantities related to the swing phase, the designed gait protocol states that the subject must land the prosthetic limb on the first force plate, then he must land the sound limb on the second force plate and he must finally stop himself when



the sound limb passes the prosthetic limb. The entire cycle must be performed by the same subject for ten times.



*Figure 4.2.1 – Trial phases. a) Prosthetic limb landing on the first force plate. b) Sound limb landing on the second force plate. c) Prosthetic limb passes the sound limb before the subjects stops the gait.*

Static acquisitions was also made to measure the weights presented below:

- Prosthetic limb system (adapter, knee prosthesis and foot prosthesis)
- Subject wearing prosthetic limb system.

This data was collected to refer the ground reaction forces to the total subject weight (subject plus prosthetic system) and then compare them with literature data for healthy subjects.

### 4.3 Data Processing

The MATLAB® scripts can be found at Appendix A – seventh and eighth paragraphs: Import of Gait Data, Recognition of Stance Phase and Data Filtering - 'data\_import.m' and Calculation of Gait Data Mean Values and Standard Deviations - 'data\_elaboration.m'.

In this paragraph the processing of raw data coming from the gait trials will be discussed. Final data will be presented in paragraph 4.4. Ground reaction forces will be compared to those acquired in healthy subjects in Richards et al. work [56]. Data was filtered and resampled and their mean value and standard deviation were computed. It has been necessary to do a further processing for markers' displacements information, since markers were placed on two different laminas (Vari-Flex® is divided in two independent parts on the sagittal plane).



Figure 4.3.1 – Schematic resume of gait data processing.

It is important to remember that ground reaction forces and COP anterior-posterior displacement will be the inputs of dynamic simulations, while markers displacements will be a method to validate the dynamic model. Therefore, the final data will be grouped in a MATLAB® structure. This structure will be easily loaded by the MATLAB® script performing the dynamic simulation.

#### 4.3.1 Stance Phase Recognition

To recognize the stance phase duration, it has been considered a vertical ground reaction force (vGRF) threshold equal to 20 N. This value has been chosen in accordance with the works of M.F. Bobbert et al. [57] and J.A. Zeni Jr. et al. [58]. Heel strike takes place when the vGRF is beyond 20 N. On the other hand, toe-off takes place when vGRF is less than 20 N.

All the dynamic and kinetic signals are referred to this time period: from heel strike to toe off. Therefore, signals time support is equal to the stance phase and it is divided in percentages of it. The swing phase, as said before will not be considered for the further studies. GRF, COP anterior-posterior displacement and marker displacements will resample so that they will be represented by 100 samples over the stance phase duration.

#### 4.3.2 Filtering

All signals are filtered with a Chebyshev low-pass (LP) filter with cut-off frequency equal to 10 Hz. Since the characteristic frequency of the gait is around 1 Hz (1 step/s), this cut-off frequency allows to distinguish the signals from noise without losing information.

The filtering process is performed using MATLAB®'s `filtfilt` function. Since GRF, COP displacement and markers information are not random signals, it is important to keep the signals morphology. This function executes an anticausal filtering to avoid phase distortion.

#### 4.3.3 Processing of Markers Displacements

Referring to Figure 4.3.2 (next page), it is possible to see that there are three couples of markers placed in the flexible region of the Vari-Flex® foot. The reason why there is a couple of them for

each region (hindfoot, midfoot and forefoot) it is that the Vari-Flex® is divided in two on the sagittal plane, so each marker of the couple could move independently with respect to the other.

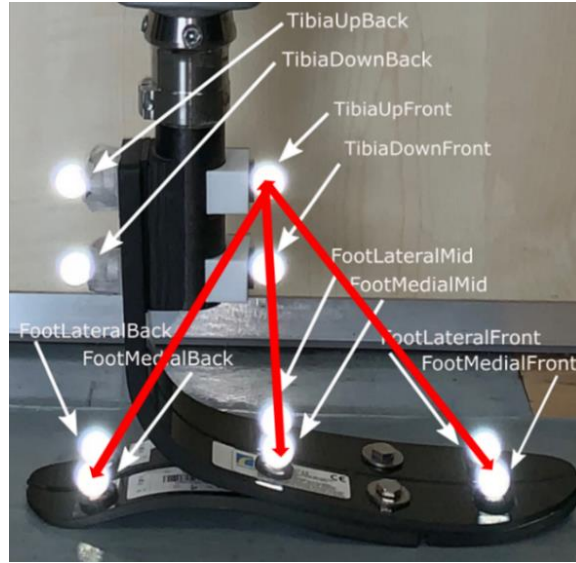


Figure 4.3.2 – Considered marker distances.

For these reasons, displacement information related to the marker couples listed below is averaged along  $y$  (inferior-superior axis) and  $z$  directions (posterior-anterior axis):

- FootLateralBack – FootMedialBack
- FootLateralMid – FootMedialMid
- FootLateralFront – FootMedialFront

N.B.: movements along  $x$  direction (medio-lateral axis) will not be considered.

Then, averaged data has been used to calculate the mean distance of each couple of markers from the TibiaUpFront marker (placed in a non-flexible region) to monitor Vari-Flex®'s deflections in each foot region (hindfoot, midfoot and forefoot). Those distances are shown in Figure 4.3.2.

#### 4.3.4 Pylon Angle Data Calculation

Pylon angle data has been calculated using the markers *TibiaUpFront* and *TibiaDownFront* because they rigidly move with respect to each other (also *TibiaUpBack* and *TibiaDownBack* couple of markers could have been used for the same purpose). Equation 4.3.1 has been considered to calculate pylon angle information (a schematic representation of the situation described with this equation can be found in Figure 4.3.3, next page):

$$\theta = \text{atan2} \left( \frac{TibiaDownFront_y - TibiaUpFront_y}{TibiaDownFront_z - TibiaUpFront_z} \right) \cdot \frac{180}{\pi} + \theta_{static}$$

Equation 4.3.1 – Trigonometric equation to determine the angle that the pylon forms with an imaginary line that is perpendicular to the ground.

Where:

$\theta$  is the pylon angle.

$\theta_{static}$  is the angle between the two markers when the prosthesis is not loaded (measured by hand).

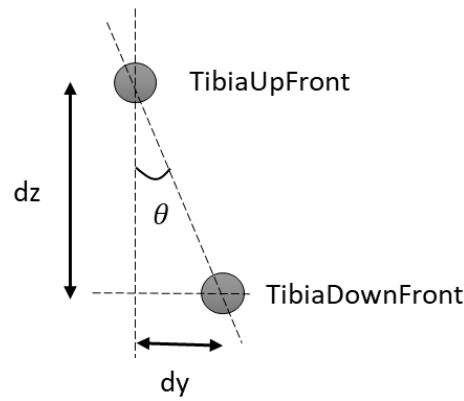


Figure 4.3.3 – Schematic representation of the logic behind Equation 4.3.1.

### 4.3.5 Mean and Standard Deviation Calculation

At this point, the signals obtained by each trial have been averaged and it has been calculated the standard deviation of them. Obviously, each trial has different time duration with respect to the others but, since each signal is referred to the percentual time duration of the stance phase, it is possible to average each sample with the referring sample of the other trials. The same logic could be applied when calculating the standard deviation of them.

## 4.4 Final Gait Data

Data presented in this section are referred to the percentage of the stance phase. But, for the sake of completeness, it is important to know that the average stance phase duration over the trials was equal to 1.23 seconds: nearly the double of a healthy subject's one (0.6 seconds [3] [11]).

### 4.4.1 Ground Reaction Forces (GRF)

The reference directions of the ground reaction forces are shown in Figure 4.4.1.

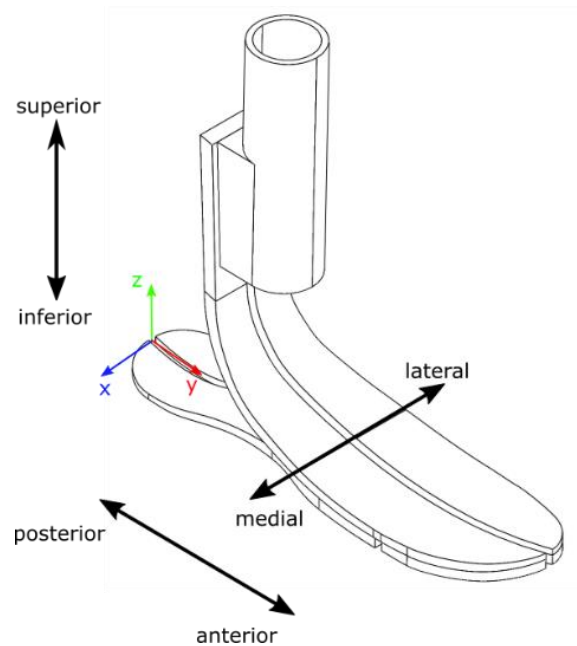


Figure 4.4.1 – Reference axes which ground reaction forces are referred to.

Inferior-superior ground reaction forces registered for each trial are shown in Figure 4.4.2 and Figure 4.4.3. Posterior-anterior GRF are shown in Figure 4.4.5 and Figure 4.4.4. Finally, medio-lateral GRF can be seen in Figure 4.4.7 and Figure 4.4.6.

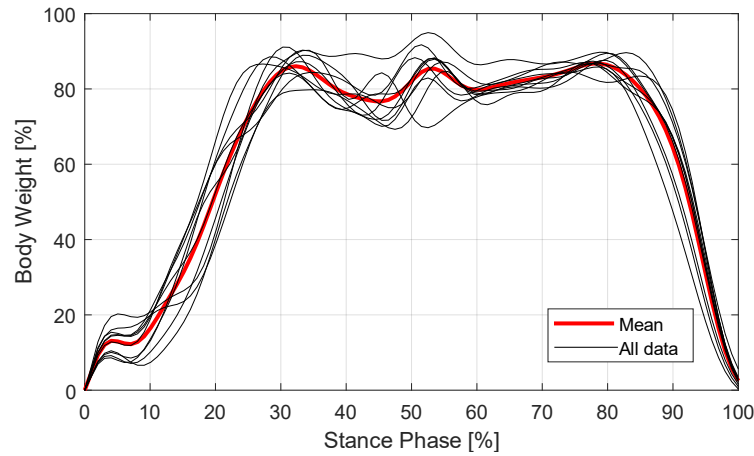


Figure 4.4.2 – Inferior-superior ground reaction force. The black lines are filtered data referring to each trial. The thicker red line is the averaged inferior-superior ground force.

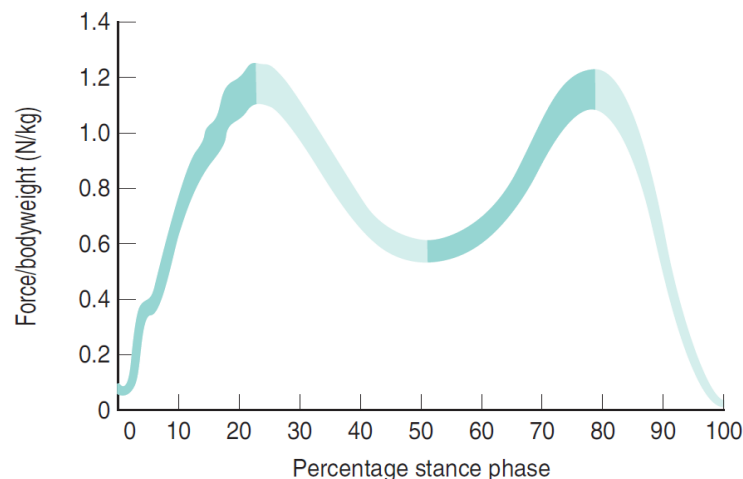
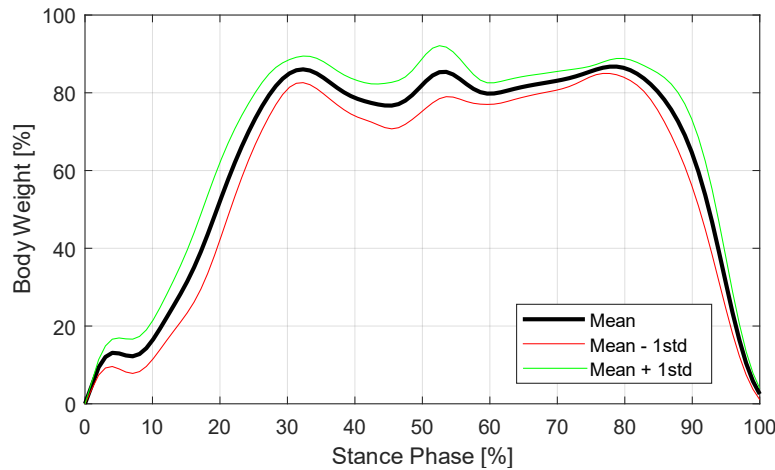


Figure 4.4.3 – Inferior-superior ground reaction forces. In the upper figure experimental processed data are presented: averaged data are represented with a black thick line, while the red and green line are respectively averaged data plus or minus the standard deviation. In the lower figure there is the inferior-superior GRF for a healthy subject [56].

It can be easily notice that inferior-superior GRF of the prothesized subject does not never reach nor passes the 100% of total bodyweight, This could happen because the subjects could help himself to

keep the balance by holding to the treadmill's lateral bars. Also, since the prosthetic knee was locked, the subject did not feel comfortable in loading completely the prosthetic limb while walking.

Nevertheless, the typical central concavity of vGRF found in health subject cannot be seen in the prosthesized one. This behaviour is probably due to the fact that the Vari-Flex® foot does not gently roll from the heel to the toe while walking, but it snaps when the load passes from the back foot to the forefoot. The result is the little peak of force that can be noticed around the 55% of the stance phase in Figure 4.4.2 (upper graphic).

Even posterior-anterior GRF (Figure 4.4.4) is lower for the prosthesized subject analysed than for a healthy people. The morphology of the two signals, however, is quite similar, with two peaks of force around 20% and 85% of stance phase: respectively, one negative and one positive. In posterior-anterior GRF plot, an anomalous peak of force around 50% of stance phase can also be noticed. This peak corresponds to the one seen in vGRF and maybe is due to the same effect.

Medio-lateral ground force is completely different for the prosthesized subject with respect to a healthy one (Figure 4.4.6, next page). Neither the morphology or the magnitude of the force are preserved. This could be related to the fact that the subject did not feel comfortable walking with the prosthesized limb and then he could not properly load the foot on medio-lateral axis.

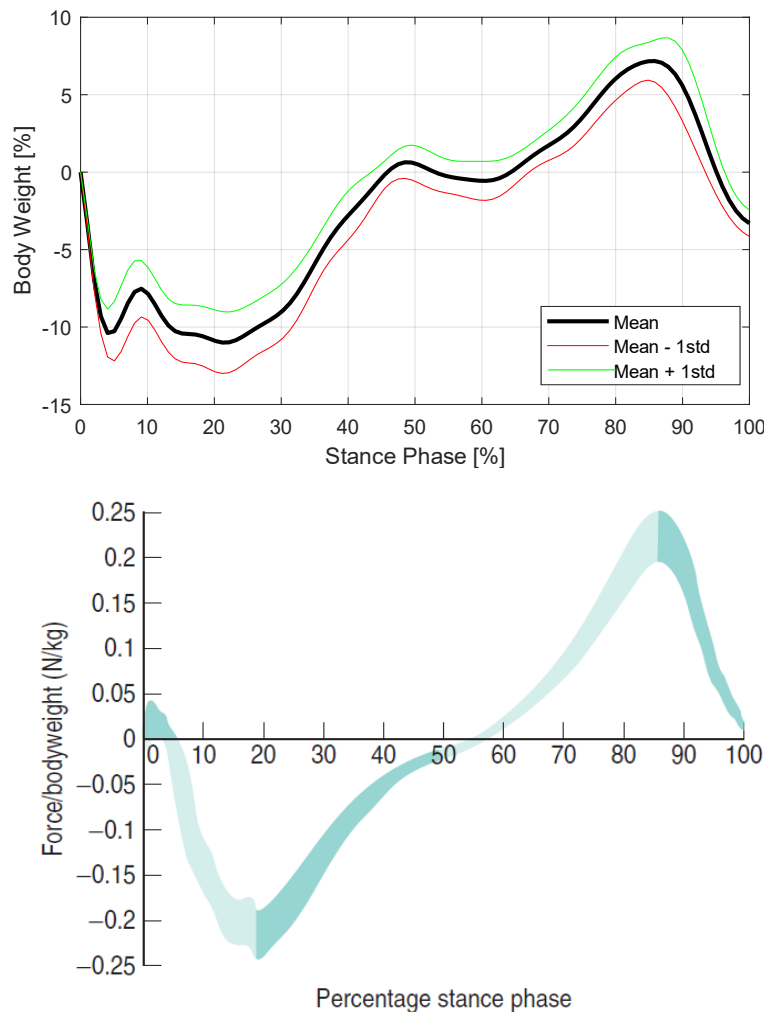


Figure 4.4.4 – Posterior-anterior ground reaction forces. In the upper figure experimental processed data are presented: averaged data are represented with a black thick line, while the red and green line are respectively averaged data plus or minus the standard deviation. In the lower figure there is the anterior-posterior GRF for a healthy subject [56].

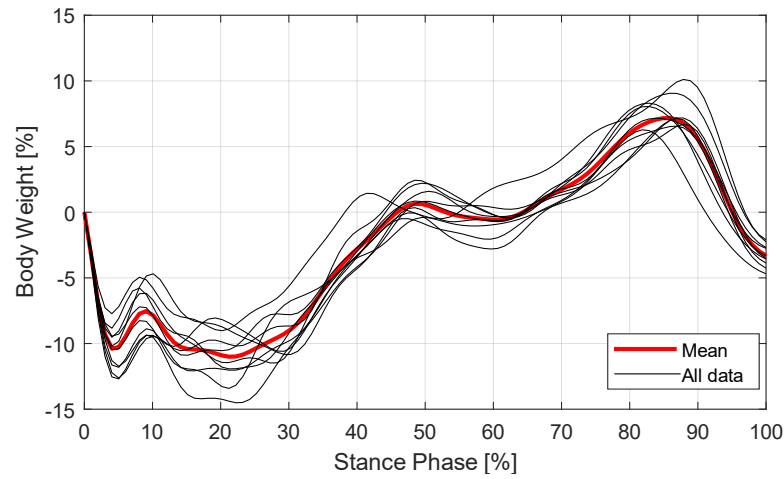


Figure 4.4.5 – Posterior-anterior ground reaction force. The black lines are filtered data referring to each trial. The thicker red line is the averaged posterior-anterior ground force.

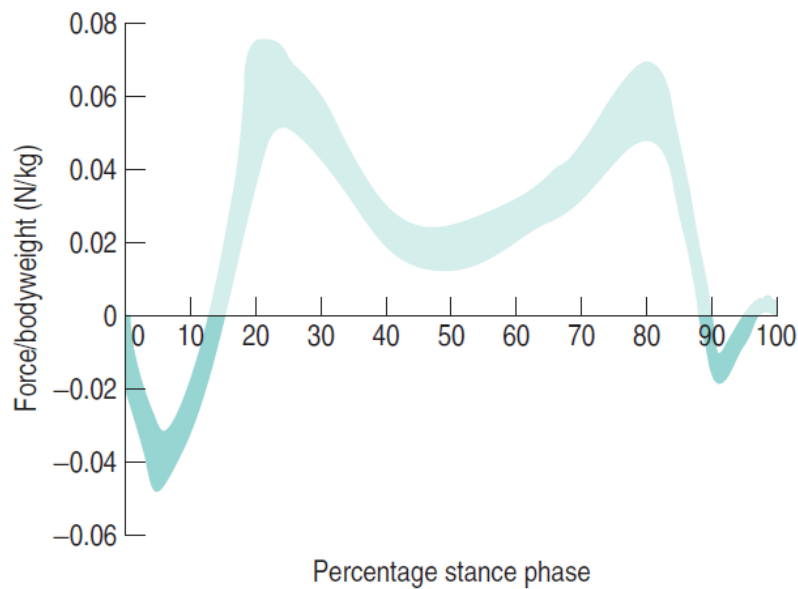
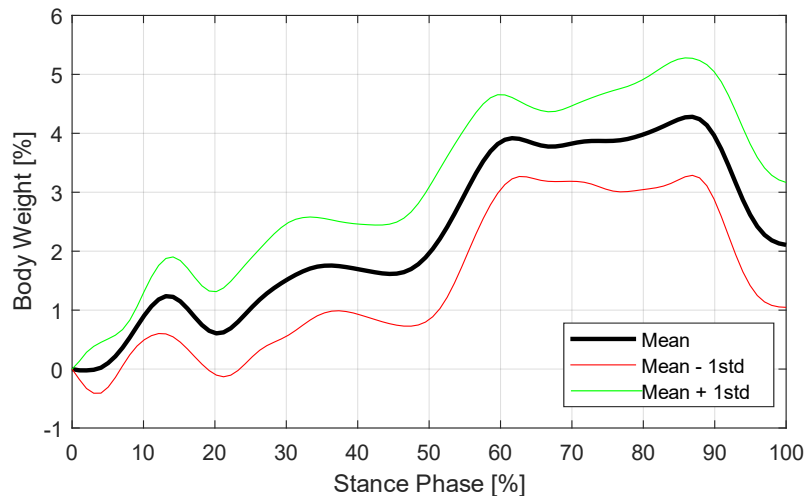


Figure 4.4.6 – Medio-lateral ground reaction forces. In the upper figure experimental processed data are presented: averaged data are represented with a black thick line, while the red and green line are respectively averaged data plus or minus the standard deviation. In the lower figure there is the medio-lateral GRF for a healthy subject [56].



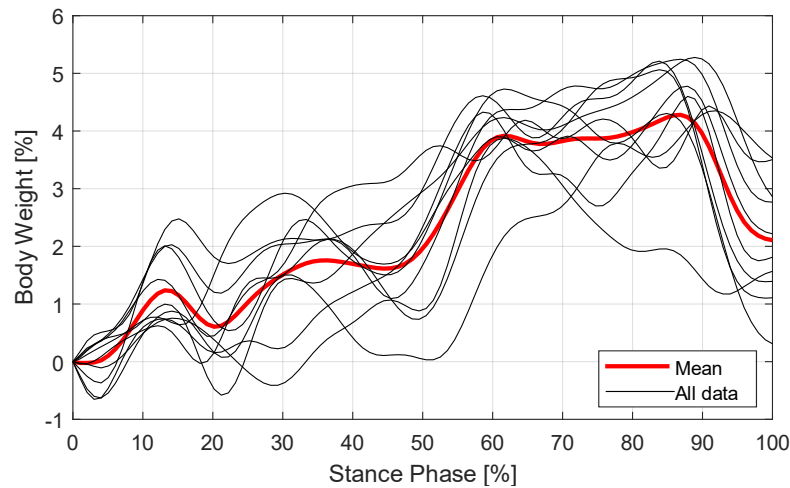


Figure 4.4.7 – Medio-lateral ground reaction force. The black lines are the filtered data referring to each trial. The thicker red line is the averaged medio-lateral ground force.

#### 4.4.2 Anterior-Posterior COP Displacement

The Centre Of Pressure (COP) of a healthy subject (Figure 4.4.9, next page) remains in the hindfoot for a third of the stance phase, then switches from the back to the forefoot with a rapid variation and finally remains under the forefoot for the last 30% of the stance phase. These events cannot be noticed when analysing the anterior-posterior COP displacement of the prothesized subject (Figure 4.4.8): in fact, his COP stays in the backfoot for mostly the first 50% of the stance phase, then rapidly switches to the forefoot from 50% to 80% of stance phase and finally remains under the forefoot for the last 20% of stance phase. Apparently, COP starts moving from back to forth around 50% of stance phase, when we could also see the vGRF peak discussed before. Therefore, even COP displacement apparently confirms the hypothesis that the prosthetic foot snaps when the load is transferred from the heel lamina to the keel lamina.

Medio-lateral COP displacement is not reported since it will be not considered in this study.

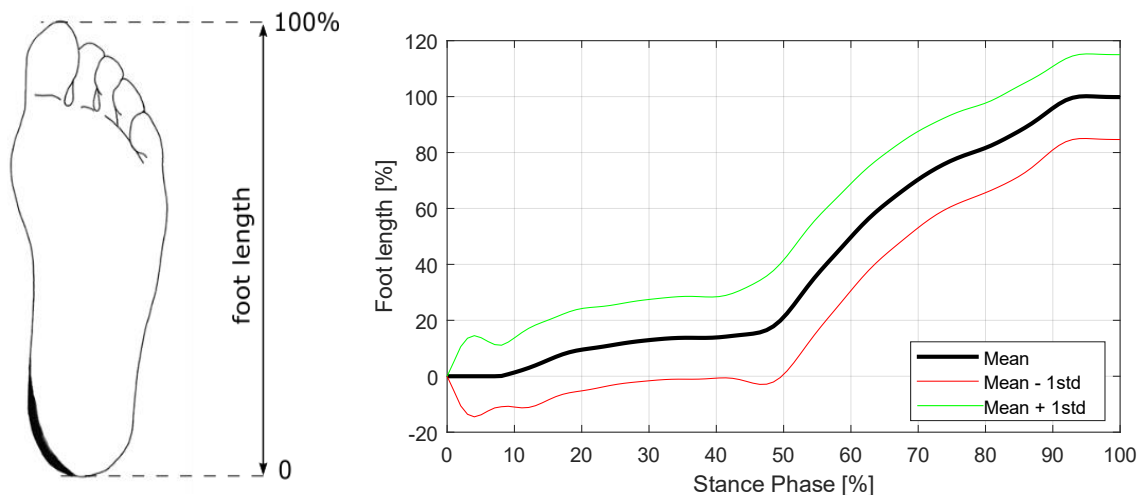


Figure 4.4.8 - Posterior-anterior COP displacement. Averaged data are represented with a black thick line, while the red and green line are respectively averaged data plus or minus one standard deviation.



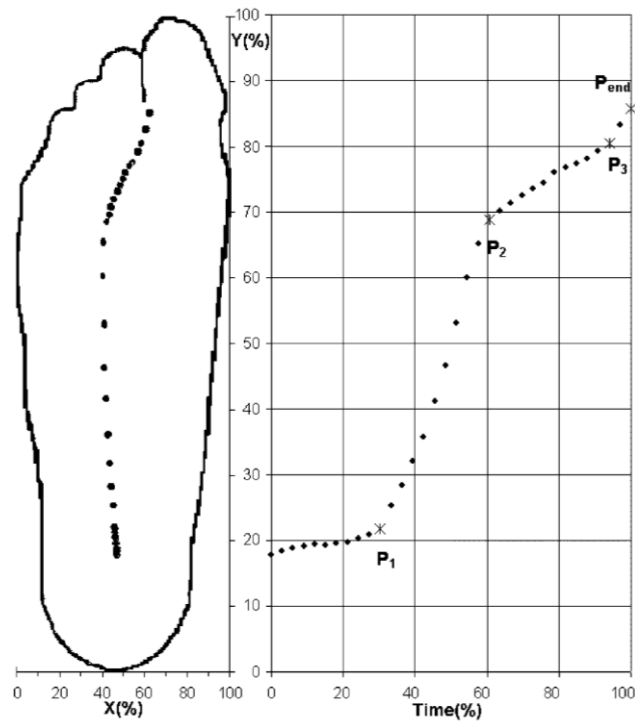


Figure 4.4.9 – Posterior-anterior COP displacement for a healthy subject [11].

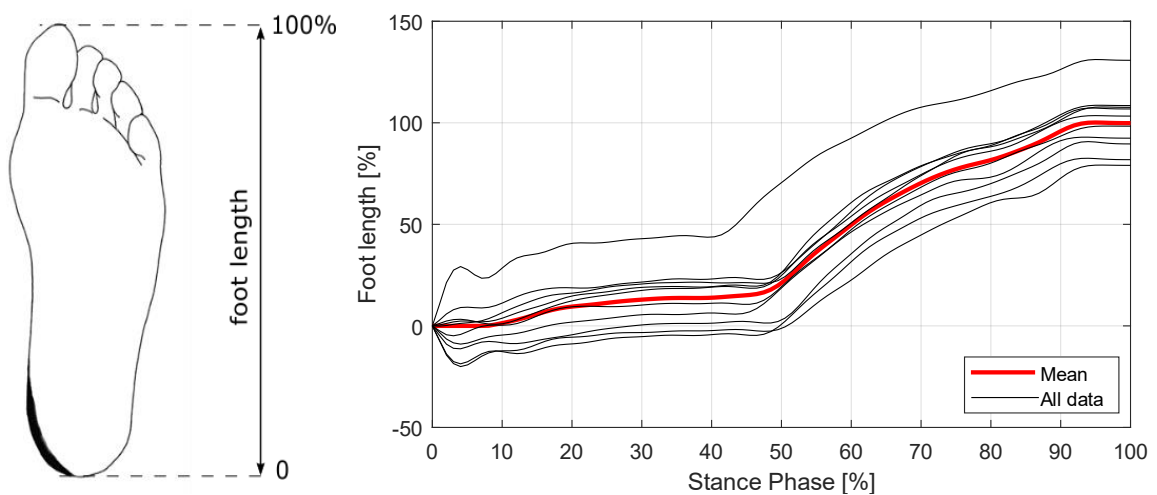


Figure 4.4.10 – Posterior-anterior COP displacement. The black lines are filtered data referring to each trial. The thicker red line is the averaged posterior-anterior COP displacement.

### 4.4.3 Pylon Angle

The pylon angle found experimentally (Figure 4.4.12, next page) is compared to the pylon angle (or “tilt angle”) provided by ISO 22675 legislation (Figure 4.4.11, next page). This legislation regulates the fatigue test on prosthetic feet in the European Union member states.

What could be noticed is that the prothesized subject touched the ground with a higher foot inclination and leave it with a lower inclination. This could happen because the subject was wearing a locked knee prosthesis and could not find a proper contact angle with the ground. Also, the subject said that he was feeling uncomfortable while loading the forefoot because he had the feeling of falling.

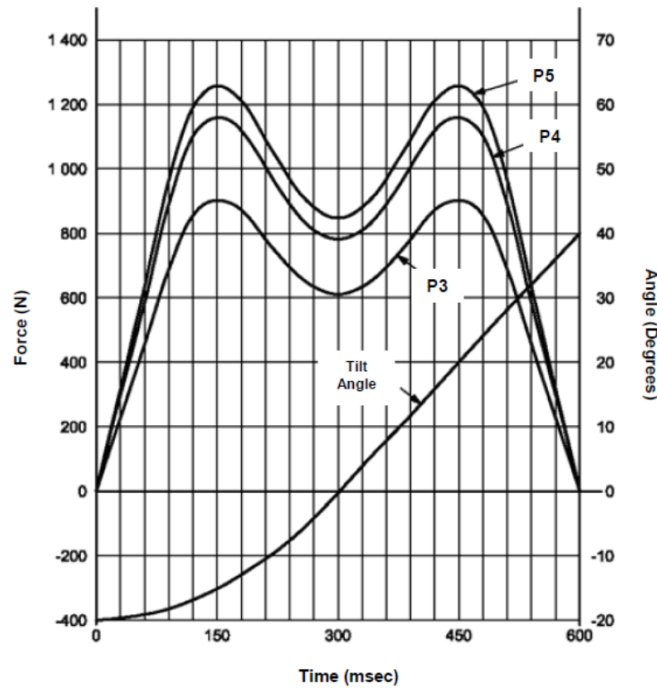


Figure 4.4.11 – Legislation ISO 22675 for fatigue test on prosthetic feet. The tilt angle refers to the already described pylon angle. In this case, the angle is referred to a period that is typically the duration of the stance phase.

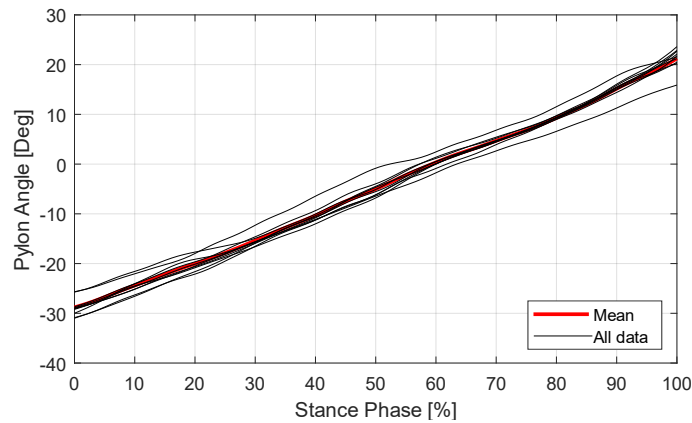


Figure 4.4.12 – Pylon angle. The angle is negative when the foot is ahead of an imaginary line perpendicular to the ground and passing through the hip joint, while is negative when the foot is behind it. The black lines are the filtered data of all trials. The thicker red line is the averaged inferior-superior ground force.

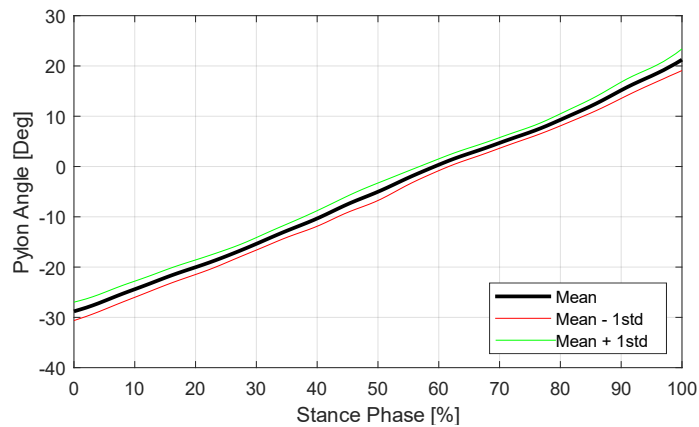


Figure 4.4.13 – Posterior-anterior COP displacement. In the upper figure experimental processed data are presented: averaged data are represented with a black thick line, while the red and green line are respectively averaged data plus or minus the standard deviation.

#### 4.4.4 Marker Distances

For marker distances there were no terms of comparison with the literature, but the FootBack marker was expected to come closer to the TibiaUpFront marker when the heel was loaded and to move away from it when the toe was loaded. On the other hand, the FootFront marker was expected to move away from TibiaUpFront when the heel was loaded and to come closer to it when the forefoot was loaded. This behaviour will be called from now on “rocker effect” and will be of great importance in the further study.

These expectations have been confirmed by the experimental results presented from Figure 4.4.14 to Figure 4.4.16.

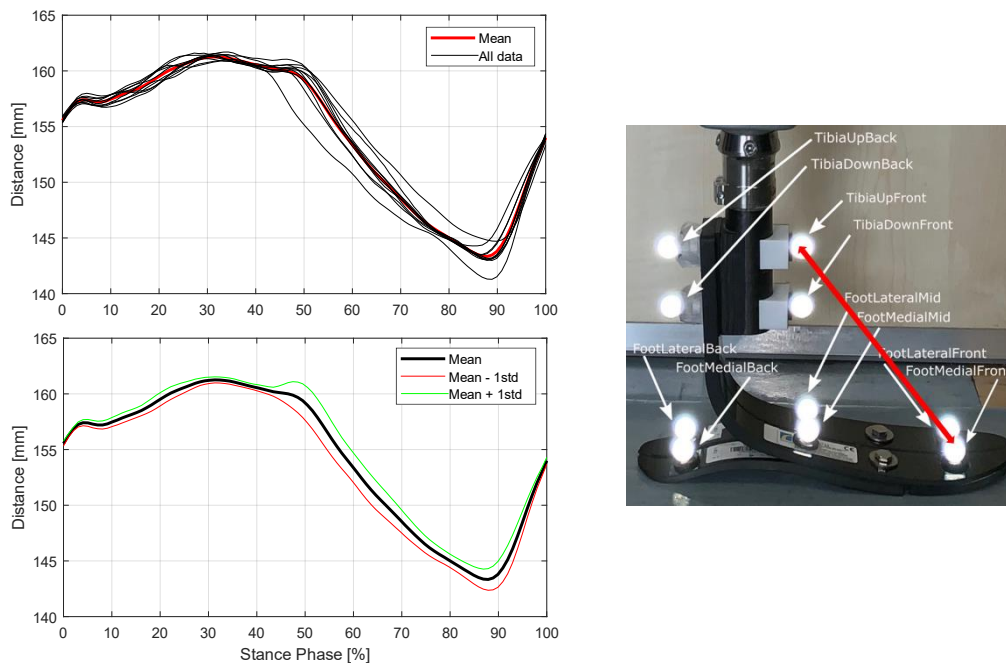


Figure 4.4.14 – Distance between FootFront markers and TibiaUpFront markers over stance phase.

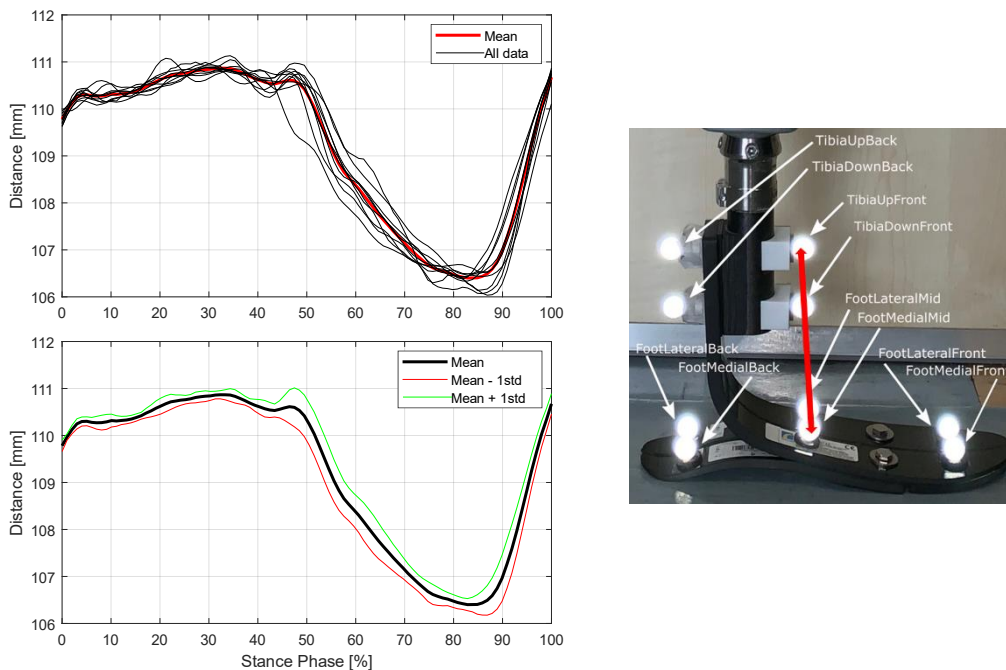


Figure 4.4.15 – Distance between FootMid markers and TibiaUpFront markers over stance phase.

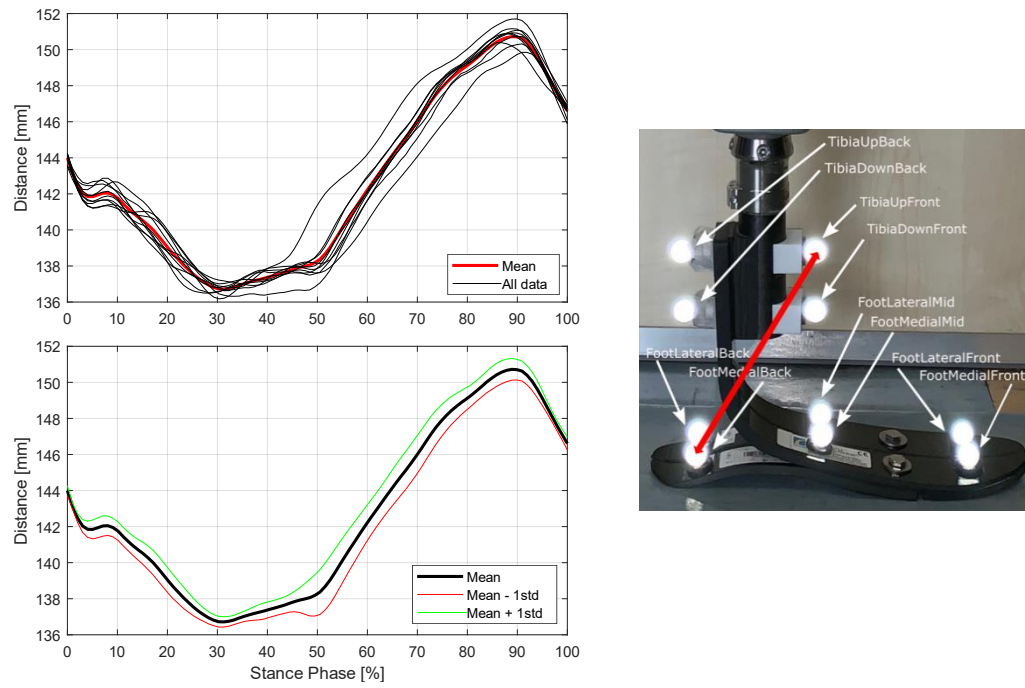


Figure 4.4.16 – Distance between FootBack markers and TibiaUpFront markers over stance phase.

## 5. Dynamic Simulations

---

*The MATLAB® script can be found at Appendix A – eighth paragraph: Dynamic Simulation – ‘vari-flex\_model.m’. The Simulink schemes are shown in Appendix B – sixth and seventh paragraphs: Former Dynamic Vari-Flex® Model – ‘sim\_vari\_flex\_dyn\_16\_9.slx’ and Modified Dynamic Vari-Flex® Model – ‘sim\_vari\_flex\_dyn\_1sr\_locked.slx’.*

This Chapter is dedicated to the description of the methods followed to reproduce a dynamic simulation of the stance phase on the Vari-Flex® foot. The inputs provided to the model and the outputs produced are presented here.

The way ground reaction forces are applied to the model produces a variation in COP displacement. Therefore, it will be necessary to discuss how the COP anterior-posterior displacement is influenced by the forces’ application method.

Finally, since from the first simulations it could be noticed that the model could not reproduce the *rocker* effect, some changes in the Simulink® model have been done. After these changes, the results obtained were more reliable to the experimental marker displacements.

### 5.1 Dynamic Simulation of Stance Phase

To run a dynamic simulation on the Vari-Flex® multibody model, different issues must be solved:

- How to apply the ground reaction forces to the model;
- How the COP varies when applying the external force to a non-continuous model;
- How to model the experimental markers in order to measure the same deflections;
- How to reproduce all the dynamic effects that the experimental results present.

In the further paragraphs all these issues will be discussed and the strategies used to overcome them will be presented. But first, the inputs and outputs which necessary to run a complete dynamic simulation of the stance phase and the chosen parameters will be introduced.

#### 5.1.1 Inputs and Outputs Signals

To proper run a dynamic simulation of the Vari-Flex® foot it is necessary to give data listed below to the model.

- Pylon angle progression
- Vertical Ground Reaction Force (vGRF)
- Horizontal Ground Reaction Force (hGRF)

COP posterior-anterior progression, instead, will be used as a control signal to proper address the point application of the GRFs. The strategies followed to apply the external forces to the model will be further discussed in Paragraph 5.1.3. Ground Reaction Forces, COP displacement and pylon angle progression data obtained from experimental measurements (Paragraphs 4.4.1 and 4.4.3) will be the main parameters.

During the simulation, the model calculates the distances between some simulated markers<sup>7</sup> that reproduce the experimental ones (TibiaUpFront, FootBack, FootMid and FootFront) and the distances between each segment midpoints and the ankle joint over time. This latter information will be useful to calculate the simulated Roll-Over-Shape (ROS) of the Vari-Flex®, a parameter widely used to characterize prosthetic feet. The procedure applied to calculate this parameter will be presented in Paragraph 5.1.5.

### 5.1.2 Parameters

The material and simulation parameters initially used to characterize joints and rigid segments properties are resumed in Table 5.1.1.

Table 5.1.1 – Material and simulation parameters for the Vari-Flex® dynamic simulation.

Parameter	Symbol	Measurement unit	Value
Young Modulus	$E$	$GPa$	55
Density	$\rho$	$g \cdot cm^{-3}$	1.8 <sup>8</sup>
Joint's rotational damping	$\beta_{R_i}$	$N \cdot m \cdot s \cdot rad^{-1}$	0.01
Joint's rotational stiffness	$k_{R,i}$	$N \cdot m \cdot rad^{-1}$	Analythical (from Equation 2.2.25 and Equation 2.2.26) Or Determined from the tuning on quasi static conditions
Segment's thickness	$H_i$	$m$	Deducted from CAD *
Segment's length	$L_i$	$m$	Calculated from <i>segmentation_info</i>
Segment's width	$W_i$	$m$	Deducted from CAD *
Simulation duration (stance phase duration)	$T$	$s$	1.23
Sampling frequency	$f_s$	$Hz$	100

\* Resumed in Table 3.2.2

### 5.1.3 Ground Reaction Forces Application

Since it is not possible to continuatively apply the forces with this kind of model, it has been necessary to choose where to apply the external forces and when. In the next paragraph the choices made and the method utilized will be discussed.

<sup>7</sup> The marker realization in Simulink® will be addressed in Paragraph 5.1.4.

<sup>8</sup> T700S composite (TORAY, Toray Composite Materials America, Inc.)

### 5.1.3.1 COP Managing

The multibody model realized is composed of discrete segments. In Simulink® it is possible to define some *frames* on these segments in order to link them to other blocks. It has been decided to create some frames on segments that forming the foot sole. These frames have been placed on the geometric centre of the lower surface (Figure 5.1.1, next page). External forces will be applied there. This choice will influence the COP progression for the computational model (issue further analysed in Paragraph 5.1.3.4).

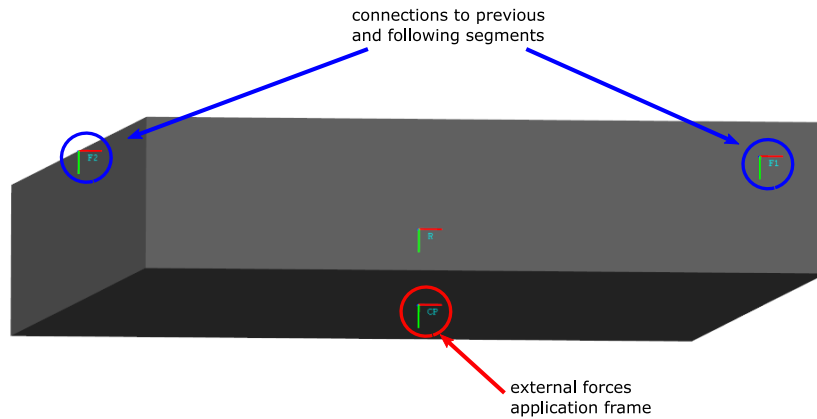


Figure 5.1.1 – Frames on foot sole's segments.

To decide which point external forces must be applied to, COP anterior-posterior progression and ground projection of segments forming the foot sole will be considered. With the use of a MATLAB® script<sup>9</sup>, it is possible to apply vGRF and hGRF on the external force application frame of the segment which is containing the COP at each instant. In Figure 5.1.2 this concept is schematized: the COP posterior-anterior progression plot is divided into 13 parts (each one represent a foot sole segment). This way, it is possible to visualize when the COP remains under each of the segments forming the foot sole.

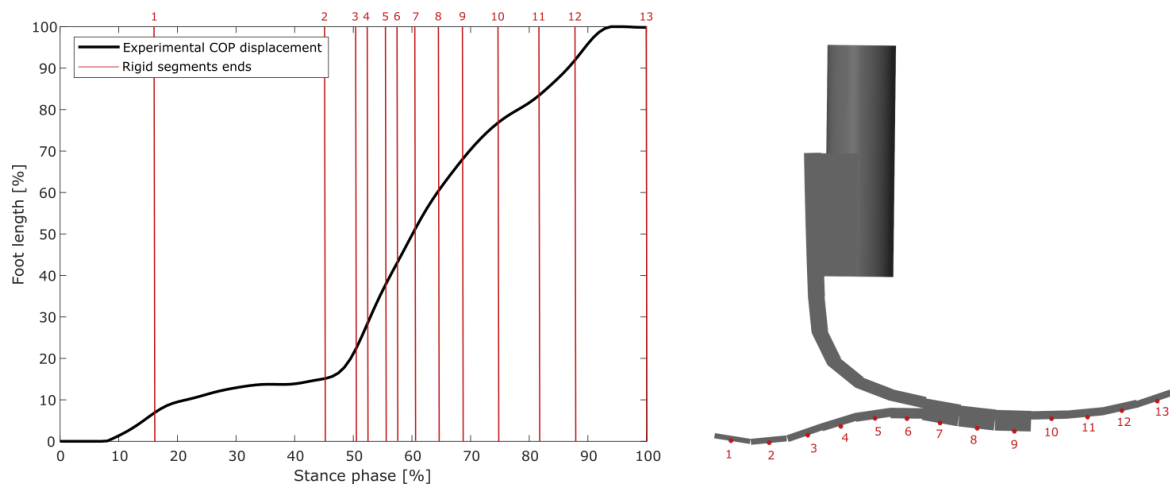


Figure 5.1.2 – COP progression over Vari-Flex® foot multibody model. Each vertical red line represents the instant when the COP switches from one segment to the following one.

<sup>9</sup> Dynamic Simulation – 'variflex\_model.m', sections "Definition of the posterior/anterior ground force acting on each segment over time [N]" and "Definition of the inferior/superior ground force acting on each segment over time [N]"

External forces could have been also applied to the starting and the ending point of each segment, but the main interest of this study is to keep the model as simple as possible. Therefore, it has been chosen to limit the number of loaded points to control during the simulation.

### 5.1.3.2 First Strategy

Once defined the points to which apply the GRFs, the first dynamic simulations have been run using the force profiles presented in Figure 5.1.3 (next page). Each different colour represents the profile of the force applied to each segment. This strategy allows to maintain ground reaction forces' experimental profiles, as it can be seen in Figure 5.1.3.

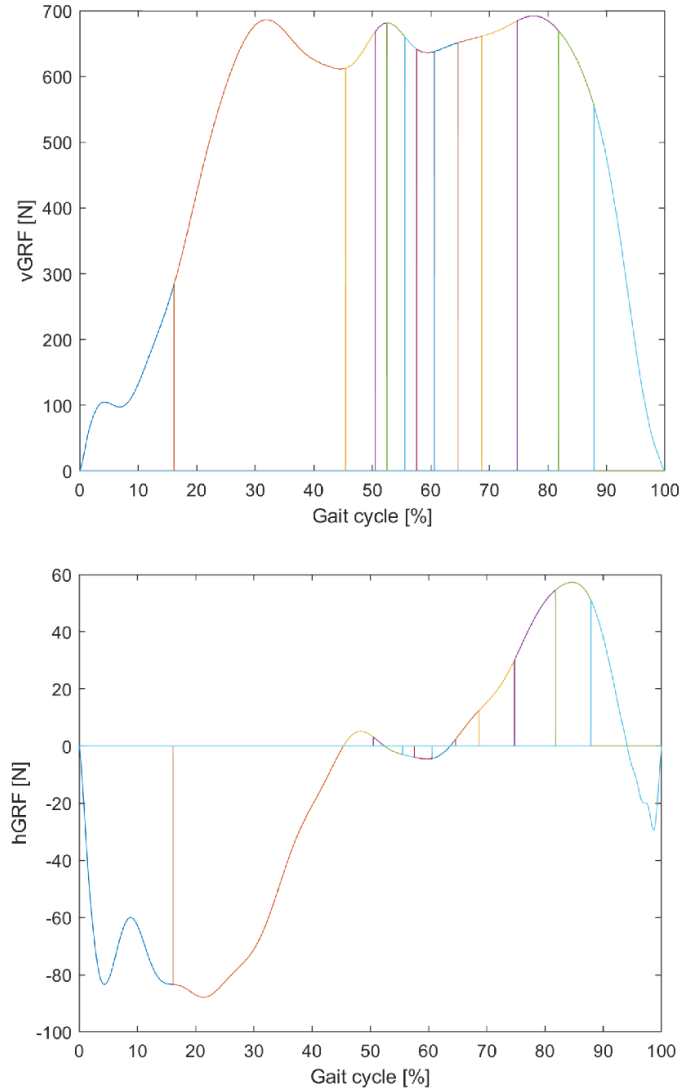


Figure 5.1.3 – First strategy's forces profiles. The upper image refers to the vertical ground reaction forces, while the lower one refers to horizontal ground reaction forces. Each vertical line represent the instant when the previous segment is unloaded and the following one becomes loaded.

In this way, each segment is loaded by proper GRFs during the correct stance phase's period.

### 5.1.3.3 Second Strategy

Using the first strategy to run the dynamic simulations, it is possible to notice that the model starts to vibrate at a certain point. As a matter of fact, unloading and loading each segment with a sudden force variation makes the model vibrate. The system, in fact, is described as a harmonic damped torsional oscillator and, as a second order dynamic system, it starts to vibrate when excited by a step



input. In this situation GRFs can be considered as step inputs, so when they are suddenly applied to a rigid segment, they make the model vibrate.

To solve this issue, few lines of MATLAB® script have been written to allow a smoother application of GRFs to each segment. Hence, each one of them is loaded and unloaded with a ramp profile of force.

To do so, the period in which the COP remains under each segment has been computed. Now it is possible to start unloading the segment from the 70% of this time period and to start loading the following one from the same instant. It has also been paid attention to not modify the overall force profile both for vGRF and hGRF.

The forces profile obtained are shown in Figure 5.1.4. The red line represents the sum of all the GRFs: it can be noticed that it follows the experimental force profile for both vGRF and hGRF.

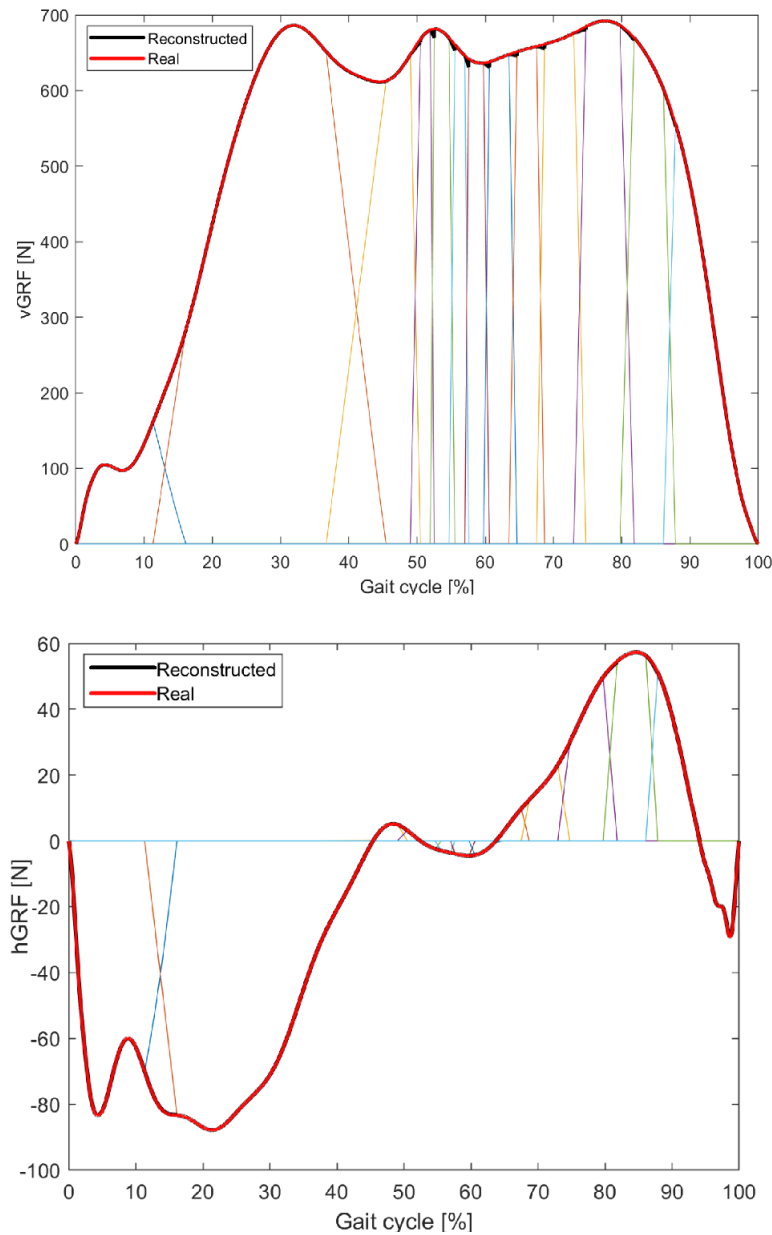


Figure 5.1.4 – Second strategy's forces profiles. The upper image refers to the vertical ground reaction forces, while the lower one refers to horizontal ground reaction forces. It can be noticed how 'reconstructed' force profiles (black thick line) and 'real' force profile (red thick line) are the same because they are not distinguishable.

This strategy allows to visibly reduce the vibrations. The output cannot be presented here, since it would be necessary to show a video of the different simulations before and after the modifications.

#### 5.1.3.4 COP Displacement Variations

This discretization of the Vari-Flex® model leads to variations in COP progression: since the GRFs remains in the same point for a period, the COP progression too becomes “discretized”. At the same time, the second forces application strategy determines COP progression’s variations: while the previous segments is being unloaded and the following one starts to be loaded, the COP moves midway between the two segments’ centres. These variations are reported in Figure 5.1.5.

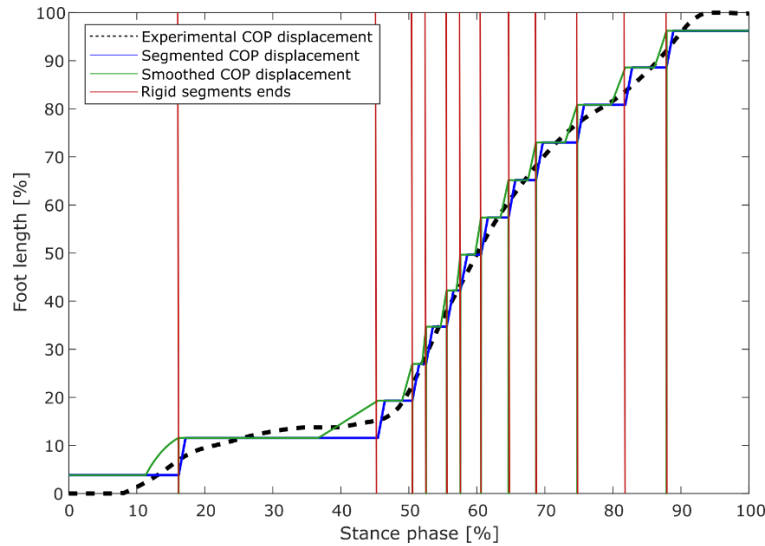


Figure 5.1.5 – COP progression for different loading conditions. The black dashed thick line represent the experimental COP posterior-anterior progression. Blue curve is the COP progression when the model is loaded following the first strategy for force application. Green curve is the COP progression when the model is loaded following the second strategy for force application.

As it can be seen, the computed COP does not differ much from the experimental one, so both force application strategies do not introduce significant errors to the modelling (RMSE% error reported in Table 5.1.2). It can also be noticed that the second strategy causes the simulated COP to anticipate the experimental one.

Table 5.1.2 - %RMSE of segmented and smoothed COP with respect to the experimental COP.

	Segmented COP	Smoothed COP
% RMSE	2.44	2.53

#### 5.1.4 Markers Modeling with Simscape

Now that the model can simulate a complete stance phase, it is important to recreate the markers within Simulink® environment. These virtual markers will be used to compute the distances between them. Then, computed distances will be compared to the ones found experimentally. This process will be fundamental to see if the multibody model works properly reproducing the real foot behaviour.

To model the marker, a Simscape *Solid* block with spherical geometry has been used. The radius considered is equal to 5 mm. Markers were modelled as rigid bodies with negligible weight to not influence the inertial properties of the foot, just as the real markers do. Hence, it has been assigned

to it a density equals to  $1 \text{ kg} \cdot \text{m}^{-3}$  (1000 times lower than the one of distilled water). The spherical body was connected to the foot structure with a *Rigid transform* block that allowed me to properly place the marker with respect to the Vari-Flex®.

It was also possible to not physically model the markers with *Solid* blocks, but it has been preferred to do so to have a visual reference when the model was running (Figure 5.1.6, next page).

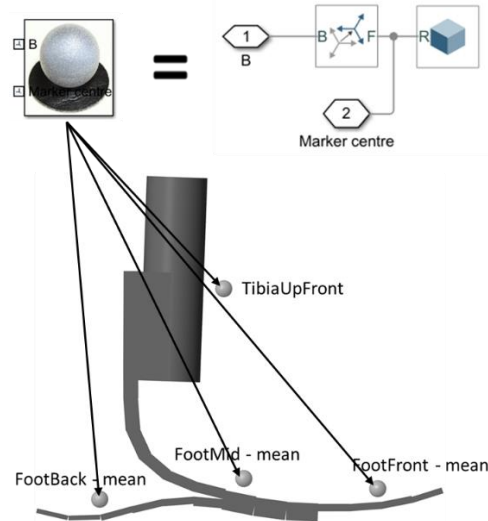


Figure 5.1.6 – Markers' modeling resuming scheme. In the upper part of the image there is the Simscape scheme created to simulate one marker. In the lower part there is the model visualization.

#### 5.1.4.1 Distance between Markers Calculation

Once modelled the markers, the last step to do is to calculate the distance between them. To achieve this, a *Transform sensor* block has been used, as shown in Figure 5.1.7. The distance is calculated between the geometrical centres of the markers. This choice reflect what the camera acquisition system does: it considers the markers' centres to define their 3D position.

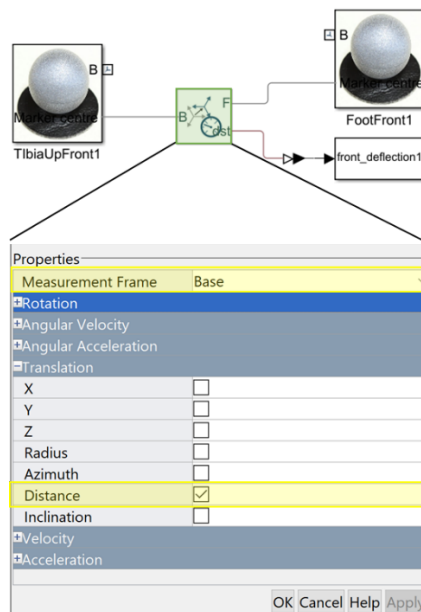


Figure 5.1.7 – Calculation of distance between simulated markers. The *Transform sensor* block is set on *Distance* calculation. The reference frame is *Base*. In this specific case the base segment will always be The geometrical centre of *TibiaUpFront* marker.

To calculate deflections, the initial offset<sup>10</sup> has been removed to the calculated distances. The three deflections calculated will be named as:

- *Back deflection* – FootBack deflection with respect to TibiaUpFront.
- *Mid deflection* – FootMid deflection with respect to TibiaUpFront.
- *Front deflection* – FootFront deflection with respect to TibiaUpFront.

### 5.1.5 ROS Calculation

The last parameter to calculate is the foot Roll-Over Shape (ROS), which is *calculated as the transformation of centre of pressure data into a shank-based coordinate system* [58]. This is an important parameter for evaluation of prosthetic feet. What will be further done is to compare the ROS curvature radius computed by the multibody model with the one found by L. Cavallaro with his FEA model.

To calculate ROS, the method proposed by A. Hansen et al. [58] in their study has been followed. Since they have acquired different experimental data to compute ROS, it has been necessary to compute the parameters used by A. Hansen et al. using different initial information. In the further paragraph the changes made will be discussed. Resuming, the main difference between the two approaches is the way the parameters are calculated and the absolute reference system position. In fact, in A. Hansen et al. work, the origin of the reference system is placed at the beginning of the force plate, while in this study the origin is placed at the top of the pylon connection.

#### 5.1.5.1 ROS Calculation on Vari-Flex Multibody Model

First, the method used by A. Hansen et al. [58] is presented, then the analogies and the differences between it and the method here used will be discussed.

A. Hansen et al. proposed a method based on markers and force platform data. Parameters and reference systems considered by A. Hansen et al. are shown in Figure 5.1.8. Ankle marker (ANKLE), knee marker (KNEE) and centre of pressure position (COP) will be the relevant points of the further discussion.

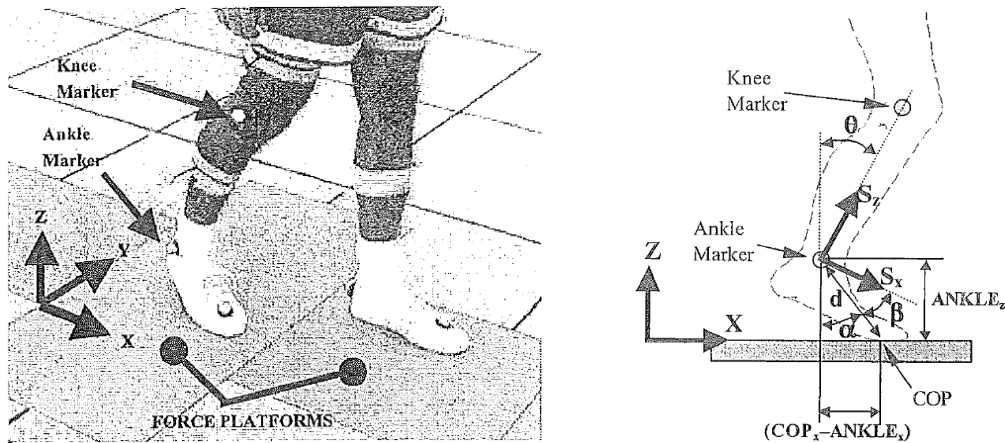


Figure 5.1.8 – Schematic explanation of the instruments used (on the left) and the parameters considered (on the right) to calculate ROS in A. Hansen et al. study [58].

The ROS calculation proposed is shown in Equation 5.1.1:

<sup>10</sup> The initial offset is the distance between markers when the foot is undeformed.

$$\begin{cases} COP_{S_x} = d \cdot \cos(\beta) \\ COP_{S_y} = -d \cdot \sin(\beta) \end{cases}$$

Equation 5.1.1 – ROS calculation in shank-based coordinate system implemented by A. Hansen et al. [58]

Where:

$d = \sqrt{(COP_x - ANKLE_x)^2 + ANKLE_z^2}$  is the distance between COP and ANKLE points.

$\beta = \frac{\pi}{2} - \theta - \alpha$  is the angle between  $\overline{ANKLE - COP}$  segment and the line perpendicular to the ground and passing through ANKLE.

$\theta = \arctan\left(\frac{KNEE_x - ANKLE_x}{KNEE_z - ANKLE_z}\right)$  is the angle that the shank forms with the line perpendicular to the ground and passing through ANKLE.

$\alpha = \arctan\left(\frac{COP_x - ANKLE_x}{ANKLE_z}\right)$  is the angle between  $\overline{ANKLE - COP}$  segment and the line perpendicular to the ground and passing through ANKLE.

The fundamental aspect of this method is that COP is always moving on X-axis with Z-coordinate equals to 0, while  $ANKLE_x$ ,  $ANKLE_z$ ,  $KNEE_x$  and  $KNEE_z$  coordinates may vary overtime. In the Vari-Flex multibody model I have implemented, the ankle joint is fixed, and COP may vary overtime. Moreover, knee markers have not been used but, it is possible to compute  $\theta$  as the angle between the markers TibiaUpFront and Tibia Down Front (as discussed in Paragraph 4.4.3)

The formulas used to calculate the ROS will be presented and justified. The parameters considered are the same of A. Hansen et al. study but reorganized to adapt to the multibody model, as shown in Figure 5.1.9. It is important to notice that in my model Y-axis corresponds to the Z-axis considered in the previous discussion.

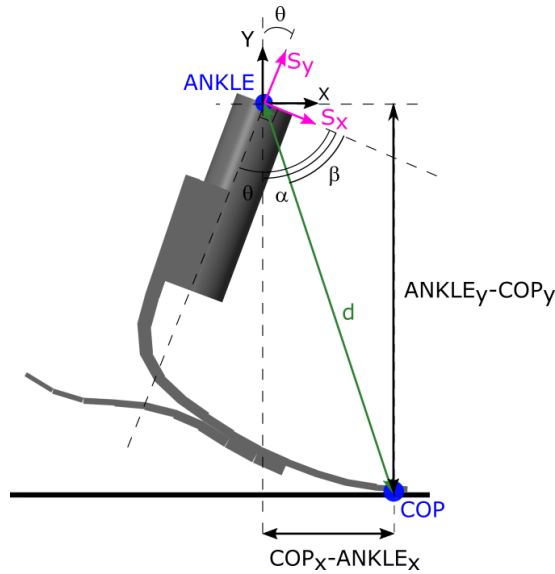


Figure 5.1.9 – Schematic representation of parameters used to evaluate ROS of Vari-Flex multibody model.

The formulas used to finally compute the ROS (Equation 5.1.1) do not change, but the way the other parameters are calculated does.

Since COP is moving along X and Y axes with respect to ANKLE and ANKLE is the origin of the reference system ( $ANKLE_x = 0, ANKLE_y = 0$ ), the distance between COP and ANKLE ( $d$ ) can be written as:

$$d = \sqrt{(COP_x - ANKLE_x)^2 + (COP_y - ANKLE_y)^2} = \sqrt{COP_x^2 + COP_y^2}$$

Equation 5.1.2 – Mathematical formula that allows to compute the distance between COP and ANKLE in Vari-Flex multibody model.

Simscape's *Transform Sensor* block admits to directly compute the distance between two points. Therefore, is not necessary to use Equation 5.1.2 but, it is exactly the formula implemented by *Transform Sensor* block.

The same logic is useful to define the formula to compute  $\alpha$ , which it can be expressed as:

$$\alpha = \arctan\left(\frac{COP_x - ANKLE_x}{COP_y - ANKLE_y}\right)$$

Equation 5.1.3 - Mathematical formula that allows to compute the angle between  $\overline{ANKLE - COP}$  and the line perpendicular to the ground and passing through ANKLE.

*Transform Sensor* blocks have always been used to retrieve information relative to COP's and ANKLE's X-coordinate and Y-coordinate positions. In Figure 5.1.10 it is possible to see the correct setting of *Transform Sensor* blocks in order to compute the previous parameters.

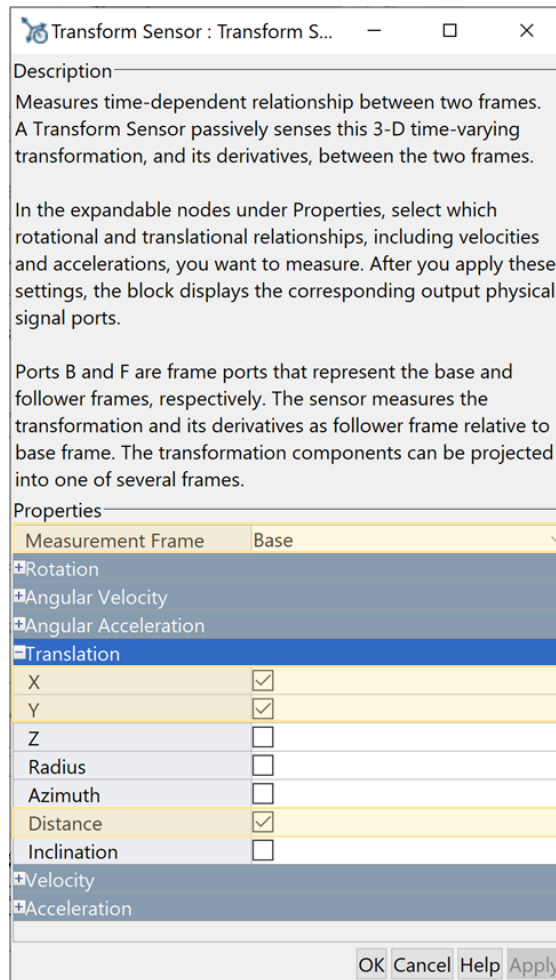


Figure 5.1.10 – Transform Sensor block settings to properly calculate  $COP_x - ANKLE_x$  (Translation – X),  $COP_y - ANKLE_y$  (Translation – Y) and d (Translation – Distance). The measurement frame is set on Base, which in this case is the ankle joint (ANKLE).

As discussed before,  $\theta$  could be reconducted to the pylon angle data. While  $\beta$  maintains the same formula used by A. Hansen et al:

$$\beta = \frac{\pi}{2} - \theta - \alpha$$

Equation 5.1.4 - Mathematical formula that allows to compute  $\beta$  angle in Vari-Flex® multibody model.

Now it is possible to calculate the ROS with the multibody model, but it is necessary to point out one last thing: since GRFs have been applied only to segments' midpoints, it has been decided to calculate the ROS when each foot sole segment reaches the maximum deflection value.

As proposed by A. Hansen et al. [59], it is possible to characterize the ROS of a foot by approximating it with a circumference. To do so, a MATLAB® function named `CircleFitByPratt` could be used. This function develops the method proposed by V. Pratt [60]. The strong point of this method is that “it works well even if data points are observed only within a small arc”, as reported by N. Chernov, the author of `CircleFitByPratt` MATLAB® function [61]. This function returns radius and centre coordinates (X,Y) of the approximant circle as outputs. The results obtained will be discussed in Paragraph 6.2.3 and compared with experimental values.

L. Cavallaro carried out the same kind of analysis with his FEA model and achieved the results shown in Figure 5.1.11.

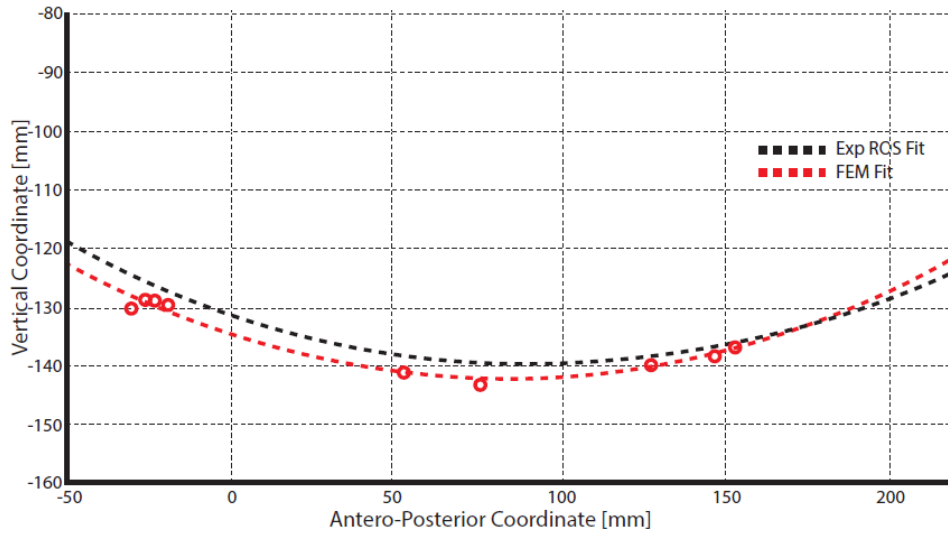


Figure 5.1.11 – Experimental (in black) and FEA (in red) fitted ROS obtained by L. Cavallaro.

From his work<sup>11</sup>, he computed a ROS radius of curvature equal to 46 cm. This value will be used to validate the multibody model developed. It is important to point out the experimental results obtained by L. Cavallaro (Exp ROS Fit) has been computed using the same experimental set described in Chapter 4.

<sup>11</sup> There are no reference about this work because L. Cavallaro paper is still to be published. He shared his results because the two works were strictly related.

## 5.2 Model Changes

Running the first dynamical simulations, it has been noticed that using the model described in Paragraph 2.5.2 the rocker effect of the foot was not reproduced by the model. In fact, the toe was not deflecting when the heel was loaded and vice versa (Figure 5.2.1, next page).

For these reasons, the Simulink® model has been modified to replicate this effect. Since it seems that the problem lies in loading transmission between front and back foot, the junction between keel and heel lamina has been identified as the probable origin of the problem. Originally, this junction was modelled as three segments connected by hinge joints. The difference between these segments and the other forming the foot is that junction segments' thickness has been assumed to be the sum of the keel and heel segments which are in contact. Moreover, the rotational stiffness of joints connecting them is the sum of the stiffnesses associated to the previously cited segments. It is important to remember that originally the junction was formed by the union of three keel spline's segments and three heel spline's segments.

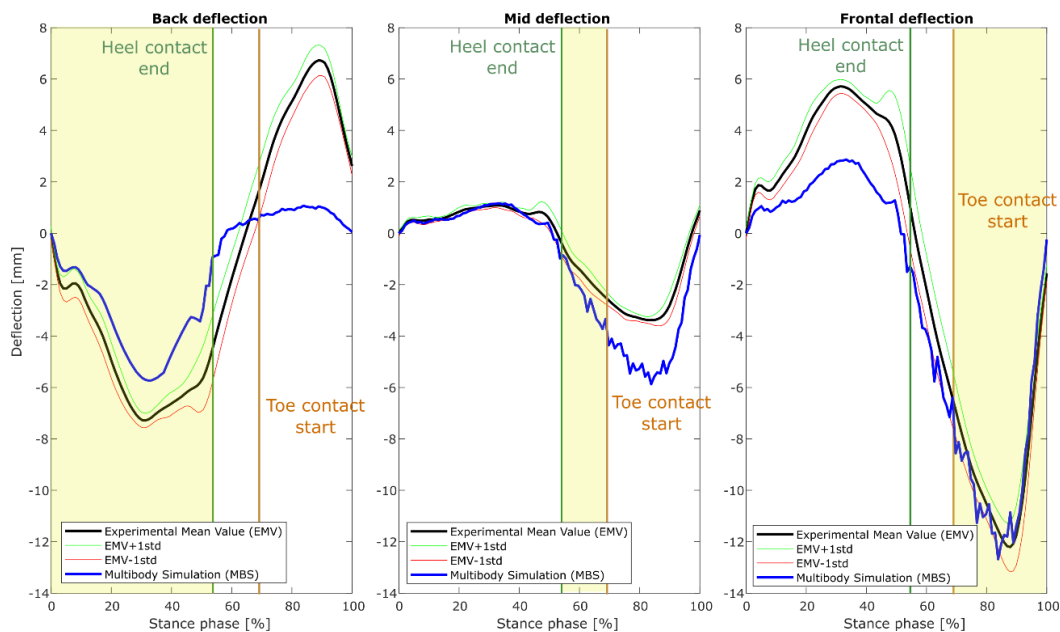


Figure 5.2.1 – Deflection of the markers on hind, mid and fore foot, calculated as explained in Paragraph 5.1.4. As it can be noticed from experimental data, when the heel lamina is loaded (from 0% to approximately 55% of the stance phase) the forefoot marker should come closer to TibiaUpFront marker, but this effect is not replicated by Multibody Simulations (MBS). The same issue may be seen when the forefoot is loaded: the backfoot marker does not move away from the TibiaUpFront marker.

It has been thought that this modeling could not reply the rocker effect because there is not transmission of linear forces between keel and heel splines. In other words, the contact between the two splines cannot be achieved with this modeling.

In order to correct the model, it is necessary to look at the real Vari-Flex® foot: the two carbon fibre laminas are joined by a screw that doesn't permit any translation or rotation (except relative rotation in the plane formed by the two laminas' surfaces, but it will be considered negligible). To reproduce the effect of the screw, a *Weld* joint that connects the two splines has been used, as shown in Figure 5.2.2.



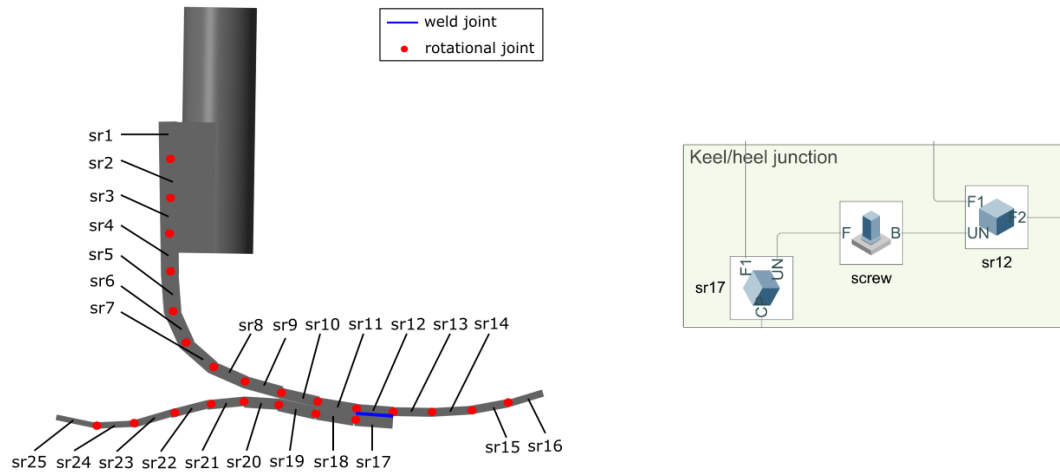


Figure 5.2.2 – Schematic representation of the Vari-Flex® multibody model after changes in junction modeling. The image on the right is the Simulink® junction model.

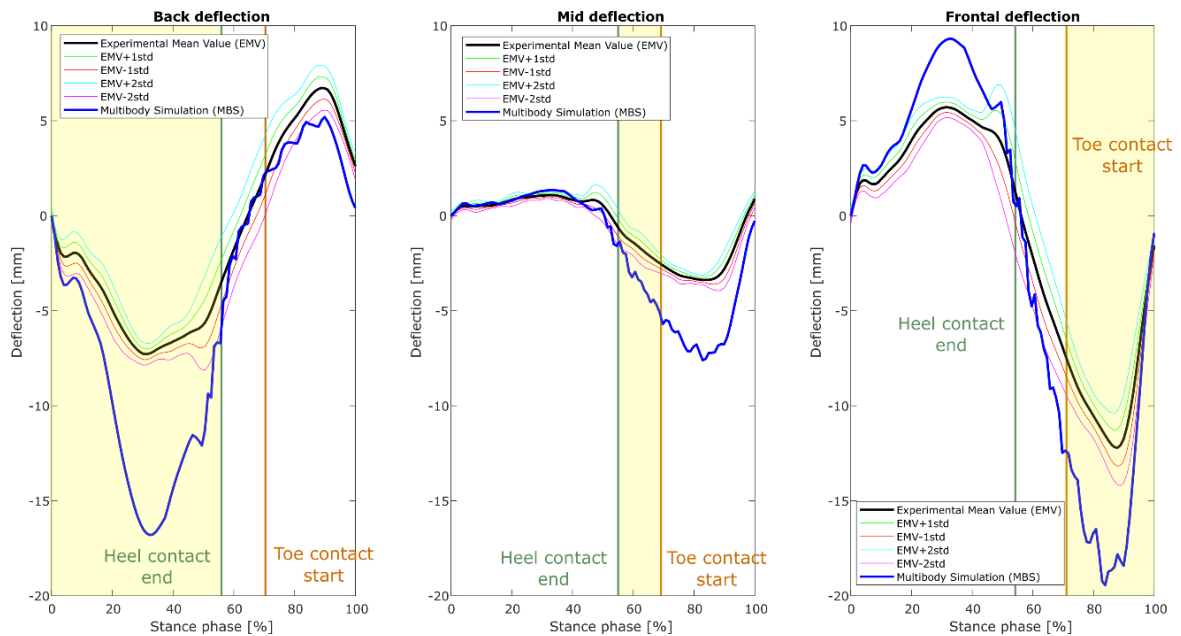


Figure 5.2.3 - Deflection of the markers on hind, mid and fore foot, calculated with the updated model.

As it can be seen, the weld joint rigidly connects the first segment of heel spline (sr17) with the twelfth one of keel spline (sr12). This way, the model could replicate the rocker effect of the Vari-Flex®, as shown in Figure 5.2.3.

Once I have seen that modeling the junction with a weld joint allowed the model to replicate *rocker effect*, I have tried to connect more than one segment and to place the weld joint in different places, as resumed in . The modelled junctions are listed down below and shown in Figure 5.2.4 (next page):

- Single weld joint between the 1<sup>st</sup> heel segment (sr17) and the 12<sup>th</sup> keel segment (sr12) – *Single* model.
- Double weld joint between 1<sup>st</sup> heel segment (sr17) and 12<sup>th</sup> keel segment (sr12) and between 2<sup>nd</sup> heel segment (sr18) and 11<sup>th</sup> keel segment (sr11) – *Double* model.
- Triple weld joint between 1<sup>st</sup> heel segment (sr17) and 12<sup>th</sup> keel segment (sr12), 2<sup>nd</sup> heel segment (sr18) and 11<sup>th</sup> keel segment (sr11) and 3<sup>rd</sup> heel segment (sr19) and 10<sup>th</sup> keel segment (sr10) – *Triple* model.

- d. Single weld joint between 2<sup>nd</sup> heel segment (sr18) and 11<sup>th</sup> keel segment (sr11) – *Single2* model

From these models, the first one has been chosen for further tuning procedures in order to reproduce the experimental deflections. To do so, the Young modulus has been modified in the range proposed by L. Cavallaro et al. [51]: 55 – 75 *GPa*. Moreover, the first model will be the one utilized to calculate the ROS.

The complete results will be presented in Paragraph 6.2.1.1 and then discussed in Paragraph 7.4.1.

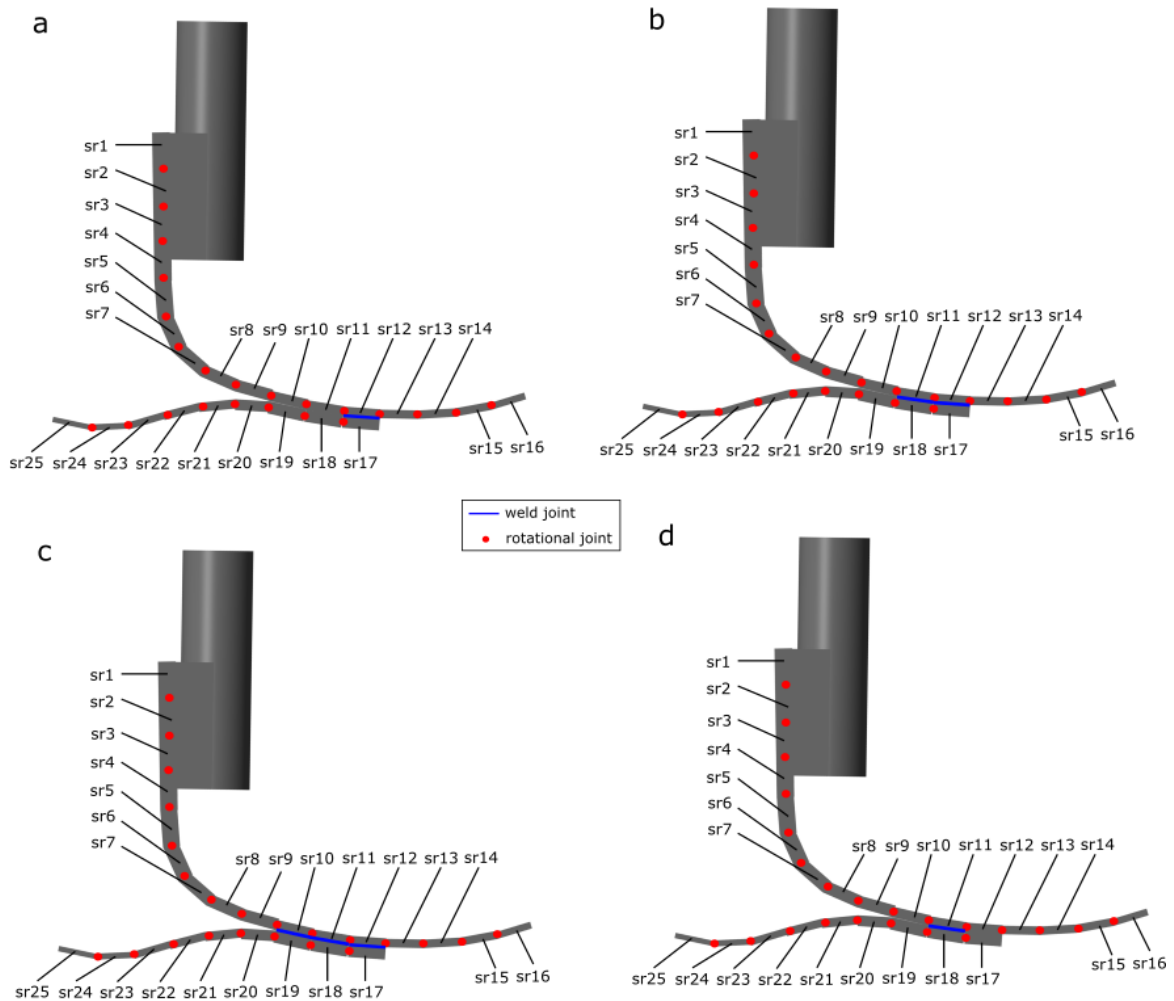


Figure 5.2.4 – Different modeling of the junction between the two laminas. The letters refer to the bulleted list above the figure. The red dots are rotational joints, while the blue lines are weld joints. a) “Single” model. b) “Double” model. c) “Triple model”. d) “Single2” model.

## 6. Results

---

This Chapter is dedicated to show the results obtained from the different test carried out on Vari-Flex® multibody model.

### 6.1 Quasi-Static Simulations on Vari-Flex® Model

In the following paragraph the differences among force-deflection curves obtained before and after tuning will be presented. The figures are referred to the different loading conditions: 20° heel touch, 10° heel touch, 10° toe touch and 20° toe touch. These results will be further discussed in Paragraph 7.1.

#### 6.1.1 Tuning Results for Each Model

In Figure 6.1.1 force vs. deflection curves obtained after stiffness tuning in each loading condition are shown. It is possible to notice that the simulated curves are linear. The possible explanation of the effect will be discussed in Paragraph 7.2.1.

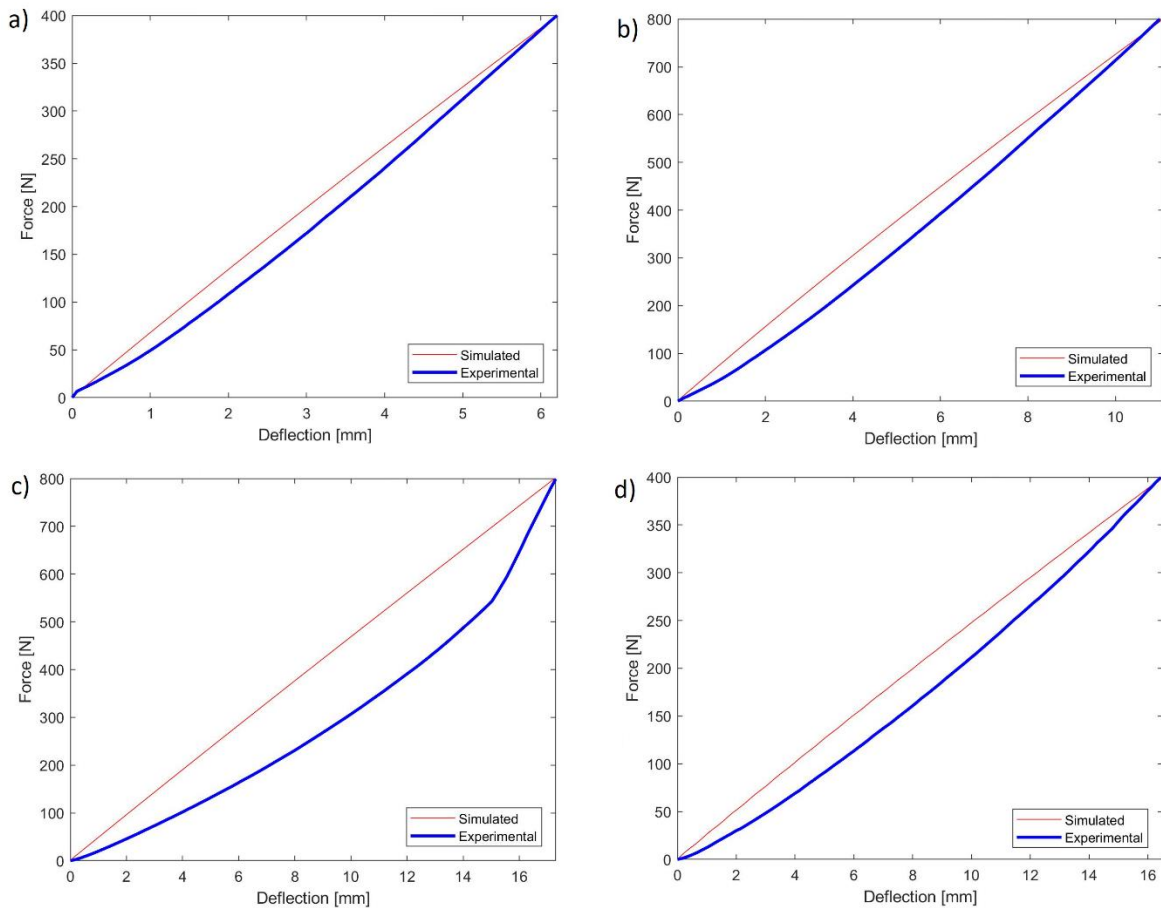


Figure 6.1.1 – Force vs. deflection experimental and simulated curves for each loading conditions. Each image refers to the tuning executed considering the single mechanical test. a) 20° heel touch. b) 10° heel touch. c) 10° toe touch. d) 20° toe touch.

### 6.1.2 Processing of Tuned Stiffness and Damping

Joints' rotational stiffness and damping, as discussed in Paragraph 3.4.2, are tuned separately for each loading conditions. Therefore, there will be four sets of tuned stiffness (Figure 6.1.2) and four sets of tuned damping (Figure 6.1.4). Data of these sets will be averaged (Figure 6.1.3 and Figure 6.1.5, the last on the following page).

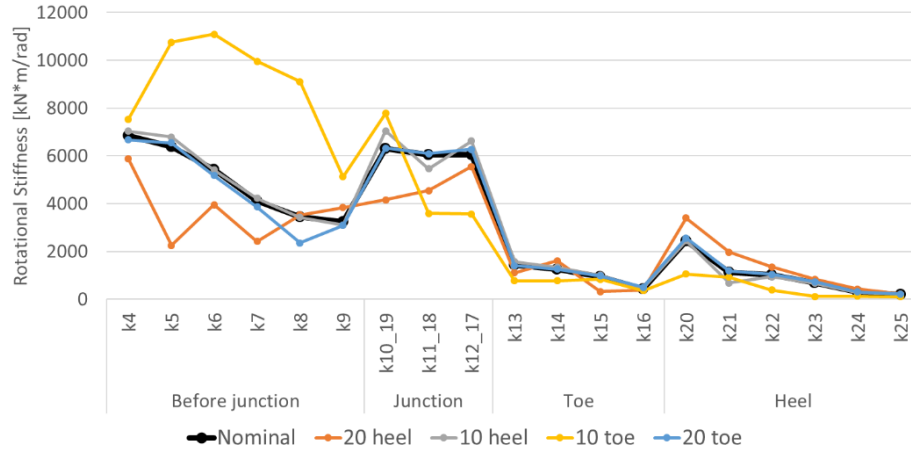


Figure 6.1.2 – Sets of tuned stiffness for each trial condition. The thick blue line represents the nominal stiffness.

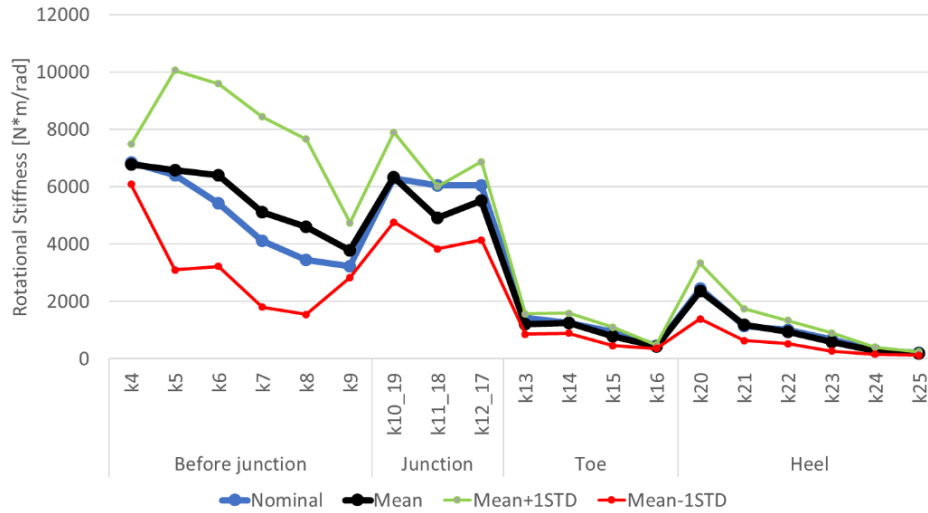


Figure 6.1.3 – Averaged tuned stiffnesses with standard deviation.

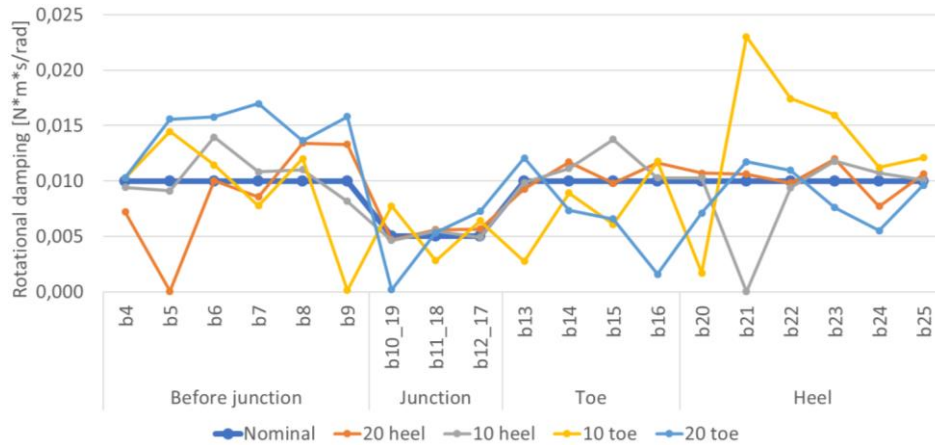


Figure 6.1.4 - Sets of tuned damping for each trial condition. The thick blue line represents the nominal damping.

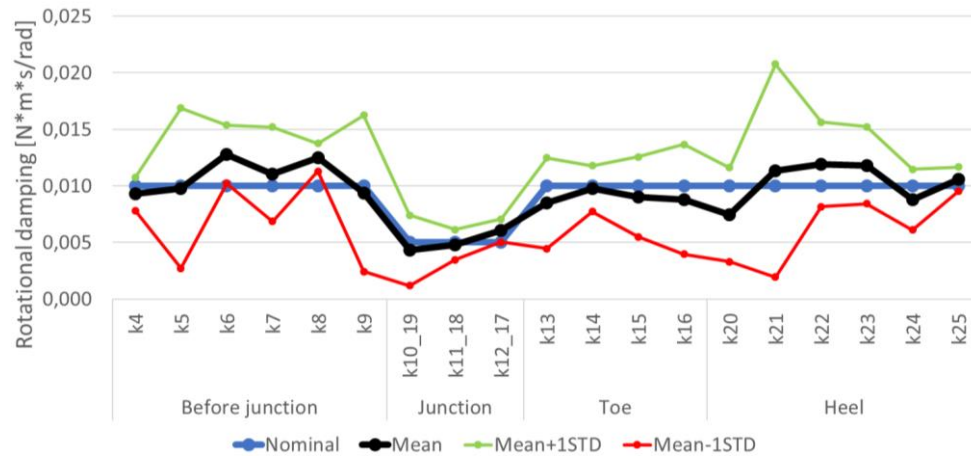


Figure 6.1.5 - Averaged tuned stiffnesses with standard deviation.

Root Mean Square Error (RMSE) between the sets of tuned stiffnesses has also been computed. This value has been referred to the nominal stiffnesses value to compute the percentage Root Mean Square Error (%RMSE), showed in Figure 6.1.6.

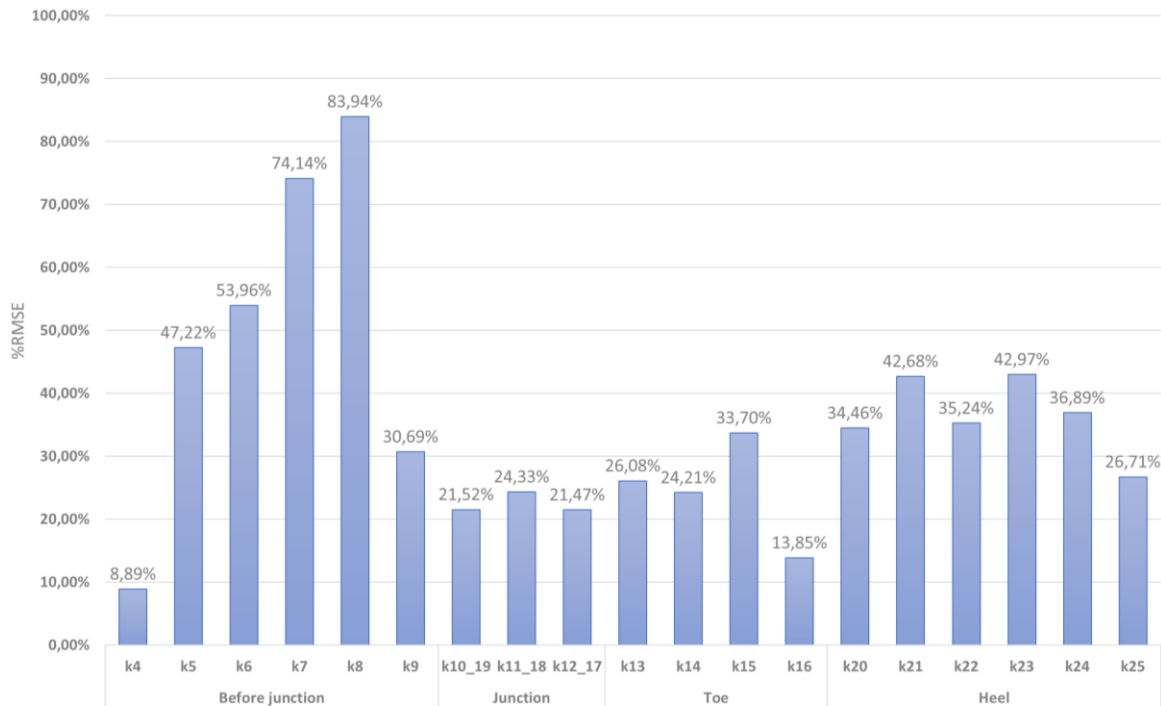


Figure 6.1.6 - % RMSE between the stiffnesses of each testing condition.

Tuned stiffnesses showed high variability between each tuning condition. This might mean that the optimization function cannot reach a local minimum shared among all the loading conditions.

### 6.1.3 Force vs. Deflection Curves Obtained with Averaged Tuned Stiffness and Damping

Averaged rotational stiffness and damping values have been used to re-run the quasi-static simulations and see if the new results were better than before. From Figure 6.1.7 to Figure 6.1.10 (next pages) the new force vs. deflection curves are shown.

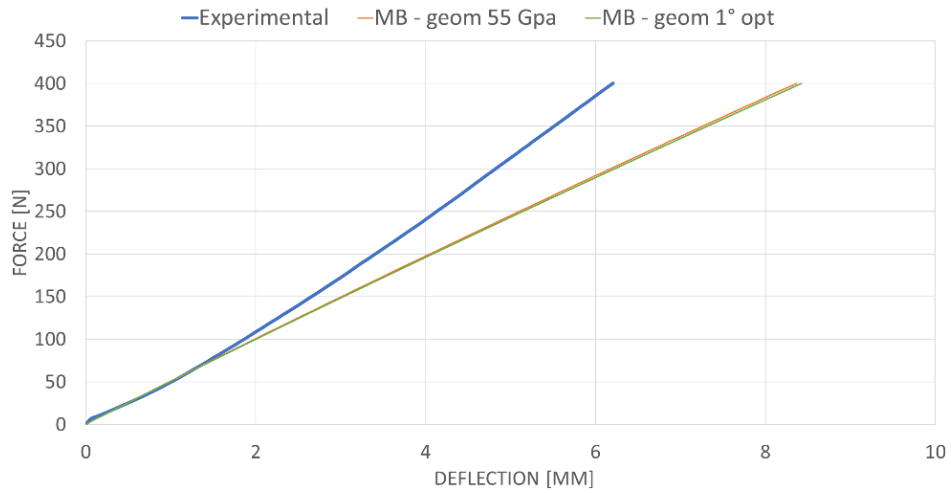


Figure 6.1.7 – Force vs. deflection diagram of 20° heel touch mechanical test. Experimental results are presented with a thick blue line. The orange line represents multibody model results before tuning. The green line represents multibody model results after tuning.

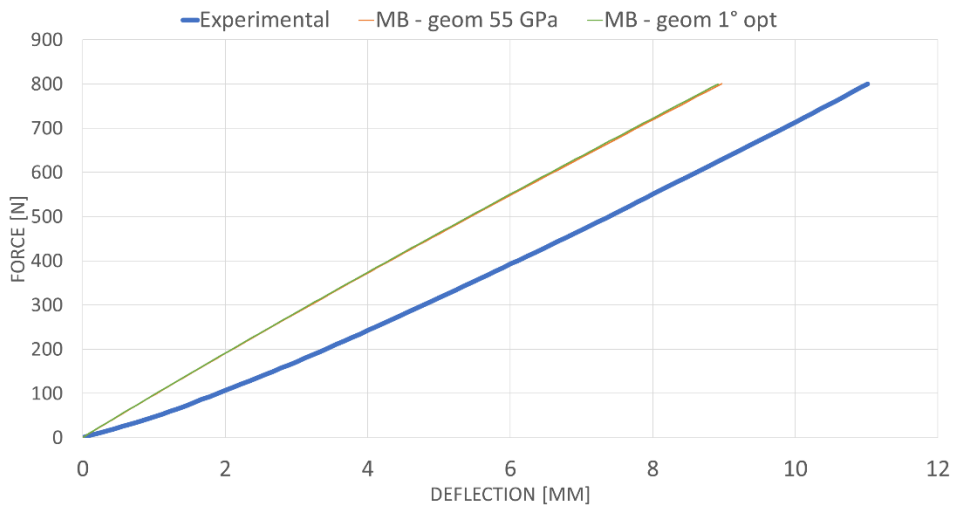


Figure 6.1.8 - Force vs. deflection diagram of 10° heel touch mechanical test. Experimental results are presented with a thick blue line. The orange line represents multibody model results before tuning. The green line represents multibody model results after tuning.

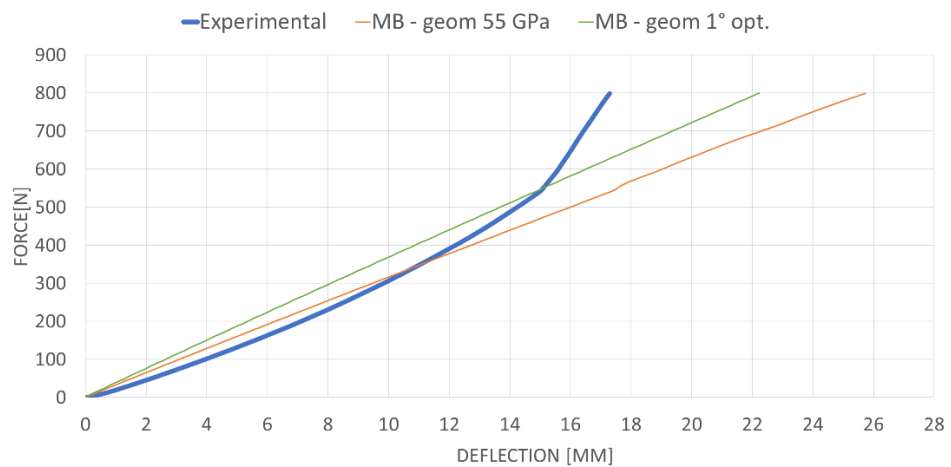


Figure 6.1.9 - Force vs. deflection diagram of 10° toe touch mechanical test. Experimental results are presented with a thick blue line. The orange line represents multibody model results before tuning. The green line represents multibody model results after tuning.

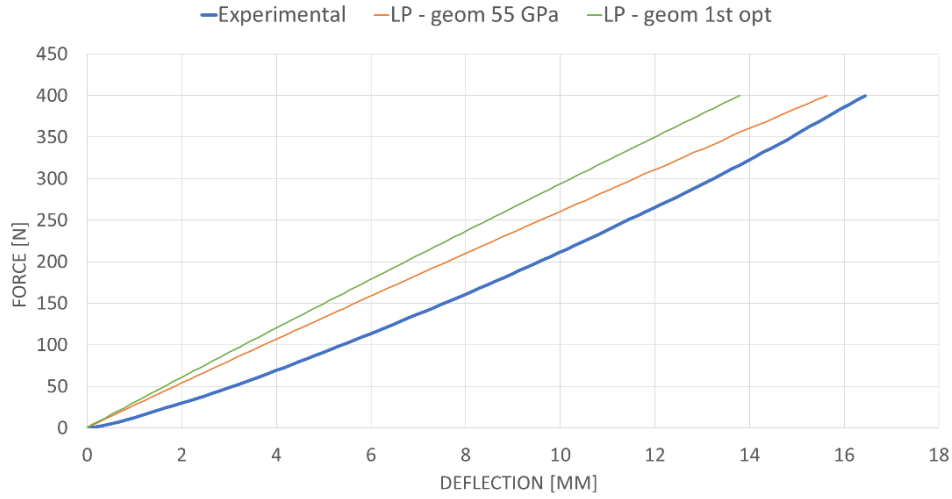


Figure 6.1.10 – Force vs. deflection diagram of 20° toe touch mechanical test. Experimental results are presented with a thick blue line. The orange line represents multibody model results before tuning. The green line represents multibody model results after tuning.

#### 6.1.4 Other Tunings on 20° Toe Touch

As discussed in Paragraph 3.4.2.2, other stiffness tunings considering 20° toe touch test have been run to see if it was possible to obtain a non-linear force-deflection curve. The results are shown in Figure 6.1.11.

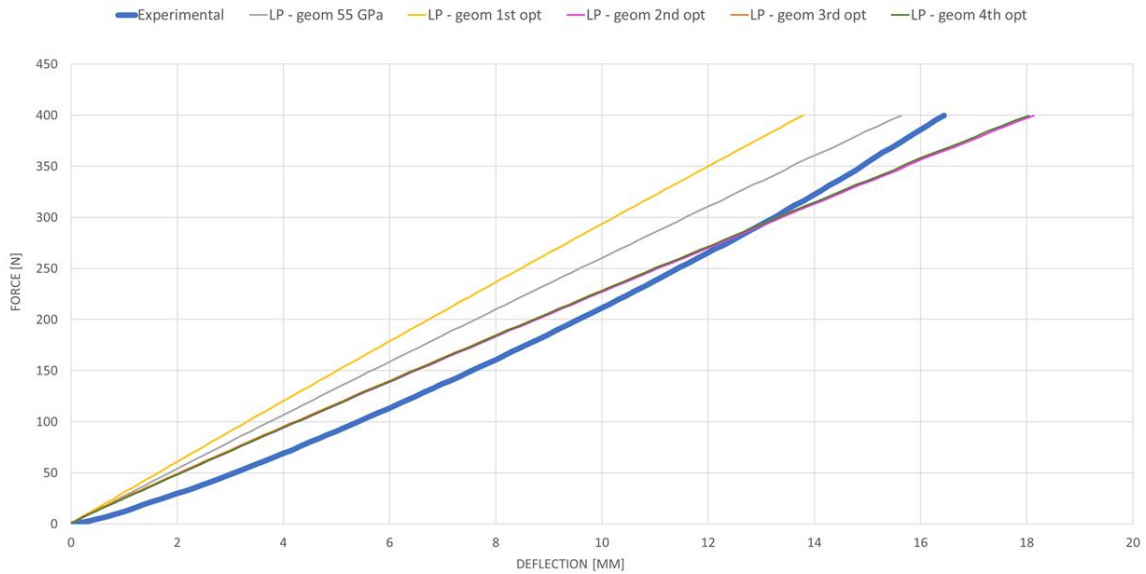


Figure 6.1.11 – Force vs. deflection curves obtained from other tuning trials executed on 20° toe touch testing conditions.

As it can be noticed, the non-linearity of force vs. deflection curve is still not achieved. This could be due to a modeling issue that will be discussed in Paragraph 7.2.1.

## 6.2 Dynamic Simulation of Stance Phase on Vari-Flex® Model

In this paragraph the deflections computed with Vari-Flex® multibody model before and after the changes applied to the junction modeling will be presented. Then, it will be presented the ROS computed using the multibody model with a single weld joint on the first heel segment with a Young modulus equal to 75 GPa (shown in Figure 5.2.2 a).

### 6.2.1 Deflection Results

To properly read the Figures presented in this Paragraph, an explanation is necessary: the yellow areas highlight the time period when the segments composing the Vari-Flex® different parts are loaded by Ground Reaction Forces (GRFs). Hence, the yellow area on the left chart represents the period when the segments forming the *heel section* are loaded by GRFs; the yellow area on the central chart represents the period when the segments forming the *heel/keel junction section* are loaded by GRFs; finally, the yellow area on the right graph represents the period when the segments forming the *forefoot section* are loaded by GRFs.

Referring to Figure 5.2.2, the previously cited sections are formed by the segments presented below:

- *Heel section*: going from the backfoot to the forefoot, it is composed by segments from *sr25* to *sr20* (included).
- *Heel/keel junction section*: going from the backfoot to the forefoot, it is composed by segments from *sr19* to *sr17* (included).
- *Forefoot section*: going from the backfoot to the forefoot, it is composed by segments from *sr13* to *sr16* (included).

In the next Paragraph, the deflections computed by the various multibody model realized will be presented. Deflections computed with the older model (described in Paragraph 2.5) have been already shown in Figure 5.2.1. Results obtained after junction modeling changes (proposed in Paragraph 5.2) will be presented below (from Figure 6.2.1 to Figure 6.2.4, last three Figures are in the next page).

Finally, deflections obtained changing Young modulus value within the range of 55 – 75 *Gpa* on *Single* multibody model will be presented. The reasons why this model has been chosen will be further discussed in Paragraph 7.4.1.

It is important to point out that the results presented by different junction models have been computed with a Young modulus value equal to 55 *GPa*.

#### 6.2.1.1 New Junction Models

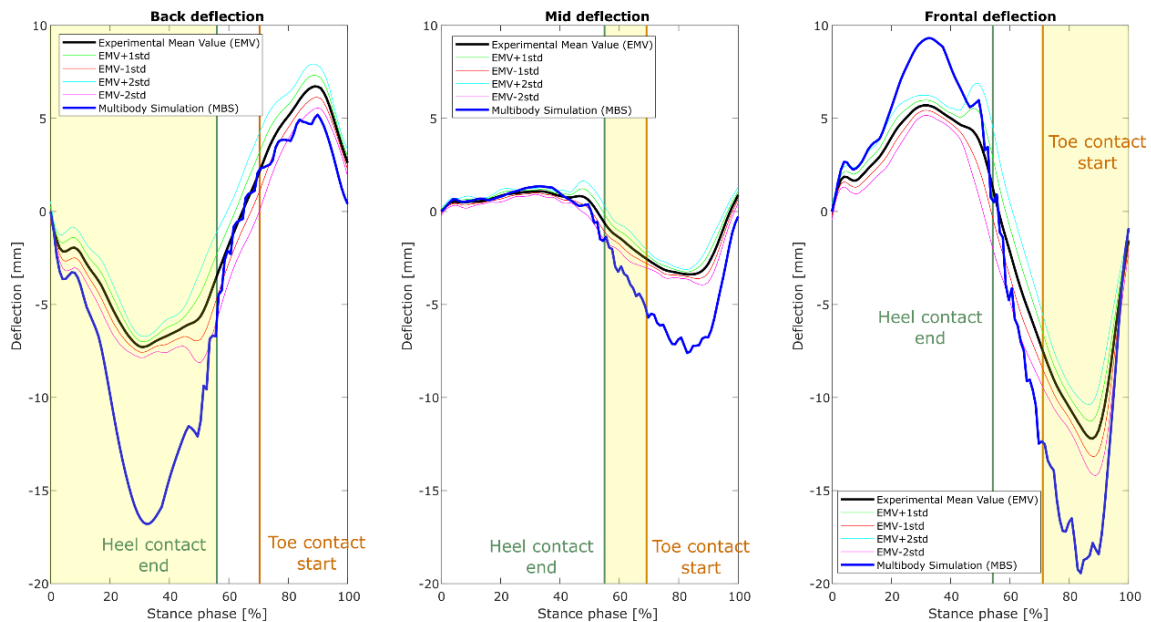


Figure 6.2.1 - Deflection of the markers on hind, mid and fore foot, computed using “Single” model.



## 6. Results

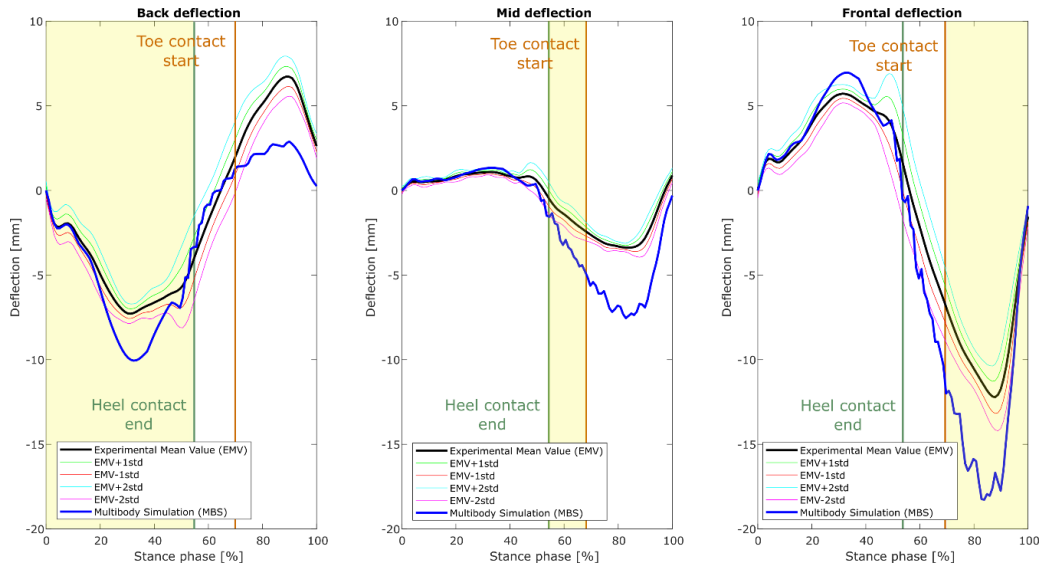


Figure 6.2.2 - Deflection of the markers on hind, mid and fore foot, computed using "Double" model.

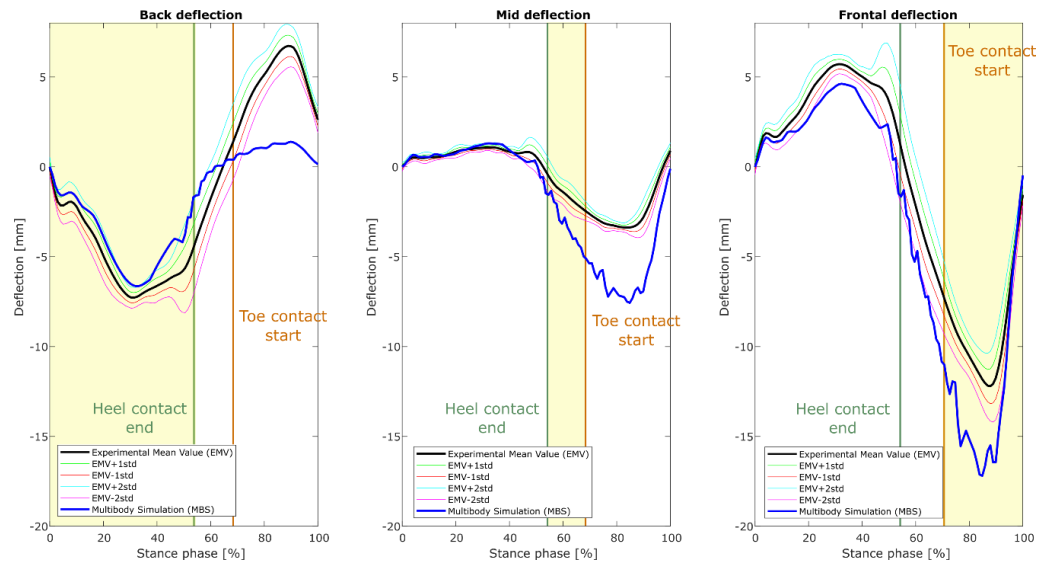


Figure 6.2.3 - Deflection of the markers on hind, mid and fore foot, computed using "Triple" model.

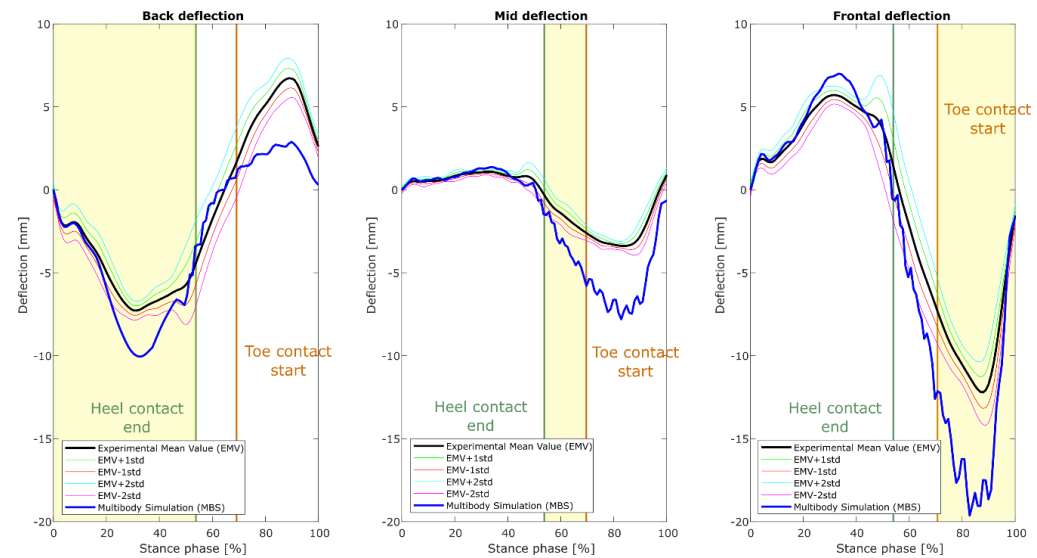


Figure 6.2.4 - Deflection of the markers on hind, mid and fore foot, computed using "Single2" model.

It is possible to notice that *Double* and *Single2* models produce nearly the same outputs.

### 6.2.1.2 Different Young Modulus

Here will be presented the results obtained varying the Young modulus within the range proposed by L. Cavallaro et al. [51], as discussed in Paragraph 5.2. The results referring to 55 *GPa* Young modulus have been already shown in Figure 6.2.1. Therefore, here will be only presented the results from 60 *GPa* to 75 *GPa* (from Figure 6.2.5 to Figure 6.2.8). Among these models, one has been chosen to further investigate its properties. The reasons behind the choice will be presented in Paragraph 7.4.1.

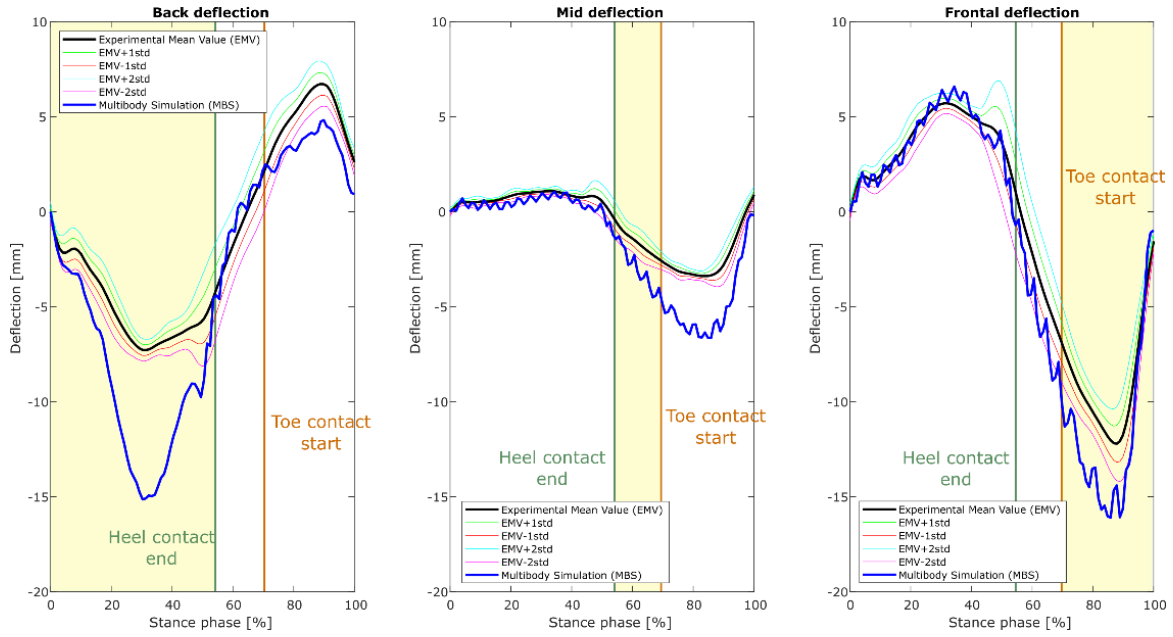


Figure 6.2.5 - Deflection of the markers on hind, mid and fore foot, computed using “Single” model and a Young modulus value equal to 60 *GPa*.

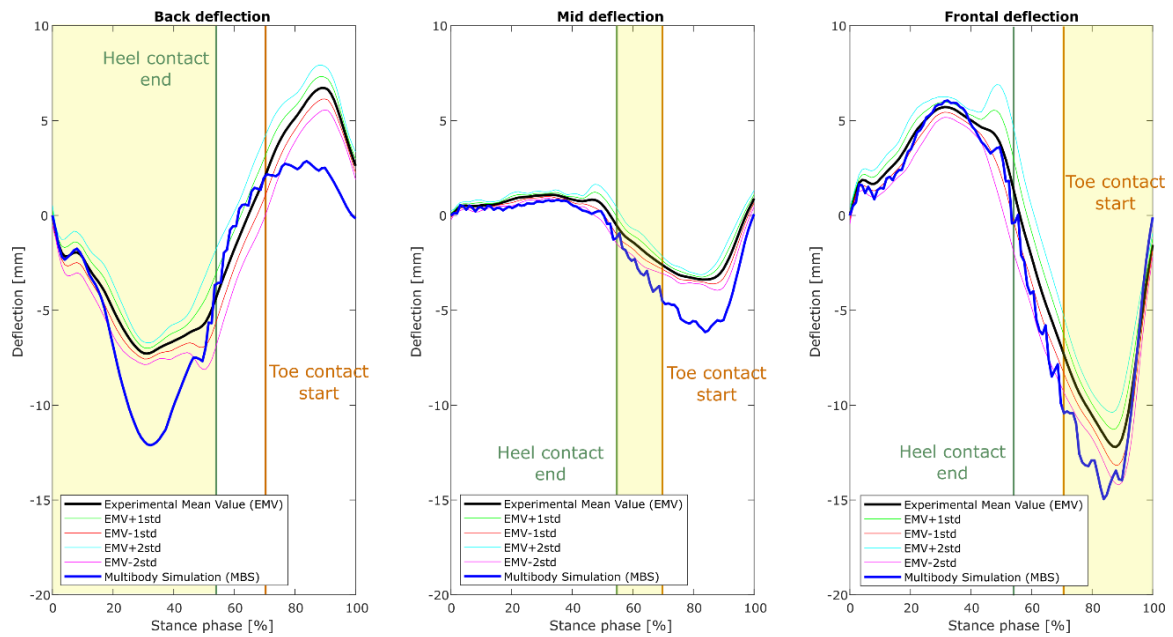


Figure 6.2.6 - Deflection of the markers on hind, mid and fore foot, computed using “Single” model and a Young modulus value equal to 65 *GPa*.

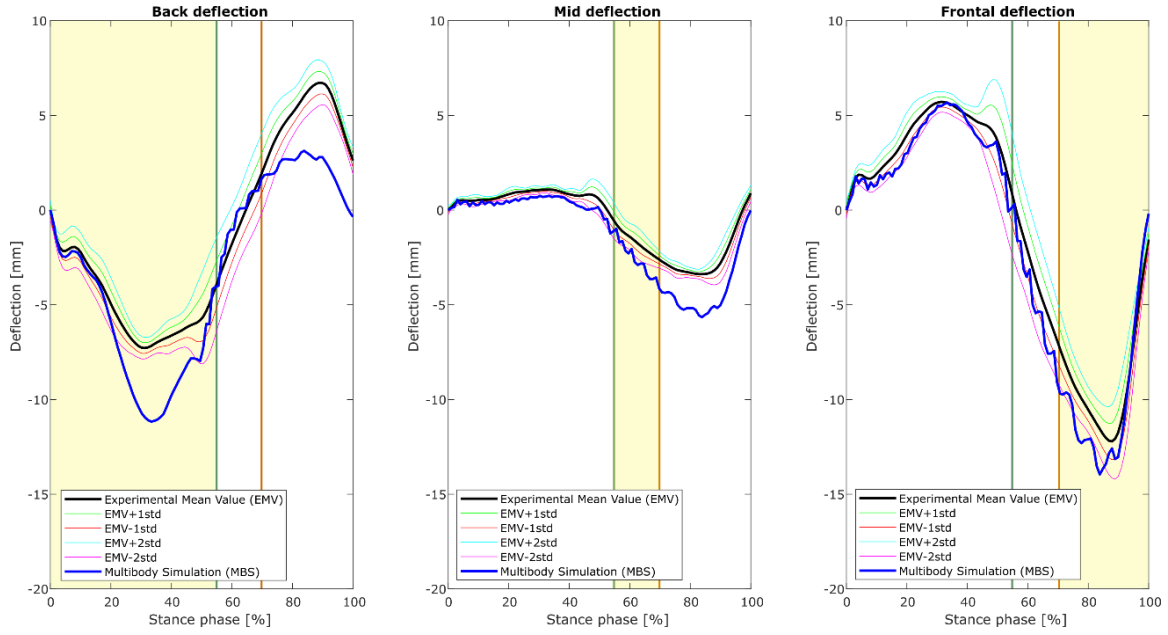


Figure 6.2.7 - Deflection of the markers on hind, mid and fore foot, computed using “Single” model and a Young modulus value equal to 60 GPa.

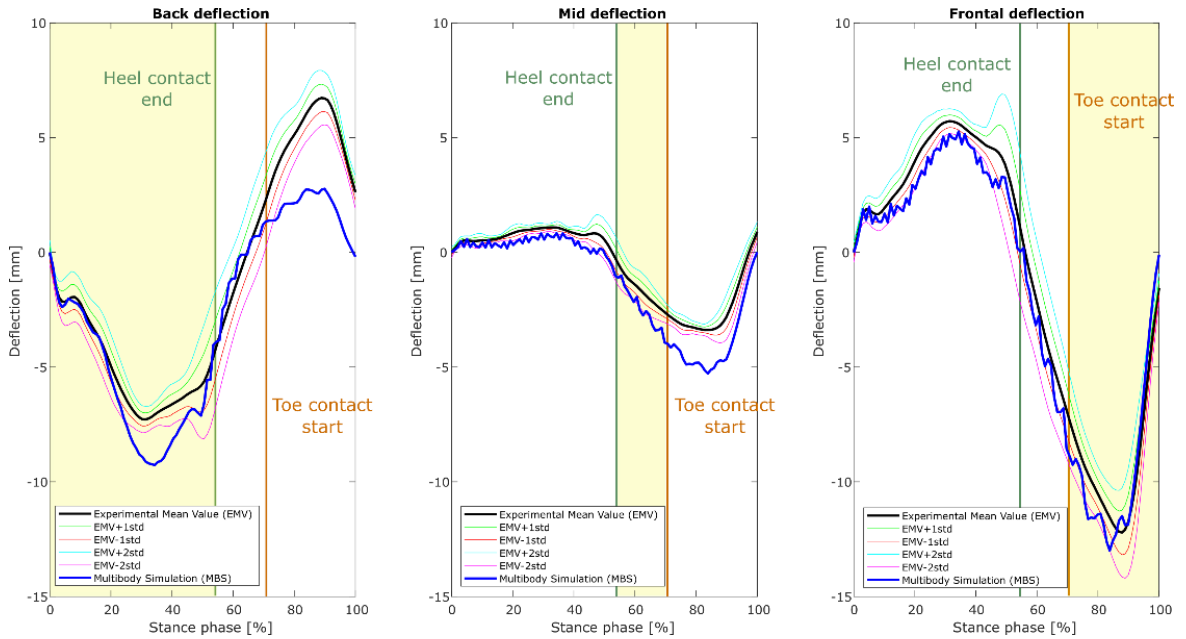


Figure 6.2.8 - Deflection of the markers on hind, mid and fore foot, computed using “Single” model and a Young modulus value equal to 75 GPa.

### 6.2.1.3 Changing Damping Value

Until now, little has been said regarding rotational damping value and it has not gone through valuable changes. For this reason, it could be interesting to see which kind of changes its variation could bring to the deflections computed by the model. It is important knowing that all further results were obtained changing the damping values of *Single* model with a Young modulus equal to 75 GPa. The damping values has been varied within the range  $0.01 - 100 \text{ N} \cdot \text{m} \cdot \text{s} \cdot \text{rad}^{-1}$ . Only  $1 \text{ N} \cdot \text{m} \cdot \text{s} \cdot \text{rad}^{-1}$  value has not been considered because simulation time were infinitely high (more than hours), probably because of model singularities. The damping was augmented by an order of magnitude at a time. Deflection results are presented from Figure 6.2.9 to Figure 6.2.12 (next pages).

## 6. Results

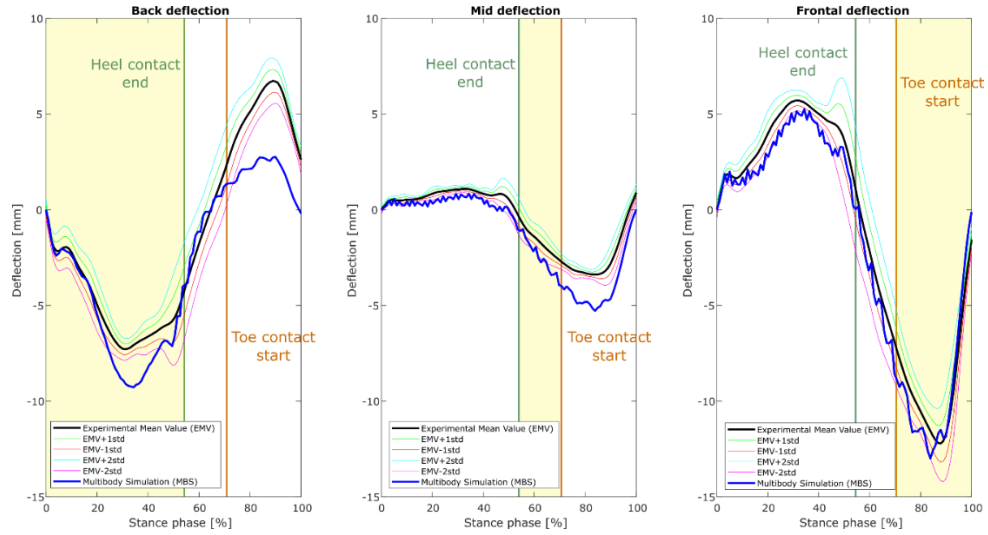


Figure 6.2.9 - Deflection of the markers on hind, mid and fore foot, computed using “Single” model and a damping value equal to  $0.01 \text{ N} \cdot \text{m} \cdot \text{s} \cdot \text{rad}^{-1}$ .

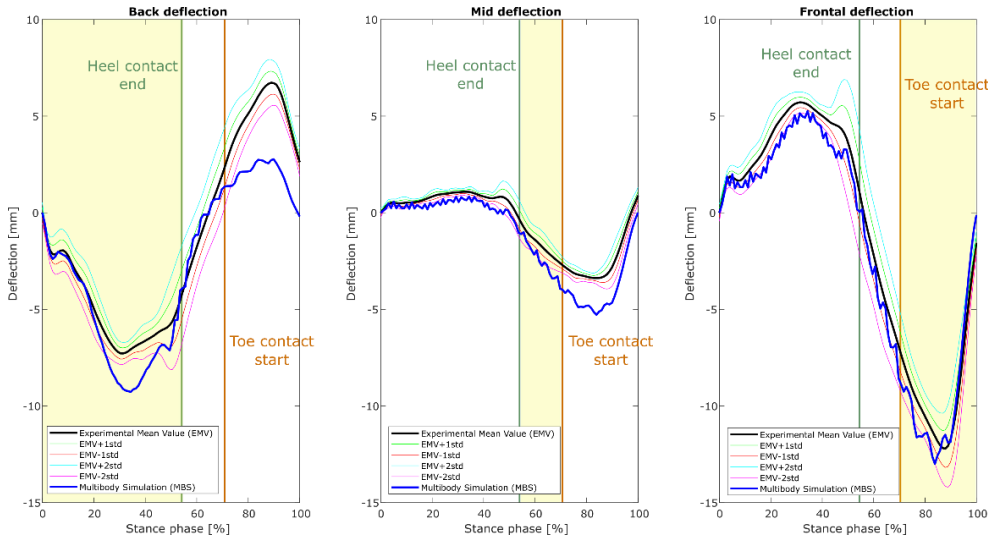


Figure 6.2.10 - Deflection of the markers on hind, mid and fore foot, computed using “Single” model and a damping value equal to  $0.1 \text{ N} \cdot \text{m} \cdot \text{s} \cdot \text{rad}^{-1}$ .

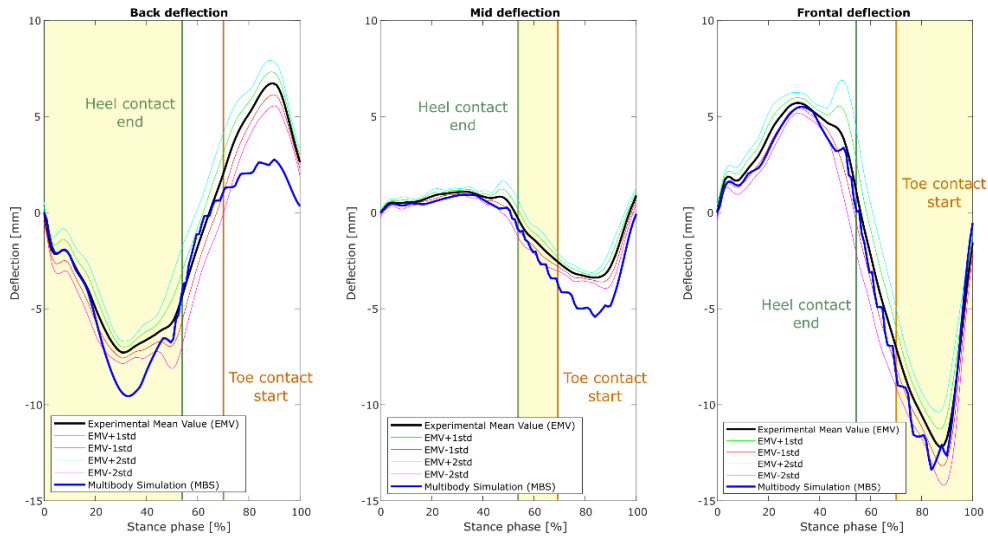


Figure 6.2.11 - Deflection of the markers on hind, mid and fore foot, computed using “Single” model and a damping value equal to  $10 \text{ N} \cdot \text{m} \cdot \text{s} \cdot \text{rad}^{-1}$ .

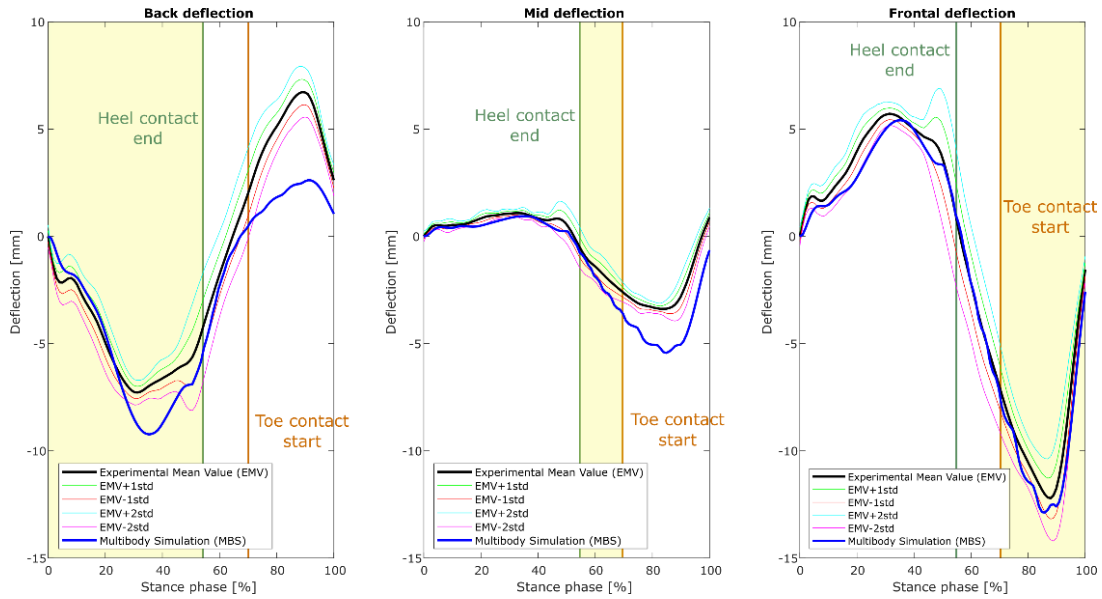


Figure 6.2.12 - Deflection of the markers on hind, mid and fore foot, computed using “Single” model and a damping value equal to  $100 \text{ N} \cdot \text{m} \cdot \text{s} \cdot \text{rad}^{-1}$ .

Apparently, the only effect introduced by damping in this model is a smoothing of deflection data. Indeed, this could be a normal behaviour because the damping increment has the effect of reducing vibrations.

### 6.2.2 Simulation Time

The time a dynamic simulation takes to run is between 1 and 7 minutes. The simulation time, under same simulation conditions, mostly depends on the number of weld joints used and damping value.

Below, it is reported a table resuming the simulation times for each different condition. First, it has been tested the simulation time keeping the damping value fixed and varying the number of weld joints considered to model the junction between the two laminas. Then, the opposite process has been adopted: with a fixed number of weld joints (one in this case), it has been changed the rotational damping value within  $0.01 - 100 \text{ N} \cdot \text{m} \cdot \text{s} \cdot \text{rad}^{-1}$  range.

Table 6.2.1 – Simulation time difference when varying the number of weld joints and keeping a fixed damping value.

Geometry model	Number of weld joints	Damping value [ $\text{N} \cdot \text{m} \cdot \text{s} \cdot \text{rad}^{-1}$ ]	Simulation time [s]
Single	1	0.01	70
Single2	1	0.01	70
Double	2	0.01	110
Triple	3	0.01	150

Table 6.2.2 - Simulation time difference when varying the damping value and keeping the same number of weld joints.

Geometry model	Number of weld joints	Damping value [ $N \cdot m \cdot s \cdot rad^{-1}$ ]	Simulation time [s]
Single	1	0.01	70
Single	1	0.1	420
Single	1	10	170
Single	1	100	170

### 6.2.3 Roll-Over Shape

From those presented, the model used to compute Vari-Flex® ROS is the *Single* one. Young modulus equal to 75 GPa and damping value equal to  $0.01 N \cdot m \cdot s \cdot rad^{-1}$  has been considered. Even if results obtained with a damping value equal to 10 or  $100 N \cdot m \cdot s \cdot rad^{-1}$  showed smoother deflection curves, it has been decided to not use those values because a damping value that high may not belong to a material such as carbon fibre.

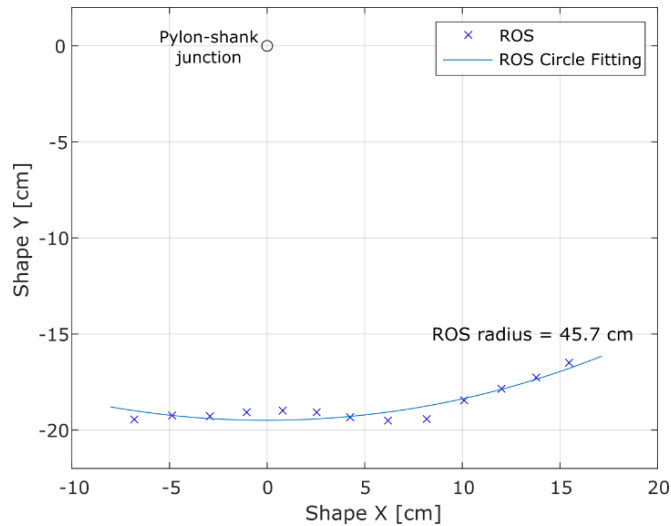


Figure 6.2.13 – ROS computed by multibody model. As it can be noticed, the radius value is like the one found by L. Cavallaro (46 cm).

It is also important to notice that ROS was not significantly affected by damping value, as reported in Table 6.2.3. Percentage absolute errors between ROS computed with the multibody model and the one obtained by L. Cavallaro are also shown in the Table below.

Table 6.2.3 – ROS radius computed using different damping values.

Damping value [ $N \cdot m \cdot s \cdot rad^{-1}$ ]	ROS radius [cm]	% Error with respect to L. Cavallaro value
0.01	44.5	3.3
0.1	45.7	0.6
10	44.9	2.4
100	45.9	0.2

## 7. Discussion and Future Developments

---

In this Paragraph the results obtained and the choices made to achieve them will be discussed. The main topics are briefly described below:

- Design of the implemented multibody model. It has been chosen to carry out the analyses with a foot composed of 25 segments interconnected by viscoelastic rotational joints, but it will be necessary to investigate other solutions to test if this is the most convenient choice in terms of valuable results.
- The way quasi-static tests are carried out influences the obtained force-deflection curves, which have a linear trend. This do not reflect the real quasi-static behaviour of the Vari-Flex® foot. Here it will be introduced a possible explanation of this issue.
- Choices made to achieve the final deflections and ROS values in stance phase dynamic analysis.

### 7.1 Multibody Model Design

In this study it has been chosen to carry out the analysis on a 25 segments multibody model of the Vari-Flex® foot (16 keel segments and 9 heel segments) but, as reported in Paragraph 2.4.4, there were other possible segmented model fulfilling the requirements to be developed.

These other models were not further tested because it has been decided to focus on the entire workflow and to reach some indicative results. These results are useful to see if multibody modeling could compute values not too different from the experimental ones.

It could be interesting to carry out these analyses with simpler models and evaluate the errors they produce and the time they take to perform a complete simulation. Maybe time costs could be further decreased. These trials could also be interesting to test if the proposed stiffness formula really can grant satisfactory results regardless the number of segments.

### 7.2 Quasi-Static Tests

Results show how implemented multibody model is still not reliable describing Vari-Flex® foot's quasi-static behaviour, since it always computes linear force-deflection relationships. This behaviour is not the one showed by experimental loading tests. Indeed, these latter tests showed non-linear force-deflection curves as results. This *linearity issue* will be further discussed in the next Paragraph.

#### 7.2.1 Linearity Issue

The reason why force-deflection curves show a linear trend is related to the way the model is loaded: as the external forces are always applied on the same point, the lever arm of the force with respect to the pylon-shank junction remains the same during the simulation. This is the reason why force-deflection relationships cannot assume any other trend than the linear one. Moreover, the same number of rotational joints is included between the force application point and the wedged pylon-shank connection. This contributes to keep the trend of the force-deflection curve linear because the total stiffness sensed by the second order system is unchanged.

To support these hypotheses, it has been tried to apply the external forces on two different segments for the 20° toe touch test. The logical flow followed is like the one utilized for dynamic tests: the

first segment has been progressively loaded and unloaded to avoid model vibrations. The second segment, then, has been progressively loaded until the maximum value of external force was reached. The force-deflection curve obtained is shown in Figure 7.2.1. It is necessary to underline that this result has not been obtained after a tuning process, but using the analytical values of rotational stiffness and damping.

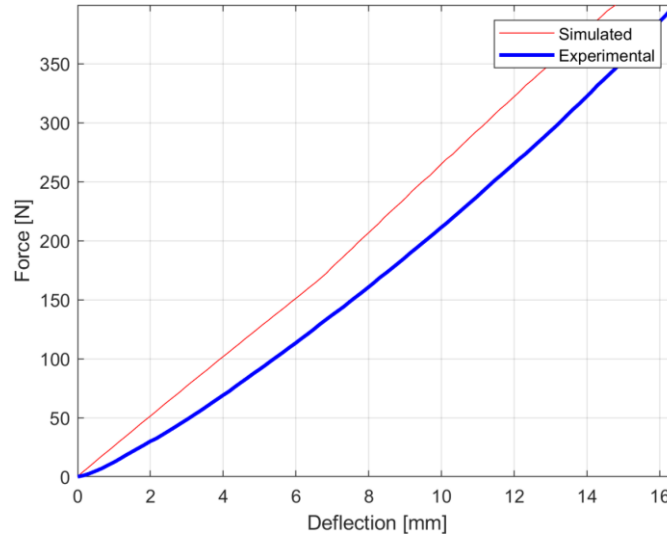


Figure 7.2.1 – Force-deflection curves for 20° heel touch quasi-static. The blue curve represents the experimental relationship. The red curve is the force-deflection relationship obtained switching the external force on two different foot sole's segments.

Although the resulting force-deflection relationship is still represented by a jagged *linear* curve, the overall trend of the new force-deflection relationship is no more linear, but it can better approximate the trend of the experimental relationship.

Since it is not possible to know where the force is applied during a mechanical test and the way the model is designed requires this kind of information, it will be necessary to implement contacts modeling in order to effectively simulate the real mechanical compressing test. This solution will be better addressed in Paragraph 7.3.1.

### 7.3 Quasi-Static Simulations Future Developments

As said in the previous Paragraph, the multibody simulations implemented could not compute non-linear force-deflection curves, but they would if force application point were moving during the simulation. It has been proposed to model the real plate compressing the prosthetic foot and implement contacts modeling in order to reproduce this behaviour.

#### 7.3.1 Contacts Modeling

Simscape Multibody *Contact Forces* library, implemented by Steve Miller [62], could be of use to model the contacts between Vari-Flex® and loading plate. In this library, he has implemented some blocks able to model contact between 2D and 3D bodies. To do so, he had to figure out how to model bodies compenetrating and how to constrain this effect. Simscape allows bodies to compenetrates without superimposed constraints. From these blocks it is possible to model the contacts between solids and calculate the contact force acting on them.

Contact modeling in this case could be useful to avoid the imposition of external force in arbitrary points of application, as it has been done in this study. Indeed, this new kind of modeling allows to



control the system with kinematic entries, like plate's displacement and velocity. In this way, it is possible to directly reproduce the real mechanical test without knowing the external force entity and its application point. Hence, the external force will be directly computed by library blocks.

Since plate displacement information is directly connected to Vari-Flex®'s deflection and the force is computed by *Multibody Contact Forces* library's blocks, it will be possible to compute the force-deflection behaviour of Vari-Flex® and possibly achieve better results than the ones obtained in this study.

Moreover, contacts modeling could allow a better reproduction of the effects deriving from the interaction between keel and heel elastic lamina when they touch: contact between the two laminas could be modelled with *Contact Forces* library's tools.

On the other hand, this kind of modeling could increase simulation time: this is a parameter to be monitored while implementing this new modeling solution, since it is fundamental to keep the multi-body analysis faster than the FEA.

## 7.4 Dynamic Tests

Regarding dynamic tests, a better description of choices made is necessary because there is not a model that perfectly reproduces the dynamic behaviour of the Vari-Flex® foot in terms of deflection. This issue is addressed in the following Paragraph.

### 7.4.1 Multibody Model Selection

After detecting the issue related with the keel/heel junction modeling, four models have been tested to improve the computed deflection values. Among these models, the *Single* one has been chosen for further implementations.

*Single* model has been chosen because it shows the best results reproducing Vari-Flex®'s "rocker effect". As it can be seen from Figure 6.2.1 to Figure 6.2.4 (Paragraph 6.2.1.1), it is the only one that achieves acceptable heel deflection values at the end of the stance phase, although it shows higher errors in other circumstances. Since the junction modeling changes have been implemented to improve the model response when reproducing the "rocker effect", it has been decided to consider this model and work on it. Moreover, *Single* model is the fastest to run among all, which is another strong point, because the aim of this study is to keep the model as fast and simple as possible and correctly compute dynamic parameters of interest.

### 7.4.2 ROS

At this point, the aim was to achieve the correct ROS radius. First, to achieve this, the Young modulus value has been tested and then it has been investigated how damping could affect the model.

It has been chosen a Young modulus value equal to 75 *GPa* because it falls within the range proposed by L. Cavallaro et al. [51] and it assures more reliable deflection results when the different regions of foot are loaded by GRFs. Unfortunately, when this Young modulus values is used, again, it is not possible to reproduce the "rocker effect" of the heel lamina. Maybe, this is definitively a limitation of the model.

The reliable deflection results, however, allow to correctly compute the ROS radius of curvature. The ROS values obtained, in fact, are really close to those obtained experimentally: as shown in Table 6.2.3, the maximum absolute percentage error committed is less than 4%.

What has been noticed is that, as expected, a stiffer foot (higher Young modulus value) increases ROS radius and that is a physical effect of elastic feet. In addition to this, the model produced higher deflection values when a lower Young modulus value was used. This is another property that may be also noticed on real prosthetic feet.

## 7.5 Dynamic Simulations Future Developments

With the multibody model developed in this study it is possible to realize a reverse dynamic analysis in order to compute interarticular forces and torques acting on the lower limb's joints. Another possible development, however, could be the insertion of the multibody model in a complex musculoskeletal model in order to compute valuable parameters like net metabolic rate (as N. P. Fey et al. [33] did).

### 7.5.1 *Contacts Modeling*

Contacts modeling could be an interesting improvement even for dynamic simulations: it can be used to analyse the same dynamic parameters using a different logic with respect to the one adopted in this study.

With contacts modeling, indeed, it is possible to give to the model the only pylon angle information as input. Moreover, this kind of information could be taken from ISO 22675 normative. Therefore, it will not be necessary to give GRFs and COP displacements as inputs anymore: these parameters will be directly computed by the model and they could be used as further validation references.

### 7.5.2 *Reverse Dynamic Analysis*

Reverse dynamic analysis is a powerful method to compute internal forces of a cinematic chain. This method is particularly interesting when applied to the human body because it is difficult to extract interarticular forces acting on anatomical joints with external instrumentation. Therefore, it could be interesting achieving this information joining the multibody model here used with a simple biomechanical model of the lower limb.

As introduced in Paragraph 2.3.3, it is possible to insert the Vari-Flex® model in a complete multibody model of the lower limb and possibly compute the forces and the torques acting on knee and hip joint on a trans-tibial amputee. Moreover, knowing kinematic parameters of the knee prosthesis, it will also be possible to compute the forces acting on the hip of a transfemoral amputee and those acting on the prosthesis itself. Those forces, indeed, could determine the prosthesis failure if they are too high.

Simscape Multibody *Contact Forces* library, again, could be of use to model the interarticular torques and forces and the contact between ground and foot prosthesis. With this type of analysis, it will be possible to compute the interarticular forces developed by a prothesized subject only knowing knee, ankle and hip kinematic data, as schematized in Figure 7.5.1.

With a musculoskeletal model, then, it will be also possible to deduct muscles tensions and see which kind of effects the foot prosthesis has on muscle activations.

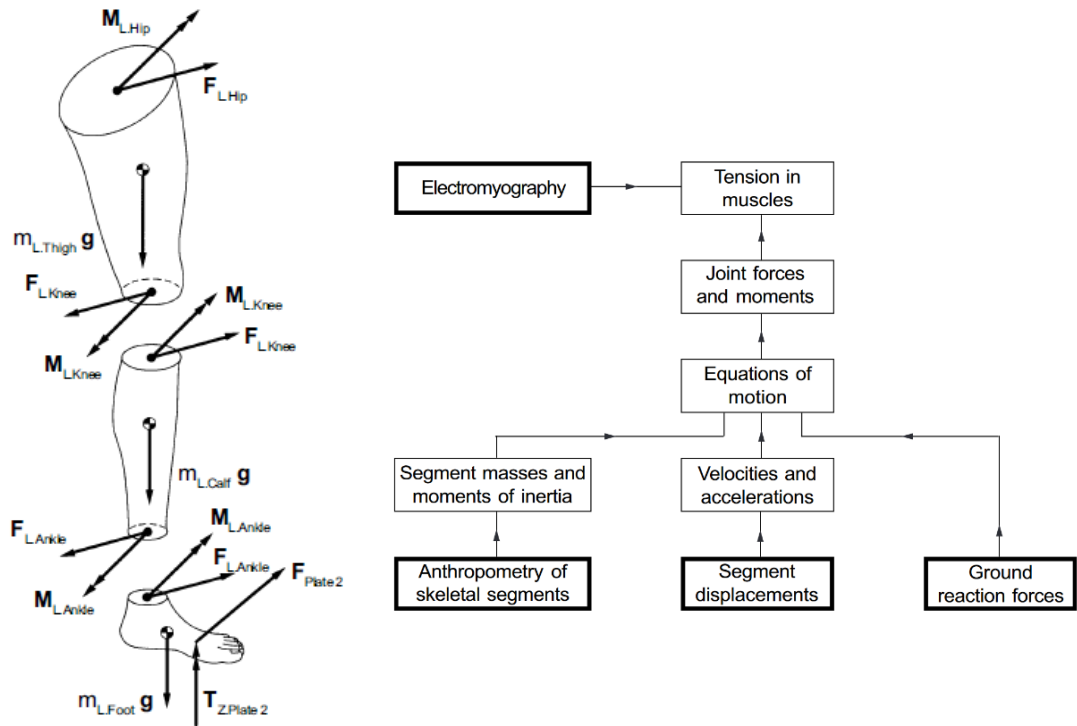


Figure 7.5.1 – On the left: schematic representation of the inverse dynamic analysis scheme for the lower limb. On the right: workflow to determine intersegmental ("joint") forces and moments. [63]



## 8. Conclusions

---

This work demonstrated that it is possible to conduct a dynamic analysis of the stance phase and obtain valuable results with a multibody model. Moreover, this kind of simulation is faster to run than a complete FEM (Finite Element Model). As a matter of fact, it is possible to compute the ROS radius of curvature with an error less than 4% in less than 10 minutes. A complete FEM could take more than one hour to reach the same result.

It is necessary to say that the study has been conducted using information coming from a single subject and that results achieved must be validated on other subjects.

There are still problems related to conducted quasi-static test, but this issue will be possibly solved with the implementation of contacts modeling.

Reverse dynamic analysis could be an interesting development of the multibody model because it could be a useful method to compute interarticular forces. Indeed, those forces are difficult to measure with experimental instrumentations, but they are fundamental to see the effects that the prosthesis produces on amputee's joints.









## A. Appendix A – MATLAB® Scripts

---

### Theoretical wedged beam model – ‘bar\_model\_theoretical.m’

```
close all
clear all
clc

%% Simulation parameters-----
fs=1000; % Sampling frequency [Hz]
T=1; % Simulation's duration [s]
t=linspace(0,T,T*fs); % Time vector [s]

%% Beam parameters-----
% Dimensions
L=1; % Total beam length [m]
H=0.1; % Beam thickness [m]
W=0.1; % Beam width [m]

% External force
fmax=1e3; % Maximum applied force
Fo.time=linspace(0,T,T*fs)'; % Fo - time vector [s]
Fo.signals.values=linspace(0,-fmax,T*fs)'; % Fo - values [N]
Fo.signals.dimension=1;

%% Material properties-----
% T700S carbon fibre density
rho=1.80; % [g/cm^3]
rho=rho/10^3*10^6; % [kg/m^3]

% Young Modulus of T700S carbon fibre composite [GPa]
E=134;

% Moment of inertia of the transverse section (b*h^3/12) [m^4]
I=(H^3*W)/12;

% Damping coefficient [N*m*s/rad]
b=0.001;

%% Theoretical results-----
Ty=abs(Fo.signals.values); % Vertical reaction force [N]
Mz=abs(Fo.signals.values)*L; % Torque on z-axis [N*m]
dx=-abs(Fo.signals.values)*L^3/(3*E*10^9*I); % Beam maximum deflection [N]
dx_max=dx(end);

% Elastic line
x=linspace(0,L,fs);
F=fmax;
ftheor=-(x.^2.*F./(6*E*10^9*I)).*(3*L-x);

%% One rigid segment simulation-----
n=1; % Number of segments
l=L/n; % Segment length [m]
lengthl=0:l:L; % Cumulative length

% Joint stiffness [N*m/rad]
k1=E*10^9*I/l; % used by P.Fey et al. (2012)

% Run simulation
out1=sim('bar_model_1.slx');

% Elastic line
x1=[0 out1.deflection.signals.values(end,1)];
f1=[0 out1.deflection.signals.values(end,2)];
```

```

%% Two rigid segments simulation-----
n=2;                % Number of segments
l=L/n;              % Segment length [m]
length2=0:1:L;      % Cumulative length

% Joint stiffness [N*m/rad]
k2=E*10^9*I/l;      % used by P.Fey et al. (2012)

% Run simulation
out2=sim('bar_model_2.slx');

% Elastic line
x2(1)=0;
f2(1)=0;
j=2;
for i=2:-1:1
    x2(j)=out2.deflection.signals.values(end,i*2-1);
    f2(j)=out2.deflection.signals.values(end,i*2);
    j=j+1;
end

%% Five rigid segments simulation-----
n=5;                % Number of segments
l=L/n;              % Segment length [m]
length5=0:1:L;      % Cumulative length

% Joint stiffness [N*m/rad]
k5=E*10^9*I/l;      % used by P.Fey et al. (2012)

% Run simulation
out5=sim('bar_model_5.slx');

% Elastic line
x5(1)=0;
f5(1)=0;
j=2;
for i=5:-1:1
    x5(j)=out5.deflection.signals.values(end,i*2-1);
    f5(j)=out5.deflection.signals.values(end,i*2);
    j=j+1;
end

%% Ten rigid segments simulation-----
n=10;               % Number of segments
l=L/n;              % Segment length [m]
length10=0:1:L;     % Cumulative length

% Joint stiffness [N*m/rad]
k10=E*10^9*I/l;     % used by P.Fey et al. (2012)

% Run simulation
out10=sim('bar_model_10.slx');

% Elastic line
x10(1)=0;
f10(1)=0;
j=2;
for i=10:-1:1
    x10(j)=out10.deflection.signals.values(end,i*2-1);
    f10(j)=out10.deflection.signals.values(end,i*2);
    j=j+1;
end

%% Twenty rigid segments simulation-----
n=20;               % Number of segments
l=L/n;              % Segment length [m]
length20=0:1:L;     % Cumulative length

```

```
% Joint stiffness [N*m/rad]
k20=E*10^9*I/1;           % used by P.Fey et al. (2012)

% Run simulation
out20=sim('bar_model_20.slx');

% Elastic line
x20(1)=0;
f20(1)=0;
j=2;
for i=20:-1:1
    x20(j)=out20.deflection.signals.values(end,i*2-1);
    f20(j)=out20.deflection.signals.values(end,i*2);
    j=j+1;
end
```

## Analytical wedged beam model - 'bar.m'

```

close all
clear all
clc

%% Simulation parameters-----
fs=1000; % Sampling frequency [Hz]
T=1; % Simulation's duration [s]
t=linspace(0,T,T*fs); % Time vector [s]

%% Parameters-----
% Dimensions
L=1; % Total body length [m]
H=0.1; % Body thickness [m]
W=0.1; % Body width [m]

% External force
fmax=1e3; % Maximum applied force
Fo.time=linspace(0,T,T*fs)'; % Fo - time vector [s]
Fo.signals.values=linspace(0,-fmax,T*fs)'; % Fo - values [N]
Fo.signals.dimension=1;

%% Material properties-----
% T700S carbon fibre density
rho=1.80; % [g/cm^3]
rho=rho/10^3*10^6; % [kg/m^3]

% Young Modulus of T700S carbon fibre composite [GPa]
E=134;

% Moment of inertia of the transverse section (b*h^3/12) [m^4]
I=(H^3*W)/12;

% Damping coefficient [N*m/(s*rad)]
b=0.001;

%% Theoretical results-----
Ty=abs(Fo.signals.values); % Vertical reaction force [N]
Mz=abs(Fo.signals.values)*L; % Torque on z-axis [N*m]
dx=-abs(Fo.signals.values)*L^3/(3*E*10^9*I); % Beam maximum deflection [N]
dx_max=dx(end);

% Elastic line
x=linspace(0,L,fs);
F=fmax;
ftheor=-(x.^2.*F./(6*E*10^9*I)).*(3*L-x);

%% Empirical coefficient for calculate stiffness-----
N(1)=1;

for i=2:20
    N(i)=N(i-1)+i^2;
end

%% One rigid segment simulation-----
n=1; % Number of segments
l=L/n; % Segment length [m]
lengthl=0:l:L; % Cumulative length

% Joint stiffness [N*m/rad]
% k1=fmax*L^2*N(n)/n^2/abs(dx_max);
k1=(3*E*10^9*I/L)*(N(n)/n^2); % analytical formula

% Run simulation
out1=sim('bar_model_1.slx');
```

```
% Elastic line
x1=[0 out1.deflection.signals.values(end,1)];
f1=[0 out1.deflection.signals.values(end,2)];

%% Two rigid segments simulation-----
n=2; % Number of segments
l=L/n; % Segment length [m]
length2=0:1:L; % Cumulative length

% Joint stiffness [N*m/rad]
% k2=fmax*L^2*N(n)/n^2/abs(dx_max);
k2=(3*E*10^9*I/L)*(N(n)/n^2); % analytical formula

% Run simulation
out2=sim('bar_model_2.slx');

% Elastic line
x2(1)=0;
f2(1)=0;
j=2;
for i=2:-1:1
    x2(j)=out2.deflection.signals.values(end,i*2-1);
    f2(j)=out2.deflection.signals.values(end,i*2);
    j=j+1;
end

%% Five rigid segments simulation-----
n=5; % Number of segments
l=L/n; % Segment length [m]
length5=0:1:L; % Cumulative length

% Joint stiffness [N*m/rad]
% k5=fmax*L^2*N(n)/n^2/abs(dx_max);
k5=(3*E*10^9*I/L)*(N(n)/n^2); % analytical formula

% Run simulation
out5=sim('bar_model_5.slx');

% Elastic line
x5(1)=0;
f5(1)=0;
j=2;
for i=5:-1:1
    x5(j)=out5.deflection.signals.values(end,i*2-1);
    f5(j)=out5.deflection.signals.values(end,i*2);
    j=j+1;
end

%% Ten rigid segments simulation-----
n=10; % Number of segments
l=L/n; % Segment length [m]
length10=0:1:L; % Cumulative length

% Joint stiffness [N*m/rad]
k10=(3*E*10^9*I/L)*(N(n)/n^2); % analytical formula

% Run simulation
out10=sim('bar_model_10.slx');

% Elastic line
x10(1)=0;
f10(1)=0;
j=2;
for i=10:-1:1
    x10(j)=out10.deflection.signals.values(end,i*2-1);
    f10(j)=out10.deflection.signals.values(end,i*2);
    j=j+1;
end
```

```
%% Twenty rigid segments simulation-----
n=20;                % Number of segments
l=L/n;              % Segment length [m]
length20=0:l:L;     % Cumulative length

% Joint stiffness [N*m/rad]
k20=(3*E*10^9*I/L)*(N(n)/n^2); % analytical formula

% Run simulation
out20=sim('bar_model_20.slx');

% Elastic line
x20(1)=0;
f20(1)=0;
j=2;
for i=20:-1:1
    x20(j)=out20.deflection.signals.values(end,i*2-1);
    f20(j)=out20.deflection.signals.values(end,i*2);
    j=j+1;
end
```

## Cartesian Coordinates Segmentation Method – ‘segmentation\_auto\_DEF.m’

```

clear all
close all
clc

%% Coordinates import-----
% Keel coordinates
fid=fopen('sagoma_keel_double_pts.txt'); % Open "points"
file containing the points x,y and z coordinates [mm] of keel silhouette
coord_keel=textscan(fid,'%f %f %f'); % Read the opened
file
coord_keel1=[-coord_keel{1,1} coord_keel{1,2}]; % Matrix contain-
ing only x and y coordinates
x_corr=coord_keel1(1,1); % x-coordinate of
the upper point on the left of the Vari-Flex silhouette
y_corr=coord_keel1(1,2); % y-coordinate of
the upper point on the left of the Vari-Flex silhouette
coord_keel=[coord_keel1(:,1)-x_corr coord_keel1(:,2)-y_corr]; % Translation of
the origin in the keel spline upper point
fclose(fid);
coord_keel_sil=coord_keel/10^3; % Conversion in
meters [m]

% Heel coordinates
fid=fopen('sagoma_heel_double_pts.txt'); % Open "points"
file containing the points x,y and z coordinates [mm] of heel silhouette
coord_heel=textscan(fid,'%f %f %f'); % Read the opened
file
coord_heel1=[-coord_heel{1,1} coord_heel{1,2}]; % Matrix contain-
ing only x and y coordinates
coord_heel=[coord_heel1(:,1)-x_corr coord_heel1(:,2)-y_corr]; % Translation of
the origin in the keel spline upper point
fclose(fid);
coord_heel_sil=coord_heel/10^3; % Conversion in
meters [m]

%% Comparison between silhouette and nominal spline-----
% Points # relative to the start and the end of the two splines
start_keel=1; % ID# of the keel spline
starting point
end_keel=33; % ID# of the keel spline en-
dig point
start_heel=1; % ID# of the heel spline
starting point
end_heel=19; % ID# of the heel spline
starting point

coord_keel=coord_keel_sil(start_keel:end_keel,:); % Nominal keel spline
coord_heel=coord_heel_sil(start_heel:end_heel,:); % Nominal heel spline

% Spline plot

%% Keel segmentation-----
% Keel spline length
j=1;
for i=2:length(coord_keel)
    len_sr_keel(j)=sqrt(sum((coord_keel(i,:)-coord_keel(i-1,:)).^2)); %
    keel rigid segments lengths
    j=j+1;
end
cum_len_sr_keel=[0 cumsum(len_sr_keel)]; %
distance from the origin of the keel spline points
L_keel=sum(len_sr_keel); % to-
tal keel spline length

```

```
% Number of segments to obtain for keel spline
prompt='\nType the number of rigid segments in which you want to divide the keel
spline:  ';
Nkeel=input(prompt);           % Number of rigid segments that form the keel
spline

% Approximate polynomial function for keel spline
method='makima';
coord_keel_fit(:,1)=interp1(cum_len_sr_keel,coord_keel(:,1),lin-
space(0,cum_len_sr_keel(end),Nkeel+1),method);
coord_keel_fit(:,2)=interp1(cum_len_sr_keel,coord_keel(:,2),lin-
space(0,cum_len_sr_keel(end),Nkeel+1),method);

%% Heel segmentation-----
% Definition of the desired keel spline's segments
prompt='\nType the number of rigid segments in which you want to divide the heel
spline:  ';
Nheel=input(prompt);           % Number of rigid segments that form the heel
spline

% Definition of the segments that are in common within the two splines
prompt='\n\nWATCH FIGURE 3 - Type the number of segments that are shared by the
keel spline and the heel spline:  ';
common_sr=input(prompt);

% Definition of the keel points from where the heel spline starts
prompt='\n\nWATCH FIGURE 3 - Type the keel point ID number that links keel and
heel spline:  ';
start_heel=input(prompt);

% Heel spline length
j=1;
for i=2:length(coord_heel)
    len_sr_heel(j)=sqrt(sum((coord_heel(i,:)-coord_heel(i-1,:)).^2));    %
    heel rigid segments lengths
    j=j+1;
end
cum_len_sr_heel=[0 cumsum(len_sr_heel)];
L_heel=sum(len_sr_heel);

% Approximate polynomial function for heel spline
coord_heel_fit(:,1)=interp1(cum_len_sr_heel,coord_heel(:,1),lin-
space(0,cum_len_sr_heel(end),Nheel+1),method);
coord_heel_fit(:,2)=interp1(cum_len_sr_heel,coord_heel(:,2),lin-
space(0,cum_len_sr_heel(end),Nheel+1),method);
j=1;

% The coincident segments selected determine the coordinates of the first
% heel segments
for i=1:common_sr+1
    if i==1
        coord_heel_fit(j,:)=coord_keel_fit(start_heel,:);
        j=j+1;
    else
        coord_heel_fit(j,:)=coord_keel_fit(start_heel-i+1,:);
        j=j+1;
    end
end

%% Final segmentation plot-----
figure(4)
plot(coord_keel_fit(:,1),coord_keel_fit(:,2),'b',coord_heel_fit(:,1),coord_heel_fit(:,2),'r','LineWidth',1.5)
hold on
plot(coord_keel_fit(:,1),coord_keel_fit(:,2),'yo-
',coord_heel_fit(:,1),coord_heel_fit(:,2),'go-','LineWidth',1)
title('Segmented foot spline'),xlabel('x position [m]'),ylabel('y position [m]')
```



```
legend('Keel silhouette','Heel Silhouette','Segmented keel spline','Segmented  
heel spline')  
axis equal  
  
%% Coordinates save - comment if the coordinate are already saved-----  
foot_coord=[coord_keel_fit; coord_heel_fit];  
str=sprintf('foot_info_%s_%s',string(Nkeel),string(Nheel));  
save(str,'foot_coord','Nkeel','Nheel','start_heel','common_sr')
```

## Quasi-Static Simulation (with Geometrical Information) –

'load\_test\_geom.m'

```
close all
clear all
clc

%% Foot silhouette import-----
% Silhouette coordinates reading
filename='silhouette.txt'; % name of the point (*.txt) file
format='%f %f %f';
sil_coord=coord_read(filename,format); % function that function reads coordinates from a points file (*.txt) generated in Rhinoceros

sil_coord=sil_coord/10^3; % conversion of the coordinates in millimetres

%% Foot segmentation import-----
load('foot_info_16_9.mat')
N1=Nkeel;
N2=Nheel;

% Points coordinates
toe_pt=N1+1; % Counting from the ankle, this is the joint referred to the toe (forefoot end)
heel_pt=N1+N2+1+1; % Counting from the ankle, this is the joint referred to the heel (hindfoot end)
heel_start_joint=start_heel; % Counting from the ankle, this is the joint referred to the heel/keel junction

image_coord=[foot_coord(1:toe_pt,:); foot_coord(toe_pt-1:-1:heel_start_joint,:);
foot_coord(toe_pt+1:heel_pt,:)];

%% Choose the test
fprintf('\nMECHANICAL TEST AVAILABLE:')
fprintf('\n\n1 - 20 deg, heel touch; \n2 - 10 deg, heel touch; \n3 - 10 deg, toe touch; \n4 - 20 deg, toe touch;');
prompt='\n\nType the test ID number: ';
IDtest=input(prompt); % number of rigid segments that form the keel spline

if IDtest~=1 && IDtest~=2 && IDtest~=3 && IDtest~=4
    error('Test not present: re-run the script and choose a valid ID number')
end

%% Geometric parameters-----
% Width (along local z-axis) [m]
W(1:N1)=[38.2 38.2 38.2 38.12 38.2 42 48 53 55 60 63.8 66 66 62 50 38]/1000;
% Keel segments
W(N1+1:N1+N2)=[66 63.8 60 53 52.4 50 50 45 35]/1000;
% Heel segments

% Thickness (along local y-axis) [m]
H(1:N1)=[8.8 8.8 8.7 8.7 8.5 7.8 6.8 6.2 6 5.2 4.7 4.5 4.3 4.2 4.1 3.5]/1000;
% Keel segments
H(N1+1:N1+N2)=[6.1 6.1 6.1 5.4 4.2 4.1 3.6 2.8 2.7]/1000;
% Heel segments % Heel segments

% Cross-sectional moment of inertia (b*h^3/12) [m^4]
I=H.^3.*W./12;

% Segments length (along local x-axis) [m]
j=1;
for i=1:max(size(foot_coord))-1
    if i==toe_pt
    else
```

```

        L(j)=sqrt(sum((foot_coord(i+1,:)-foot_coord(i,:)).^2));
        j=j+1;
    end
end

% Joints on the foot sole x-coordinates
foot_sole_pts=[foot_coord(heel_pt:-1:toe_pt+1,1)'
foot_coord(heel_start_joint+1:toe_pt,1)'];
foot_sole_sr=[heel_pt:-1:heel_start_joint+(toe_pt-heel_start_joint)+1
heel_start_joint:toe_pt];
foot_sole_dist=diff(foot_sole_pts);           % horizontal distance between the
foot_sole_points

% Foot length [m]
foot_cum_length=cumsum(foot_sole_dist);       % cumulative sum of the foot sole
distances
foot_length=sum(foot_sole_dist);              % total length heel_toe

% Total lengths of keel and heel spline
L_tot1=sum(L(1:N1));
L_tot2=sum(L(N1+1:N1+N2));

% Starter revolute joints angles [rad]
theta=zeros(1,length(L));
theta(1)=pi-atan2(foot_coord(2,1)-foot_coord(1,1),foot_coord(2,2)-
foot_coord(1,2));
j=2;
for i=3:max(size(foot_coord))
    if i==toe_pt+1
        elseif i>toe_pt && i<toe_pt+common_sr+2
            j=j+1;
        elseif i==toe_pt+common_sr+2
            l_opp(j)=sqrt(sum((foot_coord(toe_pt+common_sr+2,:)-
foot_coord(heel_start_joint-common_sr-1,:)).^2));
            A(j)=L(heel_start_joint-common_sr-1)^2+L(j)^2-l_opp(j)^2;
            B(j)=2*L(heel_start_joint-1)*L(j);
            theta(j)=acos(A(j)/B(j));
            alpha(j)=atan2(foot_coord(i,1)-foot_coord(i-1,1),foot_coord(i,2)-
foot_coord(i-1,2));
            j=j+1;
        else
            alpha(j)=atan2(foot_coord(i,1)-foot_coord(i-1,1),foot_coord(i,2)-
foot_coord(i-1,2));
            theta(j)=alpha(j-1)-alpha(j);
            j=j+1;
        end
    end
end

theta_grad=theta*180/pi;

%% Material properties-----
% Material's Young modulus [GPa]
E=55*10^9;           % Carbon Fibre (Composite)

% Material's density
rho=1.80/10^3*10^6;   % Carbon Fibre (Composite)

% Analytical joints' compliances [N*m*s/rad]
b=linspace(0.01,0.01,N1+N2);           % Carbon fibre typically has damping near 0
b4=b(4);b5=b(5);b6=b(6);b7=b(7);b8=b(8);b9=b(9);b10_19=b(10);b11_18=b(11);b12_17=
b(12);
b13=b(13);b14=b(14);b15=b(15);b16=b(16);b20=b(20);b21=b(21);b22=b(22);b23=b(23);b
24=b(24);b25=b(25);

% Analytical joints' stiffnesses [N*m/rad]
N(1)=1;
for i=2:max(N1,N2)
    N(i)=N(i-1)+i^2;           % Analytical coefficients

```

```

end
k=zeros(1,N1+N2);
k(1:N1)=(N(N1)/N1^2)*(3*E*I(1:N1)/L_tot1);
k(N1+1:N1+N2)=(N(N2)/N2^2)*(3*E*I(N1+1:N1+N2)/L_tot2);
k4=k(4);k5=k(5);k6=k(6);k7=k(7);k8=k(8);k9=k(9);k10_19=k(10)+k(19);k11_18=k(11)+k(18);k12_17=k(12)+k(17);
k13=k(13);k14=k(14);k15=k(15);k16=k(16);k20=k(20);k21=k(21);k22=k(22);k23=k(23);k24=k(24);k25=k(25);

%% Simulation parameters-----
% Sampling frequency [Hz]
fs=100;

% Simulation time (stance phase duration) [% gait cycle]
T=10;

% Time support [% gait cycle]
t=linspace(0,T,(T*fs+1));

%% Tilt angle controls-----
if IDtest==1 % 20 heel
    tilt_angle=20*pi/180;
elseif IDtest==2 % 10 heel
    tilt_angle=10*pi/180;
elseif IDtest==3 % 10 toe
    tilt_angle=-10*pi/180;
elseif IDtest==4 % 20 toe
    tilt_angle=-20*pi/180;
end

%% External vertical forces [N]-----
if IDtest==1 % 20 heel
    vGRF.time=t';
    vGRF.signals.dimensions=1;
    vGRF.signals.values=linspace(0,1200,(T*fs+1))';
elseif IDtest==2 % 10 heel
    vGRF.time=t';
    vGRF.signals.dimensions=1;
    vGRF.signals.values=linspace(0,2800,(T*fs+1))';
elseif IDtest==3 % 10 toe
    vGRF.time=t';
    vGRF.signals.dimensions=1;
    vGRF.signals.values=linspace(0,1100,(T*fs+1))';
elseif IDtest==4 % 20 toe
    vGRF.time=t';
    vGRF.signals.dimensions=1;
    vGRF.signals.values=linspace(0,550,(T*fs+1))';
end

%% Simulation start-----
if IDtest==1 % 20 heel
    out=sim('sim_vari_flex_mech_test_heel_20.slx');
elseif IDtest==2 % 10 heel
    out=sim('sim_vari_flex_mech_test_heel_10.slx');
elseif IDtest==3 % 10 toe
    out=sim('sim_vari_flex_mech_test_toe_10.slx');
elseif IDtest==4 % 20 toe
    out=sim('sim_vari_flex_mech_test_toe_20.slx');
end

%% Plots-----
% Displacement vs. External force
dy=(out.dy-out.dy(1))*10^3; % displacement [m]
figure()
plot(dy,vGRF.signals.values)
xlabel('Deflection [mm]'),ylabel('Force [N]'),title('Force vs. deflection diagram')

```

```
%% Excel saving (comment if not wanting to save)-----
if IDtest==1          % 20 heel
    xlswrite('Results_sim_test_16_9_geom.xlsx',dy,4,'G2')
    xlswrite('Results_sim_test_16_9_geom.xlsx',vGRF.signals.values,4,'H2')
elseif IDtest==2      % 10 heel
    xlswrite('Results_sim_test_16_9_geom.xlsx',dy,3,'G2')
    xlswrite('Results_sim_test_16_9_geom.xlsx',vGRF.signals.values,3,'H2')
elseif IDtest==3      % 10 toe
    xlswrite('Results_sim_test_16_9_geom.xlsx',dy,1,'G2')
    xlswrite('Results_sim_test_16_9_geom.xlsx',vGRF.signals.values,1,'H2')
elseif IDtest==4      % 20 toe
    xlswrite('Results_sim_test_16_9_geom.xlsx',dy,2,'G2')
    xlswrite('Results_sim_test_16_9_geom.xlsx',vGRF.signals.values,2,'H2')
end
```

## 2-Segments Beam Model to Be Tuned – 'bar\_optimization.m'

```
close all
clear all
clc

%% Simulation parameters-----
fs=1000; % Sampling frequency [Hz]
T=1; % Simulation's duration [s]
t=linspace(0,T,T*fs); % Time vector [s]

%% Parameters-----
% Dimensions
L=1; % Total body length [m]
H=0.1; % Body thickness [m]
W=0.1; % Body width [m]

% External force
fmax=10e2; % Maximum applied force
Fo.time=linspace(0,T,T*fs)'; % Fo - time vector [s]
Fo.signals.values=linspace(0,-fmax,T*fs)'; % Fo - values [N]
Fo.signals.dimension=1;

% Segments
n=2; % Number of segments
l=L/n; % Segment length [m]
length=0:1:L; % Cumulative length

%% Material properties-----
% T700S carbon fibre density
rho=1.80; % [g/cm^3]
rho=rho/10^3*10^6; % [kg/m^3]

% Young Modulus of T700S carbon fibre composite [GPa]
E=134;

% Moment of inertia of the transverse section (b*h^3/12) [m^4]
I=(H^3*W)/12;

% Damping coefficient [N*m/(s*rad)]
b=0.01;

% Rigid segments mass
m=l*W*H*rho;

% Rigid segments moment of inertia
Iz=1/12*m*l^2;

%% Theoretical results-----
% Beam maximum deflection [m]
dy=-abs(Fo.signals.values)*L^3/(3*E*10^9*I); % Over-time
dy_max=dy(end); % Max vertical force

% Elastic line with fmax applied
x=linspace(0,L,fs);
F=fmax;
ftheor=(x.^2.*Fo.signals.values./(6*E*10^9*I)).*(3*L-x);

%% Stiffness-----
% Empirical coefficient for calculate stiffness
N(1)=1;

for i=2:n
    N(i)=N(i-1)+i^2;
end
```

```
% Joint stiffness [N*m/rad]
for i=1:n
    k(i)=(3*E*10^9*I/L)*(N(n)/n^2);    % analytical formula
end

% k=[5.35e6 8.9e6];                    % Taken from Simulink

%% Simulation-----
% Run simulation
out=sim('bar_model_opt_2.slx');

%% Elastic line-----
X(1)=0;
f(1)=0;
j=2;
for i=n:-1:1
    X(j)=out.deflection.signals.values(end,i*2-1);
    f(j)=out.deflection.signals.values(end,i*2);
    j=j+1;
end
```

## Import of Gait Data, Recognition of Stance Phase and Data Filtering - 'data\_import.m'

```

clear
close all
clc

for j=1:10
    %% String name-----
    data_string=['Test',num2str(j),'.csv'];
    data_save=['Test',num2str(j)];

    %% Data import-----
    data=xlsread(data_string);
    load('excel_coord.mat'); % Matrix that
contains the ID# of the cells containing information in CSV files
    force_plate_info=data(5:excel_coord(j,1),1:11);
    marker_info=data(excel_coord(j,2):excel_coord(j,3),1:62);

    %% Sampling Frequencies-----
    fs_force_plate=1000; % Force plate
    fs_camera=100; % Camera

    %% Determination of stance phase-----
    % Determination of the frameID corresponding to heel-strike
    index_start=find(force_plate_info(:,5)<=-20);
    frame_start=force_plate_info(index_start(1),1);

    % Determination of the frameID corresponding to toe-off
    index_end=find(force_plate_info(index_start(1):end,5)>=-20);
    frame_end=force_plate_info(index_end(1)+index_start(1),1);

    % Isolating stance signal - force plate data
    i=find(force_plate_info(:,1)==frame_start);
    j=find(force_plate_info(:,1)==frame_end);
    force_plate_info=force_plate_info(index_start(1):index_end(1)+in-
dex_start(1),:);

    % Isolating stance signal - marker data
    i=find(marker_info(:,1)==frame_start);
    j=find(marker_info(:,1)==frame_end);
    marker_info=marker_info(i(1):j(end),:);

    %% Time info-----
    T=max(size(force_plate_info))/fs_force_plate;
    t=linspace(0,100,122);
    t2=linspace(0,T,max(size(force_plate_info)));
    t3=linspace(0,T,max(size(marker_info)));

    %% Data processing-----
    % Signal filtering - GRF
    [b1,a1]=cheby2(8,20,10/(fs_force_plate/2));
    force_plate_info_filt(:,1:6)=filtfilt(b1,a1,force_plate_info(:,3:8));
    % figure(1)
    % freqz(b1,a1,512,fs_force_plate)

    % Signal filtering - COP
    [b2,a2]=butter(10,10/(fs_force_plate/2));
    force_plate_info_filt(:,7:9)=filtfilt(b2,a2,force_plate_info(:,9:11));
    % figure(2)
    % freqz(b2,a2,512,fs_force_plate)

    % Signal filtering - Markers
    [b3,a3]=cheby2(10,20,10/(fs_camera/2));
    marker_info_filt=filtfilt(b3,a3,marker_info(:,3:62));
    % figure(3)
    % freqz(b3,a3,512,fs_camera)

```



```

% GRF & COP downsampling
for i=1:9
    temp=[flipud(force_plate_info_filt(:,i)); force_plate_info_filt(:,i);
flipud(force_plate_info_filt(:,i))];
    temp_res=resample(temp,3*122,length(temp));
    force_plate_info_filt_res(:,i)=temp_res(122+1:2*122);
end

% GRF & COP downsampling
for i=1:60
    temp=[flipud(marker_info_filt(:,i)); marker_info_filt(:,i);
flipud(marker_info_filt(:,i))];
    temp_res=resample(temp,3*122,length(temp));
    marker_info_filt_res(:,i)=temp_res(122+1:2*122);
end

%% Data organization in structures-----
% Acquisition info
Test.Fs.Units='Hz';
Test.Fs.ForcePlat=fs_force_plate;
Test.Fs.Camera=fs_camera;

Test.Time.Units='s';
Test.Time.Duration=T;
Test.Time.Support=t';

% Ground Forces
Test.GRF.Units='N';
Test.GRF.Fx=-force_plate_info_filt_res(:,1);
Test.GRF.Fy=-force_plate_info_filt_res(:,2);
Test.GRF.Fz=-force_plate_info_filt_res(:,3);

% COP displacements
Test.COP.Units='mm';
Test.COP.y=force_plate_info_filt_res(:,8)-force_plate_info_filt_res(1,8);

% Marker positions
Test.Marker_Pos.Units='mm';
Test.Marker_Pos.TibiaDownBack(:,1)=marker_info_filt_res(:,1);           % Tibia
Down Back
Test.Marker_Pos.TibiaDownBack(:,2)=marker_info_filt_res(:,2);
Test.Marker_Pos.TibiaDownBack(:,3)=marker_info_filt_res(:,3);
Test.Marker_Pos.TibiaUpBack(:,1)=marker_info_filt_res(:,4);           % Tibia
Up Back
Test.Marker_Pos.TibiaUpBack(:,2)=marker_info_filt_res(:,5);
Test.Marker_Pos.TibiaUpBack(:,3)=marker_info_filt_res(:,6);
Test.Marker_Pos.TibiaUpFront(:,1)=marker_info_filt_res(:,7);           % Tibia
Up Front
Test.Marker_Pos.TibiaUpFront(:,2)=marker_info_filt_res(:,8);
Test.Marker_Pos.TibiaUpFront(:,3)=marker_info_filt_res(:,9);
Test.Marker_Pos.TibiaDownFront(:,1)=marker_info_filt_res(:,10);        % Tibia
Down Front
Test.Marker_Pos.TibiaDownFront(:,2)=marker_info_filt_res(:,11);
Test.Marker_Pos.TibiaDownFront(:,3)=marker_info_filt_res(:,12);
Test.Marker_Pos.FootBackLateral(:,1)=marker_info_filt_res(:,13);       % Foot
Back Lateral
Test.Marker_Pos.FootBackLateral(:,2)=marker_info_filt_res(:,14);
Test.Marker_Pos.FootBackLateral(:,3)=marker_info_filt_res(:,15);
Test.Marker_Pos.FootBackMedial(:,1)=marker_info_filt_res(:,16);        % Foot
Back Medial
Test.Marker_Pos.FootBackMedial(:,2)=marker_info_filt_res(:,17);
Test.Marker_Pos.FootBackMedial(:,3)=marker_info_filt_res(:,18);
Test.Marker_Pos.FootMedLateral(:,1)=marker_info_filt_res(:,19);        % Foot
Med Lateral
Test.Marker_Pos.FootMedLateral(:,2)=marker_info_filt_res(:,20);
Test.Marker_Pos.FootMedLateral(:,3)=marker_info_filt_res(:,21);

```

---

```

    Test.Marker_Pos.FootMedMedial(:,1)=marker_info_filt_res(:,22);           % Foot
Med Medial
    Test.Marker_Pos.FootMedMedial(:,2)=marker_info_filt_res(:,23);
    Test.Marker_Pos.FootMedMedial(:,3)=marker_info_filt_res(:,24);
    Test.Marker_Pos.FootFrontLateral(:,1)=marker_info_filt_res(:,25);       % Foot
Front Lateral
    Test.Marker_Pos.FootFrontLateral(:,2)=marker_info_filt_res(:,26);
    Test.Marker_Pos.FootFrontLateral(:,3)=marker_info_filt_res(:,27);
    Test.Marker_Pos.FootFrontMedial(:,1)=marker_info_filt_res(:,28);       % Foot
Front Medial
    Test.Marker_Pos.FootFrontMedial(:,2)=marker_info_filt_res(:,29);
    Test.Marker_Pos.FootFrontMedial(:,3)=marker_info_filt_res(:,30);

    % Marker positions
    Test.Marker_Sp.Units='mm/s';
    Test.Marker_Sp.TibiaDownBack(:,1)=marker_info_filt_res(:,31);         % Tibia
Down Back
    Test.Marker_Sp.TibiaDownBack(:,2)=marker_info_filt_res(:,32);
    Test.Marker_Sp.TibiaDownBack(:,3)=marker_info_filt_res(:,33);
    Test.Marker_Sp.TibiaUpBack(:,1)=marker_info_filt_res(:,34);           % Tibia
Up Back
    Test.Marker_Sp.TibiaUpBack(:,2)=marker_info_filt_res(:,35);
    Test.Marker_Sp.TibiaUpBack(:,3)=marker_info_filt_res(:,36);
    Test.Marker_Sp.TibiaUpFront(:,1)=marker_info_filt_res(:,37);         % Tibia
Up Front
    Test.Marker_Sp.TibiaUpFront(:,2)=marker_info_filt_res(:,38);
    Test.Marker_Sp.TibiaUpFront(:,3)=marker_info_filt_res(:,39);
    Test.Marker_Sp.TibiaDownFront(:,1)=marker_info_filt_res(:,40);       % Tibia
Down Front
    Test.Marker_Sp.TibiaDownFront(:,2)=marker_info_filt_res(:,41);
    Test.Marker_Sp.TibiaDownFront(:,3)=marker_info_filt_res(:,42);
    Test.Marker_Sp.FootBackLateral(:,1)=marker_info_filt_res(:,43);       % Foot
Back Lateral
    Test.Marker_Sp.FootBackLateral(:,2)=marker_info_filt_res(:,44);
    Test.Marker_Sp.FootBackLateral(:,3)=marker_info_filt_res(:,45);
    Test.Marker_Sp.FootBackMedial(:,1)=marker_info_filt_res(:,46);       % Foot
Back Medial
    Test.Marker_Sp.FootBackMedial(:,2)=marker_info_filt_res(:,47);
    Test.Marker_Sp.FootBackMedial(:,3)=marker_info_filt_res(:,48);
    Test.Marker_Sp.FootMedLateral(:,1)=marker_info_filt_res(:,49);       % Foot
Med Lateral
    Test.Marker_Sp.FootMedLateral(:,2)=marker_info_filt_res(:,50);
    Test.Marker_Sp.FootMedLateral(:,3)=marker_info_filt_res(:,51);
    Test.Marker_Sp.FootMedMedial(:,1)=marker_info_filt_res(:,52);       % Foot
Med Medial
    Test.Marker_Sp.FootMedMedial(:,2)=marker_info_filt_res(:,53);
    Test.Marker_Sp.FootMedMedial(:,3)=marker_info_filt_res(:,54);
    Test.Marker_Sp.FootFrontLateral(:,1)=marker_info_filt_res(:,55);     % Foot
Front Lateral
    Test.Marker_Sp.FootFrontLateral(:,2)=marker_info_filt_res(:,56);
    Test.Marker_Sp.FootFrontLateral(:,3)=marker_info_filt_res(:,57);
    Test.Marker_Sp.FootFrontMedial(:,1)=marker_info_filt_res(:,58);     % Foot
Front Medial
    Test.Marker_Sp.FootFrontMedial(:,2)=marker_info_filt_res(:,59);
    Test.Marker_Sp.FootFrontMedial(:,3)=marker_info_filt_res(:,60);

    %% Data struct save-----
    save(data_save, 'Test');

    %% Clear variables-----
    clear
end

```

---

## Calculation of Gait Data Mean Values and Standard Deviations - 'data\_elaboration.m'

```
clear
close all
clc

%% Data re-organization-----
load('static_load.mat');           % Subject + adapter weight [N]
load('foot_length.mat');           % Prosthetic foot length [mm]

for i=1:10
    string=['Test',num2str(i)];
    load(string);
    % Input variables
    COPy(i,:)=Test.COP.y/foot_length*100;           % COP progression
    normalized over foot length
    GRFx(i,:)=(Test.GRF.Fx-Test.GRF.Fx(1))/static_load*100; % Medio-Lateral
    GRF normalized over subject+adapter+prosthesis weight
    GRFy(i,:)=(Test.GRF.Fy-Test.GRF.Fy(1))/static_load*100; % Horizontal GRF
    normalized over subject+adapter+prosthesis weight
    GRFz(i,:)=(Test.GRF.Fz-Test.GRF.Fz(1))/static_load*100; % Vertical GRF
    normalized over subject+adapter+prosthesis weight
    T(i)=Test.Time.Duration;           % Stance phase
    duration
    theta(i,:)=atan2(Test.Marker_Pos.TibiaUpFront(:,2)-Test.Marker_Pos.TibiaDown-
    Front(:,2),Test.Marker_Pos.TibiaUpFront(:,3)-Test.Marker_Pos.TibiaDown-
    Front(:,3))*180/pi+0.97;           % Pylon angle with respect tp the ground perpendic-
    ular direction

    % Output variables
    back_disp_y=mean([Test.Marker_Pos.FootBackMedial(:,2)';Test.Marker_Pos.Foot-
    BackLateral(:,2)']]);           % Temporary variable that contains the medium antero-
    posterior displacement of the Back markers (placed on two

    % different carbon fiber sheets)
    back_disp_z=mean([Test.Marker_Pos.FootBackMedial(:,3)';Test.Marker_Pos.Foot-
    BackLateral(:,3)']]);           % Temporary variable that contains the medium vertical
    displacement of the Back markers (placed on two

    % different carbon fiber sheets)
    dist_back(i,:)=sqrt((Test.Marker_Pos.TibiaUpFront(:,2)')-
    back_disp_y).^2+(Test.Marker_Pos.TibiaUpFront(:,3)')-back_disp_z).^2);           %
    Distance from TibiaUpFront and FootBack (mid-point) in the sagittal plane
    med_disp_y=mean([Test.Marker_Pos.FootMedMedial(:,2)';Test.Marker_Pos.FootMed-
    Lateral(:,2)']]);           % Temporary variable that contains the medium antero-pos-
    terior displacement of the Med markers (placed on two

    % different carbon fiber sheets)
    med_disp_z=mean([Test.Marker_Pos.FootMedMedial(:,3)';Test.Marker_Pos.FootMed-
    Lateral(:,3)']]);           % Temporary variable that contains the medium vertical
    displacement of the Med markers (placed on two

    % different carbon fiber sheets)
    dist_med(i,:)=sqrt((Test.Marker_Pos.TibiaUpFront(:,2)')-
    med_disp_y).^2+(Test.Marker_Pos.TibiaUpFront(:,3)')-med_disp_z).^2);           %
    Distance from TibiaUpFront and FootMed (mid-point) in the sagittal plane
    front_disp_y=mean([Test.Marker_Pos.FootFrontMe-
    dial(:,2)';Test.Marker_Pos.FootFrontLateral(:,2)']]);           % Temporary variable that
    contains the medium antero-posterior displacement of the Front markers (placed on
    two

    % different carbon fiber sheets)
    front_disp_z=mean([Test.Marker_Pos.FootFrontMe-
    dial(:,3)';Test.Marker_Pos.FootFrontLateral(:,3)']]);           % Temporary variable that
    contains the medium vertical displacement of the Front markers (placed on two
```

```
% different carbon fiber sheets)
    dist_front(i,:)=sqrt((Test.Marker_Pos.TibiaUpFront(:,2))'-
front_disp_y).^2+(Test.Marker_Pos.TibiaUpFront(:,3))'-front_disp_z).^2);    % Dis-
tance from TibiaUpFront and FootFront (mid-point) in the sagittal plane
end

%% Statistical analysis-----
% Mean values
GaitData.COPy.mean=mean(COPy);          % COP anterior-posterior dis-
placement mean value
GaitData.GRFx.mean=mean(GRFx);          % GRFx mean value
GaitData.GRFy.mean=mean(GRFy);          % GRFy mean value
GaitData.GRFz.mean=mean(GRFz);          % GRFz mean value
GaitData.T.mean=mean(T);                % Step duration mean value
GaitData.pylon_angle.mean=mean(theta);  % Pylon Angle
GaitData.dist_front.mean=mean(dist_front); % Distance from TibiaUpFront and
the mid-point between FootFrontMedial and FootFrontLateral mean value
GaitData.dist_med.mean=mean(dist_med);   % Distance from TibiaUpFront and
the mid-point between FootMedMedial and FootMedLateral mean value
GaitData.dist_back.mean=mean(dist_back); % Distance from TibiaUpFront and
the mid-point between FootBackMedial and FootBackLateral mean value

% COP control - it can't be less than zero or more than the total foot length
(out of the foot sole)
for i=1:length(Test.Time.Support)
    if GaitData.COPy.mean(i)<0
        GaitData.COPy.mean(i)=0;
    elseif GaitData.COPy.mean(i)>100
        GaitData.COPy.mean(i)=100;
    end
end

% Standard deviations
GaitData.COPy.std=std(COPy);          % COP anterior-posterior dis-
placement standard deviation
GaitData.GRFx.std=std(GRFx);          % GRFx standard deviation
GaitData.GRFy.std=std(GRFy);          % GRFy standard deviation
GaitData.GRFz.std=std(GRFz);          % GRFz standard deviation
GaitData.T.std=std(T);                % Step duration standard devia-
tion
GaitData.pylon_angle.std=std(theta);  % Pylon Angle standard deviation
GaitData.dist_front.std=std(dist_front); % Distance from TibiaUpFront and
the mid-point between FootFrontMedial and FootFrontLateral standard deviation
GaitData.dist_med.std=std(dist_med);   % Distance from TibiaUpFront and
the mid-point between FootMidMedial and FootMedLateral standard deviation
GaitData.dist_back.std=std(dist_back); % Distance from TibiaUpFront and
the mid-point between FootBackMedial and FootBackLateral standard deviation

%% Data Save-----
save('GaitData','GaitData');          % Structure containing information about GRF, COP
progression, marker distances, pylon angle and stance phase duration
```

## Dynamic Simulation – 'variflex\_model.m'

```

close all
clear
clc
load('GaitData.mat');           % Loading the structure that contains the dynamic
gait info
load('static_load.mat');        % Loading the variable that carries the info
about the weight of subject+adapter+prosthetic foot

%% Foot silhouette import-----
% Silhouette coordinates reading
filename='silhouette.txt';      % Name of the Points-format file
format='%f %f %f';
sil_coord=coord_read(filename,format); % Function that function reads coordi-
nates from a points file (*.txt)

sil_coord=sil_coord/10^3;      % generated in Rhinoceros
                                % Coordinates conversion in millime-
                                tres

%% Foot segmentation import-----
load('foot_info_16_9.mat')      % Loading the file containing segmentation
info
N1=Nkeel;                      % Number of keel spline points
N2=Nheel;                      % Number of heel spline points

% Points coordinates
toe_pt=N1+1;                   % Counting from the keel's lamina start, this
is the point referred to the toe (forefoot end)
heel_pt=N1+N2+1+1;            % Counting from the keel's lamina start, this
is the point referred to the heel (hindfoot end)
heel_start_joint=start_heel;   % Counting from the keel's lamina start, this
is the point referred to the heel/keel junction

% Matrix containing the points' coordinates that allows to plot the
% segmented spline properly
image_coord=[foot_coord(1:toe_pt,:); foot_coord(toe_pt-1:-1:heel_start_joint,:);
foot_coord(toe_pt+1:heel_pt,:)];

% Silhouette and segmentation plot
figure(1)
plot(sil_coord(:,1),sil_coord(:,2),'b','LineWidth',1)
hold on
plot(image_coord(:,1),image_coord(:,2),'ko-','LineWidth',1.5,'MarkerFaceCol-
or','r','MarkerSize',2,'MarkerEdgeColor','r')
title(['Geometric model of Vari-Flex foot - Keel segments: ' num2str(N1) '; Heel
segments: ' num2str(N2)])
xlabel('x position [m]'),ylabel('y position [m]'),axis equal
legend('Foot silhouette','Foot segmentation')

%% Geometric parameters-----
% Width (along local z-axis) [m]
W(1:N1)=[38.2 38.2 38.2 38.2 38.2 42 48 53 55 60 63.8 66 66 62 50 38]/1000;
% Keel segments
W(N1+1:N1+N2)=[66 63.8 60 53 52.4 50 50 45 35]/1000;
% Heel segments

% Thickness (along local y-axis) [m]
H(1:N1)=[8.8 8.8 8.7 8.7 8.5 7.8 6.8 6.2 6 5.2 4.7 4.5 4.3 4.2 4.1 3.5]/1000;
% Keel segments
H(N1+1:N1+N2)=[6.1 6.1 6.1 5.4 4.6 4.1 3.6 3.1 2.7]/1000;
% Heel segments

% Cross-sectional moment of inertia (b*h^3/12) [m^4]
I=H.^3.*W./12;

% Segments length (along local x-axis) [m]

```

---

```

j=1;
for i=1:max(size(foot_coord))-1
    if i==toe_pt
    else
        L(j)=sqrt(sum((foot_coord(i+1,:)-foot_coord(i,:)).^2));
        j=j+1;
    end
end

% Joints on the foot sole x-coordinates
foot_sole_pts=[foot_coord(heel_pt:-1:toe_pt+1,1)'
foot_coord(heel_start_joint+1:toe_pt,1)']; % coordinates referring to the
points forming the foot sole
foot_sole_dist=diff(foot_sole_pts);
% horizontal distance between the foot sole points

% Foot length [m]
foot_cum_length=cumsum(foot_sole_dist); % cumulative sum of the foot sole
distances
foot_length=sum(foot_sole_dist); % total foot length - it matches with
the CAD model's total length

% Total lengths of keel and heel spline [m]
L_tot1=sum(L(1:N1)); % Keel spline
L_tot2=sum(L(N1+1:N1+N2)); % Heel spline

% Starter revolute joints angles [rad]
theta=zeros(1,length(L));
theta(1)=pi-atan2(foot_coord(2,1)-foot_coord(1,1),foot_coord(2,2)-
foot_coord(1,2));
j=2;
for i=3:max(size(foot_coord))
    if i==toe_pt+1
    elseif i>toe_pt && i<toe_pt+common_sr+2
        j=j+1;
    elseif i==toe_pt+common_sr+2
        l_opp(j)=sqrt(sum((foot_coord(toe_pt+common_sr+2,:)-
foot_coord(heel_start_joint-common_sr-1,:)).^2));
        A(j)=L(heel_start_joint-common_sr-1)^2+L(j)^2-l_opp(j)^2;
        B(j)=2*L(heel_start_joint-1)*L(j);
        theta(j)=acos(A(j)/B(j));
        alpha(j)=atan2(foot_coord(i,1)-foot_coord(i-1,1),foot_coord(i,2)-
foot_coord(i-1,2));
        j=j+1;
    else
        alpha(j)=atan2(foot_coord(i,1)-foot_coord(i-1,1),foot_coord(i,2)-
foot_coord(i-1,2));
        theta(j)=alpha(j-1)-alpha(j);
        j=j+1;
    end
end

% Material properties-----
% Material's Young modulus [GPa]
E=75*10^9; % Carbon Fibre Composite

% Material's density [kg/m^3]
rho=1.8*10^3; % Carbon Fibre Composite

% Analytical joints' compliances [N*m*s/rad]
b=lininspace(100,100,N1+N2); % Carbon fiber typically has damping near 0
b2=b(2);b3=b(3);b4=b(4);b5=b(5);b6=b(6);b7=b(7);b8=b(8);b9=b(9);b13=b(13);b14=b(1
4);b15=b(15);b16=b(16); % keel spline joints
b10=b(10);b11=b(11);b12=b(12);b17=b(17);b18=b(18);b19=b(19);
% keel/heel junction joints
b20=b(20);b21=b(21);b22=b(22);b23=b(23);b24=b(24);b25=b(25);
% heel spline joints

```

---

---

```

% Analytical joints' stiffnesses [N*m/rad]
N(1)=1;
for i=2:max(N1,N2)
    N(i)=N(i-1)+i^2; % Analytical coefficients
end
k=zeros(1,N1+N2);
k(1:N1)=(N(N1)/N1^2)*(3*E*I(1:N1)/L_tot1);
k(N1+1:N1+N2)=(N(N2)/N2^2)*(3*E*I(N1+1:N1+N2)/L_tot2);

k2=k(2);k3=k(3);k4=k(4);k5=k(5);k6=k(6);k7=k(7);k8=k(8);k9=k(9);k13=k(13);k14=k(14);
k15=k(15);k16=k(16); % keel spline joints
k10=k(10);k11=k(11);k12=k(12)+k(17);k18=k(18);k19=k(19);
% keel/heel junction joints
k20=k(20);k21=k(21);k22=k(22);k23=k(23);k24=k(24);k25=k(25);
% heel spline joints

%% Other parameters-----
% Gravitational acceleration [m/s^2]
g=9.80665;

% Subject+adapter+prothetic foot weight [N]
Fw=static_load;

%% Simulation parameters-----
% Samples acquired over stance phase (simulated sampling frequency: 81,4 Hz)
ns=100;

% Resampling coefficient (times ns_new is bigger than ns)
c=100;

% Simulation time (stance phase duration) [s]
T=GaitData.T.mean;

% Time support [s]
t=linspace(0,T,ns);
t_res=linspace(0,T,ns*c);

%% Ankle controls-----
% Pylon angle [deg]
pylon_angle=GaitData.pylon_angle.mean;

% Pylon angle input signal
pylon_ang.time=t'; % Time support [s]
pylon_ang.signals.values=-pylon_angle'*pi/180; % Conversion in radians
[rad]
pylon_ang.signals.dimensions=1; % Struct dimension [1D]

%% COP displacement-----
COP_time=t; % Time support [s]
COP_displacement=GaitData.COPy.mean*foot_length/100; % COP displacement expressed as a % of foot length

% Calculation of the time interval in which COP remains in a certain segment [% stance phase]
for i=1:length(foot_cum_length)
    occurrences(i)=length(find(COP_displacement<=foot_cum_length(i)));
end
% Conversion in seconds [s]
for i=1:length(occurrences)
    permanence_time(i)=round(COP_time(occurrences(i))*ns*c)/(ns*c);
end

%% Inferior/superior ground force [N]-----
% Total inferior/superior ground force [N]
inf_sup_ground_force=GaitData.GRFz.mean*Fw/100;

% Inferior/superior ground force resampling

```

---

---

```

fs_new=ns*c; % New
number of samples
inf_sup_ground_force_res=resample(inf_sup_ground_force,fs_new,ns); % Infe-
rior/superior ground force resampled [N]

% Definition of the innferior/superior ground force acting on each segment over
time [N]
if permanence_time(1)==0
    for i=1:length(permanence_time)
        if permanence_time(i)==0
            vGRF(i).time=t_res;
            vGRF(i).signals.dimensions=1;
            vGRF(i).signals.values=zeros(length(inf_sup_ground_force_res),1);
        else
            vGRF(i).time=t_res;
            vGRF(i).signals.dimensions=1;
            vGRF(i).signals.values=zeros(length(inf_sup_ground_force_res),1);
            vGRF(i).signals.values(permanence_time(i-1)/T*fs_new+1:perma-
nence_time(i)/T*fs_new)=inf_sup_ground_force_res(permanence_time(i-
1)/T*fs_new+1:permanence_time(i)/T*fs_new);
        end
    end
else
    for i=1:length(permanence_time)
        vGRF(i).time=t_res;
        vGRF(i).signals.dimensions=1;
        vGRF(i).signals.values=zeros(length(inf_sup_ground_force_res),1);
        if i==1
            vGRF(i).signals.values(1:perma-
nence_time(i)/T*fs_new)=inf_sup_ground_force_res(1:permanence_time(i)/T*fs_new);
        else
            vGRF(i).signals.values(permanence_time(i-1)/T*fs_new+1:perma-
nence_time(i)/T*fs_new)=inf_sup_ground_force_res(permanence_time(i-
1)/T*fs_new+1:permanence_time(i)/T*fs_new);
        end
    end
end

%% Anterior/posterior ground force-----
% Total anterior/posterior ground force [N]
ant_post_ground_force=GaitData.GRFy.mean*Fw/100;

% Anterior/superior ground force resampling
fs_new=ns*c; % New
number of samples
ant_post_ground_force_res=resample(ant_post_ground_force,fs_new,ns); % Ante-
rior/posterior ground force resampled [N]

% Definition of the anterior/superior ground force acting on each segment over
time [N]
if permanence_time(1)==0
    for i=1:length(permanence_time)
        if permanence_time(i)==0
            hGRF(i).time=t_res;
            hGRF(i).signals.dimensions=1;
            hGRF(i).signals.values=zeros(length(ant_post_ground_force_res),1);
        else
            hGRF(i).time=t_res;
            hGRF(i).signals.dimensions=1;
            hGRF(i).signals.values=zeros(length(ant_post_ground_force_res),1);
            hGRF(i).signals.values(permanence_time(i-1)/T*fs_new+1:perma-
nence_time(i)/T*fs_new)=ant_post_ground_force_res(permanence_time(i-
1)/T*fs_new+1:permanence_time(i)/T*fs_new);
        end
    end
else
    for i=1:length(permanence_time)
        hGRF(i).time=t_res;

```

---



```

hGRF(i).signals.dimensions=1;
hGRF(i).signals.values=zeros(length(ant_post_ground_force_res),1);
if i==1
    hGRF(i).signals.values(1:perma-
nence_time(i)/T*fs_new)=ant_post_ground_force_res(1:permanence_time(i)/T*fs_new);
else
    hGRF(i).signals.values(permanence_time(i-1)/T*fs_new+1:perma-
nence_time(i)/T*fs_new)=ant_post_ground_force_res(permanence_time(i-
1)/T*fs_new+1:permanence_time(i)/T*fs_new);
end
end
end

%% External forces handling to reduce model vibrations - 2nd strategy-----
for i=1:length(permanence_time)
    force_start(i)=find(vGRF(i).signals.values,1);           % Starting sample
of force application
    force_end(i)=find(vGRF(i).signals.values,1,'last');       % Ending sample
of force application
    Fapp_duration(i)=length(find(vGRF(i).signals.values));    % Applied
force duration (in samples)
    perc=70;                                                  % Percentage of
forces sovrapposition
    perc=perc/100;

    % Vertical ground reaction force
    if i==1
        vGRF(i).signals.values(force_start(i):force_start(i)+ceil(Fapp_dura-
tion(i)*perc))=inf_sup_ground_force_res(force_start(i):force_start(i)+ceil(Fapp_d
uration(i)*perc));
        vGRF(i).signals.values(force_start(i)+ceil(Fapp_dura-
tion(i)*perc)+1:force_end(i))=inf_sup_ground_force_res(force_start(i)+ceil(Fapp_d
uration(i)*perc)+1:force_end(i))-lin-
space(0,inf_sup_ground_force_res(force_end(i)),length(force_start(i)+ceil(Fapp_du
ration(i)*perc)+1:force_end(i)));
    else
        vGRF(i).signals.values(force_start(i-1)+ceil(Fapp_duration(i-
1)*perc)+1:force_end(i-1)+1)=linspace(0,inf_sup_ground_force_res(force_end(i-
1)),length(force_start(i-1)+ceil(Fapp_duration(i-1)*perc)+1:force_end(i-1)+1));
        vGRF(i).signals.values(force_start(i)+ceil(Fapp_dura-
tion(i)*perc)+1:force_end(i))=inf_sup_ground_force_res(force_start(i)+ceil(Fapp_d
uration(i)*perc)+1:force_end(i))-lin-
space(0,inf_sup_ground_force_res(force_end(i)),length(force_start(i)+ceil(Fapp_du
ration(i)*perc)+1:force_end(i)));
    end

    % Horizontal ground reaction force
    if i==1
        hGRF(i).signals.values(force_start(i):force_start(i)+ceil(Fapp_dura-
tion(i)*perc))=ant_post_ground_force_res(force_start(i):force_start(i)+ceil(Fapp_
duration(i)*perc));
        hGRF(i).signals.values(force_start(i)+ceil(Fapp_dura-
tion(i)*perc)+1:force_end(i))=ant_post_ground_force_res(force_start(i)+ceil(Fapp_
duration(i)*perc)+1:force_end(i))-lin-
space(0,ant_post_ground_force_res(force_end(i)),length(force_start(i)+ceil(Fapp_d
uration(i)*perc)+1:force_end(i)));
    else
        hGRF(i).signals.values(force_start(i-1)+ceil(Fapp_duration(i-
1)*perc)+1:force_end(i-1)+1)=linspace(0,ant_post_ground_force_res(force_end(i-
1)),length(force_start(i-1)+ceil(Fapp_duration(i-1)*perc)+1:force_end(i-1)+1));
        hGRF(i).signals.values(force_start(i)+ceil(Fapp_dura-
tion(i)*perc)+1:force_end(i))=ant_post_ground_force_res(force_start(i)+ceil(Fapp_
duration(i)*perc)+1:force_end(i))-lin-
space(0,ant_post_ground_force_res(force_end(i)),length(force_start(i)+ceil(Fapp_d
uration(i)*perc)+1:force_end(i)));
    end
end
end

```

---

```

%% COP comparison - real/segmented/smoothed-----
% Segmented COP - external force application 1st strategy
seg_COP(1:occurrences(1))=(foot_cum_length(1)/2)/foot_length*100;
for i=2:length(occurrences)
    seg_COP(occurrences(i-1)+1:occurrences(i))=(foot_cum_length(i-1)+diff(foot_cum_length(i-1:i))/2)/foot_length*100;
end

% Smoothed COP
supportv=[fliplr(COP_displacement) COP_displacement fliplr(COP_displacement)];
% Support vector with the COP displacement flipped left-right

% and added before and after the original COP vector
supportv_res=resample(supportv,fs_new,ns);
% Resampled support vector
COP_res=supportv_res(fs_new:2*fs_new-1);
% Resampled COP

for i=1:length(foot_cum_length)
    if i==length(foot_cum_length)
        smooth_COP(force_start(i):force_end(i))=linspace(foot_cum_length(i-1)+diff(foot_cum_length(i-1:i))/2,foot_cum_length(i-1)+diff(foot_cum_length(i-1:i))/2,length(force_start(i):force_end(i)));
    else
        force_base_segment=vGRF(i).signals.values(force_start(i)+ceil(Fapp_duration(i)*perc)+1:force_end(i));
        force_follower_segment=vGRF(i+1).signals.values(force_start(i)+ceil(Fapp_duration(i)*perc)+1:force_end(i));
        w=(force_base_segment-force_follower_segment)./(force_base_segment+force_follower_segment);
        if i==1
            midpoint=foot_cum_length(i);
            smooth_COP(force_start(i):force_start(i)+ceil(Fapp_duration(i)*perc))=linspace(foot_cum_length(i)/2,foot_cum_length(i)/2,length(force_start(i):force_start(i)+ceil(Fapp_duration(i)*perc)));
            for j=1:length(w)
                if w(j)>=0
                    weighted_COP(j)=midpoint-w(j)*(foot_cum_length(i)/2);
                elseif w(j)<0
                    weighted_COP(j)=midpoint-w(j)*diff(foot_cum_length(i:i+1))/2;
                end
            end
        else
            midpoint=foot_cum_length(i);
            smooth_COP(force_start(i):force_start(i)+ceil(Fapp_duration(i)*perc))=linspace(foot_cum_length(i-1)+diff(foot_cum_length(i-1:i))/2,foot_cum_length(i-1)+diff(foot_cum_length(i-1:i))/2,length(force_start(i):force_start(i)+ceil(Fapp_duration(i)*perc)));
            for j=1:length(w)
                if w(j)>=0
                    weighted_COP(j)=midpoint-w(j)*diff(foot_cum_length(i-1:i))/2;
                elseif w(j)<0
                    weighted_COP(j)=midpoint-w(j)*diff(foot_cum_length(i:i+1))/2;
                end
            end
        end
        smooth_COP(force_start(i)+ceil(Fapp_duration(i)*perc)+1:force_end(i))=weighted_COP;
        clear weighted_COP
    end
end
clc

%% Start simulation-----
out=sim('sim_vari_flex_dyn_lsr_locked.slx');

%% Deflection analysis and comparison with experimental values-----

```

---

---

```

% Time support [% stance phase]
t_def=linspace(0,100,100);

% Frontal deflection [mm]
front_def=GaitData.dist_front.mean-GaitData.dist_front.mean(1); %
Experimental averaged data - 10 trials
fd_std=GaitData.dist_front.std; %
Standard deviation of experimental data - 10 trials
front_deflection=(out.front_deflection(1:end-1)-out.front_deflection(1))*1000; %
Offset removing (initial distance) and conversion in mm

% Mid deflection [mm]
mid_def=GaitData.dist_med.mean-GaitData.dist_med.mean(1); %
Experimental averaged data - 10 trials
md_std=GaitData.dist_med.std; %
Standard deviation of experimental data - 10 trials
mid_deflection=(out.mid_deflection(1:end-1)-out.mid_deflection(1))*1000; %
Offset removing (initial distance) and conversion in mm

% Back deflection [mm]
back_def=GaitData.dist_back.mean-GaitData.dist_back.mean(1); %
Experimental averaged data - 10 trials
bd_std=GaitData.dist_back.std; %
Standard deviation of experimental data - 10 trials
back_deflection=(out.back_deflection(1:end-1)-out.back_deflection(1))*1000; %
Offset removing (initial distance) and conversion in mm

%% ROS calculation-----
% Calculation of alpha angle [rad]
t=1;
for i=1:length(permanence_time)
    if i==1
        for j=2:floor(permanence_time(i)/T*100)+1
            alpha(t)=atan2(out.ROS(j,(i-1)*3+1),-out.ROS(j,(i-1)*3+2));
            d(t)=out.ROS(j,(i-1)*3+3);
            t=t+1;
        end
    else
        for j=floor(permanence_time(i-1)/T*100)+2:floor(perma-
nence_time(i)/T*100)+1
            alpha(t)=atan2(out.ROS(j,(i-1)*3+1),-out.ROS(j,(i-1)*3+2));
            d(t)=out.ROS(j,(i-1)*3+3);
            t=t+1;
        end
    end
end
alphadeg=alpha*180/(pi/2); % Alpha angle [deg]

% Calculation of beta angle [rad]
beta=pi/2-(pylon_angle*pi/180)-alpha;
betagrad=beta*180/pi; % Beta angle [deg]

% ROS's components calculation [m]
RollOverShapeX=d.*cos(beta); % ROS component along shank-based X axis
RollOverShapeY=-d.*sin(beta); % ROS component along shank-based Y axis

%% ROS plot-----
% Instants of maximum deflection for each foot sole segment
ROSPts=[floor(permanence_time(1:end-2)/T*100) floor(permanence_time(end-2:end-
1)/T*100)+1];

% Calculation of the circle that approximates the experimental ROS [m]
R=CircleFitByPratt([RollOverShapeX(ROSPts) RollOverShapeY(ROSPts)']); %
Function that computes radius and centre's coordinates of the approximant arc of
circle
ROSCentreX=R(1); % X-coord of the centre
ROSCentreY=R(2); % Y-coord of the centre
ROSRadius=R(3); % Circle radius

```

---

```
% Calculation of the circle coordinates that form the arc of circle
% containg the computed ROS
theta=linspace(-pi*5/9,-pi*3.4/9,1e3);
x=ROSRadius*cos(theta)+ROSCentreX;          % X coordinates
y=ROSRadius*sin(theta)+ROSCentreY;          % Y coordinates
str=sprintf('ROS radius = %0.2f cm',ROSRadius*100)
```

## Other Functions

### 'coord\_read.m'

```
function coord=coord_read(filename,format)
% COORD_READ is a function that reads coordinates from a Points file (*.txt)
% generated in Rhinoceros
%   Filename = name of the *.txt file
%   Format = format of the field to read
% Open the coordinates text file
fid=fopen(filename);
% Reading coordinates
coord=textscan(fid,format);
coord=[-coord{1,1} coord{1,2}];
coord=[coord(:,1)-coord(1,1) coord(:,2)-coord(1,2)];
% Close the coordinates text file
fclose(fid);
end
```

### 'CircleFitByPratt.m' [61]

```
function Par = CircleFitByPratt(XY)

%-----
%
%   Circle fit by Pratt
%   V. Pratt, "Direct least-squares fitting of algebraic surfaces",
%   Computer Graphics, Vol. 21, pages 145-152 (1987)
%
%   Input:  XY(n,2) is the array of coordinates of n points x(i)=XY(i,1),
%           y(i)=XY(i,2)
%
%   Output: Par = [a b R] is the fitting circle:
%               center (a,b) and radius R
%
%   Note: this fit does not use built-in matrix functions (except "mean"),
%         so, it can be easily programmed in any programming language
%-----

n = size(XY,1);      % number of data points

centroid = mean(XY); % the centroid of the data set

%   computing moments (note: all moments will be normed, i.e. divided by n)

Mxx=0; Myy=0; Mxy=0; Mxz=0; Myz=0; Mzz=0;

for i=1:n
    Xi = XY(i,1) - centroid(1); % centering data
    Yi = XY(i,2) - centroid(2); % centering data
    Zi = Xi*Xi + Yi*Yi;
    Mxy = Mxy + Xi*Yi;
    Mxx = Mxx + Xi*Xi;
    Myy = Myy + Yi*Yi;
    Mxz = Mxz + Xi*Zi;
    Myz = Myz + Yi*Zi;
    Mzz = Mzz + Zi*Zi;
end

Mxx = Mxx/n;
Myy = Myy/n;
Mxy = Mxy/n;
```

```

Mxz = Mxz/n;
Myz = Myz/n;
Mzz = Mzz/n;

%    computing the coefficients of the characteristic polynomial

Mz = Mxx + Myy;
Cov_xy = Mxx*Myy - Mxy*Mxy;
Mxz2 = Mxz*Mxz;
Myz2 = Myz*Myz;

A2 = 4*Cov_xy - 3*Mz*Mz - Mzz;
A1 = Mzz*Mz + 4*Cov_xy*Mz - Mxz2 - Myz2 - Mz*Mz*Mz;
A0 = Mxz2*Myy + Myz2*Mxx - Mzz*Cov_xy - 2*Mxz*Myz*Mxy + Mz*Mz*Cov_xy;
A22 = A2 + A2;

epsilon=1e-12;
ynew=1e+20;
IterMax=20;
xnew = 0;

%    Newton's method starting at x=0

for iter=1:IterMax
    yold = ynew;
    ynew = A0 + xnew*(A1 + xnew*(A2 + 4.*xnew*xnew));
    if (abs(ynew)>abs(yold))
        disp('Newton-Pratt goes wrong direction: |ynew| > |yold|');
        xnew = 0;
        break;
    end
    Dy = A1 + xnew*(A22 + 16*xnew*xnew);
    xold = xnew;
    xnew = xold - ynew/Dy;
    if (abs((xnew-xold)/xnew) < epsilon), break, end
    if (iter >= IterMax)
        disp('Newton-Pratt will not converge');
        xnew = 0;
    end
    if (xnew<0.)
        fprintf(1,'Newton-Pratt negative root: x=%f\n',xnew);
        xnew = 0;
    end
end

%    computing the circle parameters

DET = xnew*xnew - xnew*Mz + Cov_xy;
Center = [Mxz*(Myy-xnew)-Myz*Mxy , Myz*(Mxx-xnew)-Mxz*Mxy]/DET/2;

Par = [Center+centroid , sqrt(Center*Center'+Mz+2*xnew)];




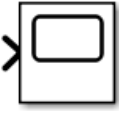


end %    CircleFitByPratt

```


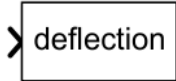

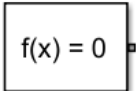
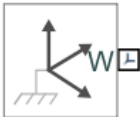


## B. Appendix B – Simulink® Schemes

### Simulink®/Simscape's Blocks Legend

Table B.0.1 – Legend of Simulink®/Simscape's blocks utilized

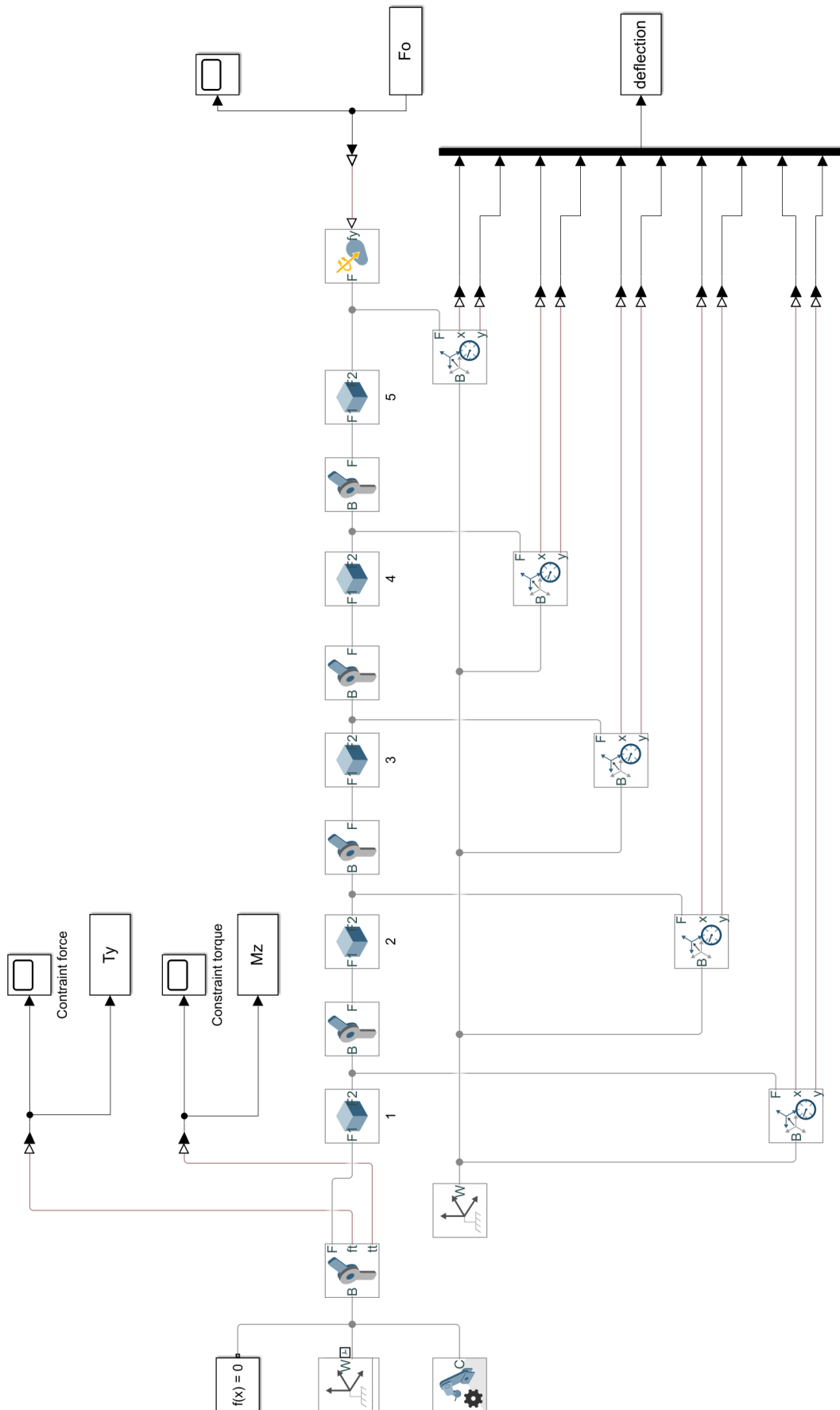
Block's image	Block's Name	Description <sup>12</sup>
	Solid	Represents a solid combining a geometry, an inertia and mass, a graphics component, and rigidly attached frames into a single unit. A solid is the common building block of rigid bodies. The Solid block obtains the inertia from the geometry and density, from the geometry and mass, or from an specified inertia tensor.
	Revolute Joint	Represents a revolute joint acting between two frames. This joint has one rotational degree of freedom represented by one revolute primitive. The joint constrains the origins of the two frames to be coincident and the z-axes of the base and follower frames to be coincident, while the follower x-axis and y-axis can rotate around the z-axis.
	Rigid Transform	Defines a fixed 3-D rigid transformation between two frames. Two components independently specify the translational and rotational parts of the transformation. Different translations and rotations can be freely combined.
	Scope	Displays time-domain signals on screen (also while simulation in running).
	External Forces and Torques	Applies an external force and torque at the attached frame. The force and torque are specified by the physical signal inputs.
	Transform Sensor	Measures time-dependent relationship between two frames. A Transform Sensor pas-

<sup>12</sup> From Simulink®'s block description

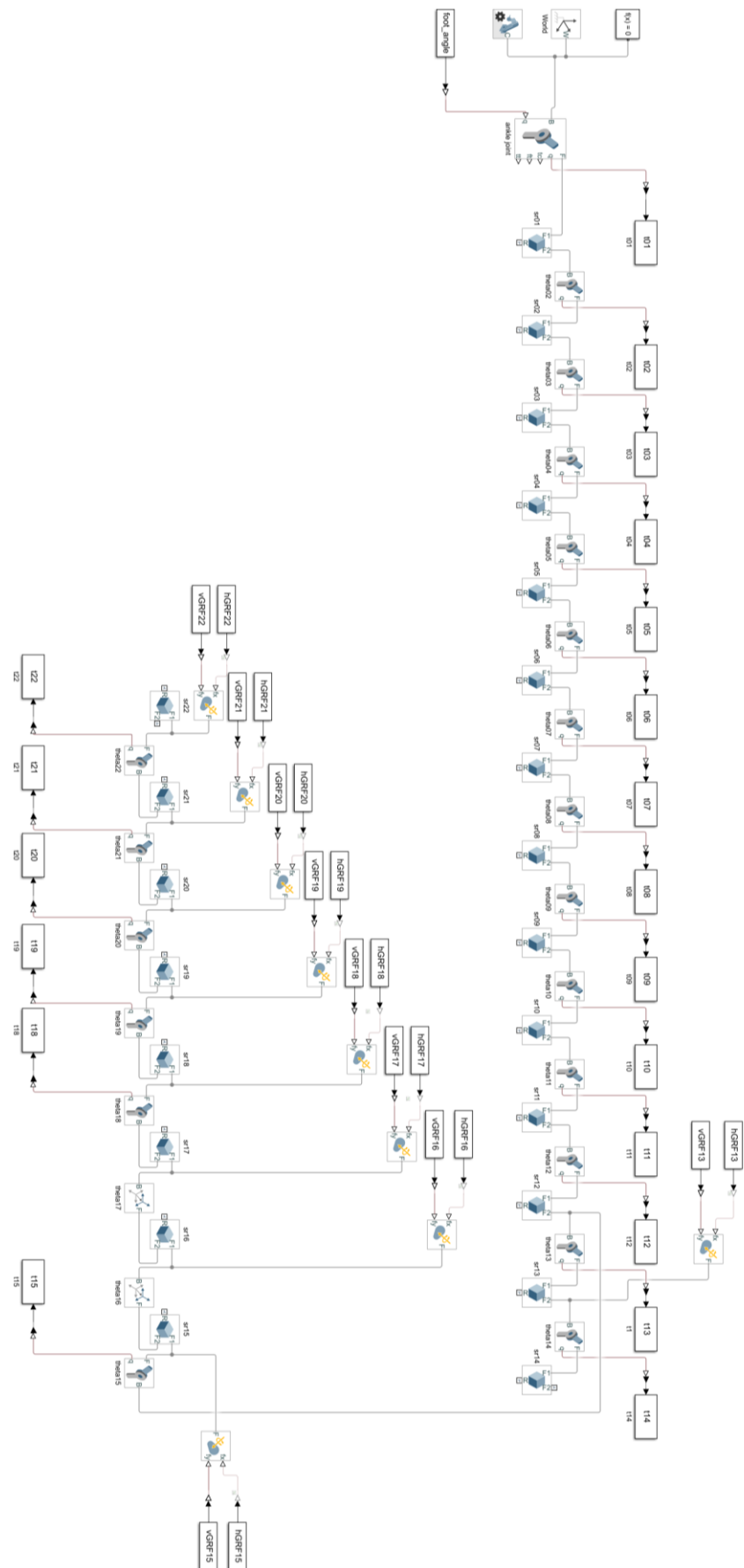
		sively senses this 3-D time-varying transformation, and its derivatives, between the two frames.
	From Workspace	Reads data values specified in timeseries, matrix, or structure format from the MATLAB workspace, model workspace, or mask workspace.
	To Workspace	Writes input to specified timeseries, array, or structure in a workspace.
	MUX	Merges different signals in one single output.
	Solver Configuration	Defines solver settings to use for simulation.
	World Frame	Provides access to the world or ground frame, a unique motionless, orthogonal, right-handed coordinate frame predefined in any mechanical model. World frame is the ground of all frame networks in a mechanical model.
	Mechanism Configuration	Sets mechanical and simulation parameters that apply to an entire machine, the target machine to which the block is connected.
	Simulink-PS and PS-Simulink Converter	Convert the unitless Simulink input signal to a Physical Signal and vice versa.



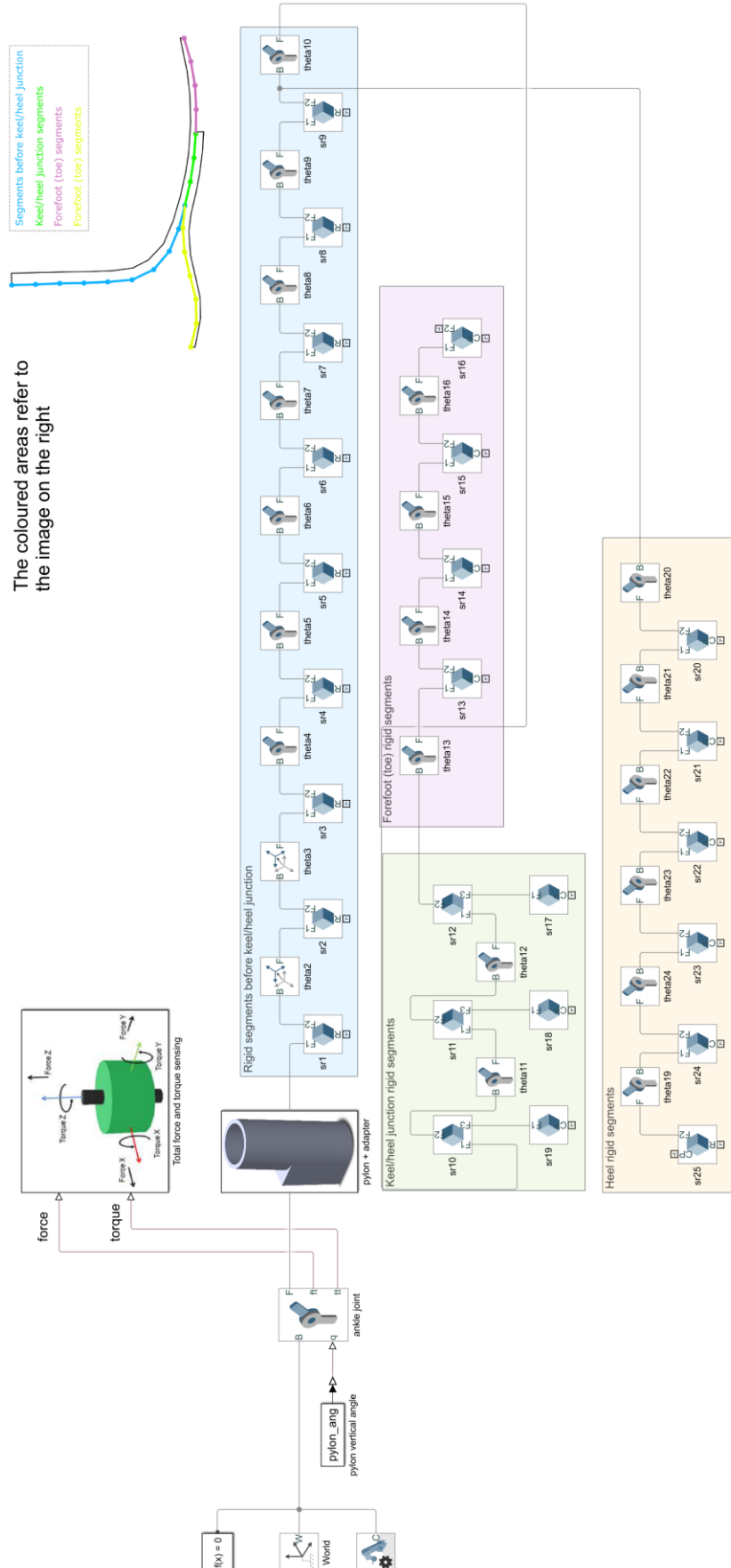
## 5-Segments Wedged Beam Model – ‘bar\_model\_5.slx’



# Highlander® multibody model – 'sim\_highlander\_v6.slx'

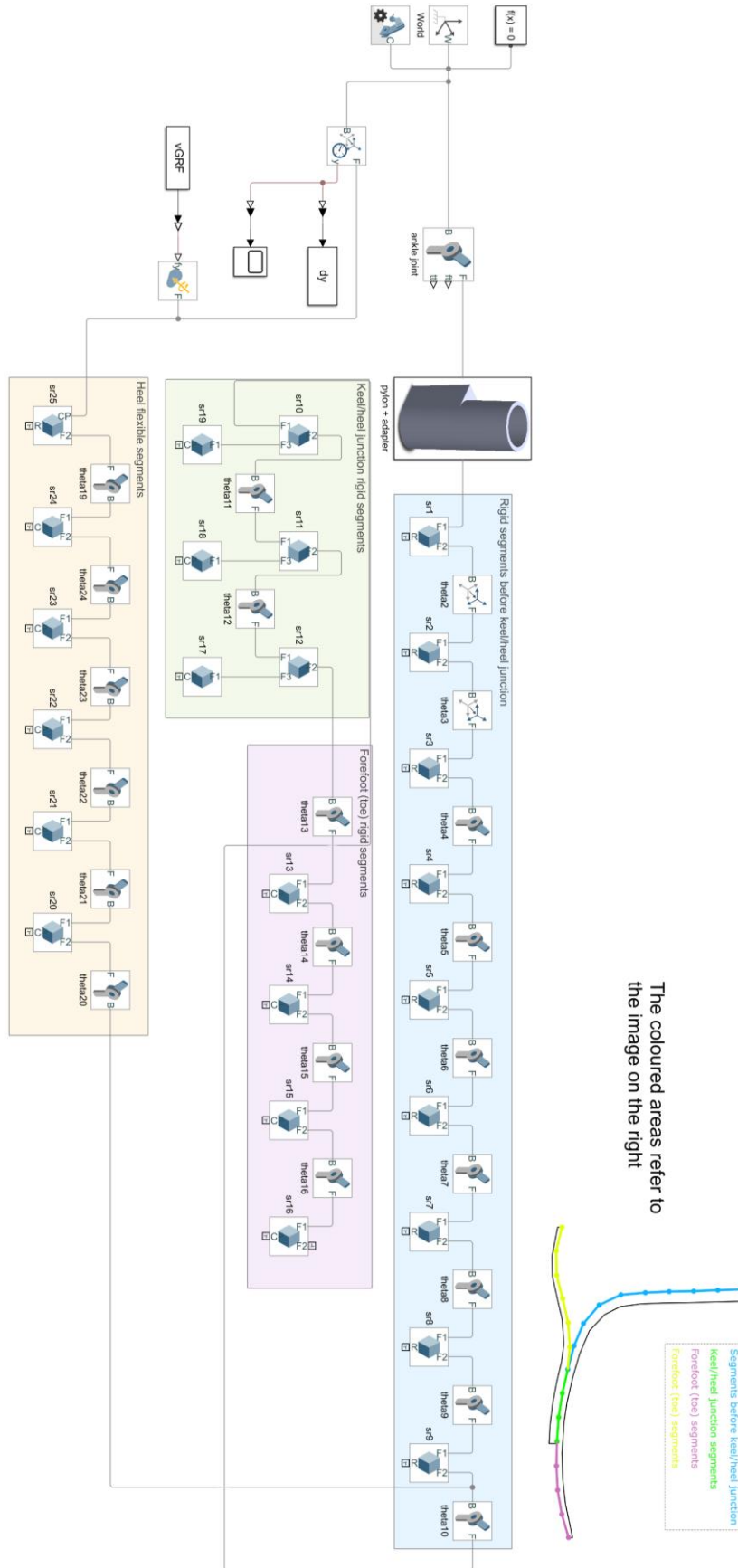


# Vari-Flex® multibody model - 'sim\_vari\_flex\_16\_9\_geom.slx'

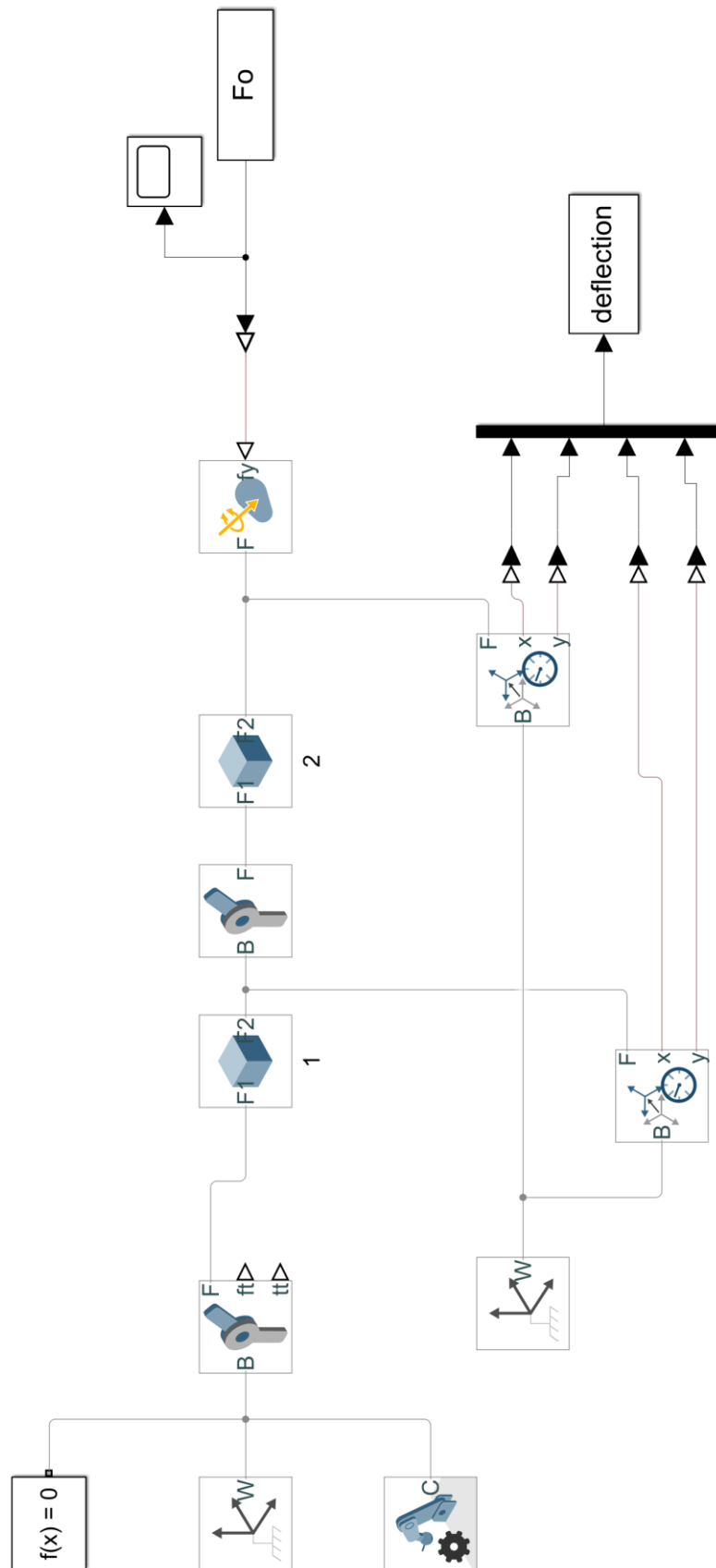


## Quasi-Static Simulation 20 Heel Vari-Flex® Model –

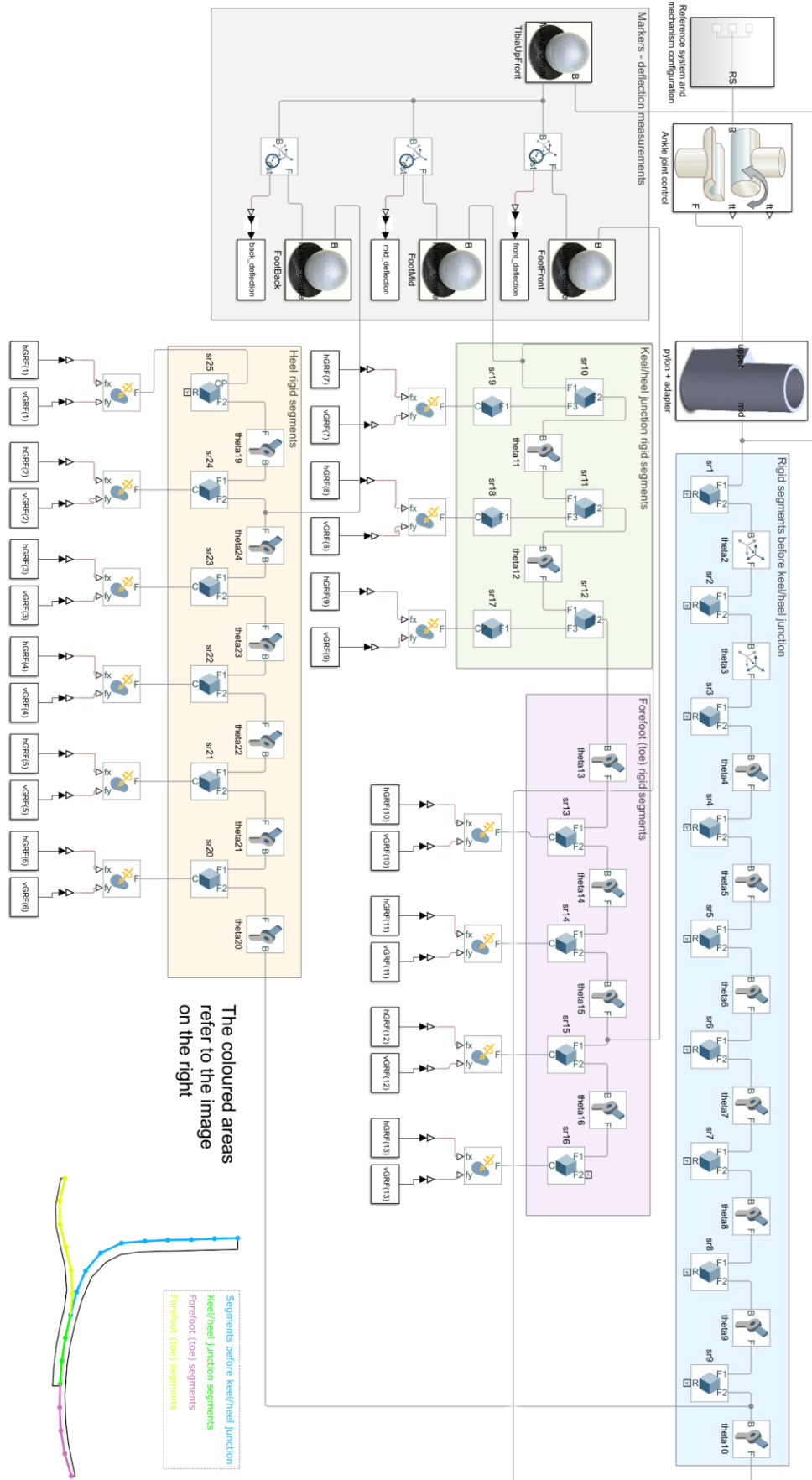
'sim\_vari\_flex\_mech\_test\_heel\_20.slx'



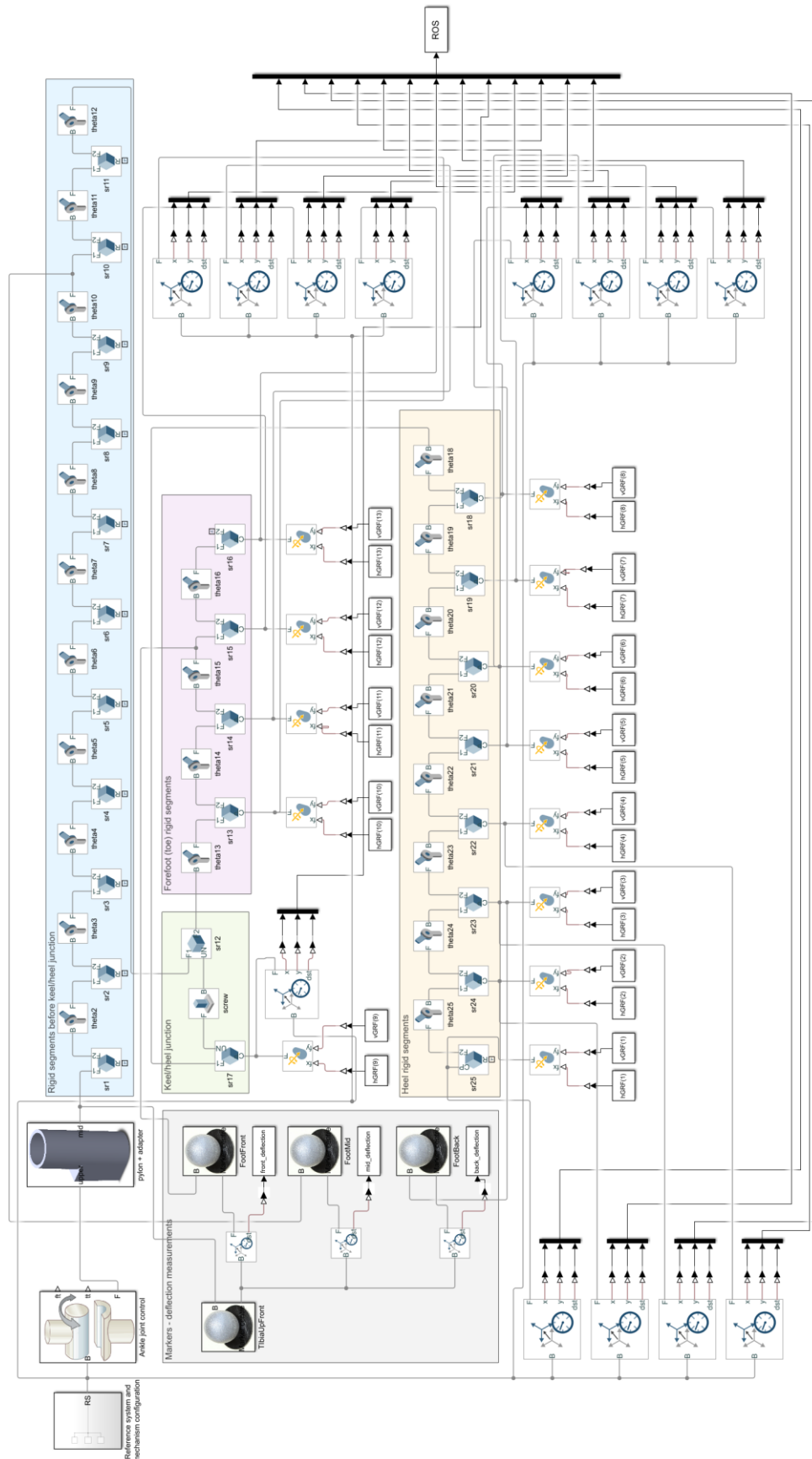
## 2-Segments Beam Model to Be Tuned – 'bar\_model\_opt\_2.slx'



# Former Dynamic Vari-Flex® Model – 'sim\_vari\_flex\_dyn\_16\_9.slx'

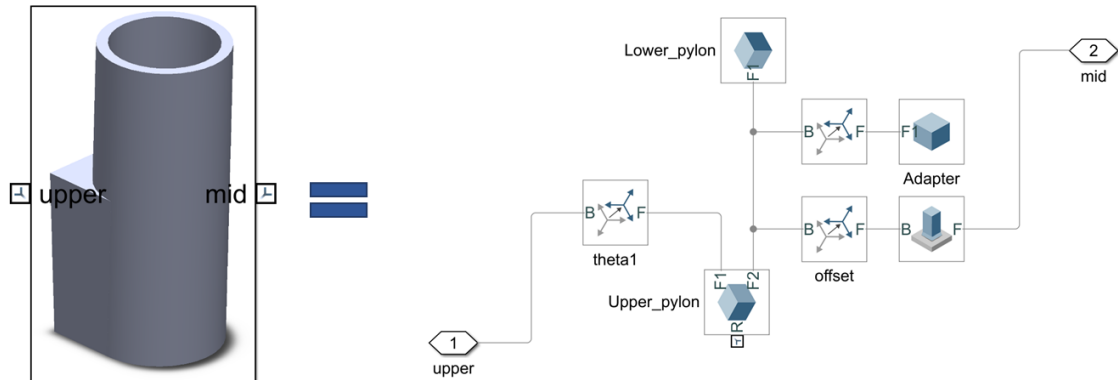


# Modified Dynamic Vari-Flex® Model – 'sim\_vari\_flex\_dyn\_1sr\_locked.slx'

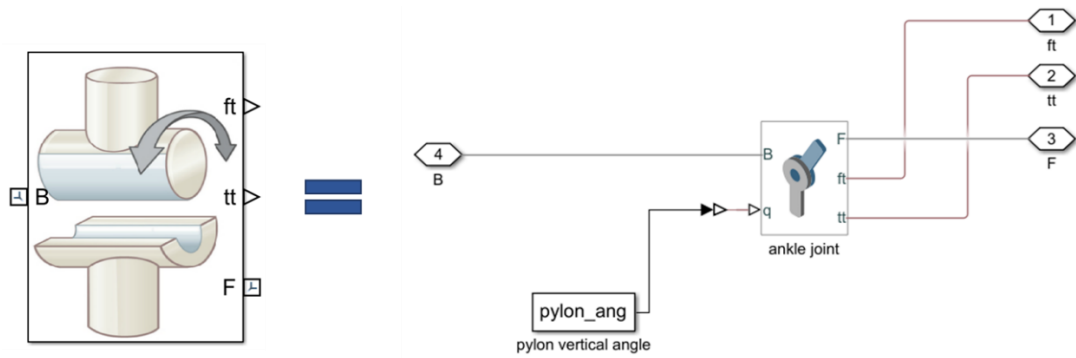


## Subsystems

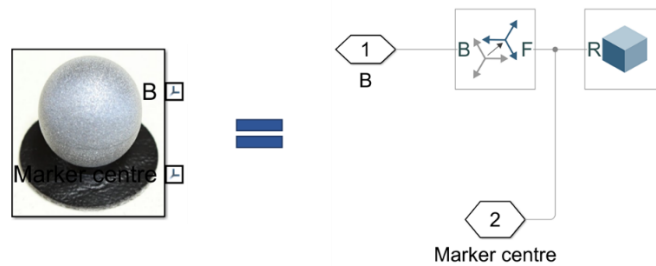
### *Pylon + Adapter*



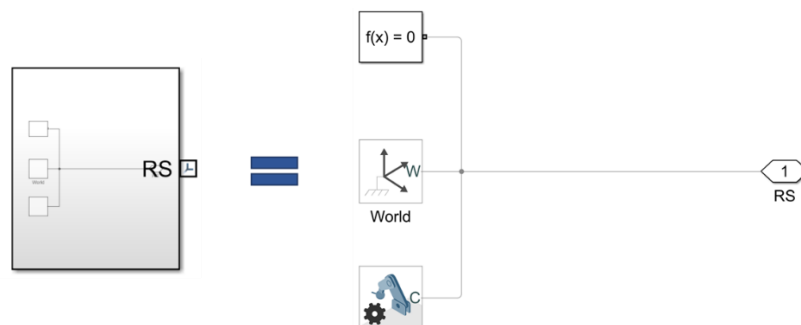
### *Ankle Joint Control*



### *Marker*



### *Reference system and mechanism configuration*





## References

---

- [1] B. Blackwood, T. J. Yuen, B. J. Sangeorzan and W. R. Ledoux, "The midtarsal joint locking mechanism," *Foot Ankle Int.*, vol. 26, no. 12, pp. 1074-80, December 2005.
- [2] P. contributors, "Foot and Ankle Structure and Function," Physiopedia, 2019 July 19. [Online]. Available: [https://www.physio-pedia.com/index.php?title=Foot\\_and\\_Ankle\\_Structure\\_and\\_Function&oldid=217145](https://www.physio-pedia.com/index.php?title=Foot_and_Ankle_Structure_and_Function&oldid=217145).
- [3] C. W. Chan and A. Rudins, "Foot Biomechanics During Walking and Running," *Mayo Clin Proc*, vol. 69, pp. 448-461, 1994.
- [4] P. Abrahams, *Atlante del corpo umano: una guida completa per comprendere il corpo umano*, DIX Editore, 2009, pp. 222-231.
- [5] R. Donatelli, "Normal Biomechanics of the Foot and Ankle," *Journal of Orthopaedic & Sports Physical Therapy*, vol. 7, no. 3, pp. 92-95, 1985.
- [6] J. H. Hicks, "The Mechanics of the Foot - The Plantar Aponeurosis and the Arch," *Journal of Anatomy*, vol. 88, no. 1, pp. 25-30, 1954.
- [7] V. H. Frankel and M. Nordin, *Basic Biomechanics of the Skeletal System*, Philadelphia: Lea & Febiger, 1980.
- [8] "Cambridge Dictionary," [Online]. Available: <https://dictionary.cambridge.org/it/dizionario/inglese/gait>.
- [9] P. contributors, "Gait," Physiopedia, 2019 June 18. [Online]. Available: <https://www.physio-pedia.com/index.php?title=Gait&oldid=215024>.
- [10] R. A. Mann and J. Hagy, "Biomechanics of walking, running and sprinting," *The American Journal of Sports Medicine*, vol. 8, no. 5, pp. 345-350, 1980.
- [11] M. Schmid, G. Beltrami, D. Zambarbieri and G. Verni, "Centre of pressure displacements in trans-femoral amputees during gait," *Gait & Posture*, vol. 21, pp. 255-262, 2005.
- [12] K. Ziegler-Graham, E. J. MacKenzie, P. L. Ephrim, T. G. Travison and R. Brookmeyer, "Estimating the Prevalence of Limb Loss in the United States: 2005 - 2050," *Archives of Physical Medicine and Rehabilitation*, no. 89, pp. 422-429, 2008.
- [13] H. Claessen, M. Narres, B. Haastert, W. Arend, F. Hoffmann, S. Morbach, G. Rumenapf, T. Kvitkina, H. Friedel, C. Gunster, I. Schubert, W. Ullrich, B. Westerhoff, A. Wilk and A. Icks, "Lower-extremity amputations in people with and without diabetes in Germany, 2008-2012 – an analysis of more than 30 million inhabitants," *Clinical Epidemiology*, no. 10, pp. 475-488, 2018.
- [14] F. L. Lombardo, M. Maggini, A. De Bellis, G. Seghieri and R. Anichini, "Lower Extremity Amputations in Persons with and without Diabetes in Italy: 2001-2010," *PLoS ONE*, vol. 9, no. 1, 2014.

- [15] N. Holman, R. Young and W. Jeffcoate, "Variation in the Recorder Incidence of Amputation of the Lower Limb in England," *Diabetologia*, no. 55, pp. 1919-1925, 2012.
- [16] S. Fosse, A. Hartemann-Heurtier, S. Jacqueminet, G. Ha Van, A. Grimaldi and A. Fagot-Campagna, "Incidence and Characteristics of Lower Limb Amputations in People with Diabetes," *Diabetic Medicine*, no. 26, pp. 391-396, 2009.
- [17] E. J. Peters, M. R. Childs, R. P. Wunderlich, L. B. Harkless, D. G. Armstrong and L. A. Lavery, "Functional Status of Persons With Diabetes-Related Lower-Extremity Amputations," *Diabetes Care*, vol. 24, no. 10, pp. 1799-1804, 2001.
- [18] I. D. F. contributors, "Guidelines," International Diabetes Federation, 2017. [Online]. Available: <https://www.idf.org/e-library/guidelines/119-idf-clinical-practice-recommendations-on-diabetic-foot-2017.html>.
- [19] N. Cho, J. Shaw, S. Karuranga, Y. Huang, J. da Rocha Fernandes, A. Ohlrogge and B. Malanda, "IDF Diabetes Atlas: Global estimates of diabetes prevalence for 2017 and projections for 2045," *PlumX Metrics*, vol. 138, pp. 271-281, Apr 2018.
- [20] I. D. F. contributors, "What is diabetes," International Diabetes Federation, 2019. [Online]. Available: <https://www.idf.org/aboutdiabetes/what-is-diabetes.html>.
- [21] W. Contributors, "Diabetes Mellitus," Wikipedia, the Free Encyclopedia, 8 August 2019. [Online]. Available: <https://en.wikipedia.org/w/index.php?title=Diabetes&oldid=909854418>.
- [22] C. Liapis, K. Balzer and F. Benedetti-Valentini, "Diabetic Foot," in *Vascular Surgery. European Manual of Medicine*, Berlin, Heidelberg, Springer, 2007, pp. 501-521.
- [23] F. H. F. contributors, "Diabetes Complications and Amputation Prevention," American College of Foot and Ankle Surgeons, 2019. [Online]. Available: <https://www.foothealthfacts.org/conditions/diabetic-complications-and-amputation-prevention#>.
- [24] P. J. Kim and J. Steinberg, "Complications of the diabetic foot.," *Endocrinology & Metabolism Clinics of North America*, vol. 4, no. 42, pp. 833-847, Dec 2013.
- [25] S. C. Mishra, K. C. Chhatbar, A. Kashikar and A. Mehndiratta, "Diabetic Foot," 16 November 2017. [Online]. Available: <https://www.bmj.com/content/bmj/359/bmj.j5064.full.pdf>.
- [26] B. S. Godfrey, "Lower Limb Prosthetics," 20 September 2013. [Online]. Available: <https://now.aapmr.org/lower-limb-prosthetics/>.
- [27] G. Tombolini, "I Piedi Protesici," in *Protesi di Arto Inferiore*, Manfredonia (FG), 2010.
- [28] P. G. Adamczyk, M. Roland and M. H. Hahn, "Sensitivity of biomechanical outcomes to independent variations of hindfoot and forefoot stiffness in foot prosthesis.," *Human Movement Science*, no. 54, pp. 154-171, April 2017.
- [29] E. Klood, A. Hansen, S. Fatone and M. Edwards, "Effects of prosthetic foot forefoot flexibility on oxygen cost and subjective preference rankings of unilateral transtibial prosthesis users," *Journal of Rehabilitation Research & Development*, vol. 47, no. 6, pp. 543-552, 2010.

- [30] K. E. Zelik, S. H. Collins, P. G. Adamczyk, A. D. Segal, G. K. Klute, D. C. Morgenroth, M. E. Hahn, M. S. Orenduff, J. M. Czerniecki and A. D. Kuo, "Systematic Variation of Prosthetic Foot Spring Affects Center-of-Mass Mechanics and Metabolic Cost During Walking," *Neural Systems and Rehabilitation Engineering*, vol. 19, no. 4, pp. 411-419, August 2011.
- [31] S. U. Raschke, M. S. Orenduff, J. L. Mattie, D. E. Kenyon, Y. O. Jones, D. Moe, L. Winder, A. S. Wong, A. Moreno-Hernandez, J. M. Highsmith, D. J. Sanderson and T. Kobayashi, "Biomechanical characteristics, patient preference and activity level with different prosthetic feet: a randomized double blind trial with laboratory and community testing," *Journal of Biomechanics*, no. 48, pp. 146-152, 2015.
- [32] N. P. Fey, G. K. Klute and R. R. Neptune, "The influence of energy storage and return foot stiffness on walking mechanics and muscle activity in below-knee amputees," *Clinical Biomechanics*, no. 26, pp. 1025-1032, June 2011.
- [33] N. P. Fey, G. K. Klute and R. R. Neptune, "Optimization of Prosthetic Foot Stiffness to Reduce Metabolic Cost and Intact Knee Loading During Below-Knee Amputee Walking: A Theoretical Study," *Journal of Biomechanical Engineering*, vol. 134, pp. 111005/1-111005/10, November 2012.
- [34] V. A. contributors, "Osteoarthritis (OA) | Causes, symptoms, treatments," Versus Arthritis, 2019. [Online]. Available: <https://www.versusarthritis.org/about-arthritis/conditions/osteoarthritis/>.
- [35] D. C. Norvell, J. Czerniecki, G. E. Reiber, C. Maynard, J. A. Pecoraro and N. S. Wiess, "The prevalence of knee pain and symptomatic knee osteoarthritis among veteran traumatic amputees and non amputees," *Archives of Physical Medicine and Rehabilitation*, vol. 86, pp. 487-493, 2005.
- [36] D. C. Morgenroth, A. D. Segal, K. E. Zelik, J. M. Czernicki, G. K. Klute, P. G. Adamczyk, M. S. Orenduff, M. E. Hahn, S. H. Collins and A. D. Kuo, "The effect of prosthetic foot push-off on mechanical loading associated with knee osteoarthritis in lower limb extremity amputees," *Gait & Posture*, vol. 34, pp. 502-507, 2011.
- [37] 6. McGraw-Hill Dictionary of Scientific & Technical Terms, *metabolic cost*, The McGraw-Hill Companies, Inc, 2003.
- [38] C. Curtze, A. L. Hof, H. G. van Keeken, J. P. Halbertsma, K. Postema and B. Otten, "Comparative roll-over analysis of prosthetic feet," *Journal of Biomechanics*, vol. 42, pp. 1746-1753, 2009.
- [39] P. G. Adamczyk, S. H. Collins and K. D. Arthur, "The advantages of a rolling foot inhuman walking," *The Journal of Experimental Biology*, vol. 209, pp. 3953-3963, July 2006.
- [40] A. H. Hansen, D. S. Childress and E. H. Knox, "Roll-over shapes of human locomotor systems: effects of walking speed," *Clinical Biomechanics*, vol. 19, pp. 407-414, 2004.
- [41] A. Hansen, "Effects of alignment on the roll-over shapes of prosthetic feet," *Prosthetics and Orthotics International*, vol. 32, no. 4, pp. 390-402, December 2008.
- [42] J. W. Leonard and J. H. Nath, "Comparison of finite element and lumped parameter methods for oceanic cables," *Engineering Structures*, vol. 3, pp. 153-167, July 1981.

- [43] S. M. Rigney, A. Simmons and K. Lauren, "A prosthesis-specific multi-link segment of lower-limb amputee sprinting," *Journal of Biomechanics*, vol. 49, pp. 3185-3193, July 2016.
- [44] J. Hoover and S. A. Meguid, "Analytical viscoelastic modelling of whiplash using lumped parameter," *International Journal of Mechanics and Materials in Design*, vol. 11, pp. 125-137, March 2015.
- [45] S. Miller, T. Soares, Y. Van Weddingen and J. Wendlandt, "Modeling Flexible Bodies with Simscape Multibody Software," The MathWorks, Inc., 2017. [Online].
- [46] M. contributors, *Simscape Multibody Getting Started Guide*, Natick, MA: The MathWorks, Inc., 2019.
- [47] A. Rohatgi, "WebPlotDigitizer," April 2019. [Online]. Available: <https://automeris.io/WebPlotDigitizer>.
- [48] G. Bovi, M. Rabuffetti, P. Mazzoleni and M. Ferrarin, "A multiple-task gait analysis approach: Kinematic, kinetic and EMG reference data for healthy young and adult subjects," *Gait & Posture*, vol. 33, p. 6.13, 2011.
- [49] D. A. Winter, "Anthropometry," in *Biomechanics and Motor Control of Human Movement*, 4th ed., Hoboken, New Jersey: John Wiley & Sons, Inc., 2009, pp. 82-86.
- [50] M. contributors, "interp1," [Online]. Available: <https://it.mathworks.com/help/matlab/ref/interp1.html#References>.
- [51] L. Cavallaro, C. Ferraresi, F. Tessari, C. De Benedictis and G. Milandri, "Studio numerico e sperimentale di piede protesico e valutazione degli effetti prodotti sulla deambulazione," Torino, 2018.
- [52] I. M. Daniel and O. Ishai, *Engineering Mechanics of Composite Materials*, New York - Oxford: Oxford University Press, 2006.
- [53] T. M. Contributors, "Simulink Design Optimization - User's Guide," The Mathworks, Inc., September 2019. [Online]. Available: [https://it.mathworks.com/help/pdf\\_doc/slido/slido\\_ug.pdf](https://it.mathworks.com/help/pdf_doc/slido/slido_ug.pdf).
- [54] T. M. Contributors, "Simulink Design Optimization - Getting Started Guide," The MathWorks, Inc., September 2019. [Online]. Available: [https://it.mathworks.com/help/pdf\\_doc/slido/slido\\_gs.pdf](https://it.mathworks.com/help/pdf_doc/slido/slido_gs.pdf).
- [55] N. Pham and B. M. Wilamowski, "Improved Nelder Mead's Simplex Method and Applications," *Journal of computing*, vol. 3, no. 3, pp. 55-63, March 2011.
- [56] J. Richards, A. Chohan and R. Erande, "Biomechanics," in *Tidy's Physiotherapy*, Churchill Livingstone, 2013, pp. 331-368.
- [57] M. F. Bobbert, H. C. Schamhardt and M. B. Nigg, "Calculation of Vertical Ground Reaction Force Estimates During Running from Positional Data," *Journal of Biomechanics*, vol. 24, no. 12, pp. 1095-1105, 1991.

- [58] J. A. Zeni, J. G. Richards and J. S. Higginson, “Two Simple Methods for Determining Gait Events during Treadmill and Overground Walking Using Kinematic Data,” *Gait & Posture*, vol. 27, pp. 710-714, 2008.
- [59] A. Hansen, S. A. Guard and D. S. Childress, “The determination of foot/ankle roll-over shape: Clinical and research applications,” in *Pediatric Gait, 2000. A new Millennium in Clinical Care and Motion Analysis Technology*, 2000.
- [60] V. Pratt, “Direct Least-Squares Fitting of Algebraic Surfaces,” *Computer Graphics*, vol. 21, no. 4, pp. 145-152, April 1987.
- [61] N. Chernov, “Circle Fit (Pratt method),” MathWorks, Jan 2009. [Online]. Available: <https://it.mathworks.com/matlabcentral/fileexchange/22643-circle-fit-pratt-method>. [Accessed November 2019].
- [62] S. Miller, “Simscape Multibody Contact Forces Library,” April 2019. [Online]. Available: <https://it.mathworks.com/matlabcentral/fileexchange/47417-simscape-multibody-contact-forces-library>.
- [63] C. L. Vaughan, B. L. Davis and J. O'Connor, Dynamics of Human Gait, 2nd Edition ed., Cape Town, South Africa: Kiboho Publishers, 1999.



# Ringraziamenti

---

I primi ringraziamenti vanno alle persone che hanno reso possibile e seguito l'intero lavoro di Tesi. Ringrazio in particolare il Prof. Carlo Ferraresi, l'Ing. Federico Tessari, l'Ing. Giovanni Milandri e l'Ing. Carlo De Benedictis per il costante supporto durante tutto il percorso, per aver condiviso con me dubbi e perplessità ed avermi aiutato con la loro esperienza a superarli.

Voglio ringraziare tutto il team del dipartimento di Rehab Technologies dell'Istituto Italiano di Tecnologia (IIT) di Genova per avermi fatto sentire parte del team e aver condiviso con me le loro idee. Un ringraziamento particolare va a: l'Ing. Matteo Laffranchi, coordinatore del gruppo di ricerca, che ha ritagliato del tempo per assistere alle presentazioni; il Dott. Lorenzo Cavallaro, per aver condiviso con me i risultati delle sue analisi; l'Ing. Marco Freddolini per avermi assistito durante i test di analisi del cammino.

Un grande grazie va ai colleghi e agli amici che mi hanno accompagnato durante parte del percorso e a quelli che mi accompagnano tuttora, a chi mi sostiene da più lontano e a chi mi è più vicino. Voglio quindi ringraziare Alice, Mattia e i ragazzi dell'Aula Tesisti, che mi hanno accompagnata in questo percorso e l'hanno reso meno pesante con il loro supporto e la loro allegria; i miei compagni di corso Alessandra, Elisa, Enrica, Mattia e Orlando, con cui ho trascorso questi anni di Magistrale e che mi hanno permesso di affrontarli sempre con un sorriso in più; i miei amici del Liceo, che rallegrano sabati sera, feste e Capodanni ormai da molti anni; le mie amiche Giulia e Maria Chiara che, anche se lontane, mi sono sempre vicino con il cuore.

Ringrazio Lorenzo, il mio ragazzo, che mi accompagna, supporta e sopporta da ormai due anni. Non è stato sempre facile affrontare le sfide che questo percorso ci ha messo davanti, ma ce l'abbiamo fatta. Insieme.

Voglio ringraziare anche le compagne di squadra di Torino e le ex compagne di squadra di Varese: le prime sono ormai la mia seconda famiglia da parecchi anni, le seconde mi hanno adottato e permesso di non abbandonare questo grande amore che è la pallanuoto.

Colgo l'occasione per ringraziare anche coach Ionut Cismaru, che mi ha insegnato a lottare con le unghie e con i denti e non si è mai risparmiato nello sgridarmi quando accennavo a mollare. Insieme a lui, ringrazio tutti gli allenatori con cui ho lavorato in questi anni: ognuno di voi mi ha aiutato a crescere come persona e come atleta.

Infine, ringrazio le persone che sono con me proprio dall'inizio: i miei genitori e la mia famiglia. Grazie perché mi avete permesso di studiare e seguire le mie passioni. Mi avete spronato quando stavo per mollare, dato una mano a rialzarmi quando cadevo e gioito con me quando ho raggiunto infine gli obiettivi. Questo primo traguardo, a cui spero di aggiungerne molti altri, è anche vostro.